

# **Roles of miR-3085-3p in skeletal development and osteoarthritis**

**Lingzi Niu**

Thesis submitted for the degree of Doctor of Philosophy

School of Biological Sciences  
University of East Anglia

2021

This copy of the thesis has been supplied on condition that anyone who consults it is understood to recognise that its copyright rests with the author and that use of any information derived therefrom must be in accordance with current UK Copyright Law. In addition, any quotation or extract must include full attribution.

# Abstract

Osteoarthritis (OA) is a progressive arthritis characterized by cartilage degradation, subchondral bone sclerosis and synovial inflammation. MicroRNAs are endogenous non-coding short RNAs, which repress gene expression. Numerous microRNAs have been reported to be involved in pathogenesis of OA. MiR-3085-3p is a novel microRNA that is selectively expressed in human cartilage and targets ITGA5. This project unravelled roles of miR-3085-3p in the skeletal development and progression of OA, following the optimization of time and dosage across experiments.

Overexpression of miR-3085-3p decreased expression of ITGA5 in DF1, SW1353, HeLa and C28/I2 in various assays including qRT-PCR, Western blotting and Luciferase assay. dosage and transfection time of miR-3085-3p mimic were optimized in different cell lines and assays.

MiR-3085-3p regulated cartilage homeostasis and chondrocyte function through decreasing the expression of ACAN and COL2A1, and various signalling pathways. MiR-3085-3p increased IL-1 $\beta$  induced MMP13, but transiently downregulated NF $\kappa$ B signalling by targeting MYD88. It repressed TGF $\beta$ /SMAD signalling by targeting SMAD2, SAMD3, and SMAD4. MiR-3085-3p potentiated canonical WNT/ $\beta$ -catenin signalling pathway characterized by promoting the luciferase activity of WNT3A-induced TOPFLASH reporter as well as the expression of WNT3A-induced AXIN2.

MiR-3085-3p took a vital part in human bone marrow MSC differentiation. During chondrogenesis, overexpression of miR-3085-3p decreased the expression of chondrocyte marker genes including ACAN, COL2A1, COL10A1 and SOX9. It led to delayed chondrogenic pellet formation and less GAG component. Taking advantage of microarray and RNA sequencing datasets, we found that JUN and FOS were potential targets of miR-3085-3p, and miR-3085-3p promoted IL-1 induced MMP-13 via JNK/AP-1 pathway. In adipogenesis, adipogenic marker genes (CEBP $\alpha$  and PPAR $\gamma$ ) were decreased, and lipid droplet accumulation was inhibited, at the presence of miR-3085-3p. whilst in osteogenesis, miR-3085-3p enhanced both the expression of osteoblast markers (COL1, ALPL) and the calcification. CMTM3, LBH and CTDSP2 were further validated as direct targets of miR-3085-3p by qRT-PCR and Luciferase assay. SiRNA against these 3 genes demonstrated a similar promotion of osteogenesis.

We did not successfully generate the miR-3085-3p null mice due to embryonic lethality. Lethality was also observed in the ITGA5 cartilage-specific knockout mice. Significant developmental defects in skeletal development and possible accelerated progression of osteoarthritis were revealed in ITGA5 cartilage-specific knockout mice, suggesting that ITGA5 is crucial in these processes. MiR-3085-3p potentially has negative effects on skeletal development and osteoarthritis by targeting ITGA5.

## **Access Condition and Agreement**

Each deposit in UEA Digital Repository is protected by copyright and other intellectual property rights, and duplication or sale of all or part of any of the Data Collections is not permitted, except that material may be duplicated by you for your research use or for educational purposes in electronic or print form. You must obtain permission from the copyright holder, usually the author, for any other use. Exceptions only apply where a deposit may be explicitly provided under a stated licence, such as a Creative Commons licence or Open Government licence.

Electronic or print copies may not be offered, whether for sale or otherwise to anyone, unless explicitly stated under a Creative Commons or Open Government license. Unauthorised reproduction, editing or reformatting for resale purposes is explicitly prohibited (except where approved by the copyright holder themselves) and UEA reserves the right to take immediate 'take down' action on behalf of the copyright and/or rights holder if this Access condition of the UEA Digital Repository is breached. Any material in this database has been supplied on the understanding that it is copyright material and that no quotation from the material may be published without proper acknowledgement.

# Contents

Abstract .....	2
List of figures .....	8
List of tables .....	12
List of appendices .....	13
List of abbreviations .....	14
Acknowledgement .....	20
Chapter 1 Introduction .....	21
1.1 Structure of a synovial joint .....	21
1.1.1 Synovium .....	23
1.1.2 Subchondral bone .....	23
1.1.3 Articular cartilage .....	23
1.2 Pathophysiology of skeletal development and osteoarthritis .....	28
1.2.1 Endochondral ossification in skeletal development and osteoarthritis .....	28
1.2.2 Pathologic matrix degradation .....	29
1.2.3 Molecules and signalling pathways involved in modulating chondrocytes behaviours and cartilage .....	31
1.3 Animal modelling in osteoarthritis .....	44
1.4 MicroRNAs .....	47
1.4.1 Biosynthesis of microRNAs .....	47
1.4.2 MicroRNAs in mesenchymal stem cell differentiation .....	49
1.4.3 MicroRNAs in osteoarthritis .....	51
1.5 Discovery of miR-3085 .....	58
1.6 Hypotheses and aims .....	59
Chapter 2 Materials and methods .....	60

2.1 Cell lines and cell culture .....	60
2.2 Sub-cloning.....	60
2.2.1 Genomic DNA extraction.....	60
2.2.2 DH5 $\alpha$ competent cells preparation.....	61
2.2.3 Plasmid construction.....	61
2.2.4 Site-directed mutagenesis of pmirGLO constructs.....	64
2.3 Transient transfection using Lipofectamine 3000.....	66
2.3.1 Transfection for Luciferase assay .....	66
2.3.2 Transfection for qRT-PCR.....	66
2.4 Stimulation of signalling pathways.....	67
2.5 Dual-GLO luciferase assay.....	67
2.6 Total RNA Isolation from cultured cells.....	67
2.7 Reverse transcription.....	68
2.7.1 Cells to cDNA.....	68
2.7.2 MiRCURY LNA Universal cDNA synthesis.....	68
2.8 Quantitative real-time polymerase chain reaction (qRT-PCR).....	69
2.9 Western blotting.....	70
2.10 Human MSCs differentiation.....	70
2.10.1 Chondrogenesis induction.....	70
2.10.2 Osteogenesis induction.....	71
2.10.3 Adipogenesis induction .....	71
2.11 Alcian Blue staining .....	72
2.12 Alizarin Red S straining .....	72
2.13 Oil Red O staining.....	72
2.14 Glycosaminoglycan (GAG) assay .....	73
2.14.1 Chondrogenic pellets digestion .....	73

2.14.2 DMMB staining.....	73
2.14.3 Double-stranded DNA quantification .....	74
2.15 Generation of transgenic mice model .....	74
2.16 Genotyping .....	76
2.17 DMM modelling.....	77
2.18 Whole mount skeletal preparation and staining .....	78
2.19 Tissue processing.....	78
2.20 Tissue sectioning .....	80
2.21 Histological staining .....	80
2.22 Growth plate measurement .....	83
2.23 Histologic scoring for osteoarthritis severity.....	84
2.24 Statistical analysis .....	85
Chapter 3 Optimizing of effective dosage and time of miR-3085-3p on ITGA5 in cell lines.....	86
3.1 Introduction.....	86
3.2 Results.....	87
1.1.1 MiR-3085-3p is highly expressed in human osteoarthritic chondrocytes..	87
1.1.2 Overexpression of miR-3085-3p decreases the expression of ITGA5 mRNA .....	88
1.1.3 MiR-3085-3p supresses ITGA5 by targeting seed sites within 3'UTR .....	92
1.1.4 ITGA5 protein is downregulated by miR-3085-3p .....	94
3.3 Discussion .....	97
Chapter 4 Investigating roles of miR-3085-3p in chondrocyte function .....	99
4.1 Introduction.....	99
4.2 Results.....	100
4.2.1 MicroRNA-3085-3p and extracellular matrix genes.....	100
4.2.2 MicroRNA-3085-3p and NFkB signalling.....	101

4.2.3 MicroRNA-3085-3p and TGF $\beta$ signalling .....	103
4.2.4 MicroRNA-3085-3p and WNT signalling .....	105
4.3 Discussion .....	106
Chapter 5 Exploring effects of miR-3085-3p on human bone marrow mesenchymal stem cell differentiation.....	108
5.1 Introduction .....	108
5.2 Results.....	109
5.2.1 Differential expression of miR-3085-3p during human BMMSC differentiation.....	109
5.2.2 MiR-3085-3p suppresses human BMMSC chondrogenesis.....	110
5.2.3 JUN and FOS are potential target genes of miR-3085-3p in human chondrocytes.....	114
5.2.4 MiR-3085-3p contributes to IL-1 $\beta$ -induced MMP-13 expression by activating JNK/AP-1 pathway.....	124
5.2.5 MiR-3085-3p inhibits human BMMSC adipogenesis.....	126
5.2.6 MiR-3085-3p enhances human BMMSC osteogenesis.....	129
5.2.7 CMTM3, CTDSP2 and LBH are target genes of miR-3085-3p during osteogenesis.....	132
5.2.8 Depletion of CMTM3, CTDSP2 and LBH promotes human MSC osteogenesis.....	139
5.3 Discussion .....	143
Chapter 6 Phenotyping the ITGA5 cartilage-specific knockout mice.....	147
6.1 Lethality of miR-3085-3p null mice.....	147
6.2 Rationale for the generation of ITGA5 cartilage-specific knockout mice.....	150
6.3 Results.....	151
6.3.1 Decreased ITGA5 expression across a tissue panel in the ITGA5 cartilage-specific knockout mice .....	151
6.3.2 Embryonic defects in the ITGA5 cartilage-specific knockout mice .....	152

6.3.3 Impaired postnatal development in the ITGA5 cartilage-specific knockout mice .....	156
6.3.4 Accelerated osteoarthritis progression in the ITGA5 cartilage-specific knockout mice .....	158
6.4 Discussion .....	161
Chapter 7 General discussion and future direction .....	164
7.1 Validation and optimization .....	165
7.2 MiR-3085-3p in cartilage homeostasis and chondrocyte function.....	165
7.3 MiR-3085-3p in human BMMSC differentiation .....	167
7.4 ITGA5 cartilage-specific knockout mice.....	169
Reference.....	171
Appendices .....	208
Publications.....	216

# List of figures

Figure 1.1 Schematic picture of normal (A) and osteoarthritic (B) synovial joints.....	22
Figure 1.2 Normal articular cartilage, illustrating the different patterns of the morphology, density of chondrocytes, as well as the orientation of collagen network in different layers. ....	24
Figure 1.3 Structure and organization of a typical aggrecan .....	26
Figure 1.4 Signalling pathways involved in chondrocyte function related to OA.....	31
Figure 1.5 Schematic structures of integrin heterodimers .....	33
Figure 1.6 Canonical and alternative NFκB activation pathways.....	38
Figure 1.7 Overview of canonical and non-canonical WNT signalling pathways.....	41
Figure 1.8 Scheme of TGF-β signalling.....	43
Figure 1.9 Schematic diagram of the Cre-loxP system .....	45
Figure 1.10 Schematic diagram of the mechanism of CRISPR-Cas9 system in gene editing.....	46
Figure 1.11 Schematic diagram of the biogenesis of miRNA .....	48
Figure 1.12 Identified differentially expressed microRNAs in normal and osteoarthritic articular cartilage .....	52
Figure 2.1 Schematic construct of COL2A1-Cre and ITGA5 in transgenic mice .....	75
Figure 2.2 Breeding scheme for ITGA5 cartilage-specific knock out mice .....	76
Figure 2.3 Representative growth plate of proximal tibia.....	83
Figure 3.1 The relative expression levels of miR-3085-3p (A) and ITGA5 (B) in different cell lines .....	87
Figure 3.2 Dose dependent response in qRT-PCR.....	89
Figure 3.3 Time course investigation of ITGA5 mRNA via qRT-PCR.....	90
Figure 3.4 Expression level of ITGA5 is detected by qRT-PCR in primary chondrocytes.....	91
Figure 3.5 Dose dependent response in luciferase assay.....	93
Figure 3.6 Time course in luciferase assay .....	94
Figure 3.7 Western blot analysis was performed to determine the protein levels of ITGA5 at 72 hours after transfection of miR-3085-3p mimic at indicated concentrations.....	95

Figure 3.8 Time course investigation of ITGA5 protein using western blotting.....	96
Figure 4.1 Luciferase assay of 3'utr constructs of ACAN and COL2A1 .....	100
Figure 4.2 Regulation of miR-3085-3p in IL-1 $\beta$ -induced MMP13 in HACs .....	101
Figure 4.3 Regulation of MYD88 by miR-3085-3p.....	102
Figure 4.4 Regulation of TGF $\beta$ /SMAD signalling by miR-3085-3p .....	103
Figure 4.5 Regulation of miR-3085-3p on SMADs .....	104
Figure 4.6 Regulation of miR-3085-3p on WNT3A signalling .....	105
Figure 5.1 The relative expression of miR-3085-3p during human MSC differentiation .....	109
Figure 5.2 Expression of marker genes for chondrocytes during chondrogenesis .	111
Figure 5.3 Regulation of marker genes by miR-3085-3p mimic throughout chondrogenesis.....	111
Figure 5.4 Regulation of marker genes by miR-3085-3p inhibitor throughout chondrogenesis.....	112
Figure 5.5 Sulphated glycosaminoglycans contents of chondrogenic pellets.....	112
Figure 5.6 Representative chondrogenic pellets stained with Alcian Blue.....	113
Figure 5.7 Profile of candidate target genes of miR-3085-3p during chondrogenesis .....	117
Figure 5.8 Expression of candidate genes of miR-3085-3p that downregulated by mimic and upregulated by inhibitor in HACs.....	120
Figure 5.9 Expression of candidate genes of miR-3085-3p that downregulated by mimic alone in HACs.....	121
Figure 5.10 Expression of candidate genes of miR-3085-3p that downregulated by both mimic and inhibitor in HACs .....	122
Figure 5.11 Luciferase assay of 3'utr constructs of JUN and FOS.....	123
Figure 5.12 Time course of IL-1 induced JUN, FOS and MMP-13 mRNA expression and JNK protein level in HACs .....	125
Figure 5.13 Regulation of marker genes for adipocytes during adipogenesis .....	126
Figure 5.14 Regulation of marker genes by miR-3085-3p mimic and inhibitor across adipogenesis. ....	127
Figure 5.15 Oil Red O staining for cytoplasmic triacylglycerol of adipocytes.....	128
Figure 5.16 Regulation of marker genes for osteoblast during osteogenesis.....	129

Figure 5.17 Regulation of marker genes by miR-3085-3p mimic and inhibitor across osteogenesis. ....	130
Figure 5.18 Alizarin Red S staining for calcification across osteogenesis .....	131
Figure 5.19 Profile of candidate target genes of miR-3085-3p across osteogenesis .....	134
Figure 5.20 Expression of candidate genes of miR-3085-3p that downregulated by mimic and upregulated by inhibitor in HACs.....	136
Figure 5.21 Luciferase assay of 3'UTR constructs of CMTM3, CTDSP2 and LBH. ....	137
Figure 5.22 Expression of candidate targets of miR-3085-3p across osteogenesis. ....	138
Figure 5.23 Expression of markers and candidate targets of miR-3085-3p that regulated by siRNAs during osteogenesis.....	140
Figure 5.24 Alizarin Red S staining for calcification across osteogenesis under effects of siRNAs.....	141
Figure 5.25 Schematic overview of regulation of miR-3085-3p, siRNAs on target genes and downstream pathways involved in osteogenesis .....	146
Figure 6.1 Picture illustrated the sequence of alleles from selective genetically altered founders heterozygous mice. ....	148
Figure 6.2 Genotyping images of miR-3085-3p null strain .....	148
Figure 6.3 Expression of miR-3085-3p in offspring generated by founder #11 .....	149
Figure 6.4 Expression of ITGA5 in a tissue panel of ITGA5 cartilage-specific knockout strain. ....	151
Figure 6.5 Sagittal sections from embryos of ITGA5 cartilage-specific knockout mice .....	153
Figure 6.6 Sections from representative E17.5 embryo tissues .....	153
Figure 6.7 Whole mount skeletal preparation of embryos of ITGA5 cartilage-specific knockout mice .....	154
Figure 6.8 Quantification of the length of long bones of ITGA5 cartilage-specific knockout mice. ....	155
Figure 6.9 Growth plates ITGA5 cartilage-specific knockout mice at p21 were analysed in proximal heads of tibia. ....	157
Figure 6.10 Mice weight monitoring.....	158

Figure 6.11 Representative images of knee joints of ITGA5 cartilage-specific knockout mice at 10 weeks following Sham or DMM surgery ..... 159

Figure 6.12 Histological analysis of four compartments of knees via OARSI scoring system..... 160

## List of tables

Table 1.1 Summary of studies on the roles of microRNAs in cartilage extracellular matrix homeostasis and chondrocyte functions involved in OA.....	56
Table 2.1 PCR reaction for 3'UTR fragments.....	62
Table 2.2 Touch-down PCR program for 3'UTR fragments.....	62
Table 2.3 Fast digestion of DNA by double restriction enzymes.....	63
Table 2.4 DNA ligation reaction.....	63
Table 2.5 QuikChange Lightning Multi Site-Directed Mutagenesis reaction.....	65
Table 2.6 QuikChange Lightning Multi Site-Directed Mutagenesis PCR program....	65
Table 2.7 Standard qRT-PCR cycle conditions.....	69
Table 2.8 MicroRNA qRT-PCR cycle conditions.....	69
Table 2.9 Preparation for a GAG standard curve.....	73
Table 2.10 Protocol for preparing a dsDNA standard curve.....	74
Table 2.11 Genotyping PCR reaction.....	77
Table 2.12 Genotyping PCR program.....	77
Table 2.13 Tissue processing program.....	79
Table 2.14 Haematoxylin and eosin staining protocol for paraffin embedded tissue sections.....	81
Table 2.15 Safranin O and Fast Green staining protocol for paraffin embedded tissue sections.....	82
Table 2.16 OARSI semi-quantitative scoring system. This scoring system was proposed for histologic scoring of osteoarthritis in mice.....	84
Table 5.1 Summary of seed sites of miR-3085-3p seating within the 3'UTR of candidate target genes during chondrogenesis.....	118
Table 5.2 Summary of seed sites of miR-3085-3p seating within the 3'UTR of candidate targets during osteogenesis.....	135
Table 5.3 Results of Pearson correlation test between influence of siRNAs and miR-3085-3p on osteogenesis.....	142
Table 6.1 Information of pups from F1 litters of miR-3085-3p null strain.....	149

## List of appendices

Appendix 1 Primers for pmirGLO construction .....	208
Appendix 2 Primers for QuikChange Lightning Multi Site-Directed Mutagenesis ...	209
Appendix 3 Primers and probes for GOI qRT-PCR.....	210
Appendix 4 Primer sets for genotyping PCR. ....	213
Appendix 5 Expression level of miR-3085-3p after transfection of miR-3085-3p mimic in hBMMSC differentiation.....	214

## List of abbreviations

Abbreviation	Definition
<b>ACAN</b>	aggrecan
<b>ACAN</b>	aggrecan
<b>ACL</b>	anterior cruciate ligament transection
<b>ADAMTS</b>	a disintegrin and metalloproteinase with thrombospondin-like motifs
<b>AKT</b>	protein kinase B
<b>ALPL</b>	alkaline phosphatase
<b>ASAP</b>	Home Office Animals (Scientific Procedures) Act 1986
<b>ATG10</b>	autophagy-related gene 10
<b>BAFF-R</b>	B cell-activating factor receptor
<b>BMMSC</b>	bone-marrow-derived mesenchymal stem cell
<b>BMP</b>	bone morphogenetic protein
<b>BMPR2</b>	bone morphogenetic protein receptor type 2
<b>CAMKII</b>	calcium/calmodulin-sensitive protein kinase II
<b>CAPE</b>	caffeic acid phenethyl ester
<b>CD248</b>	CD248 molecule
<b>CEBP</b>	CCAAT / enhancer binding protein
<b>CH25H</b>	cholesterol 25-hydroxylase
<b>CHST3</b>	carbohydrate sulfotransferase 3
<b>CK1</b>	casein kinase I
<b>CMTM3</b>	CKLF like MARVEL transmembrane domain containing 3
<b>COL11A1</b>	collagen type XI alpha 1 chain
<b>COL1A1</b>	collagen type I alpha 1 chain
<b>COL1A2</b>	collagen type I alpha 2 chain
<b>COL2A1</b>	collagen type II alpha 1 chain
<b>COL9A2</b>	collagen type IX alpha 2 chain
<b>COMP</b>	cartilage oligomeric matrix protein
<b>Co-SMAD</b>	common-mediator SMAD
<b>CRISPR</b>	clustered regularly interspaced short palindromic repeats

<b>CRTAC1</b>	cartilage acidic protein 1
<b>CS</b>	chondroitin sulphate
<b>CSPG4</b>	chondroitin sulphate proteoglycan 4
<b>CTDSP2</b>	CTD small phosphatase 2
<b>CYP1B1</b>	cytochrome P450 1B1
<b>DAB2</b>	DAB adaptor protein 2
<b>DAG</b>	diacylglycerol
<b>DDR2</b>	discoidin domain receptor 2
<b>DLL1</b>	delta like canonical notch ligand 1
<b>DMEM</b>	Dulbecco's modified eagle medium
<b>DMM</b>	destabilization of the medial meniscus
<b>DMMB</b>	1,9-Dimethylmethylene blue
<b>DSB</b>	double-stranded DNA break
<b>EC</b>	endothelial cell
<b>ECM</b>	extracellular matrix
<b>EDTA</b>	ethylenediaminetetraacetic acid
<b>EFHD1</b>	EF-hand domain family member D1
<b>EFNA1</b>	ephrin A1
<b>EGF</b>	epidermal growth factor
<b>ERK</b>	extracellular signal-regulated kinase
<b>EZH2</b>	enhancer of zeste homolog 2
<b>FAK</b>	focal adhesion kinase
<b>FBS</b>	fetal bovine serum
<b>FBXO32</b>	F-box protein 32
<b>FGF</b>	fibroblast growth factor
<b>FGFR</b>	fibroblast growth factor receptor
<b>FN-f</b>	fragments of fibronectin
<b>FOS</b>	Fos proto-oncogene, AP-1 transcription factor subunit
<b>FRS2</b>	fibroblast growth factor receptor substrate 2
<b>FRZB</b>	frizzled-related protein B
<b>FUT4</b>	fucosyltransferase 4

<b>GAG</b>	glycosaminoglycan
<b>GLDN</b>	gliomedin
<b>GOI</b>	genes of interest
<b>GRB2</b>	growth factor receptor-bound protein 2
<b>GSK3<math>\beta</math></b>	glycogen synthase kinase 3 beta
<b>HAC</b>	human primary articular chondrocyte
<b>HDAC2</b>	histone deacetylase 2
<b>HDR</b>	homology-directed repair
<b>HMGB1</b>	high mobility group box chromosomal protein 1
<b>HSPG</b>	heparan sulphate proteoglycans
<b>IBMX</b>	3-isobutyl-1-methylxanthine
<b>ID1</b>	inhibitor of DNA binding 1, HLH protein
<b>I-EGF</b>	integrin epidermal growth factor-like domain
<b>IFN</b>	interferon
<b>IGF</b>	insulin-like growth factor
<b>IGFBP5</b>	insulin like growth factor binding protein 5
<b>IHC</b>	immunohistochemistry
<b>IKK</b>	I $\kappa$ B kinases
<b>IL</b>	interleukin
<b>ISH</b>	in situ hybridization
<b>ITGA5</b>	integrin alpha 5
<b>I<math>\kappa</math>B</b>	inhibitor of NF $\kappa$ B
<b>JAK</b>	Janus kinase
<b>JNK</b>	c-Jun N-terminal kinase
<b>JUN</b>	Jun proto-oncogene, AP-1 transcription factor subunit
<b>KLF6</b>	Kruppel like factor 6
<b>KO</b>	knock out
<b>KPNA3</b>	karyopherin subunit alpha 3
<b>KS</b>	keratan sulphate
<b>LBH</b>	limb bud and heart development
<b>LEF-1</b>	lymphoid enhancer factor 1

<b>LFC</b>	lateral femoral condyle
<b>LMW-HA</b>	low molecular weight hyaluronan
<b>LRP</b>	low-density lipoprotein receptor-related protein
<b>LTP</b>	lateral tibial plateau
<b>LT<math>\beta</math>-R</b>	lymphotoxin beta receptor
<b>LYN</b>	LYN proto-oncogene, Src family tyrosine kinase
<b>MAPK</b>	mitogen-activated protein kinase
<b>MEK</b>	mitogen-activated protein kinase kinase
<b>MFC</b>	medial femoral condyle
<b>miRNA</b>	microRNA
<b>MMP</b>	matrix metalloproteinase
<b>MSC</b>	mesenchymal stem cell
<b>mTOR</b>	mammalian target of rapamycin
<b>MTP</b>	medial tibial plateau
<b>MYD88</b>	myeloid differentiation factor 88
<b>NBF</b>	neutral buffered formalin
<b>NEK2</b>	NIMA-related kinase 2
<b>NFAT</b>	nuclear factor of activated T-cells
<b>NFIA</b>	nuclear factor I A
<b>NFKBIA</b>	NFKB inhibitor alpha
<b>NF<math>\kappa</math>B</b>	nuclear factor kappa-light-chain-enhancer of activated B cells
<b>NGDS</b>	next generation deep sequencing
<b>NHEJ</b>	non-homologous end-joining
<b>NOS2</b>	nitric oxide synthase 2
<b>OA</b>	osteoarthritis
<b>OAF</b>	out at first homolog
<b>OCN</b>	osteocalcin
<b>OPN</b>	osteopontin
<b>PCP</b>	planar cell polarity
<b>PDK1</b>	phosphoinositide-dependent kinase 1
<b>PGE2</b>	prostaglandin E2

<b>PGRN</b>	progranulin
<b>PI3K</b>	phosphoinositide 3-kinases
<b>PKC</b>	protein kinase C
<b>PLC</b>	phospholipase C
<b>PLEKHF1</b>	pleckstrin homology and FYVE domain containing 1
<b>PP2A</b>	Protein phosphatase 2
<b>PPAR</b>	peroxisome proliferator activated receptor
<b>PSI</b>	plexin/semaphorin/integrin
<b>PTEN</b>	phosphatase and tensin homolog
<b>PTGS2</b>	prostaglandin-endoperoxide synthase 2
<b>PTH1H</b>	parathyroid hormone-like hormone
<b>PTP1B</b>	protein tyrosine phosphatase non-receptor type 1
<b>RAB3IL1</b>	RAB3A interacting protein like 1
<b>RHAMM</b>	receptor for hyaluronan mediated motility
<b>RIP</b>	receptor-interacting protein
<b>RISC</b>	RNA-induced silencing complex
<b>ROCK</b>	Rho-associated kinase
<b>ROR<math>\alpha</math></b>	retinoic acid-related orphan receptor alpha
<b>R-SMAD</b>	receptor associated SMAD protein
<b>RTK</b>	receptor tyrosine kinase
<b>RT-PCR</b>	real time polymerase chain reaction
<b>RUNX2</b>	Runt-related transcription factor 2
<b>SBE</b>	CAGAC smad binding element
<b>SCARA3</b>	cavenger receptor class A member 3
<b>SCIN</b>	scinderin
<b>SEM</b>	standard error of the mean
<b>SERPINE1</b>	serpin family E member 1
<b>shRNA</b>	short hairpin RNA
<b>siRNA</b>	small interfering RNA
<b>SIRT1</b>	silent information regulator 1
<b>SLC25A28</b>	solute carrier family 25 member 28

<b>SMAD</b>	mothers against decapentaplegic homolog
<b>SMURF1</b>	SMAD ubiquitin regulatory factor 1
<b>SOS</b>	son of sevenless protein
<b>STAT</b>	Janus kinase-signal transducer and activator of transcription
<b>TAK1</b>	transforming growth factor beta-activated kinase 1
<b>TBRI</b>	TGF $\beta$ type I receptor
<b>TBR2</b>	TGF $\beta$ type II receptor
<b>TCF</b>	T-cell factor
<b>TGF</b>	transforming growth factor
<b>TGFBR3</b>	transforming growth factor beta receptor 3
<b>TIMP</b>	tissue inhibitors of metalloproteinase
<b>TLR</b>	toll-like receptor
<b>TNF</b>	tumour necrosis factor
<b>TNIP1</b>	TNFAIP3 interacting protein 1
<b>TRADD</b>	tumour necrosis factor receptor type 1-associated DEATH domain protein
<b>TRAF</b>	tumour necrosis factor receptor-associated factor
<b>TRIF</b>	TIR-domain-containing adapter-inducing interferon- $\beta$
<b>TSC22D3</b>	TSC22 domain family member 3
<b>T-SSR</b>	tyrosine site-specific recombinases
<b>TXNIP</b>	thioredoxin interacting protein
<b>TYMP</b>	thymidine phosphorylase
<b>UC-MSC</b>	umbilical cord mesenchymal stem cell
<b>UTR</b>	untranslated region
<b>VEGF</b>	vascular endothelial growth factor
<b>vWFPC</b>	von-Willebrand factor cleaving protease
<b>WIF-1</b>	WNT inhibitory factor 1
<b>WNT</b>	wingless and int-1
<b>WT</b>	wild type

# Acknowledgement

As a Chinese saying goes, "one day teacher, one day father." I would like to express my sincere gratitude to my supervisor, Professor Ian Clark, who guide me into and bring me up in the world of research. Thanks are due to Dr Tracey Swingler, my second supervisor, for all her help and care in the lab, and Professor Andrea Munsterberg for her kind suggestions and comments.

I would like to thank all the Clark lab members, Dr Rosemary Davidson, Dr Linh Le, Perry Smith, past and present, for their friendship and assistance during my PhD.

I would like to thank Professor Stephen Robinson for kindly giving his ITGA5 mice to me, without which, my animal experiment would not have been possible.

I thank all staff in DMU – Simon, Rich, John, Emma, Anya, Imogen for their kindness to me and my mice.

I also want to thank folks in Newcastle University, Professor David Young, Dr Matt Barter, Dr Yao Hao ang Hua Lin for their sharing and collaboration in experimental techniques.

I thank Professor Tom Wileman, who gave me the opportunity working in his group, enriching my experience in animal experiments.

Special thanks are due to Dr Zhengyu Zhang, Dr Huanyu Li, Dr Weijiao Zhang, and Dr Nan Cheng. I appreciate their accompany and feeding in the lab and life.

I thank Arthritis Action and FFWG for funding me during my PhD.

Last but not least, I thank my father Jigeng Niu and my stepmother Xiuping Wang who gave me endless support and encouragement in my life. Finally, I would present my profound longing for my mother who gave me life, and your soul is always living in me.

# Chapter 1 Introduction

Osteoarthritis (OA), the most common type of arthritis found worldwide and a leading cause of disability, has exerted a great negative impact on the health and quality of life of the elderly (1). In epidemiologic studies, 8.75 million people aged or over 45 year-old were suffering from OA in UK in 2019 (2). an estimated 13.4% of adults in U.S. were clinically diagnosed with OA in 2017, and the prevalence of it steadily increases with age (3). The importance of OA not only derives from its high incidence and health detriment but also its heavy economic burden on both individuals and society, in terms of loss of productivity and cost of care and treatment. OA most commonly involves the weight-bearing and frequently active joints, including hips, knees, the lumbar and cervical spine, metatarsophalangeal and interphalangeal joints, which can cause pain, swelling, stiffness, deformity and dysfunction of these joints (4). The pattern and progression of joints involved in OA is strikingly affected by age, gender, mechanical, biochemical and genetic factors. Although the aetiology of OA is still not fully understood, the pathogenesis is characterized by cartilage damage, subchondral bone sclerosis, and synoviopathy, among which the erosion, degradation and deficiency of cartilage are regarded as the core pathology (Figure 1.1). Existing therapies for OA are focused on pain and improving function and quality of life with disease using analgesics, anti-inflammatory drugs, and surgery in late stage. Comprehensive and individualized interventions are required to manage OA.

## 1.1 Structure of a synovial joint

Synovial joints, namely diarthroses, the most mobile type of joints in the body, usually consist of the following components:

As shown in Figure 1.1, each bone taking part in the synovial joint is covered by hyaline cartilage (rarely, as in the case of temporomandibular joint, by fibrocartilage), and the joint is surrounded by a fibrous capsule. The outer layer of the capsule is a fibrous membrane that is continuous with the periosteum of the bones forming the joint, reinforced by ligaments. The inner synovial membrane encloses the joint and is responsible for producing the synovial fluid that help lubricate the joint surfaces. Certain synovial joints may have additional structures such as articular discs, bursae

or fatty pads. Intra articular discs or menisci are made up of fibrocartilage and may be complete or incomplete. Complete discs divide the joint cavity into two components. Bursae are small sacs located between the bones and muscles or tendons, filled with synovial fluid and thought to reduce friction. Articular fat pads are also covered in synovial membrane. They distribute synovial fluid evenly and reduce stress on the joint (5).

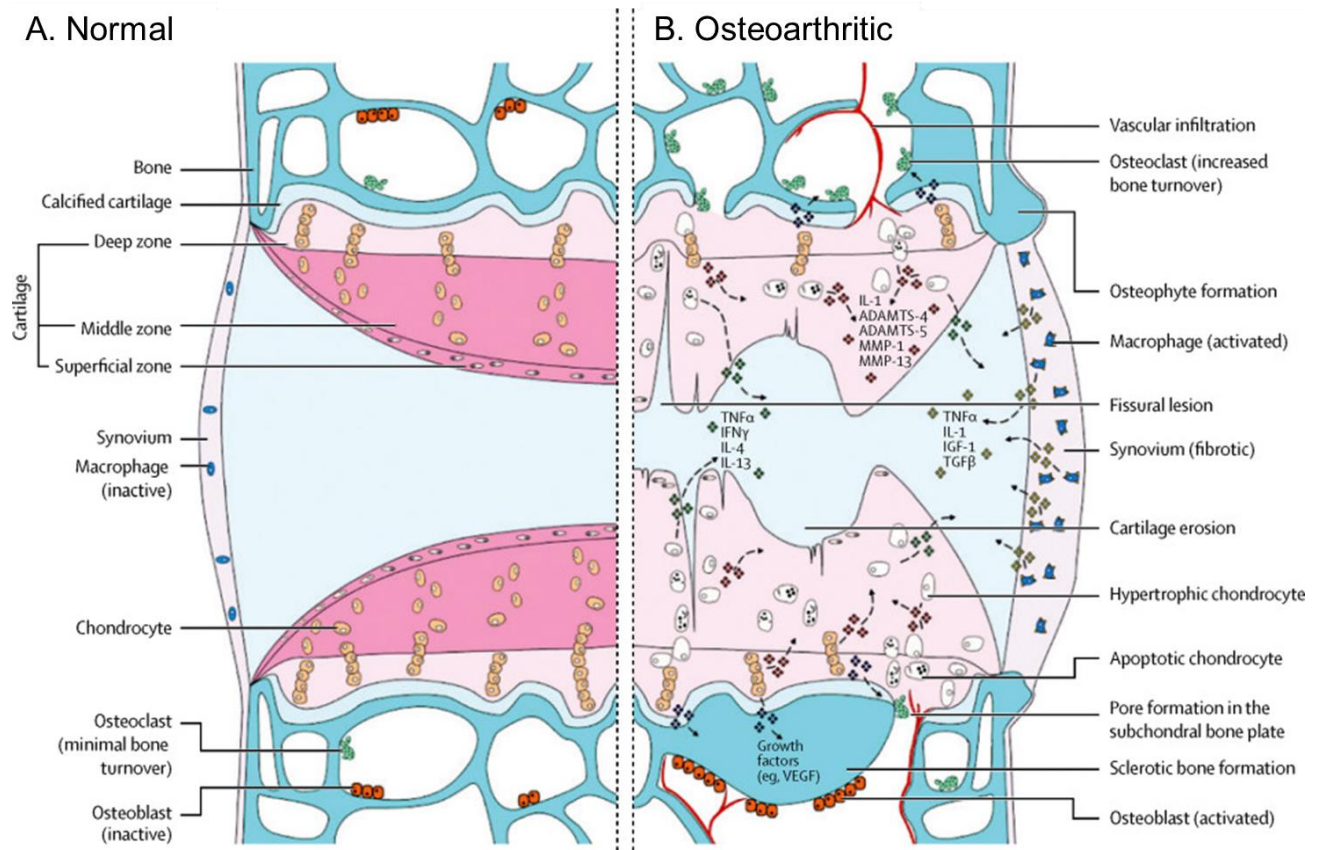


Figure 1.1 Schematic picture of normal (A) and osteoarthritic (B) synovial joints. (A) Structures in normal joint, including articular cartilage, synovium, and bone. (B) Pathological changes of structures and signalling pathways that occurred in osteoarthritis. ADAMTS, a disintegrin and metalloproteinase with thrombospondin-like motifs; IFN, interferon; IGF, insulin-like growth factor; IL, interleukin; MMP, matrix metalloproteinase; TGF, transforming growth factor; TNF, tumour necrosis factor; VEGF, vascular endothelial growth factor. Adapted with permission from (6).

### **1.1.1 Synovium**

Synovium can become hyperplastic, inflammatory, fibrotic, and detritus-rich in OA. It is intriguing to speculate that the synoviopathy is indispensable in the progression of OA. In early OA, synovial hyperplasia and hypertrophy are found with increased cytoplasmic volume, proliferation of synovial lining cells, development of villi or folds in the membrane, and vascular engorgement which affects the ability of the synovium to provide nutrients for the articular cartilage. In addition, lymphocytic infiltration including B-lymphocytes, plasma cells as well as T-lymphocytes can be detected, with the influx of inflammatory cells further perpetuating the cycle of cartilage degeneration. Fibrotic synoviopathy is commonly identified in the late stage of OA, characterized by capsular fibrosis responsible for the joint stiffness. Detritus-rich synovitis is another form of synoviopathy that occurs in the end-stage of OA, mostly resulting from bone and cartilage fragments attached or incorporated to synovial membrane.(7)

### **1.1.2 Subchondral bone**

During the course of OA, the subchondral bone might suffer from corrosion and rupture on the surface and, and microfractures of the trabeculae bone. The mechanical pressures are therefore transmitted to the marrow cavity together with focal necrosis, and cysts ensues in the subchondral bone. There is a responding upregulation in osteoblastic activity, thereby thickness of subchondral bone plate (8) increases and new bone outgrows on bone edges (9). Furthermore, vascular engorgement and bone marrow oedema largely contribute to the clinical features of subchondral sclerosis (10).

### **1.1.3 Articular cartilage**

#### **1.1.3.1 Extracellular matrix**

Articular cartilage is an aneural, avascular and alymphatic connective tissue, sparsely populated with chondrocytes and primarily composed of extracellular matrix (ECM), covering the ends of bones in synovial joints. It is an elastic, resilient tissue that distributes the shock load and enables low-friction movement to protect the underlying bone. The properties of cartilage are dependent on the composition and structure of the ECM, and chondrocytes contribute to the homeostasis of this matrix. It is the combination of collagen and proteoglycan (predominantly aggrecan) that establishes

a stable collagen fibril network to ensure the framework and shape of cartilage and provides a negative charge density with aggrecan molecules being able to repel each other and retain water, regulating the compressibility and maintaining the shape of cartilage. The cartilage can be predominantly divided into four zones according the components and arrangement of chondrocytes and ECM from the superficial to deep layers. The superficial zone is smooth with flattened chondrocytes and thinner collagen fibres arranged in parallel with the surface, while the deeper layer contains round cell morphology and thicker fibres perpendicular to the surface and merges with a calcified layer that interlocks with the subchondral bone. Between the superficial and deeper zones, there is a transition layer with collagen and chondrocytes randomly arranged. (Figure 1.2) The proportion of the major collagen constituents don't dramatically vary in different zones in mammalian articular cartilage.

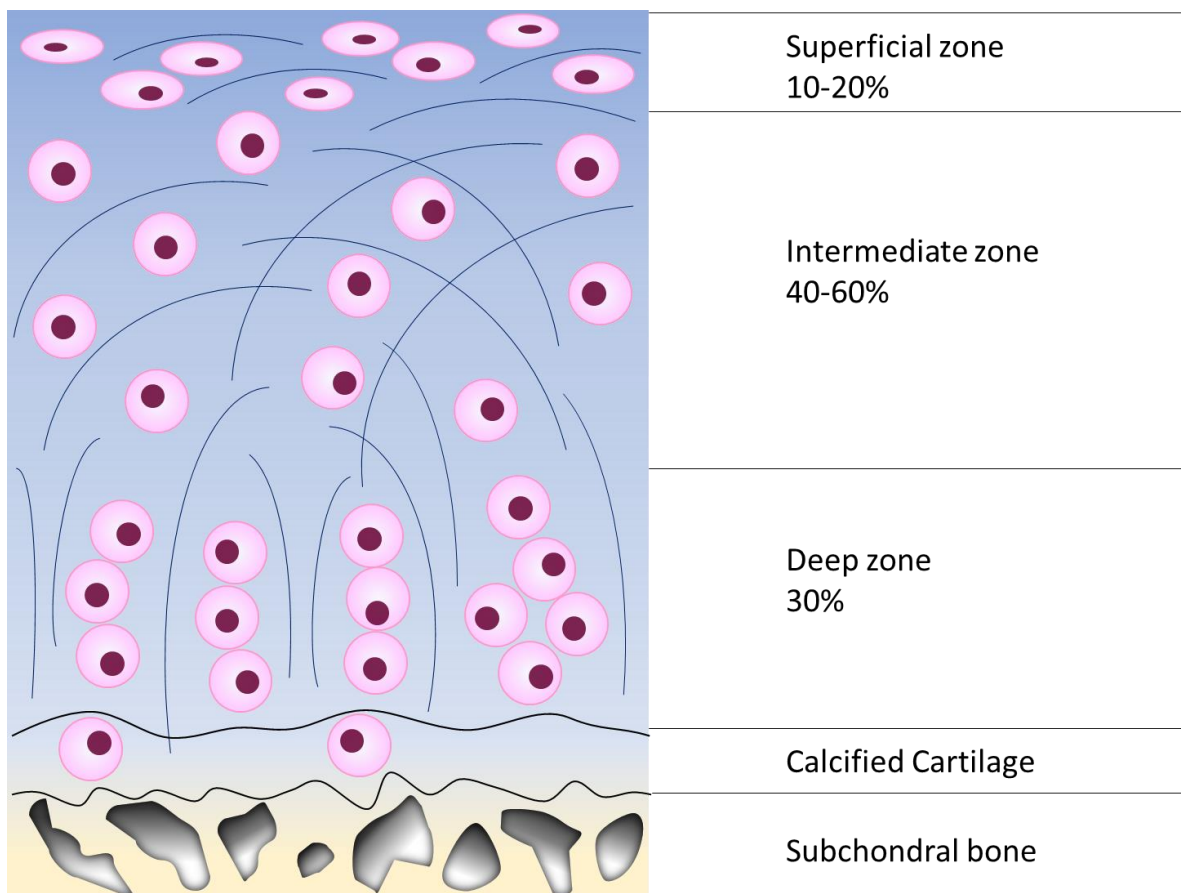


Figure 1.2 Normal articular cartilage, illustrating the different patterns of the morphology, density of chondrocytes, as well as the orientation of collagen network in different layers.

#### 1.1.3.1.1 Collagen network

The predominant matrix fibril constituent is type II collagen which forms a structural scaffold (11). It is primarily secreted by chondrocytes as a procollagen comprising a triple helix of  $\alpha$ -chains and aggregates into fibrils after the C- and N-termini are cleaved off by tolloid family proteinases and ADAMTS2, 3 or 14 (12). Subsequently, cross-links are formed. Evidence has accumulated that these fibrils can develop a heteropolymer covalently connected with a minor proportion of other type collagens, notably type XI and IX, to establish the core fibril network (13-16). The assemblage of collagen fibrils is under the regulation of a number of molecules including decorin, fibromodulin and lumican. In addition, both collagen type IX and XI appear to play an important role in regulating structure and interactions with other matrix molecules, such as matrilins and cartilage oligomeric matrix protein (COMP) (17).

#### 1.1.3.1.2 Aggrecan

Aggrecan (ACAN), a large aggregating proteoglycan, is also an important part of the network, made up of a core protein with three globular domains (G1, G2, G3) and two interglobular segments to which are bound the glycosaminoglycan (GAG) sidechains (Figure 1.3). A number of repeats of chondroitin sulphate (CS) and keratan sulphate (KS) disaccharides, together with other oligosaccharides units, form the linear GAG polysaccharide (18). Each CS has a building block of a D-glucuronate with a negatively charged carboxyl group and an N-acetyl galactosamine with a sulphate, while KS contains a D-galactose and an N-acetylglucosamine. The CS chains are clustered into 2 domains. The KS chains are shorter and enriched near to the N-terminal of the core protein. One molecule of aggrecan is estimated to contain around 30 such chains. Many aggrecans are bound to a hyaluronan (also a GAG, but not sulphated), thereby assembling into a large aggregates with fixed and intensive negative charges to trap the water, in turn, contribute to the compressive property of articular cartilage (19).

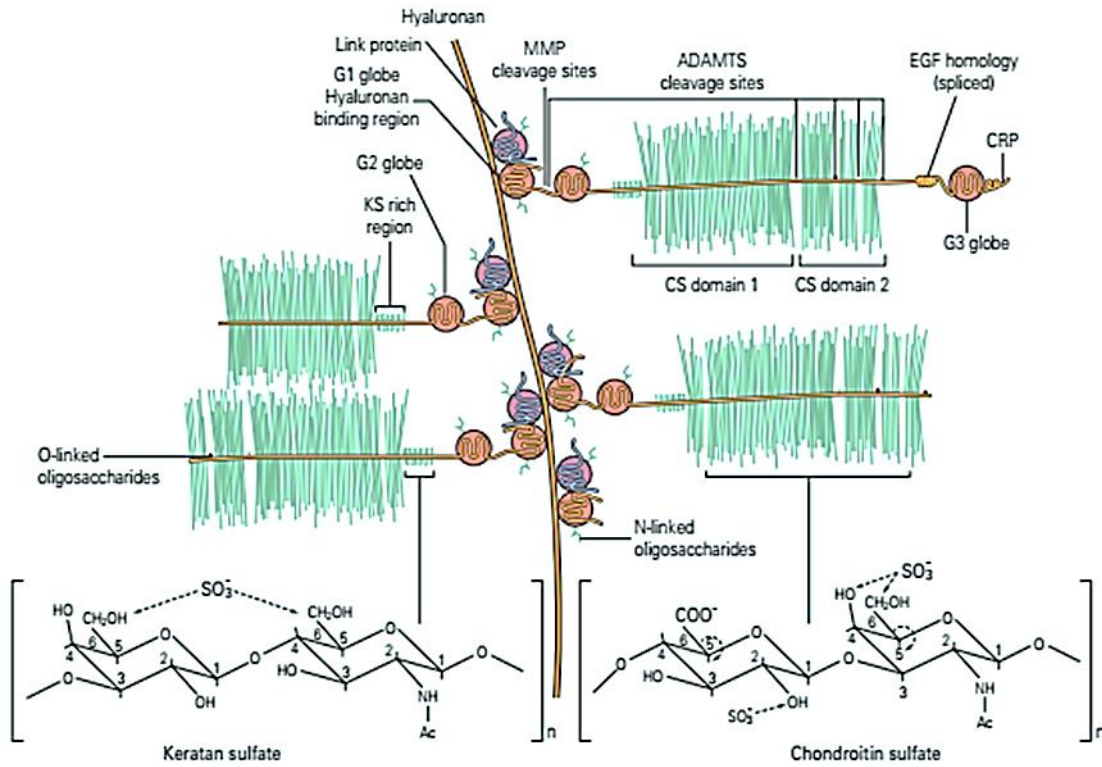


Figure 1.3 Structure and organization of a typical aggrecan. The sites for cleavage by the ADAMTS and MMP aggrecanases are indicated. ADAMTS, a disintegrin and metalloproteinase with thrombospondin-like motifs; CS, chondroitin sulphate; EGF, epidermal growth factor; KS, keratan sulphate; MMP, matrix metalloproteinase. Adapted with permission from (20).

### **1.1.3.2 Chondrocyte**

Chondrocytes are the unique cells embedded in the articular cartilage, playing a significant part in maintaining the structure, function, and integrity of cartilage by delicately regulating both synthetic and catabolic processes in response to environmental changes within the ECM. They are responsible for the turnover of the ECM in their immediate vicinity by breaking down the damaged matrix components, caused by mechanical and physical events and producing new molecules to repair. Chondrocytes in different location of articular cartilage vary in terms of morphology and metabolic function. In the superficial zone, they are flat and have a greater density than those in deeper layers. Normal chondrocytes sit in a lacuna, the territorial matrix rich in type VI collagen, and have little cell to cell contact, characterized by small number of mitochondria indicating their low rate of oxygen consumption. In contrast, chondrocytes, especially in the deep/radial zone, have abundant endoplasmic reticula and Golgi apparatus, which give them the capacity of protein synthesis and the sulfation of the polysaccharides from the side chains of proteoglycans. Importantly, chondrocytes are responsible for obtaining feedback of the environmental changes via various cell surface receptors such as integrins (21, 22), discoidin domain receptor 2 (DDR-2) (23), heparan sulphate proteoglycans (HSPG) (24), CD44 and receptor for hyaluronan mediated motility (RHAMM) (25, 26).

## **1.2 Pathophysiology of skeletal development and osteoarthritis**

### **1.2.1 Endochondral ossification in skeletal development and osteoarthritis**

It is quite interesting that not only the component and structure of the articular cartilage but also many biological processes which occur in the progression of OA mimic the pattern of the chondral evolution, including changes in the chondrocytic differentiation, matrix anabolism, proliferation, matrix catabolism, calcification, and apoptosis. Chondrocytes are differentiated from mesenchymal stem cells (MSCs). The zone most distant from the ossification contains resting chondrocytes and undergoes a relatively frequent mitosis and cluster into a multicellular layer to achieve proliferation. Following this is a hypertrophic phase characterized by dramatically enlarged mature chondrocytes and increasing secretion of type X collagen. Hypertrophic chondrocytes then die, and the ECM becomes mineralized and degraded with an onset of MMP13 expression. Besides, blood vessel invasion enables endothelial cells (ECs) to vascularize the developing bone, and the bone vessels undergo mineralization to form a template for osteoblasts laying down for mineralizing bone (27, 28). Meanwhile, osteoclasts get involved to remove the matrix while osteoblasts assist in the formation and deposition of calcified bone (29, 30).

A series of genes has been reported to have important influence on the fetal developmental process and confirmed in OA (30, 31). For example, expression of SOX9, a typical transcription factor expressed in chondroprogenitor cells and at a high level in chondrocytes, indicates the differentiation to the chondrocyte phenotype, is downregulated in OA (32). Overexpression of SOX9 in passaged human primary chondrocytes increases COL2A1 expression and improves their capacity to rebuild the ECM, suggesting a recovery in chondrocyte phenotype (33). Nonetheless, the onset and upregulation of MMP13 expression implies raised matrix catabolism potentially linked to hyperplastic differentiation, a similar feature observed in osteoarthritic chondrocytes (34).

## 1.2.2 Pathologic matrix degradation

There are various hypotheses that may inform the pathology of cartilage and joint degeneration, such as mechanical overload, matrix proteolysis, age-related deterioration of the structure and function of cartilage matrix and chondrocytes, and increasing damage to the genomic DNA of the chondrocytes leading to a changed cellular phenotype. Ultimately, it is the breakdown and erosion of the cartilage ECM that plays a crucial role in the progression of OA and signifies the stage of this disease.

All joint tissues can be involved in OA including synovium, ligaments as well as the subchondral bone but the predominant pathogenesis is the degradation of the cartilage ECM from the very early stage. There is a delicate balance between the anabolism and catabolism of the ECM in healthy articular cartilage with ongoing tissue remodelling. However, in OA, the equilibrium is disturbed with the balance towards degradation, together with the loss of population and function of chondrocytes, therefore a failure to maintain homeostasis.

The main threat to the ECM which determines the integrity of cartilage are catabolic enzymes that degrade aggrecan and the collagen network. A disintegrin and metalloproteinase with thrombospondin motifs (ADAMTSs) and matrix metalloproteinase (MMPs) are two principal classes of proteinases belonging to two constituent branches of the metzincin superfamily (35, 36), that are closely associated with cartilage degradation. Humans have 19 ADAMTS genes and 24 MMP genes, which encode 19 ADAMTSs and 23 MMPs (37, 38). On the basis of domain composition and substrate preference, ADAMTSs can be subgrouped into aggrecanase/ proteoglycanase (ADAMTS1, 4, 5, 8, 9, 15 and 20), procollagen N-propeptidases (ADAMTS2, 3 and 14), COMP proteinase (ADAMTS7 and 12), von-Willebrand factor cleaving protease (vWFCP) (ADAMTS13) and others (ADAMTS 6, 10, 16, 17, 18 and 19) (39). Likewise, MMPs are assembled into collagenase (MMP 1, 8 and 13), gelatinase (MMP2 and 9), stromelysins (MMP3, 10 and 11), matrilysins (MMP7 and 26), membrane type MMPs (MMP14, 15, 16, 17, 24 and 15) and others (MMP12, 19, 20, 21, 23, 27 and 28) (38). Furthermore, both ADAMTSs and MMPs can be inhibited by tissue inhibitors of metalloproteinase (TIMPs) (37, 40). These proteinases are notable for their involvement in development and diseases primarily through remodelling ECM (41-43).

Aggrecan proteolysis precedes and is independent of collagen breakdown primarily caused by the activity of aggrecanases from the ADAMTSs, particularly ADAMTS4 and ADAMTS5 (44, 45). The cleavage occurring in the inter-globular domain could remove the CS chains leading to an accumulation of the shortening of aggrecan and the loss of the fixed negative charge density when exceeding the limited capacity of chondrocytes to repair. Additionally, the interglobular cleavage site is also a target of MMPs, further contributing to the degradation of aggrecans (46, 47).

Fibrillar collagen is mainly degraded by MMPs, characterized by their collagenolytic ability to specifically cleave the triple helix destabilizing the collagens. In OA, the expression levels of a number of MMPs are dysregulated, for instance, MMP1, MMP2, MMP3, MMP8, MMP9, MMP13, MMP16 and MMP28 have been reported significantly increased in cartilage (48, 49), among which MMP13, a collagenase with high specific activity against type II collagen, plays a vital role in disease progression.

Moreover, in cartilage, the deficiency of anabolic factors such as insulin-like growth factor 1 (IGF1) and bone morphogenetic proteins (BMPs) in combination with a rising impact of catabolic factors such as interleukin-1 $\beta$  (IL-1 $\beta$ ) and tumour necrosis factor- $\alpha$  (TNF $\alpha$ ) can lead to an overexpression of ADAMTSs and MMPs. Taken as a whole, when the breakdown of the cartilage ECM is no longer counterbalanced by the synthesis, degradation ensues.(50, 51)

### 1.2.3 Molecules and signalling pathways involved in modulating chondrocytes behaviours and cartilage

It is known that chondrocytes have the capacity to balance the delicate metabolism of cartilage ECM in response to altered loads and tissue damage. They are able to obtain external feedback guided in this endeavour by receptors at the cell surface. A network of various molecules and signalling cascades signals are responsible for either changing the cellular morphology by engaging the cytoskeleton or altering cellular function by regulating gene expression and protein synthesis (Figure 1.4). In this project, the transmembrane receptors, integrins, and classic signalling pathways including NFκB signalling pathway, TGFβ signalling pathway and WNT signalling pathway are emphasized on.

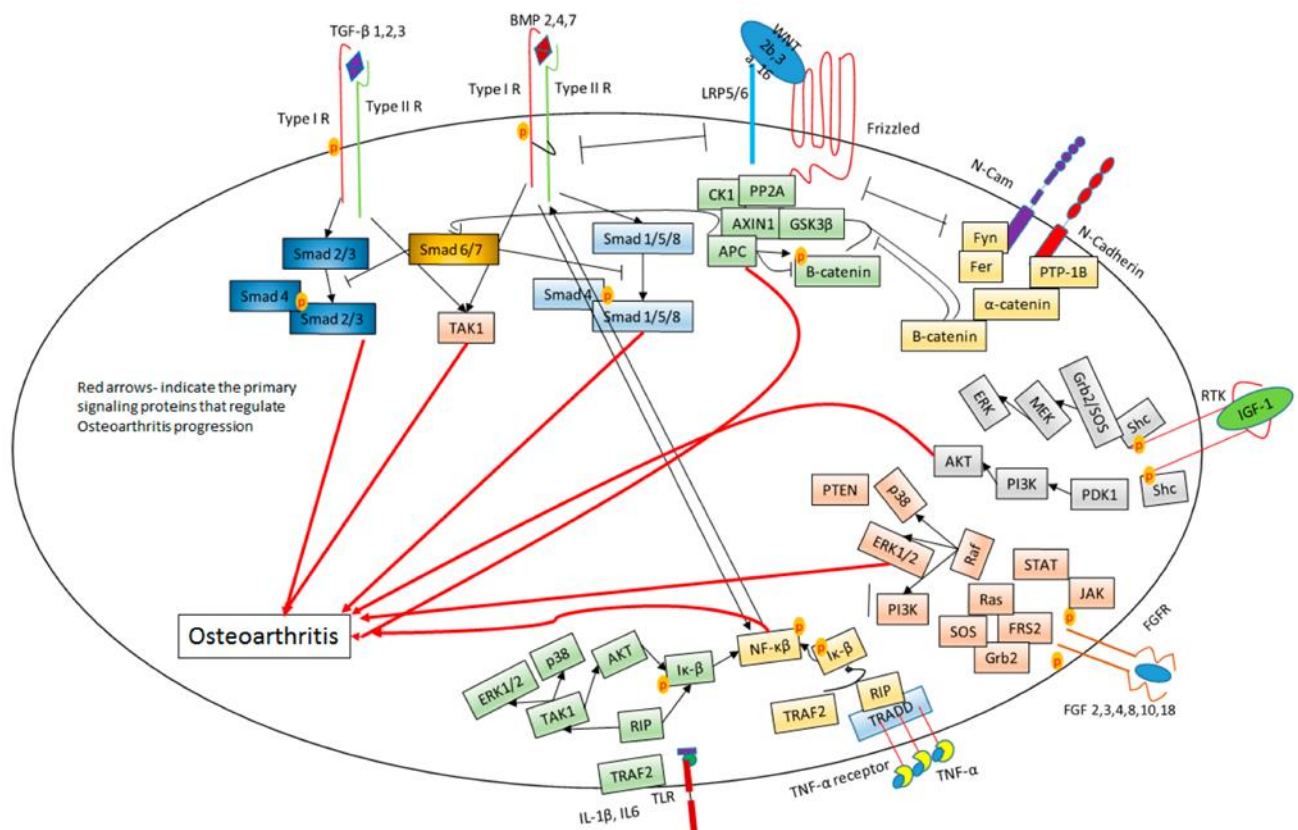


Figure 1.4 Signalling pathways involved in chondrocyte function related to OA. The majority of signalling cascades that contribute to the development and progression of OA includes TGFβ/SMAD, WNT, NF-κB, MAPK, PI3K/AKT and STAT pathways. Red arrows present dominant signalling molecules participating in OA. Black arrows indicate the activation processes, while bars indicate the inhibition. AKT, protein kinase B; BMP, bone morphogenetic protein; CK1, casein kinase I; ERK, extracellular signal-regulated kinase; GRB2, growth factor receptor-bound protein 2; FGF, fibroblast growth factor; FGFR, fibroblast growth factor receptor; FRS2, fibroblast growth factor receptor substrate 2; GSK3β, glycogen synthase kinase 3 beta; IGF-1, insulin-like growth factor 1; Iκ-β, inhibitor of NF-κB; IL, interleukin; JAK, Janus kinase; LRP, low-density lipoprotein receptor-related protein; MAPK, mitogen-activated protein kinase; MEK, mitogen-activated protein kinase kinase; NF-κB, nuclear factor kappa-light-chain-enhancer of activated B cells; PDK1, phosphoinositide-dependent kinase 1; PI3K, phosphoinositide 3-kinases; PP2A, protein phosphatase 2; PTEN, phosphatase and tensin homolog; PTP1B, protein tyrosine phosphatase non-

*receptor type 1; RTK, receptor tyrosine kinase; RIP, receptor-interacting protein; SMAD, mothers against decapentaplegic homolog; SOS, son of sevenless protein; TGF, transforming growth factor  $\beta$ ; TLR, toll-like receptor; TNF- $\alpha$ , tumour necrosis factor-alpha; TRAF, tumour necrosis factor receptor-associated factor; TRADD, tumour necrosis factor receptor type 1-associated DEATH domain protein; STAT, Janus kinase-signal transducer and activator of transcription; TAK1, transforming growth factor beta-activated kinase 1; WNT, wingless and int-1. Taken with permission from (52).*

### **1.2.3.1 Integrins**

Typically, integrins are membrane-spanning heterodimeric proteins that contain an  $\alpha$  subunit noncovalently bound to a  $\beta$  subunit. There have been 18  $\alpha$  subunits and 8  $\beta$  subunits reported, which can form 24 integrin heterodimers with various functions (53). The  $\alpha$  subunits consist of a seven-bladed  $\beta$ -propeller, thigh, calf-1, and calf-2 domains. 9 of the  $\alpha$  subunits contain an  $\alpha$  I domain, which is inserted in the  $\beta$ -propeller domain. Every  $\beta$  subunit has a  $\beta$  I domain ( $\alpha$  I domain like region), a hybrid domain, a plexin/semaphorin/integrin (PSI) domain, integrin epidermal growth factor-like (I-EGF) domains and a  $\beta$  tail domain. The I domain determines integrin ligand specificity, and the cytoplasmic tail of  $\beta$  integrin plays an essential role of connecting to intracellular proteins.(53-55) The conformation determines the activity of integrin heterodimers. In the inactive state, the extracellular legs are bent, and the ligand-binding head is buried close the cell membrane, by which the binding site of integrin is covered and reducing the affinity to ligand. At the same time, the transmembrane and intracellular regions of  $\alpha$  and  $\beta$  subunits are close to each other. In the active conformation, the headpiece is open, the legs are extended and the intracellular tails are separated.(Figure 1.5) (54, 56)

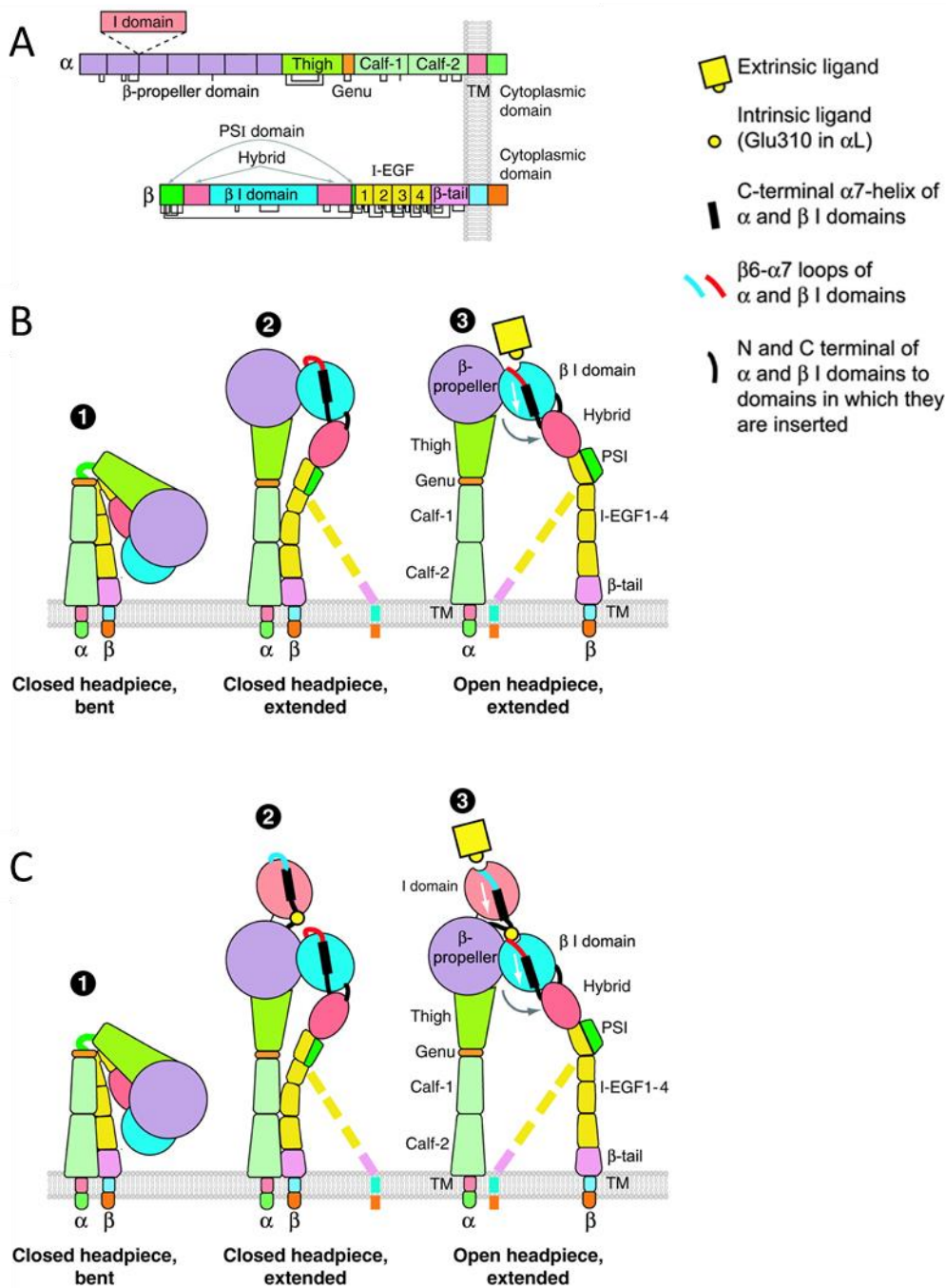


Figure 1.5 Schematic structures of integrin heterodimers. (A) Representative structure of integrin  $\alpha$  and  $\beta$  subunits. (B) Bent (1) and extended (2,3) conformations of integrin heterodimers where the  $\alpha$  subunit does not contain the  $\alpha$  I domain. (C) Bent (1) and extended (2,3) conformations of integrin heterodimers where the  $\alpha$  subunit contains the  $\alpha$  I domain. I-EGF, integrin epidermal growth factor-like; PSI, plexin/semaphorin/integrin domain, Adapted with permission from (54).

Specific subunits of integrin combine to give specificity of ligand binding. Cytoplasmic domains interact with actin cytoskeleton through talin and vinculin, as well as intracellular signalling associated proteins such as focal adhesion kinase (FAK) and protein kinase C (PKC). The ability of integrins to mutually transduce signals between cells and ECM enables them to induce mechanotransduction, cellular adherence, proliferation, differentiation, and gene expression (22, 57, 58).

Integrin  $\alpha 5\beta 1$  is one of the integrin dimers primarily expressed in chondrocytes, which can recognize fibronectin (59). Fibronectin is a matrix glycoprotein that has role in guiding matrix assembly and cell migration. It can be cleaved by MMPs into fibronectin fragments. The accumulation of fibronectin fragments containing the heparin-binding domain was observed in the degradation of ECM and further contribute to the destruction of cartilage (19, 60). Although the details were not known, fragments of fibronectin (FN-f), when added to cartilage in explant culture, as well as injected into the joint, could stimulate chondrocytes to produce proteases and induce cartilage breakdown (60, 61). A study of disc degeneration demonstrated that fibronectin fragments in the ECM can upregulate the expression of integrin  $\alpha 5\beta 1$ , active extracellular signal-regulated kinase (ERK) and promote the expression of MMP9 and MMP13, resulting to apoptosis of nucleus pulposus cells (62). It has also been reported that integrin  $\alpha 5\beta 1$  gets involved in the modulation of the expression of MMPs in chondrocytes, thereby affecting the synthesis of extracellular matrix (63). Besides, it has been shown that ITGA5 is essential in differentiation of that prehypertrophic chondrocyte toward hypertrophy during skeletal development (64). Tanaka et al. found that when chondrocytes undergo dedifferentiation when cultured in monolayer, Integrin $\alpha 5\beta 1$  can mediate dedifferentiation of chondrocytes cultured in monolayer by induction of the expression type I and type III non-cartilaginous procollagen (65). In OA, ITGA5 was found decreased in early stage of OA, and recovered in at a late stage, also indicating a correlation with chondrocyte differentiation during OA progression (66).

Additionally, integrin  $\alpha 5\beta 1$  is an essential mechanoreceptor by which chondrocytes respond to mechanical load. In normal chondrocytes, cell membrane hyperpolarization occurred rapidly after mechanically stimulation, which activated ion channels and activates integrin  $\alpha 5\beta 1$  receptor (59, 67), possibly leading to an autocrine or paracrine

of interleukin 4 (IL-4) (68). IL-4 can change the ratio of MMPs to TIMPs by inhibiting the expression of IL-1-induced MMP3 (69, 70). However, in osteoarthritic chondrocytes, cyclical pressurization gave rise to membrane depolarization due to an altered mechanical signalling transduction via integrin  $\alpha 5\beta 1$  (71). Interestingly, when tension was applied, integrin  $\alpha 5\beta 1$ -fibronectin adhesive bonds were strengthened giving rise to the downstream phosphorylation of FAK (72). Moreover, the synovial joints specific ablation of ITGA5 in mice demonstrated more active biomechanical properties in femoral condyle cartilage, compared with controls (73). These findings indicate that integrin  $\alpha 5\beta 1$ /ITGA5 takes a precise control of the development and progression of OA.

### 1.2.3.2 NFκB signalling pathway

Inflammatory signalling pathways alter functions of chondrocytes exert an important impact in the progression of OA. These signalling cascades can be induced by different factors including mechanical loads, matrix breakdown products, and proinflammatory cytokines such as IL-1, IL-6 tumour necrosis factor alpha (TNFα), subsequently affecting gene expression profiles and cellular behaviour of chondrocytes.

TLRs (Toll-like receptors) mediate innate immunity response, both exogenous and endogenous ligand recognition (e.g. ds-DNAs, heat shock proteins, hyaluronan oligosaccharides) by which can evoke activation of proinflammatory cytokines and costimulatory factors, exacerbate the inflammatory response involved in joint destruction of OA (74). TLR-2 and 4 have been reported to be upregulated in the damaged part of osteoarthritic cartilage and strongly give rise to the increased level of MMPs, NO and prostaglandin E2 (PGE2) and catabolism of ECM via NFκB pathway (75). TLR-mediated signalling largely relies on adaptor molecules such as myeloid differentiation factor 88 (MYD88) and TIR-domain-containing adapter-inducing interferon-β (TRIF) (76). Several endogenous products including low molecular weight hyaluronan (LMW-HA), high mobility group box chromosomal protein 1 (HMGB-1) and FN-f have been reported to play an important role in critically modulate matrix catabolism and chondrocyte hypertrophic differentiation through the MYD88-dependent TLR 2/4 signalling pathway in chondrocytes and OA progression. (77-79)

NFκB (nuclear factor-kappa B), as a key transcription factor, is critical in regulating proliferation, differentiation and apoptosis of chondrocytes by mediating the expression of inflammatory genes, cytokines and matrix degradation enzymes during skeletal development and osteoarthritis (80, 81). The NFκB family consists of RelA (p65), RelB, c-Rel, NFκB1 (p50 or p105) and NFκB2 (p52 or p100), among which RelA/p50 is the most common heterodimer in mammalian cells. Commonly, the canonical NFκB pathway is activated by binding ligand to Toll-like or T-cell receptors and leads to the induction of the IκB kinases (IKKα/IKKβ/IKKγ-NEMO). IKKs mediate the ubiquitin-induced degradation of inhibitory NFκB proteins (IκB), releasing RelA/p50 dimers. Subsequently, the activated RelA/p50 dimers translocate into nucleus and regulates the transcription of target genes. An alternative pathway triggered by B cell-

activating factor receptor (BAFF-R), CD40-R, or lymphotoxin beta receptor (LT $\beta$ -R) activates IKK $\alpha$  kinase and induces the maturation of p100. The activated RelB/p52 dimers migrate into nucleus and stimulate the transcriptional activity of target genes. (Figure 1.6)

In articular cartilage, NF $\kappa$ B signalling pathway can be initiated by the activation of receptors for mechanical stress, FN-f or cytokines. The activated NF $\kappa$ B transcription factors subsequently elicit the expression of multiple MMPs, ADAMTS, apoptotic molecules (COX2, NO, PGE2), chemokines (IL-8), and cytokines (TNF- $\alpha$ , IL-1 $\beta$ , and IL-6) that induce cartilage deterioration. Additionally, these NF $\kappa$ B mediated chemokines and cytokines in turn act in a positive feedback to activate the NF $\kappa$ B signalling pathway (82-85). Moreover, due to persistent NF $\kappa$ B activation, articular chondrocytes could transform from pre-hypertrophy to terminal hypertrophy resulting in chondrocyte calcification and osteophyte formation (86, 87). Animal research suggested that intra-articular injection of inhibitors of NF $\kappa$ B, such as caffeic acid phenethyl ester (CAPE) (88, 89) and resveratrol (90-92) were capable of protecting cartilage from degradation in surgically induced OA rabbits through inhibiting TNF/IL-1-induced NF $\kappa$ B signalling. Accordingly, after the negative regulation of NF $\kappa$ B by small interfering RNA (siRNA), short hairpin RNA (shRNA) or microRNA (miRNA), the levels of large number of cytokines, chemokines, ADAMTS and MMPs have decreased (93-95). All these studies confirm the close involvement of NF $\kappa$ B signalling pathway during the development and progression of OA.

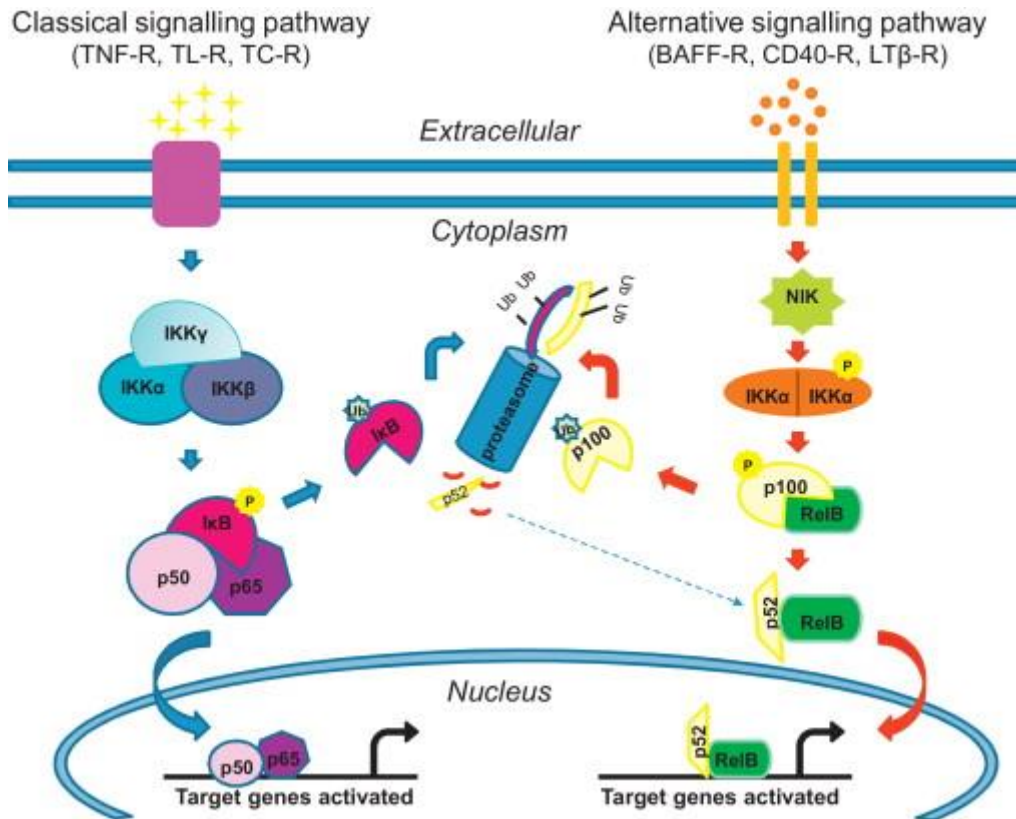


Figure 1.6 Canonical and alternative NFκB activation pathways. The classic NFκB pathway is activated by binding ligand to Toll-like or T-cell receptors (TNF-R, TL-R, or TC-R) and leads to the induction of the IκB kinases (IKKα/IKKβ/ IKKγ-NEMO). IKKs mediate the ubiquitin-induced degradation of inhibitory NF-κB proteins (IκB), releasing RelA/p50 dimers. Subsequently, the activated RelA/p50 dimers translocate into nucleus and regulates the transcription of target genes. The alternative pathway triggered by BAFF-R, CD40-R, or LTβ-R activates IKKα kinase and induces the maturation of p100. The activated RelB/p52 dimers migrate into nucleus and stimulate the transcriptional activity of target genes. Adapted with permission from (81)

### 1.2.3.3 WNT signalling pathway

The WNT signalling pathway is a highly conserved pathway that includes 19 WNT genes (96), the transmembrane receptors, and 3 pathways which are the canonical WNT/ $\beta$ -catenin pathway (97, 98) and two non-canonical pathways - WNT/ $\text{Ca}^{2+}$  pathway (99, 100) and WNT/planar cell polarity (PCP) pathway (101, 102).

Canonical WNT ligands, including WNT1, WNT3, WNT3A and WNT7A (103), combine with the transmembrane receptors, frizzled (Fzd) and the co-receptor, low-density lipoprotein receptor-related protein (LRP5/6), leading to the inactivation of glycogen synthase kinase 3 $\beta$  (GSK-3 $\beta$ ). This further inhibits the GSK-3 $\beta$ -mediated ubiquitination and degradation of  $\beta$ -catenin.  $\beta$ -catenin then accumulates in the cytoplasm and translocated to the nucleus, where it binds to the transcription factor lymphoid enhancer factor 1 (LEF-1)/ T-cell factor (TCF) to regulate the transcription of downstream target genes.(96) (Figure 1.7A)

The WNT/ $\beta$ -catenin signalling participates in multiple developmental processes of bone and joint development, plays an important role in chondrocyte differentiation, proliferation, hypertrophy and apoptosis, and is closely related to the occurrence and progression of OA (104, 105). Previous study has reported that  $\beta$ -catenin protein levels in chondrocytes are significantly upregulated in patients with osteoarthritis or in the case of cartilage damage. Its transcriptional activity is activated by WNT7A to induce the dedifferentiation of articular chondrocytes, inhibition of COL2 expression and promotion of MMP13 expression, by which accelerating cartilage degeneration (106). WNT inhibitory factor 1 (WIF-1) has a predominant expression in the upper-face of epiphyseal cartilage during late embryonic and postnatal development of the mouse, and be able to block WNT3A-induced WNT/ $\beta$ -catenin signalling pathway (107). In addition, the expression of Wif-1 has a negative correlation with the disease severity in the cartilage of knee OA patients (108). Moreover, frizzled-related protein B (FRZB) is an extracellular antagonist of WNT signalling. Deletion of FRZB enhances the accumulation of  $\beta$ -catenin and increases the expression of MMPs in the IL-1 $\beta$  stimulated chondrocytes, thereby aggravating the progression of OA (109).

The non-canonical pathway can be predominately induced by WNT4, WNT5A and WNT11, which is  $\beta$ -catenin independent (110). In the active WNT/ $\text{Ca}^{2+}$  pathway, the

production of inositol 1,4,5-trisphosphate (IP3) and diacylglycerol (DAG) is triggered as the result of the activation of phospholipase C (PLC). The intracellular  $Ca^{2+}$  release is then upregulated by IP3, which in turn stimulates protein kinase C (PKC), calcium/calmodulin-sensitive protein kinase II (CAMKII) and calcineurin. Subsequently, nuclear factor of activated T-cells (NFAT) is induced and gets involved in the regulation of cell adhesion and migration. (Figure 1.7B) (99, 100) While in the PCP pathway, activity of small GTPases including Rac1 and RhoA is stimulated, which activated the downstream effector Rho-associated kinase (ROCK) and c-Jun N-terminal kinase (JNK), thereby leading to the activation of JUN and the actin cytoskeleton reorganization. (Figure 1.7C) (101, 102)

Increasing evidence has been shown that the non-canonical WNT signalling pathway play a critical part in the development and progression of OA. WNT5A was found expressed in the proliferative and prehypertrophic chondrocytes of the developing long bones of mice. Additionally, both knockout and overexpression of WNT5A in mice resulted in deferred chondrocyte differentiation and bone formation, suggesting that WNT5A signalling is crucial in skeletal development.(111) In human osteoarthritic chondrocytes, higher level of WNT5A was detected. Furthermore, WNT5A can stimulate the CAMKII and JNK signalling, together with decreased ACAN and increased MMP1 and MMP13 production, thereby exacerbating the catabolic activity in articular cartilage.(112)

Collectively, WNT signalling functionally regulates chondrocytes with regard to skeletal development and OA progression.

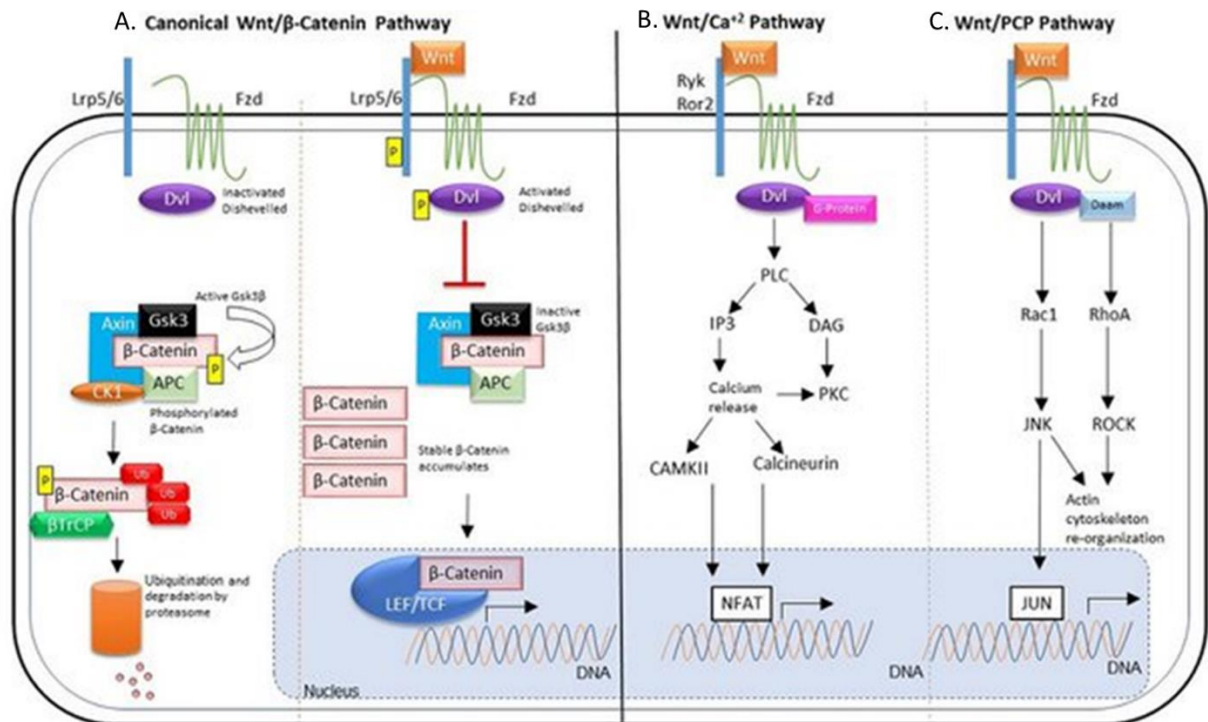


Figure 1.7 Overview of canonical and non-canonical WNT signalling pathways. (A) Canonical WNT/β-catenin pathway. WNT ligands combine with Fzd and Lrp5/6 co-receptors, leading to the inactivation of GSK-3β. This further inhibits the GSK-3β-mediated ubiquitination and degradation of β-catenin. β-catenin then accumulates in the cytoplasm and translocated to the nucleus, where it binds to the transcription factor LEF1/TCF to regulate the transcription of downstream target genes. (B) Non-canonical WNT/Ca<sup>2+</sup> pathway. The production of IP3 and DAG is triggered as the result of the activation of PLC. The intracellular Ca<sup>2+</sup> release is then upregulated by IP3, which in turn stimulates PKC, CAMKII and calcineurin. Subsequently, NFAT is induced. (C) Non-canonical WNT/PCP pathway. Activity of small GTPases including Rac1 and RhoA is stimulated, which activated the downstream effector ROCK and JNK, thereby leading to the activation of JUN and the actin cytoskeleton reorganization. APC, adenomatous polyposis coli; βTrcp, beta-transducin repeats-containing protein; CaMKII, calcium/calmodulin-sensitive protein kinase II; CK1, casein kinase 1; Dvl, dishevelled; DAG, diacylglycerol; Fzd, Frizzled; Gsk3, glycogen synthase kinase 3; IP3, inositol 1,4,5-triphosphate; JNK, c-Jun N-terminal kinase; LEF1, lymphoid enhancer factor 1; LRP5/6, lipoprotein receptor related protein 5/6; NFAT, nuclear factor of activated T-cells; PKC, protein kinase C; PLC, phospholipase C; Rac1, Rac Family Small GTPase 1; RhoA, Ras homolog gene family, member A; ROCK, Rho-associated kinase; TCF, T-cell factor. Adapted with permission from (113)

#### 1.2.3.4 TGF $\beta$ /SMAD signalling pathway

TGF $\beta$  (transforming growth factor  $\beta$ ) superfamily is a large family of multifunctional growth factors including BMPs (bone morphogenetic proteins), TGF $\beta$ s, GDFs (growth and differentiation factors), Activin/Inhibin and Nodal, taking a vital part in the development and homeostasis of a variety of tissues (114). TGF $\beta$  receptors are clustered into three types, type I receptors (TBR1, also termed ALKs), type II receptors (TBR2, BMPRII, etc.) and type III receptors. Type I receptors binds to TGF $\beta$  ligands and activate SMADs (small mother against decapentaplegic), where type I receptors act downstream the type II receptors. In signal transduction, TGF $\beta$ s bind to type II receptors, which recruit and phosphorylate type I receptors. SMADs are the main signal transducers for TGF $\beta$  signalling pathway. When the type I receptor is activated, the intracellular signal is initiated by the phosphorylation of the receptor-associated SMAD protein (R-SMAD).(114) TBR2-ALK5 complex activates SMAD2 and SMAD3, while TBR2-ALK1 activates SMAD1, SMAD5 and SMAD8 (115, 116). The activated R-SMADs form an isomeric complex with the common-mediator SMAD (Co-SMAD, Smad4 in mammals) and translocate to the nucleus. (117, 118) Once in the nucleus, the SMAD complex contacts with other DNA-binding transcription elements (SBE) through the MH1 domain to regulate target genes. SMAD6 and SMAD7 are inhibitory SMAD that inhibit the TGF $\beta$  signal transduction by interfering the combination of R-SMADs to SMAD4 (117, 118) (Figure 1.8)

In human bone-marrow-derived mesenchymal stem cells (BMMSCs), inhibition of SMAD2/3 phosphorylation prevented chondrogenesis, while SMAD1/5/8 led to inhibition of terminal differentiation of chondrocyte and mineralization (119). SMAD6 and SMAD ubiquitin regulatory factor 1 (SMURF1) are major inhibitors of SMAD1/5/8 signalling. Mice overexpressing Smad6 in chondrocytes demonstrated repression of Smad1/5/8 phosphorylation and progressive dwarfism (120). Previous study reported that in papain and L-cysteine induced OA rats, expression of TGF $\beta$ 1, phospho-SMAD2/3 and ALK5 elevated. Inhibiting T $\beta$ RI led to a protective effect on OA progression, indicating that suppression of TGF $\beta$ 1/SMAD signalling pathway could improve cartilage damage during OA (121). Interestingly, genome-wide association analysis revealed that mutations in TGF $\beta$ 1 gene indicates reduced TGF $\beta$  response, leading to increased susceptibility to OA (122-124). Besides, mutations in the SMAD3

gene have also been reported to act as a risk factor of OA (125-127). Taken together, TGF $\beta$ /SMAD signalling pathway closely participate in skeletal development and OA aetiology and progression.

There are other signalling pathways that participate in the regulation of chondrocyte function and OA pathogenesis, such as mitogen-activated protein kinase (MAPK) signalling, Notch signalling. Multiple signalling pathways interact with each other and together contributes to OA development and progression (128).

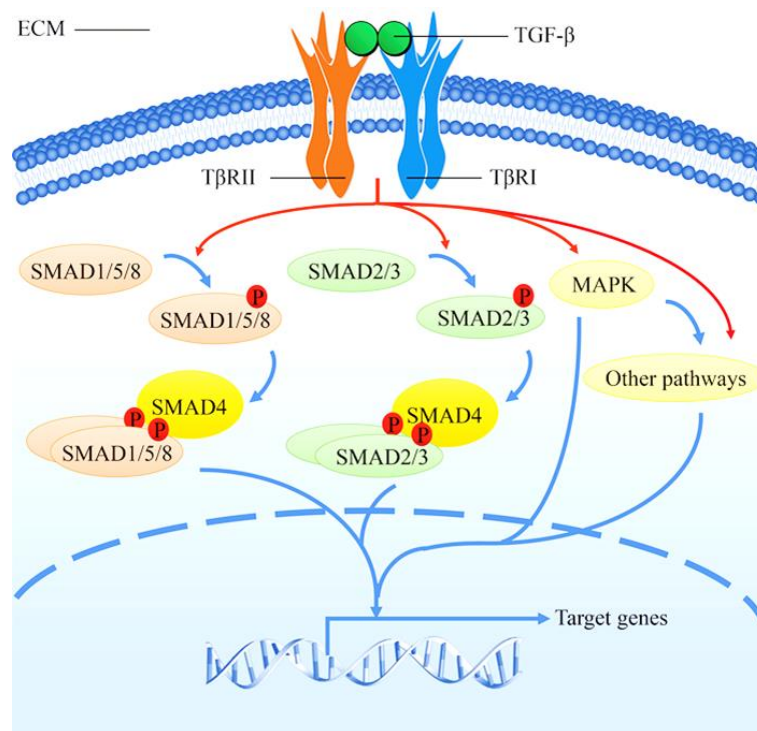


Figure 1.8 Scheme of TGF- $\beta$  signalling. TGF- $\beta$  binds to T $\beta$ RI and T $\beta$ RII. T $\beta$ RII transphosphorylates T $\beta$ RI and induce SMAD2/3 pathway, SMAD1/5/8 pathway and non-SMAD-dependent signalling pathways, such as the MAPK signalling pathway. Adapted with permission from (129).

### 1.3 Animal modelling in osteoarthritis

One of the most commonly employed animal models are the mouse models. The validity of the mouse model arises from its ability to replicate various human diseases. There is a common sequence in genetic complexity between the mouse and the human beings (130, 131). It has been found that out of about 40000 working genes in both humans and mice, no more than 3% are unique to either of them in terms of the sequencing of the genome(132). Secondly, all the mice that are used in a particular study usually come from a similar genetic background. That is to say that the mice could have been backcrossed or that they arise from one genetic strain via inbreeding (133). The result is that all the subjects to be used in the study are genetically identical to each other. That is vital in the elimination of the complexities that arise from instances of genetic variations as well as genetic polymorphism. Also, the gap between different generations of the mice is relatively short, typically three months.

Experimental models capable of reproducing the changes that occur in OA can be valuable, especially for studying these alterations across the timecourse of the disease with the possibility of sequential evaluation of the disease lesions. There are various animal models used for studying osteoarthritis. There is spontaneous model that OA naturally occurs in such animals like mice and Guinea pigs, manifestations of which include the occurrence of joint space narrowing, cartilage lesions, alterations in cartilage matrix molecules, and osteophyte formation(134). Another common type of mouse model employed is the induction of the disease through an Intraarticular injection of monoiodoacetate (130), papain, trypsin, hyaluronidase or collagenase (135). The post-traumatic occurrence of the disease is initiated by inducing damages to the joints of the animals through surgery. A textbook case is the destabilization of the medial meniscus (DMM) and/or anterior cruciate ligament transection (ACLT). The post-traumatic nature of the DMM model of osteoarthritis has several similarities in pathogenesis as well as pathology as osteoarthritis in human beings.(136-138)

There are also transgenic models which are commonly applied. Especially, the Cre-loxP system is widely utilized in the generation of conditional gene modified mice. Cre recombinase is one of the tyrosine site-specific recombinases (T-SSRs). It recognizes the sequence of a particular DNA fragment termed loxP. It is able to precisely cleave

DNA sequences between two loxP sites (139, 140). Regarding the mechanism of the Cre-loxP system, a Cre recombinase recognizes two loxP sites, and then Cre cuts the loxP flanked (floxed) DNA (Figure 1.9A). Although the Cre-loxP system is primarily applied for gene excision, it also has the capability to induce inversion and translocation of the DNA fragment between two loxP sites, depending on the orientation and location of the two repeat loxP sites. To generate conditional transgenic mice using Cre-loxP system, Cre-driver strain where Cre is driven by promoter or enhancer of the tissue of interest, and floxed strain where the target gene is flanked by two repeat loxP sites are crossed (Figure 1.9B). This system enables researchers to study genes of interest in a specific spatiotemporal manner. Most importantly, many tissue specific Cre tool mice have been generated and available.

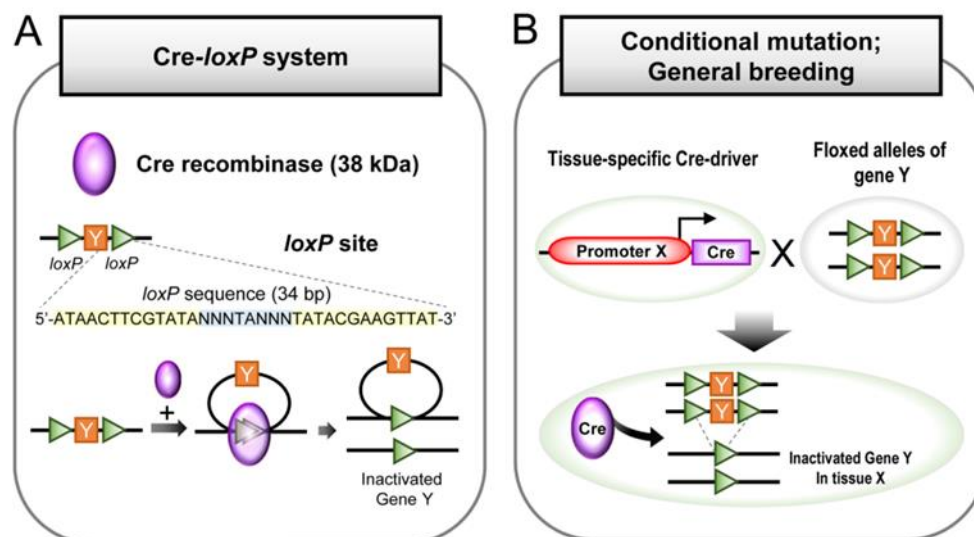


Figure 1.9 Schematic diagram of the Cre-loxP system. (A) Cre recombinase recognizes two repeat loxP sites. (B) Generation of conditional mutation using Cre-driver strain and floxed-DNA containing strain. Adapted with permission from (141).

Recently, the CRISPR-Cas9 system has innovated biomedical research and facilitated the development of genomic editing dependent therapies. The two are an abbreviation of clustered regularly interspaced short palindromic repeats (CRISPR) and CRISPR-associated proteins (Cas) respectively, developed from an immune defence mechanism of prokaryotic organisms (bacteria and archaea) (142). A designed guiding RNA (gRNA) binds to its target DNA sequence by base pairing, direct the Cas9 protein and generate double-stranded DNA break (DSB) at specific genomic location, exploiting the non-homologous end-joining (NHEJ) or the homology-directed repair

(HDR) pathway for gene knock-out, knock-in or point mutations. (Figure 1.10) The technique enables the modification of the genome of animals whereby the CRISPR-Cas9 is injected into the embryos leading to modification of the genome. The mice that are generated from such embryos are genotypically sequenced to establish whether they possess the desired genomic changes, and those that do maintain such modifications are bred to ascertain germline transmission. Taking advantage of CRISPR-Cas9 system, miR-455 knock out mice have been successfully generated in our lab.

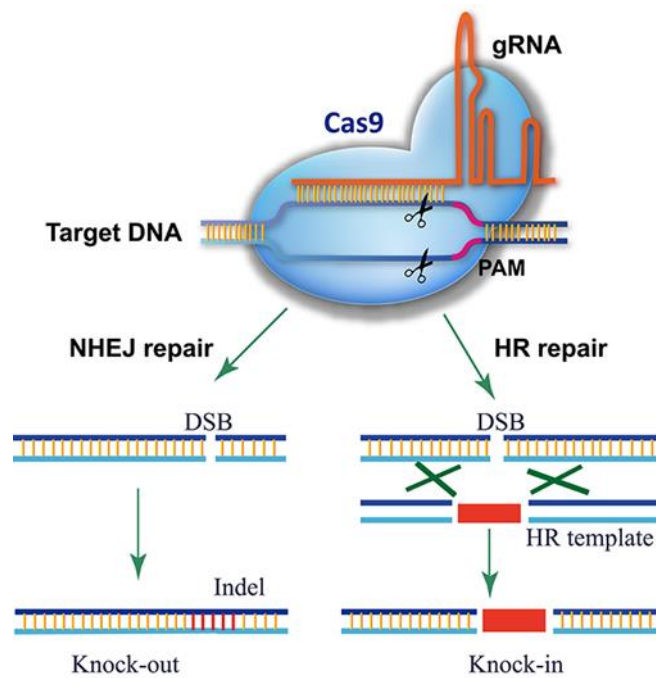


Figure 1.10 Schematic diagram of the mechanism of CRISPR-Cas9 system in gene editing. A guiding RNA is designed, which can either bind to Cas9 or target to a specific DNA sequence, to direct Cas9 to the target gene. DSBs are generated, exploiting the NHEJ repair pathway to achieve gene knock-out, while the HDR pathway to make knock-in. DSB, double-stranded DNA break; NHEJ, non-homologous end-joining; HDR, homology-directed repair. Taken with permission from(143).

## 1.4 MicroRNAs

### 1.4.1 Biosynthesis of microRNAs

MicroRNAs (miRNAs) refer to a class of endogenous non-coding single-stranded short RNA molecules containing 18-25 nucleotides, widely found in eukaryotes. The majority of miRNA genes are located in the non-coding regions between genes or within gene introns, termed intergenic and intronic miRNAs respectively. They are highly conserved across the process of evolution, and participate in diverse physiological or pathological activities, negatively regulating the gene expression by complementary base-pairing with their target mRNAs to achieve either inhibition of translation or direct degradation of mRNA targets. A miRNA can have multiple target genes, in turns, a gene can be simultaneously regulated by different kinds of miRNAs.

As shown in Figure 1.11, Typically, miRNAs are derived from single-stranded precursor RNAs, transcribed by RNA polymerase, that contain complementary sequences that allow them to fold back on themselves to form a double-stranded RNA, termed pri-miRNA, with a stem-loop at one end. This pri-miRNA is then cleaved near its terminal loop by a microprocessor complex combining Drosha and DGCR8/Pasha to generate a pre-miRNA that has a 3' overhang at one end. The pre-miRNA is exported to the cytoplasm by exportin-5 where it is cleaved by Dicer into a small double-stranded miRNA that has a 3' overhang at both ends. The duplex RNA assembles with a protein complex containing an Argonaute protein (commonly Ago1), leading to the separation of the strands and removal of the passenger strand which will be eventually degraded. Many pre-miRNAs generate two mature miRNAs, named with suffix of 3p or 5p depending on the distance from which terminal of the pre-miRNA. The single-stranded guide miRNA is then incorporated into an RNA-induced silencing complex (RISC) and binds to a complementary region on an mRNA, mostly the 3' untranslated regions (3' UTR), and inhibits translation of the message or alternatively leads to destabilization and degradation of the mRNA. The manner by which miRNA regulates the target mRNA depends on the complementarity of base-pairing. For instance, in majority of plants, where complementarity is complete or nearly complete, the cleavage of target mRNA is induced; when mRNA binds to its targets with imperfect complementarity, mainly in mammals, the translation of message from mRNA is blocked. (144)

Mechanisms by which miRNAs might decrease gene expression at the translational level have been a matter of considerable controversy. Generally, the RISC can interfere with translation initiation, where the complex either inhibits the interaction between eIF4E and the 5' end of the mRNA or prevents the assembly of the complete ribosome from its subunits. The RISC can also take effect at some point after translation has been initiated, leading to the degradation of the nascent protein as well as the release of the ribosomes from the mRNA. In addition, decapping and/or deadenylation enzymes can be recruited by the RISC to promote the degradation of mRNA. (145)

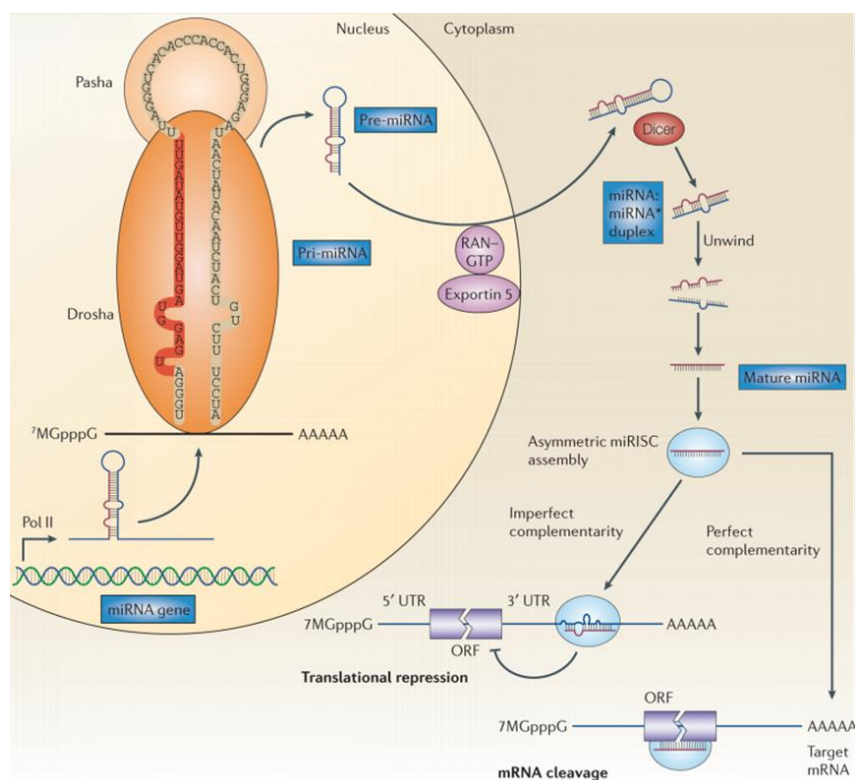


Figure 1.11 Schematic diagram of the biogenesis of miRNA. The miRNA is generally synthesized by RNA polymerase II as a primary transcript with a 5' cap and poly(A) tail. This primary transcript folds itself to form a hairpin-shaped pri-miRNA, which is then cleaved by Drosha into a shorter pre-miRNA. The pre-miRNA is exported to the cytoplasm where it gives rise to a small double-stranded miRNA after processing by Dicer. The double-stranded miRNA becomes disassembled and incorporated into a RISC complex. Most plant miRNAs are precisely complementary to the mRNA, which tends to induce the cleavage of the mRNA, otherwise inhibits translation of the mRNA. Taken with permission from (144).

## **1.4.2 MicroRNAs in mesenchymal stem cell differentiation**

Mesenchymal stem cells (MSCs) are stem cells characterized with potential of self-renewal and multiple differentiation. Upon regulated by a variety of factors, MSCs can differentiate into chondrocytes, osteoblasts, and adipocytes, which can be utilized in tissue repair and engineering.

### **1.4.2.1 MicroRNA and chondrogenesis**

SOX9 is a key transcription factor in the early stage of chondrogenesis, promoting the expression of type II, IX, XI collagen and Aggrecan (146). It has been confirmed that miR-145 can directly target SOX9 by seed sites in the 3'UTR and inhibit the formation of chondrogenesis of murine bone marrow MSCs (BMMSCs) in the early stage of chondrogenic differentiation. Overexpression of miR-145 can reduce the expression of SOX9 at the protein level, thereby reducing the expression of chondrocyte markers - COL2A1, ACAN and COMP. On the contrary, inhibition of the expression of miR-145 significantly increased the expression of SOX9 and collagen type IX alpha 2 chain (COL9A2), collagen type XI alpha 1 chain (COL11A1) (147). Similarly, miR-495 also has a negative regulation on SOX9, that is, overexpression of miR-495 can decrease the expression of SOX9, while inhibition of miR-495 can increase the expression of SOX9 (148).

MicroRNAs also regulate chondrogenesis by regulating bone morphogenetic protein 2 (BMP2). In vitro studies of murine BMMSCs showed that miR-99a directly suppressed bone morphogenetic protein receptor type 2 (BMPR2) at early stage and inhibited chondrogenesis. Consistently, knockdown of miR-99a can promote chondrogenesis, while silencing BMPR2 attenuated the inhibition of miR-99a on the process (149).

MicroRNAs can exert their effect through TGF $\beta$ /SMAD pathway. It has been demonstrated that miR-193b shows a dose dependent downregulation of the expression of TGF $\beta$ 2 and TGF $\beta$  receptor 3 (TGFB3), the phosphorylation of SMAD3 and early chondrogenesis in chondrogenic human adipose-derived mesenchymal stem cells (150). TGF $\beta$  signalling pathway is also reported to be inhibited by miR-193b through targeting SMAD3 (151), strongly suggesting that miR-193b inhibit chondrogenesis by preventing regulated by TGF $\beta$ /SMAD signalling.

The activity of WNT signals is crucial in chondrogenesis as well as the pathogenesis and progression of OA, and can be regulated by microRNAs (104, 107, 152-155). WNT3A was found increased in the cartilage of OA patient concomitant with a decreased expression of miR-410. Furthermore, WNT3A was verified to be a direct target of miR-410. Accordingly, overexpression of miR-410 increased the marker genes including SOX9, COL2A1 and ACAN of chondrocytes during chondrogenesis (156). In addition, WNT5A, regarded as a ligand that activates non-canonical WNT signalling pathways, has been reported to be targeted by exosomal miR-92a-3p, thereby promoting chondrocyte proliferation and cartilage development (157).

#### **1.4.2.2 MicroRNAs and osteogenesis / adipogenesis**

Runt-related transcription factor 2 (RUNX2) is a master specific transcription factors during osteoblast differentiation (158, 159). It has been reported that miR-133 could directly downregulate the expression of RUNX2 by bind to the 3'UTR of RUNX2 mRNA, thereby inhibiting osteogenic differentiation of mice premyogenic C2C12 cells (160). MiR-23b targeted RUNX2 in a similar manner in the osteogenesis of human bone marrow MSCs (hBMMSC). Consistently, overexpression of miR-23b significantly decreased the activity of alkaline phosphatase (ALPL), which is a key osteoblast marker, resulting in severe bone lose in mice (161). Recently, miR-550, was detected to be the greatly downregulated microRNAs during osteogenesis. Similarly, RUNX2 was predicted to be a target of miR-505. It was decreased by miR-505 mimics and increased by miR-505 inhibitors in mouse progenitor osteoblasts (MC3T3-E1 cells), and further regulated the expression of ALPL, osteopontin (OPN) and osteocalcin (OCN) (162).

MicroRNAs are involved in osteogenesis by regulating signalling pathways including TGF $\beta$ /SMAD signalling pathway and WNT signalling pathway. Studies have shown that miR-135 represses the expression of SMAD5 (160), and miRNA-214 inhibits BMP2 by binding to its 3'UTR (163), revealing that microRNAs could negatively regulate osteogenesis by disrupting TGF $\beta$ /SMAD signalling pathway. It has been shown that miR-139-5p plays roles in hBMMSCs osteogenesis through mediating canonical WNT signalling pathway by decreasing  $\beta$ -catenin and FZD4 (164). Furthermore, miR-26b was found to promote osteogenesis of hBMMSCs by targeting

GSK3 $\beta$  which is known to be the key kinase that phosphorylates  $\beta$ -catenin in canonical WNT pathway (165).

In addition, adipose tissues have drawn increasing attention as actors in the pathogenesis of OA, in terms of both biomechanical factors and metabolic factors including adipokines such as leptin, adiponectin, resistin, visfatin, omentin-1 and vaspin (166-169). Interestingly, reduced adipogenesis capacity of hBMSCs has been depicted, characterized by decreased lipid deposition (170). In adipogenesis, peroxisome proliferator activated receptors (PPARs) and CCAAT / enhancer binding proteins (CEBPs) are two predominant regulators (171). MiR-27 has been shown to play an important part in inhibiting adipogenesis by targeting PPAR $\gamma$  and CEBP $\alpha$  (172-174). Karbiener et al. revealed that miR-27b decreased across adipogenesis, while overexpression of miR-27b inhibited the expression of PPAR $\gamma$  and CEBP $\alpha$ . Luciferase assay further validated that miR-27b regulates adipocyte differentiation through specifically binding to PPAR $\gamma$  mRNA (174). MiR-27a, another member of the miR-27 family, was found reduced in obese mice and also attenuated adipogenesis by targeting PPAR $\gamma$  protein in 3T3-L1 preadipocytes, suggesting that miR-27 family may be a negative regulator of adipocyte differentiation (172).

Moreover, a study elucidated that during the osteogenic differentiation of hBMSCs, miR-27b-3p could inhibit calcification as well as the expression of osteogenesis markers including ALPL, OCN and osterix, whilst suppression of miR-27-3p promoted this process(175). Likewise, the expression of osteoblast marker genes such as ALP, BGLAP and BMP4 were upregulated by miR-149-3p, leading to a promotion of the differentiation of murine BMSCs into osteoblasts. Meanwhile, miR-149-3p could suppress the expression of adipocyte marker genes CEBP $\alpha$ , CEBP $\beta$  and PPAR $\gamma$ , and thus inhibit the differentiation of BMSCs into adipocytes (176). These studies suggest that microRNAs could have dual regulation of both osteogenesis and adipogenesis.

### **1.4.3 MicroRNAs in osteoarthritis**

Up to now, researchers have reported numerous miRNAs that are associated with OA. These miRNAs are likely to exert their influence on functions of chondrocytes and the homeostasis and structure of ECM by regulating the expression of target genes.

### 1.4.3.1 MicroRNAs profile in osteoarthritis

MicroRNA expression profiles have been characterized by several studies, based on bioinformatic analysis. When comparing the expression profiles of 365 miRNAs in OA and normal knee articular cartilage, 9 miRNAs were found upregulated while 7 miRNAs were downregulated in OA patients (177). Also, Jones et al. have screened 157 human miRNAs extracted from primary OA patients undertaking surgery of knee replacement and healthy individuals, 17 miRNAs were identified selectively expressed in OA cartilage, where 6 microRNAs demonstrated significant increase and 3 microRNAs showed decrease (178). In another large cohort of miRNAs in human osteoarthritic chondrocytes, 7 microRNAs were identified differentially expressed in osteoarthritis, with 1 upregulated and 6 downregulated, indicating a comprehensive regulation of miRNAs in OA (179). Interestingly, in a study exploring the microRNAs interactome with mRNAs in OA cartilage, 62 miRNAs and 238 mRNAs built up a interaction network, providing evidence of microRNAs' potentials in the regulation of OA pathophysiology (180). (Figure 1.12)

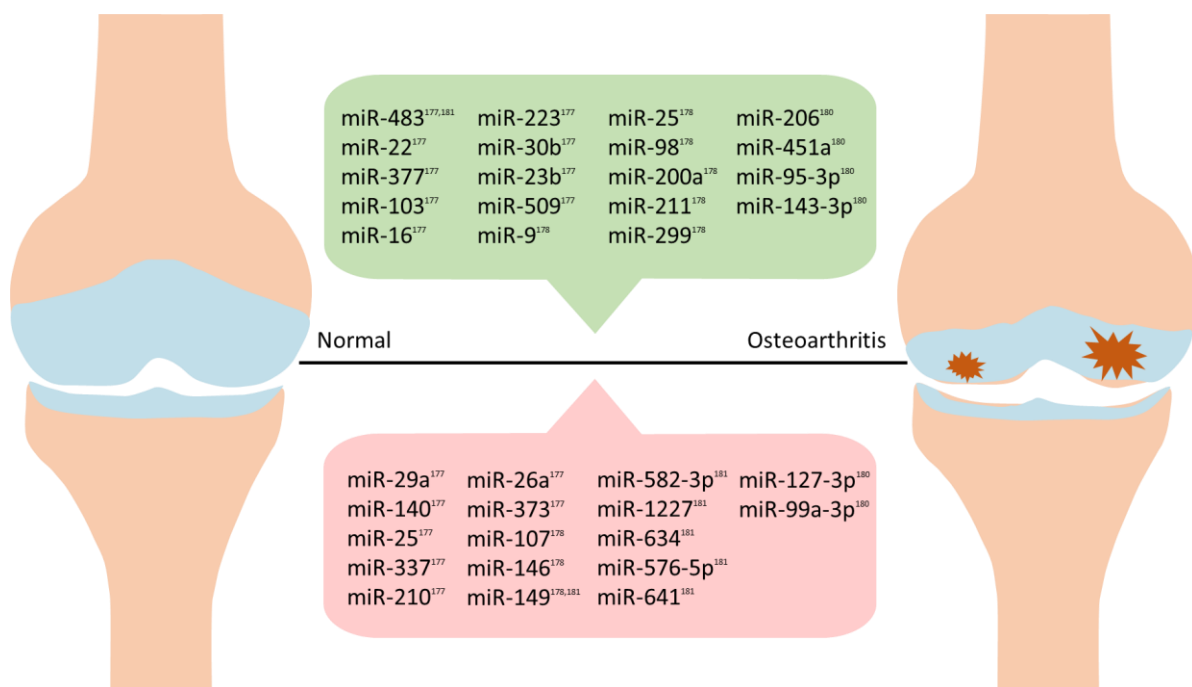


Figure 1.12 Identified differentially expressed microRNAs in normal and osteoarthritic articular cartilage. Profiling of microRNAs were carried out by microarray, RNA sequencing or qRT-PCR, followed by bioinformatic functional analysis. Green rectangle presents upregulated microRNAs, while pink rectangle shows downregulated microRNAs, in osteoarthritic cartilage with relevance to chondrocyte functions. Data are derived from (177, 178, 180, 181).

### **1.4.3.2 MicroRNAs and extracellular matrix of cartilage**

There is a dynamic balance between the synthesis and degradation of the cartilage ECM (83). If the anabolic activity cannot counterbalance the catabolic activity, ECM homeostasis is disrupted, and cartilage starts to deteriorate. Numerous studies have reported that MMP13 (46, 182, 183), ADAMTS4 (184, 185) and ADAMTS5 (47, 184, 185) are the two main hydrolytic enzymes leading to the degradation of extracellular matrix in cartilage, where MMP13 mainly degrades type II collagen and ADAMTS4 and ADAMTS5 degrades aggrecan.

Involvement of microRNAs in regulation of cartilage homeostasis has been widely investigated (Table 1.1). It has been reported that miR-26a and miR-26b were downregulated in patients with osteoarthritis, and they participated in cartilage degradation through various ways. After transfecting miR-26a mimics, type IX collagen, type X collagen and CD200 represented significant reduction in expression in mouse primary epiphyseal chondrocytes (186). In addition to the downregulation of MMP3, MMP9, MMP13 and prostaglandin-endoperoxide synthase 2 (PTGS2), the overexpression of miR-26a or miR-26b gave rise to detained p65 transduction from cytoplasm to nucleus through targeting karyopherin subunit alpha 3 (KPNA3) which is a key mediator of the p65/p50 translocation involved in the activation of NFκB signalling pathway (187). MiR-26a and miR-26b were further found to suppress fucosyltransferase 4 (FUT4) by which to increase aggrecan and type II collagen as well as decrease MMP13 and ADAMTS5, resulting in attenuating ECM destruction, promoting chondrocyte proliferation and inhibiting apoptosis (188). These studies suggest that miR-26a and miR-26b are closely involved in the regulation of cartilage ECM homeostasis. MiR-92a-3p was also reduced in OA patients. It directly targeted not only ADAMTS4 and ADAMTS5 which attenuated the cartilage catabolism (189), but also histone deacetylase 2 (HDAC2) leading to enhanced histone H3 acetylation on promoters of ACAN, COMP and COL2A1, thereby promoting the expression of ECM genes and cartilage development (190). Recently, a study on MSC exosomes revealed that exosomal miR-92a-3p took part in both chondrogenesis of human BMSCs and cartilage degeneration in OA mice, through WNT signalling pathway by repressing the expression of WNT5A (157). In addition, the CH25H/CYP7B1/RORα axis by which the cholesterol metabolism was regulated, contributed to ECM

degradation (191). MiR-10a-3p exerted an inhibitory effects CH25H/CYP7B1/ROR $\alpha$  axis by binding to the 3'UTR of cholesterol 25-hydroxylase (CH25H), accordingly retarding cartilage destruction during the pathogenesis of osteoarthritis (192). By contrast, the expression of miR-122 was upregulated in knee OA cartilage. The expression of aggrecan and type II collage decreased at the presence of miR-122 mimics, whilst increased by miR-122 inhibitors, implicated as a role player in maintenance of cartilage ECM homeostasis by targeting silent information regulator 1 (SIRT1) (193).

### **1.4.3.3 MicroRNAs and chondrocyte function**

As the only cellular element of articular cartilage, chondrocytes take a crucial part in the maintenance of cartilage structure and function. Disruption of the chondrocyte cell phenotype and behaviour can give rise to the development and progression of OA (194).

Myriad research has been carried out to elucidate the roles of microRNAs in regulating chondrocyte functions (Table 1.1). MiR-29b-3p was highly expressed in patients with osteoarthritis. It could promote chondrocyte apoptosis, and correspondingly the occurrence of osteoarthritis by targeting granulin precursors, progranulin (PGRN), and the injection of miR-29b-3p antagonist in the knee joints of surgically induced OA rats can ameliorate the cartilage loss (195). Additionally, miR-29b was involved in the IL-1 $\beta$  induced CDK4 mediated chondrocyte apoptosis by targeting parathyroid hormone-like hormone (PTH1H) (196). Similarly, expression of miR-486-5p was upregulated in osteoarthritic cartilage. It was demonstrated that miR-486-5p directly repressed SMAD2 and thus impeded TGF $\beta$ /SMAD signalling pathway. Overexpression of miR-486-5p inhibited the proliferation and migration of the cells, and decreased the expression of ACAN and COL2A1, leading to the occurrence of osteoarthritis (197). Moreover, miR-20 was reported to target autophagy-related gene 10 (ATG10), and inhibit chondrocyte proliferation and autophagy via PI3K/AKT/mTOR signalling pathway(198). MiR-34a could also inhibiting the PI3K/AKT signalling pathway by directly depressing the Notch ligand Delta-like 1 (DLL1), resulting in the decrease of total PI3K and phospho-AKT proteins in osteoarthritic chondrocytes, thereby inducing cell apoptosis (199). Furthermore, in the knee joint of surgically induced OA rats, articular chondrocyte apoptosis and cartilage destruction were attenuated after

injection of miR-34a antagonist (199). On the contrary, miR-138 levels were significantly reduced in osteoarthritis cartilage. P65, a key member of the NF- $\kappa$ B subunits, was verified as a direct target of miR-138. In both human primary osteoarthritic chondrocytes and SW1353 cells, the protein levels of p65, PTGS2 and IL-6 were downregulated at the presence of miR-138 mimic (200). Another study demonstrated that overexpression of miR-138 effectively decreased NIMA-related kinase 2 (NEK2) in combination with  $\beta$ -catenin which is a core component of WNT/ $\beta$ -catenin signalling pathway, while chondrocyte proliferation was enhanced and apoptosis was hindered (201).

#### **1.4.3.4 MicroRNAs and treatment**

It is known that a number of miRNAs have close correlation with OA, providing potential targets for OA treatment. However, the application of miRNAs in clinical phase is still limited.

MiR-181a-5p demonstrated an elevated expression in the degenerated cartilage of OA facet and knee joints. Therefore, locked nucleic acid antisense oligonucleotides against miR-181-5p were intraarticularly injected in the facet and knee joints of DMM modelling OA mice, and demonstrated a protective effect on cartilage featured by alleviation of chondrocyte apoptosis and cartilage destruction (202). Reversely, miR-93-5p had a lower expression in knee OA. The delivery of lentiviruses packaging miR-93-5p elevated the level of miR-93-5p in the knees of ACLT-induced OA rats, by which ameliorated the severity of cartilage degeneration and slowed the progression of OA (203). By other means, MSCs can induce microRNAs in vivo. For instance, in DMM induced OA rats, human umbilical cord mesenchymal stem cells (hUC-MSCs) overexpressing miR-140-5p contributed to the improvement of chondrocyte functions and regeneration of impaired cartilage (204). Moreover, intervention in the regulatory factors of microRNAs is another promising strategy for treating OA. Enhancer of zeste homolog 2 (EZH2) has been proved to inhibit the expression of miR-138 by inducing the methylation of the promoter of miR-138, thereby accelerating cartilage destruction. Rescue experiments using small interfering RNA against EZH2 effectively mitigated chondrocyte apoptosis and catabolic activities (205). All this research sheds a light on the potential of miRNAs as a novel therapy in osteoarthritis.

Table 1.1 Summary of studies on the roles of microRNAs in cartilage extracellular matrix homeostasis and chondrocyte functions involved in OA.

MicroRNA	Expression in OA	Effect on OA	Target gene	Pathway	Pathological process in OA	Experiment subject	Ref
<b>MiR-26a</b> <b>MiR-26b</b>	Decrease	Protective	CD200, COL2A1, COL9A1		ECM homeostasis	MPECs, HEK 293 cells	(186)
			KPNA3	NF-κB	ECM homeostasis	HPACs	(187)
			FUT4	NF-κB	ECM homeostasis, Chondrocyte proliferation	HPACs, Surgically induced OA rats (ACLT)	(188)
<b>MiR-92a-3p</b>	Decrease	Protective	ADAMTS4, ADAMTS5		ECM homeostasis	HBMMSCs, HPACs	(189)
			HDAC2	Histone H3 acetylation	ECM homeostasis, Chondrogenesis	HBMMSCs, HPACs, Collagenase-induced OA mice	(190)
			WNT5A	WNT	ECM homeostasis, Chondrogenesis	HBMMSCs, HPACs, Collagenase-induced OA mice	(157)
<b>MiR-10a-3p</b>	Decrease	Protective	CH25H	CH25H/CYP7B1/RORα	ECM homeostasis	Surgically induced OA rats (ACLT), HEK 293T cells	(192)
<b>MiR-122</b>	Increase	Detrimental	SIRT1		ECM homeostasis	HPACs, SW1353 cells	(193)
<b>MiR-29b</b>	Increase	Detrimental	PGRN		Chondrocyte apoptosis and proliferation, ECM homeostasis	HPACs, SW1353 cells, Surgically induced OA rats	(195)
			PTH1H	PTH1H/CDK4/RUNX2	Chondrocyte apoptosis and proliferation, ECM homeostasis	HPACs, HEK 293T cells, Surgically induced OA mice (DMM)	(196)
<b>MiR-486-5p</b>	Increase	Detrimental	SMAD2	TGFβ/SMAD	Chondrocyte proliferation and migration	HPACs, CHON-001 chondrocytes	(197)
<b>MiR-20</b>	Increase	Detrimental	ATG10	PI3K/AKT/mTOR	Chondrocyte proliferation and autophagy	MPACs	(198)
<b>MiR-34a</b>	Increase	Detrimental	DLL1	PI3K/AKT	Chondrocyte apoptosis and senescence	HPACs, Hs 819.T cells, Surgically induced OA rats	(199)

MicroRNA	Expression in OA	Effect on OA	Target gene	Pathway	Pathological process in OA	Experiment subject	Ref
MiR-138	Decrease	Protective	P65	NF-κB	Chondrocyte inflammation	HPACs, SW1353 cells, HEK 293T cells	(200)
			NEK2	WNT/β-catenin	Chondrocyte apoptosis and proliferation	Surgically induced OA mice (DMM)	(201)

ACL, anterior cruciate ligament transection; ADAMTS, a disintegrin and metalloproteinase with thrombospondin motifs; AKT, protein kinase B; ATG10, autophagy related 10; CDK4, cyclin-dependent kinase 4; CD200, cluster of differentiation 200; CH25H, cholesterol 25-Hydroxylase; COL10A1, collagen type X alpha 1; COL9A1, collagen type IX alpha 1; CYP11B1, cytochrome P450 11B1; DLL1, delta like canonical notch ligand 1; DMM, destabilization of the medial meniscus; ECM, extracellular matrix; FUT4, fucosyltransferase 4; HBMMSC, human bone marrow mesenchymal stem cells; HDAC2, histone deacetylase 2; HEK, human embryonic kidney; HPAC, human primary articular chondrocytes; KPNA3, karyopherin subunit alpha 3; MPAC, murine primary articular chondrocytes; MPEC, murine primary epiphyseal chondrocytes; mTOR, mammalian target of rapamycin; NEK2, NIMA Related Kinase 2; PGRN, progranulin; PI3K, phosphoinositide 3-kinases; PTHLH, parathyroid hormone like hormone; RORα, retinoic acid-related orphan receptor alpha; RUNX2, Runt-related transcription factor 2; SIRT1, sirtuin 1; TGFβ, transforming growth factor beta.

## 1.5 Discovery of miR-3085

Taking advantage of next generation deep sequencing (NGDS) and subsequent validation experiments, a novel microRNA #11 was identified and is selectively expressed in OA articular cartilage by Crowe et al. in our lab (206). The microRNA candidate #11 shares the equivalent sequence as the miR-3085-3p in mice and rats, by inspecting the whole genome. The miR-3085 in mice and rats is intergenic, whilst the human miR-3085-3p is annotated within an intron of cartilage acidic protein 1 (CRTAC1) previously known as CEP-68.

Moreover, ITGA5 is demonstrated to be a direct target of miR-3085-3p. QRT-PCR demonstrated a decrease in response to miR-3085-3p in human primary chondrocytes. A luciferase reporter was constructed with the 3'UTR of ITGA5 inserted downstream the firefly luciferase. This reporter was transiently transfected together with mimic of 3085 into SW1353. Luciferase activity reduced at the presence of miR-3085-3p. This was rescued by mutations in seed sites for miR-3085-3p compared with wild type 3'UTR construct. In addition, Western blot showed that miR-3085-3p was as effective as an siRNA to ITGA5 in decreasing protein levels of ITGA5 in human primary chondrocytes.(206)

## 1.6 Hypotheses and aims

MiR-3085-3p is a novel miRNA denoted in human and preferentially expressed in cartilage. This microRNA is located in an intron of the cartilage-expressed gene CRTAC1 which and has been shown to target ITGA5 and MyD88 gene directly. Besides, miR-3085-3p can also down-regulate the expression of MMP13, although there is no seed sequence in MMP13 gene, indicating that downstream pathways are potentially targeted (206). The purpose of this research is to explore the influence of miR-3085-3p on cartilage development and homeostasis and open new insight on disease mechanisms and therapeutic interventions of osteoarthritis. Our hypothesis is that miR-3085-3p takes part in skeletal development and osteoarthritis. Therefore, our aims are:

1. Optimise assays to measure the effect of miR-3085-3p on its targets by qRT-PCR, Western blotting, and Luciferase assay, using dose-response and time course assays in a variety of cell lines.
2. Explore the roles of miR-3085-3p in cartilage homeostasis and chondrocyte function.
3. Investigate the influence of miR-3085-3p on the differentiation of human mesenchymal stem cells.
4. Generate the miR-3085 null mouse and analyse the function of miR-3085-3p in OA pathogenesis.
5. Characterize the ITGA5 cartilage-specific knock out mice and examine its effects on skeletal development and OA progression.

# Chapter 2 Materials and methods

## 2.1 Cell lines and cell culture

DF1 is a spontaneously immortalized chicken dermal fibroblast cell line (a kind gift from Prof. Andrea Munsterberg, UEA, UK). The chondrosarcoma cell line SW1353 was derived from human chondrosarcoma of humerus and purchased from ATCC. Human primary articular chondrocytes (HACs) were directly obtained and digested from excised osteoarthritic knee joints from patients(207). Human bone marrow mesenchymal stem cells (hBMMSCs) were a kind gift from Dr Matt Barter, Newcastle University, which are isolated from commercial human bone marrow mononuclear cells of 3 donors (Lonza) (208).

SW1353 and HAC cells were maintained in DMEM, low glucose, GlutaMAX™ supplement containing 10% (v/v) heat-inactivated fetal bovine serum (FBS), 100 units/mL penicillin, and 100 µg/mL streptomycin (All from Gibco, Thermo Fisher Scientific) at 37°C in 5% (v/v) CO<sub>2</sub>. Human MSCs are cultured in mesenchymal stem cell growth medium (MSCGM™, Lonza) with all the other conditions conserved.

## 2.2 Sub-cloning

### 2.2.1 Genomic DNA extraction

The genomic DNA (gDNA) was extracted from SW1353 cells using a lysis buffer containing 100mM Tris-HCl pH8 (Thermo Fisher Scientific), 1% (w/v) SDS (Thermo Fisher Scientific), 100mM NaCl (Thermo Fisher Scientific), 50mM EDTA (Thermo Fisher Scientific) and 200µg/mL Proteinase K (Sigma-Aldrich, Merck). SW1353 cells from a 75cm<sup>2</sup> cell culture flask were digested by 0.25% (w/v) trypsin-EDTA and centrifuged at 1000 g for 5 minutes. Cells were washed in 500µL DPBS (Gibco, Thermo Fisher Scientific) and resuspended in 500µL lysis buffer and incubated at 55°C for 3 hours. 500µL Phenol: Chloroform: Isoamyl Alcohol 25:24:1 saturated with 10mM Tris, pH8.0, 1mM EDTA was added and mixed thoroughly with lysates, followed by 15 minutes centrifugation at 12000g at 4°C. The clear aqueous phase was transferred into a new Eppendorf tube. An equal volume of chloroform (Sigma-Aldrich, Merck) was added, mixed and centrifuged for 15 minutes at 12000g at 4°C. The

aqueous phase was transferred to a new Eppendorf and a double volume of 100% (v/v) ethanol (Sigma-Aldrich, Merk) was added and mixed by gently inverting, left to precipitate at -20°C overnight, and centrifuged at 12000g for 15 minutes at 4°C. The supernatant was discarded, and DNA pellets were washed with 70% (v/v) ethanol and subsequently centrifuged at 12000g for 15 minutes at 4°C twice. Supernatant was removed and DNA pellets were dried at room temperature for 3-5 minutes and eventually dissolved in 250µL nuclease-free H<sub>2</sub>O (Sigma-Aldrich, Merk).

## **2.2.2 DH5α competent cells preparation**

A single DH5α colony was picked from a LB agar plate and incubated in 5mL LB broth (Thermo Fisher Scientific) in a shaking incubator at 180rpm, 37°C, overnight. 1mL bacterial culture was transferred into 100mL LB broth, and further incubated for approximately 3 hours until OD600 was between 0.4 and 0.5, indicating cells were in the logarithmic growth phase. The bacterial culture was split into 2x50 mL centrifuge tubes, left in ice for 30 minutes and centrifuged at 1500g for 10 minutes at 4°C. Pellets were gently resuspended in 10mL sterile 0.1M CaCl<sub>2</sub> and incubated in ice for 30 minutes, followed by centrifugation at 1500g for 10 minutes at 4°C. Pellets were eventually resuspended in 1mL sterile 0.1M CaCl<sub>2</sub> containing 15% (v/v) glycerol and aliquoted into 100µL per Eppendorf tube. Aliquots were snap frozen in liquid nitrogen and immediately stored at -80°C.

## **2.2.3 Plasmid construction**

### **2.2.3.1 3' untranslated region fragments amplification**

3'UTR fragments of genes of interest were amplified with Q5<sup>®</sup> Hot Start High-Fidelity DNA Polymerase (New England Biolabs) using a touch-down PCR program. Primers were designed with specified restriction sites added to the 5'-end (Appendix 1) and gDNA extracted from SW1353 cells. PCR reactions and program were set up as Table 2.1 and Table 2.2.

Table 2.1 PCR reaction for 3'UTR fragments.

Component	Reaction
<b>gDNA</b>	100ug
<b>5x Q5 reaction buffer</b>	10µl
<b>25mM dNTPs</b>	0.4µl
<b>10µM forward primer</b>	2.5µl
<b>10µM reverse primer</b>	2.5µl
<b>Q5 Hot Start high-fidelity DNA polymerase</b>	0.5µl (1 unit)
<b>Nuclease-free water</b>	To 50µl

Table 2.2 Touch-down PCR program for 3'UTR fragments.

Step	Temperature	Time
<b>Initial denaturation</b>	95°C	30 seconds
<b>15 cycles</b>	95°C	10 seconds
	70°C (-1°C per cycle)	30 seconds
	72°C	30 seconds/kb
	95°C	10 seconds
<b>20 cycles</b>	55°C	30 seconds
	72°C	30 seconds/kb
	72°C	2 minutes
<b>Final extension</b>	72°C	2 minutes
<b>Final hold</b>	4°C	Indefinitely

### 2.2.3.2 Gel purification and quantification

PCR products were loaded and separated through 1.5% (w/v) agarose gel. Desired bands were precisely excised under UV light and subsequently purified using NucleoSpin gel and PCR clean-up kit (Takara) following manufacturer's instruction (209). Concentrations of eluate were measured using a NanoDrop™ spectrophotometer (Thermo Fisher Scientific).

### 2.2.3.3 Restriction Digestion

PmirGLO Dual-luciferase miRNA target expression vector (Promega) and purified PCR products were digested using indicated FastDigest restriction enzymes (Thermo Fisher Scientific). Digestion reactions were set up as Table 2.3, followed by incubation for 30 minutes at 37°C, gel purification and quantification described in 2.2.3.2.

Table 2.3 Fast digestion of DNA by double restriction enzymes.

Component	Reaction
DNA	500ng
10x FastDigest green buffer	2µl
FastDigest restriction enzymes I	1µl
FastDigest restriction enzymes II	1µl
Nuclease-free water	To 20µl

### 2.2.3.4 Ligation

The digested and purified vector and PCR products were ligated at a molar ratio of 1:3 using T4 DNA ligase (New England Biolab). Ligations were performed as Table 2.4 at 16°C overnight.

Table 2.4 DNA ligation reaction.

Component	Reaction
Vector DNA	30ng
Insert DNA	3 times of vector in mole
T4 DNA ligase	0.33µl (1 Weiss unit)
Nuclease-free water	To 10µl

### **2.2.3.5 Transformation**

100µl DH5α competent cells were thawed on ice and 5µl ligation mixture was added, incubated on ice for 30 minutes and then heat shocked for 90 seconds in water bath at 42°C. 500µl LB broth was added and incubated on ice for 3 minutes, before shaking in an incubator at 180rpm for 1 hour at 37°C. Transformed cells were centrifuged at 6000g for 2 minutes and resuspended in 100µl LB. All transformed cells were plated onto LB agar plate containing 100mg/mL ampicillin (Sigma-Aldrich, Merk) and incubated at 37°C overnight.

### **2.2.3.6 Plasmid verification**

#### **2.2.3.6.1 Colony PCR**

A single colony was picked and incubated in 500µl LB broth supplemented with 100mg/mL ampicillin at 37°C in a shaking incubator at 180rpm for 1 hour. 1.5µl medium was applied for colony PCR according to 2.2.3.1 with an extended initial denaturation up to 3 minutes.

#### **2.2.3.6.2 Plasmid Preparation**

Colonies containing plasmids with desired inserted fragments were incubated in a shaking incubator in 5mL LB broth with 100mg/mL ampicillin at 37°C overnight.

Bacterial culture was harvested by centrifugation at 6800g for 2 minutes, from which plasmids were isolated using GeneJET Plasmid Miniprep Kit (Thermo Fisher Scientific) following manufacturer's instruction (210).

Purified plasmids were further verified by digestion with double restriction enzymes according to 2.2.3.3 and confirmed by Sanger sequencing (Source BioScience) using T7 reverse primer.

### **2.2.4 Site-directed mutagenesis of pmirGLO constructs**

Single or multiple miR-3085-3p target sites (AGCCAG), which were present within the inserted 3'UTR region of pmirGLO, were mutated into appropriate restriction sites using the QuikChange Lightning Multi Site-Directed Mutagenesis Kit (Agilent). The mutagenic oligonucleotide primers (Appendix 2) for desired points mutation were designed using the online QuikChange Primer Design Program (Agilent) individually and corresponded to the opposite strand of the plasmid. Mutagenesis reactions were

prepared as Table 2.5. The mutant strand was synthesized in the thermal cycling conditions indicated as Table 2.6. 0.4µL Dpn I restriction enzyme was added directly to the PCR products and mixed gently and thoroughly. Reactions were then incubated at 37 °C for 30 minutes. 5µL Dpn I-treated PCR product was transformed into 100 µL DH5α competent cells as described in 2.2.3.5. Mutagenesis colonies were picked, purified and verified by restriction enzyme digestion and DNA sequencing as described in 2.2.3.6.2.

*Table 2.5 QuikChange Lightning Multi Site-Directed Mutagenesis reaction.*

<b>Component</b>	<b>Reaction</b>
<b>Plasmid DNA</b>	50ng
<b>10× QuikChange Lightning Multi reaction buffer</b>	1µL
<b>dNTPs mix</b>	0.4µL
<b>QuikSolution</b>	0.3µL
<b>10 µM mutagenic primers</b>	1µL each for 1-3 primers. 0.5µL for 4-5 primers
<b>QuikChange Lightning Multi enzyme blend</b>	0.4µL
<b>Nuclease-free water</b>	To 10µL

*Table 2.6 QuikChange Lightning Multi Site-Directed Mutagenesis PCR program.*

<b>Step</b>	<b>Temperature</b>	<b>Time</b>
<b>Initial denaturation</b>	95°C	2 minutes
<b>30 cycles</b>	95°C	20 seconds
	55°C	30 seconds
	65°C	30 seconds/kb
<b>Final extension</b>	65°C	5 minutes
<b>Final hold</b>	4°C	Indefinitely

## **2.3 Transient transfection using Lipofectamine 3000**

### **2.3.1 Transfection for Luciferase assay**

DF1 and SW1353 cells were plated in 96-well plates at a density of  $8 \times 10^3$  cells/well and  $5 \times 10^3$  cells/well, respectively, and grown to 80%-90% confluence.

1. MiRCURY LNA miRNA mimic (Qiagen) or inhibitor (Qiagen) of miR-3085-3p, mimic negative control (Qiagen) or inhibitor negative control A (Qiagen) were prepared in 5 $\mu$ L Opti-MEM™ Medium (Gibco, Thermo Fisher Scientific). 0.15 $\mu$ L Lipofectamine™ 3000 (Invitrogen, Thermo Fisher Scientific) were diluted in 5 $\mu$ L Opti-MEM™ Medium. These two solutions were then mixed well and incubated for 10–15 minutes at room temperature. 10 $\mu$ L of the DNA-lipid mixture was finally added to each well to achieve a final concentration at 50nM mimic or 25nM inhibitor and negative controls in total 100 $\mu$ L. Transfected cells were subsequently incubated at 37°C in 5% (v/v) CO<sub>2</sub> for 24 hours. Medium was changed into fresh Opti-MEM™ Medium the next day.

2. 100ng pmirGLO Dual-Luciferase vector were added to 5 $\mu$ L Opti-MEM™ Medium (Gibco, Thermo Fisher Scientific) with a combination of 0.2 $\mu$ L P3000 reagent (Invitrogen, Thermo Fisher Scientific) for each well. The plasmid contained Firefly luciferase with an insertion of the 3'UTR sequence from ITGA5 downstream and Renilla luciferase acting as a reference reporter for normalization. 0.15 $\mu$ L Lipofectamine™ 3000 (Invitrogen, Thermo Fisher Scientific) were diluted in 5 $\mu$ L Opti-MEM™ Medium (Gibco, Thermo Fisher Scientific) for each well. After mixing and 10–15 minutes incubation at room temperature, complex was added to each well. Cells were then put in 37°C incubator with 5% (v/v) CO<sub>2</sub> and investigated 48 hours after transfection. For the time-course experiment, cells are harvested and analysed at desired time points after transfection.

### **2.3.2 Transfection for qRT-PCR**

The transfection method for qRT-PCR was the same as the first step described above. After transfection, SW1353 cells and HACs were incubated at 37°C in 5% (v/v) CO<sub>2</sub> for 48 hours, followed by reverse transcription. 100nM MiR-3085-3p mimic or 50nM inhibitor, and corresponding negative controls were transfected in hBMSCs and incubated for 72 hours prior to differentiation induction.

## **2.4 Stimulation of signalling pathways**

Luciferase reporters including p(CAGA)<sub>12</sub>-luc, kB-luc and TOPFlash were used for the measurement of Smad2/3, NF-κB and canonical Wnt signalling pathways respectively. Following transfection as described in 2.3.1, transfected cells were serum starved for 24 hours and then treated with recombinant human TGFβ<sub>1</sub> (4μg/l), IL-1β (5μg/l) or Wnt3a (100μg/l) (R&D Systems) for the desired time.

## **2.5 Dual-GLO Luciferase assay**

Cells were removed from the incubator, and medium changed to 50μL/well. According to the Dual-Glo Luciferase Assay System (Promega) instructions, 50μL Dual-Glo reagent was added to each well. After reaction at room temperature for 15 min, lysates were transferred to a white opaque 96-well plate and Firefly luminescence was measured. Subsequently, 50μL Dual-Glo Stop & Glo reagent was added, followed by incubation for 15 min at room temperature, and Renilla luminescence was measured using a multilabel plate reader (EnVision 2103, PerkinElmer).

## **2.6 Total RNA Isolation from cultured cells**

According to the user guidance (211), Cells were harvested in 500μl of Trizol reagent (Invitrogen, Thermo Fisher Scientific) after removing the growth media and washing with DPBS (Gibco, Thermo Fisher Scientific) from a 6-well plate. 250μl chloroform (Sigma-Aldrich, Merck) was added per 500μl Trizol, vortexed for 15 seconds and incubated at room temperature for 10mins. The mixture was centrifuged at 12000g for 10min, at 4°C. The aqueous layer was transferred into a new Eppendorf. 500μl of isopropanol (Sigma-Aldrich, Merck) was subsequently added, mixed and left for 10min at room temperature, followed by centrifuging at 12000g at 4°C for 10min. The supernatant was discarded, and the pellet was resuspended and washed in 75% (v/v) ethanol (Sigma-Aldrich, Merck). Samples were then briefly vortexed and then centrifuged for 5 mins at 7500g at 4°C. The pellet was air dried for 5-10 mins after removing supernatant. Finally, pellets were suspended in 20μl nuclease free water (Sigma-Aldrich, Merck) and stored at -80°C for further use. A NanoDrop™

spectrophotometer (Thermo Fisher Scientific) and Experion™ Automated Electrophoresis System (BioRad) were used to quantify and qualify of the extracted RNA, according to the manufacturer's instruction (212).

## **2.7 Reverse transcription**

### **2.7.1 Cells to cDNA**

Medium was removed and the cells in 96-well plate were washed with ice-cold Dulbecco's phosphate-buffered saline (DPBS, Gibco, Thermo Fisher Scientific) twice. Afterwards, 30µL Cells-to-cDNA II cell lysis buffer (Ambion, Thermo Fisher Scientific) was added to each well. Lysates were transferred to a 96-well PCR plate immediately and heated at 75°C for 15 min to inactivate RNases. All lysates were DNase I treated to remove genomic DNA contaminants by adding 1 unit DNase I and 3µL DNase I buffer (10x) per well and sequentially incubated 37°C for 15mins followed by inactivation at 75°C for 10mins. 8µL of DNase-treated samples were transferred to a new 96-well PCR plate. 200ng random primers (Invitrogen, Thermo Fisher Scientific) and 3µL of 10mM dNTP mix (Bioline) were added and heated at 70°C for 5mins to initiate priming. Following this, a mixture containing 0.5µL Moloney Murine Leukemia Virus (M-MLV) reverse transcriptase (200units/µL) (Invitrogen, Thermo Fisher Scientific), 4µL First Strand buffer (5x) (Invitrogen, Thermo Fisher Scientific), 2µL 0.1M dithiothreitol (DTT) (Invitrogen, Thermo Fisher Scientific), 40 units RNasin ribonuclease inhibitor (Promega) and 1µL water (Sigma-Aldrich, Merck) was added per well, followed by 37°C for 50 minutes and 75°C for 15 minutes. Samples were stored at -20°C after adding 30µL of water.

### **2.7.2 MiRCURY LNA Universal cDNA synthesis**

Total isolated RNA was adjusted to 5ng/µL and 2µL was transferred to a 96-well PCR plate, mixed with 2µL Reaction Buffer (5x) (Qiagen), 1µL enzyme mix (Qiagen) and nuclease-free water to achieve a final volume of 10µL. The plate was heated at 42°C for an hour followed by 95°C for 5minutes. cDNA templates were diluted 1/80 and 4µL was used for qRT-PCR analysis of miRNA.

## 2.8 Quantitative real-time polymerase chain reaction (qRT-PCR)

To each reaction for analysis of mRNA, 5µL cDNA templates obtained following Cells-to-cDNA protocol or 10µL cDNA templates from reverse transcription using isolated RNA, 2x PCR master mix (Bioline), 100nM forward and reverse primers and 200nM probe were mixed to make up a total volume of 25µL. MicroAmp optical plates (Applied Biosystem, Thermo Fisher Scientific) were sealed by adhesive cover film. QRT-PCR was carried out in an ABI Prism 7500 Sequence Detector (Applied Biosystem, Thermo Fisher Scientific), with the qRT-PCR program set as Table 2.7. Universal probes and primers were designed through Roche Universal ProbeLibrary Assay Design Centre for detecting the relative mRNA expression level of genes of interest (GOI), normalized to the 18S rRNA housekeeping gene. Sample was discarded if the Ct value for the housekeeping gene was more than 1.5Ct from the median. Details of primers were listed in Appendix 3.

*Table 2.7 Standard qRT-PCR cycle conditions.*

Step	Temperature	Time
<b>Initial denaturation</b>	95°C	10 minutes
<b>40 Cycles</b>	95°C	15 seconds
	60°C	1 minute

To each reaction for analysis of miRNA, miR-3085 and the housekeeping reference U6, 4µL cDNA templates obtained following miRCURY LNA™ Universal cDNA synthesis protocol (Qiagen) (213), 5µL PCR master mix, 1µL primer set and 0.18µL SYBR® green dye fluorescence were mixed to give a total volume of 10µL. QRT-PCR was performed following cycle conditions according to Table 2.8 in the ABI Prism 7500 Sequence Detector.

*Table 2.8 MicroRNA qRT-PCR cycle conditions.*

Step	Temperature	Time
<b>Initial denaturation</b>	95°C	10 minutes
<b>40 cycles</b>	95°C	15 seconds
	60°C	1 minute

## **2.9 Western blotting**

Cultured cells were harvested and lysed with 100 $\mu$ L radio immunoprecipitation assay (RIPA) lysis and extraction buffer with protease inhibitor cocktail III (Thermo Fisher Scientific) after removing culture medium and washing by DPBS, followed by centrifuging at 10000rpm at 4°C for 10 mins. Protein extracts were quantified using the Bio-Rad Protein Assay (Bio-Rad) based on the Bradford method (214, 215). Samples were adjusted to 100 $\mu$ g solubilized protein in a 2 $\mu$ L loading buffer containing Bromophenol Blue (Sigma-Aldrich, Merk) and 1 $\mu$ L 1M DTT (Sigma-Aldrich, Merk). Samples were gently mixed and heated at 95°C for 5 minutes and then separated by 9% (w/v) polyacrylamide sodium dodecyl sulphate-polyacrylamide gel electrophoresis (SDS-PAGE). After separation, proteins were transferred to polyvinylidene difluoride (PVDF) membranes which were then blocked in the 5% (w/v) milk solution at room temperature for 1h and probed with 1:5000 diluted primary rabbit antibody against GAPDH (#2118, Cell Signaling Technology), and 1:1000 diluted primary rabbit antibodies against ITGA5 (ab150361, Abcam), phospho-SAPK/JNK (#4671S, Cell Signaling Technology) and JNK (#9258S, Cell Signaling Technology) at 4°C overnight. Membranes were briefly washed with tris-buffered saline (150mM NaCl, 50mM Tris-HCl, pH7.6) containing 0.1% Tween 20 detergent (TBST) for 15 mins for three times and subsequently probed with the 1:10000 diluted HRP-conjugated goat anti-rabbit IgG (H+L) secondary antibody (Thermo Fisher Scientific) for an hour at room temperature. Similarly, membranes were washed with TBST for another three times for 15 minutes. Then membranes were visualized using a Bio-Rad imaging system, after processed with the SuperSignal™ West Pico PLUS chemiluminescent substrate (Thermo Fisher Scientific) (216). Acquired blotting images were analysed by the Image J software.

## **2.10 Human MSCs differentiation**

### **2.10.1 Chondrogenesis induction**

1x10<sup>5</sup> hBMSCs/well in 100 $\mu$ L growth medium were seeded and centrifuged in a U-bottom 96-well plate at 500g for 5 mins, left to adhere overnight. 10nM miRNA mimic

or 50nM inhibitor and corresponding negative controls were transfected using Lipofectamine™ 3000, and then incubated for 3 days before chondrogenic induction. Medium were changed into chondrogenesis inductive medium composed of high-glucose DMEM containing 10ng/mL recombinant human TGF-β3 (R&D system), 100nM dexamethasone, 1xITS-1 premix, 40µg/mL L-proline, and 50µg/mL 2-Phospho-L-ascorbic acid (all unspecified reagents are from Sigma-Aldrich, Merk), and replaced every 3 days up to 14 days.

### **2.10.2 Osteogenesis induction**

HMSCs were plated at  $5 \times 10^3$  cells/well in flat 96-well plates and  $1 \times 10^5$  /well in flat 48-well plates in growth medium. The next day, transfections were carried out using Lipofectamine™ 3000 with 50nM miRNA mimic, 25nM inhibitor or 50nM FlexiRube siRNAs (Qiagen) and negative controls (AllStars negative control for siRNA, Qiagen) for 2 days prior to osteogenic induction. OsteoMAX-XF™ osteogenesis medium (Sigma-Aldrich, Merk) were changed every 2 or 3 days up to 5 days.

### **2.10.3 Adipogenesis induction**

HMSCs were suspended in growth medium and plated at  $5 \times 10^3$  cells/well in flat 96-well plates. 100nM miRNA mimic, 50nM inhibitor or negative controls were transfected using Lipofectamine™ 3000 the next day. After 2 days post transfection, medium was changed into adipogenesis induction medium consisting of high-glucose DMEM supplemented with 10% (v/v) FBS, 1µM dexamethasone, 20nM IGF-1 (R&D system), 10ng/µL insulin, 500nM 3-isobutyl-1-methylxanthine (IBMX), 60µM indomethacin and 2µM rosiglitazone (all unspecified reagents are from Sigma-Aldrich, Merk) and left for 48 hours. Adipogenesis differentiation medium was replaced by maintenance medium composed of high-glucose DMEM supplemented with 10% FBS (v/v) and 10ng/µL insulin and left for 24 hours. This induction/maintenance cycle was repeated till 21 days.

## **2.11 Alcian Blue staining**

After removing induction medium, chondrogenic pellets were gently washed with DPBS once and fixed in 4% (v/v) formaldehyde (Sigma-Aldrich, Merk) for 1 hour at room temperature, followed by washing twice with double-distilled water for 5 mins each. Water was removed and 200 $\mu$ L/well 1% (w/v) Alcian Blue solution (Sigma-Aldrich, Merk) was added. Chondrogenic pellets were stained and incubated at room temperature overnight. Staining solution was removed, and pellets were washed by 0.1M HCl for 3 times (5 minutes each) and double-distilled water (ddH<sub>2</sub>O) subsequently. Pellets were imaged using Axio Cam MRc camera (Ziss) under an inverted microscope (Axiovert 40 CFL, Zeiss).

## **2.12 Alizarin Red S staining**

Osteogenic induction medium was removed, cells were fixed and washed as described in 2.11 and incubated with 40mM Alizarin Red S (pH4.2) at room temperature. Cells were then thoroughly washed using double-distilled water for 4 times (5 minutes for each) to remove excessive staining. The whole view of each well was photographed using a digital camera (Sony). Dye was eluted with 100 $\mu$ L/well 10% (w/v) cetylpyridinium (Sigma-Aldrich, Merk) in DPBS. Eluents were then transferred into a 96-well plate, and absorbance was measured at 595 nm in the EnVision plate reader (PerkinElmer).

## **2.13 Oil Red O staining**

Oil Red O stock solution (Sigma-Aldrich, Merk) was 3:2 diluted in double-distilled water and filtered through 0.2 $\mu$ m filter (Minisart, Sartorius) to prepare working solution just before use. The adipogenic inductive cells were fixed and washed as described in 2.11 and then excessively washed with 60% (v/v) isopropanol twice for 5 minutes each, left to air dry thoroughly. 100 $\mu$ L/well Oil Red O solution was added and incubated for 30 minutes at room temperature, followed by washing three times with ddH<sub>2</sub>O. Stained cells were photographed using the camera (Axio Cam MRc

camera, Ziss) fitted on an inverted microscope (Axiovert 40 CFL, Zeiss). Dye was eluted with 50 $\mu$ L/well 100% (v/v) isopropanol and measured at 492nm.

## 2.14 Glycosaminoglycan (GAG) assay

### 2.14.1 Chondrogenic pellets digestion

Following removal of chondrogenesis induction medium, chondrogenic pellets were gently washed with DPBS once and digested at 65°C overnight in 110 $\mu$ L/well papain buffer consisting of 250 $\mu$ g papain enzyme, 20 $\mu$ L 0.05M EDTA, 10 $\mu$ L 0.05M cysteine-HCl and 80 $\mu$ L 0.1M phosphate buffer pH6.5 (all from Sigma-Aldrich, Merk).

### 2.14.2 DMMB staining

GAGs are large branch polysaccharides that are negatively charged, which can be analytically detected by 1,9-Dimethylmethylene blue (DMMB) (217). The DMMB solution (pH3) was made up with 16mg DMMB, 3.04g glycine, 2.37g NaCl and 95mL 0.1M HCl in 1L ddH<sub>2</sub>O. (all from Sigma-Aldrich, Merk).

Chondroitin sulphate (CS) was used for a nine-point standard curve. Serial dilutions of 1mg/mL CS stock solution were carried out to prepare standard working solutions at concentrations ranging from 0ng/ $\mu$ L to 40ng/ $\mu$ L according to Table 2.9.

Table 2.9 Preparation for a GAG standard curve.

Standard concentration of CS	Volume of phosphate buffer	Volume of CS stock (1mg/mL)
0ng/ $\mu$ L	200 $\mu$ L	0 $\mu$ L
5ng/ $\mu$ L	199 $\mu$ L	1 $\mu$ L
10ng/ $\mu$ L	198 $\mu$ L	2 $\mu$ L
15ng/ $\mu$ L	197 $\mu$ L	3 $\mu$ L
20ng/ $\mu$ L	196 $\mu$ L	4 $\mu$ L
25ng/ $\mu$ L	195 $\mu$ L	5 $\mu$ L
30ng/ $\mu$ L	194 $\mu$ L	6 $\mu$ L
35ng/ $\mu$ L	193 $\mu$ L	7 $\mu$ L
40ng/ $\mu$ L	192 $\mu$ L	8 $\mu$ L

40µL digestion solution or standard working solution and 250µL DMMB solution were added and mixed in each well of a flat 96-well plate. Fluorescence was read at 530 nm (218) using a multilabel plate reader (EnVision 2103, PerkinElmer). Reaction and measurement were performed in duplicate.

### 2.14.3 Double-stranded DNA quantification

Digestion solution was directly diluted 1 in 50 in 1xTE buffer (10mM Tris-HCl pH8, 1mM EDTA pH8), while SYBR Green I (Invitrogen, Thermo Fisher Scientific) was diluted 1 in 1000. An eight-point standard curve was prepared and created using 5 ng/µL lambda double-stranded DNA stock solution (λDNA, Takara), following Table 2.10. 100µL/well diluted digestion solution and 100µL/well diluted SYBR Green I were added and mixed in a 96-well plate. Plate was incubated for 30 minutes in the dark at room temperature. Fluorescence of samples was measured in a 495nm/530nm excitation/emission filters set (219).

*Table 2.10 Protocol for preparing a dsDNA standard curve.*

Standard concentration of λDNA	Volume of TE buffer	Volume of λDNA stock (5ng/µL)
0ng/µL	800µL	0µL
0.03125ng/µL	795µL	5µL
0.0625ng/µL	790µL	10µL
0.125ng/µL	780µL	20µL
0.25ng/µL	760µL	40µL
0.5ng/µL	720µL	80µL
1ng/µL	640µL	160µL
2ng/µL	480µL	320µL

## 2.15 Generation of transgenic mice

Mice were maintained in the Disease Modelling Unit (DMU) of University of East Anglia. 3-5 mice were housed in an individually ventilated cage with 542cm<sup>2</sup> floor area with ambient temperature at 23±2°C and humidity at 40-60%. Mice were provided with continual access to certified standard grained-based diet and water.

maintained at All usage of mice was under the regulation of Home Office Animals (Scientific Procedures) Act 1986 (ASPA).

MiR-3085-3p null mice were generated using CRISPR/Cas9 technology by the Genome Editing Unit (GEU) of University of Manchester. Founders were bred forward with wild type (WT) C57BL/6.

COL2A1-Cre mice were purchased from Dr Attila Aszodi, Ludwig-Maximilians-University of Munich. This strain expresses Cre recombinase controlled by the promoter of gene COL2A1, enabling cartilage specific deletion of floxed gene fragments (220) (Figure 2.1A). For maintenance, COL2A1-Cre positive mice were crossed with WT mice to ensure a heterozygous Cre genotype.

ITGA5-floxed mice were kindly given by Professor Stephen Robinson, Quadrum Institute. This strain contains genetically modified ITGA5 alleles with the 255bp of exon1 flanked by loxP sites (221) (Figure 2.1B and C).

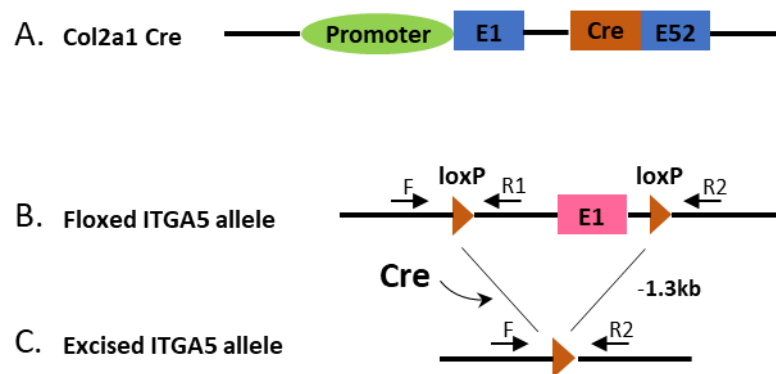


Figure 2.1 Schematic construct of COL2A1-Cre and ITGA5 in transgenic mice. (A) Structure of the COL2A1-Cre generation. (B) Structure of floxed ITGA5 allele. (C) Structure of excised allele where the exon 1 is cleaved by COL2A1-Cre. An 821bp floxed ITGA5 fragment can be amplified by primers F and R1. A 521bp excised ITGA5 fragment can be amplified by primer F and R2. F, forward primer; R1, reverse primer 1; R2, reverse primer 2. Sequence of primers is listed in Appendix4.

ITGA5 cartilage-specific knock out mice were generated following the breeding scheme shown in Figure 2.2. Homozygous ITGA5<sup>Fl</sup> mice were crossed with COL2A1-Cre mice to obtain heterozygous ITGA5<sup>Fl/WT</sup> Col2a1<sup>Cre</sup> mice. The ITGA5 cartilage-specific knock out mice (ITGA5<sup>Col2a1Cre</sup>) were generated by crossing the heterozygous ITGA5<sup>Fl/WT</sup> Col2a1<sup>Cre</sup> mice and homozygous ITGA5<sup>Fl</sup> mice. The ITGA5<sup>Col2a1Cre</sup> mice were further maintained and expanded by crossing with ITGA5<sup>Fl</sup> mice.

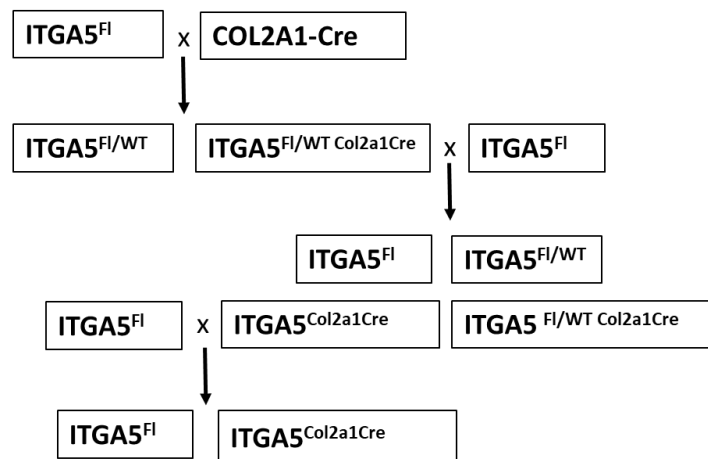


Figure 2.2 Breeding scheme for ITGA5 cartilage-specific knock out mice.

## 2.16 Genotyping

Ear biopsies were sampled by a sterile puncher, and DNA was extracted and amplified using REDEExtract-N-Amp™ Tissue PCR Kit (Sigma-Aldrich) and designed primers (Appendix4). 100µL Extraction Solution and 25µLTissue Preparation Solution were mixed and added to 1.5mL eppendorf tube containing the ear biopsy. After incubation at room temperature for 10 minutes, sample was further incubated at 95°C for 3 minutes. 100µL of Neutralization Solution B was added and vortexed. The extracts can be applied for genotyping PCR or kept at 4°C. PCR reactions and program were set up as Table 2.11 and Table 2.12. PCR products were loaded and separated through 1.5% agarose gel. The gel was then stained for 30 minutes in TAE buffer containing 0.1% (w/v) ethidium bromide (Thermo Fisher Scientific) and was visualized using a gel recording system equipped with ultraviolet light source and camera. Genotypes were defined based on sizes of visualized amplicons.

Table 2.11 Genotyping PCR reaction.

Component	Reaction
Tissue extract	4 $\mu$ L
REExtract-N-Amp PCR Reaction Mix	10 $\mu$ L
10 $\mu$ M forward primer	1 $\mu$ L
10 $\mu$ M reverse primer	1 $\mu$ L
Nuclease-free water	4 $\mu$ L
Total volume	20 $\mu$ L

Table 2.12 Genotyping PCR program.

Step	Temperature	Time
Initial denaturation	94°C	3 minutes
10 cycles	94°C	1 minute
	63°C (decreases 1°C per cycle)	1 minute
	72°C	1 minute
	95°C	1 minute
20 cycles	53°C	1 minute
	72°C	1 minute
	72°C	10 minutes
Final extension	72°C	10 minutes
Final hold	4°C	Indefinitely

## 2.17 DMM modelling

Destabilization of the medial meniscus (DMM) surgery was kindly performed by Dr Tracey Swingler, University of East Anglia, following the protocol described in (222) to induce osteoarthritic pathogenesis. Under aseptic conditions, 12-week-old male mice were inhale anaesthesia with isoflurane, 3% (v/v) of which used for induction and 2% (v/v) for maintenance. 2.5 $\mu$ g Vetergestic (Ceva Animal Health) was then administered through subcutaneous injection. The joint capsule of right knee was opened through incision medial to the parapatellar ligament. The medial meniscotibial ligament (MML)

of right knee was identified and fully severed using a fine-tipped tweezer. Capsule was closed using Vicryl 6-0 round-bodied needle suture kit (Ethicon), followed by suturing the dermal layer using Ethilon 5-0 reverse-cutting needle suture kit (Ethicon). Mice were returned to house cage when recovered and weight bearing. Vetergestic was administered daily for 3 days and weight was monitored daily for 7 days post-surgery. Sham surgery was operated by opening the capsule and then suturing the dermal incision without cutting MML. Right knees were harvested 10 weeks and processed as desired.

## **2.18 Whole mount skeletal preparation and staining**

Whole mount skeletal preparation and staining was executed on embryos at E16.5, E17.5 and E18.5, optimized based on the protocol described in (223). Pregnant females were timed-mated and sacrificed by cervical dislocation at desired gestation time points. Embryos were exfoliated and collected from uterus, followed by fixation in 95% (v/v) ethanol (Thermo Fisher Scientific) for 24 hours at room temperature. Embryos were skinned and eviscerated, and subsequently penetrated in acetone for 24 hours at room temperature. Embryos were then stained in 0.03% (w/v) Alcian Blue solution (Sigma-Aldrich, Merk) for 24 hours at room temperature, followed by initially washing in 70% (v/v) ethanol twice for 1 hour and fixing in 95% (v/v) ethanol overnight at room temperature. To preclear the specimen, embryos were incubated in 1% (w/v) potassium hydroxide (Thermo Fisher Scientific) for 1 hour, and then transported and counterstained in 0.001% (w/v) Alizarin Red S solution (Sigma-Aldrich, Merk) for 4 hours at room temperature. The Alizarin Red S solution was replaced by 50% (v/v) glycerol: 50% (w/v) potassium hydroxide solution for at least 4 days until non-skeletal tissue became clear. To store in a long term, stained sample was transferred into 80% glycerol.

## **2.19 Tissue processing**

Embryos at E15.5, E16.5 and E17.5 were harvested and fixed in 10% (v/v) neutral buffered formalin (NBF, Sigma-Aldrich, Merk) overnight at room temperature. One

quarter of the specimen were trimmed off sagittally to open the cranial, thoracic and peritoneal cavities and expose inner tissues, followed by further fixation for 8 hours.

Mice at 21 days old (P21) were sacrificed by cervical dislocation or carbon dioxide. Knees were dissected, where skin and excess muscles were removed. Subsequently, knee joints were fixed in 10% NBF for 24 hours and decalcified in 14% ethylenediaminetetraacetic acid (EDTA, pH7.2, Sigma-Aldrich, Merk) for 7 days. Similarly, mice at 10 weeks post-operation were euthanized and entire knees were fixed in 10% NBF for 24 hours and then decalcified in 20% (v/v) formic acid (Thermo Fisher Scientific) in distilled water for 22-24 hours.

After fixation and decalcification, tissues were transferred to 70% ethanol and stored at 4 °C until subsequent processing in a tissue processor (Leica, ASP 300S) overnight. Processing program was set up as Table 2.13. The next day, processed tissues were immersed in molten paraffin (Paralast, Sigma-Aldrich, Merk) in the embedding station (Leica, EG1150). Embryos and p21 knees were placed sagittally, surgically induced knees were embedded coronally, and cooled on top of the precooling platform. These tissue blocks were kept at room temperature till sectioning.

*Table 2.13 Tissue processing program.*

<b>Reagent</b>	<b>Time</b>	<b>Temperature</b>
<b>Ethanol 70%</b>	1 hour	Room temperature
<b>Ethanol 80%</b>	1.5 hours	Room temperature
<b>Ethanol 90%</b>	2 hours	Room temperature
<b>Ethanol Absolute</b>	1 hour	Room temperature
<b>Ethanol Absolute</b>	1.5 hours	Room temperature
<b>Ethanol Absolute</b>	2 hours	Room temperature
<b>Xylene</b>	0.5 hour	Room temperature
<b>Xylene</b>	1 hour	Room temperature
<b>Xylene</b>	1.5 hours	Room temperature
<b>Paraffin Wax</b>	1 hour	62 °C
<b>Paraffin Wax</b>	2 hours	62 °C
<b>Paraffin Wax</b>	2 hours	62 °C

## **2.20 Tissue sectioning**

Paraffin embedded tissue were serial sectioned at an interval of 5µm using microtome (Microm, HM355S) fitted with a microtome blade (MX35 Ultra, Thermo Fisher Scientific). Serial sections floated on the surface of warm water at 42°C to get flattened, and then collected by glass slides (Thermo Fisher Scientific). For knees specifically, sections were placed on slides one by one. 3 sections were placed on each slide to allow for the coverage of different aspects of the joint. 25 slides carrying 75 sections, spanning 375µm thickness of the knee. Slides were labelled in order and dried overnight at 37 °C and stored at room temperature.

## **2.21 Histological staining**

Embryonic sections were stained by Harris Haematoxylin Solution (Sigma-Aldrich, Merk) and Eosin Y Solution (Sigma-Aldrich, Merk) to generally differentiate cell and tissue structures. The Haematoxylin and Eosin staining was performed following the steps indicated in Table 2.14.

Safranin O and Fast Green staining was applied on formalin-fixed paraffin-embedded tissue sections of knee joints as described in Table 2.15.

Stained sections were mounted with DPX mounting medium (Thermo Fisher Scientific) and covered by cover glasses (Thermo Fisher Scientific), followed by air drying overnight at room temperature. Stained sections were observed and pictured under bright field microscope (Axioplan 2, Zeiss) equipped with AxioCam HRc camera (Ziss).

Table 2.14 Haematoxylin and eosin staining protocol for paraffin embedded tissue sections.

<b>Reagent</b>	<b>Time</b>
<b>Histoclear</b>	5 minutes
<b>Histoclear</b>	5 minutes
<b>Ethanol absolute</b>	5 minutes
<b>Ethanol 80%</b>	5 minutes
<b>Ethanol 70%</b>	5 minutes
<b>Rinsing under running tap water</b>	5 minutes
<b>Harris Haematoxylin Solution</b>	2 minutes
<b>Rinsing under running tap water</b>	5 minutes
<b>1% HCl in 70% Ethanol</b>	15 seconds
<b>Rinsing under running tap water</b>	10 seconds
<b>0.1% Sodium bicarbonate solution</b>	1 minutes
<b>Rinsing under running tap water</b>	5 minutes
<b>Eosin Y solution</b>	30 seconds
<b>Ethanol 70%</b>	2 minutes
<b>Ethanol 80%</b>	2 minutes
<b>Ethanol absolute</b>	2 minutes
<b>Histoclear</b>	5 minutes
<b>Histoclear</b>	5 minutes

Table 2.15 Safranin O and Fast Green staining protocol for paraffin embedded tissue sections.

<b>Reagent</b>	<b>Time</b>
<b>Histoclear</b>	5 minutes
<b>Histoclear</b>	5 minutes
<b>Ethanol absolute</b>	5 minutes
<b>Ethanol 95%</b>	5 minutes
<b>Ethanol 75%</b>	5 minutes
<b>Ethanol 50%</b>	5 minutes
<b>Rinsing under running tap water</b>	5 minutes
<b>0.06% Fast Green solution</b>	5 minutes
<b>1% acetic acid solution</b>	10-15 seconds
<b>0.1% Safranin O solution</b>	5 minutes
<b>Ethanol 95%</b>	1 minutes
<b>Ethanol absolute</b>	1 minutes
<b>Ethanol absolute</b>	1 minutes
<b>Histoclear</b>	2 minutes
<b>Histoclear</b>	2 minutes

## 2.22 Growth plate measurement

Using Image J, resting, proliferative and hypertrophic zones were defined in every 5 slides with 15 sections at 25 $\mu$ m interval for one sample. Area of each zone was measured, and the percentage of entire growth plate area was calculated (Figure 2.3). Average of percentages of total 15 sections was used to presented one sample for statistical analysis.

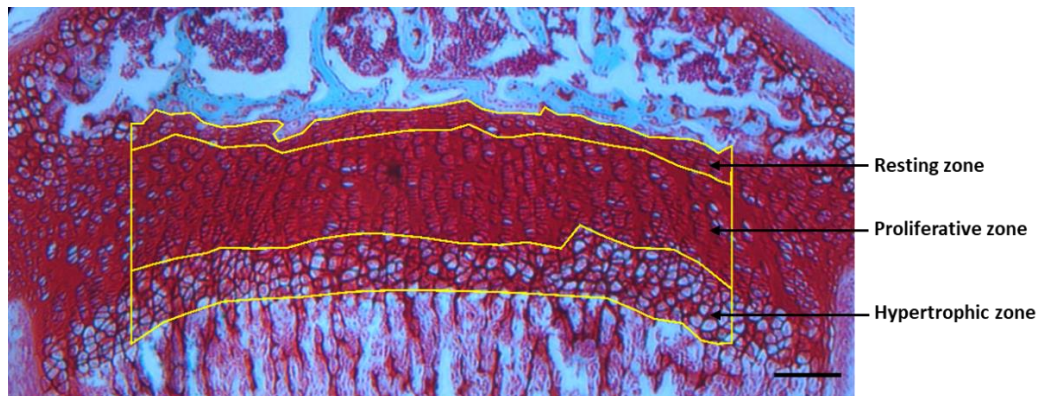


Figure 2.3 Representative growth plate of proximal tibia. Safranin O and Fast Green stained p21 knee section showed proximal tibia growth plate. Resting, proliferative and hypertrophic zones were indicated in yellow polygons for measurement. Scale bar, 100 $\mu$ m.

## 2.23 Histologic scoring for osteoarthritis severity

Among the 25 slides obtained as described in 2.20, every 5 slides with 15 sections at 25µm interval were used for analysis. The severity of osteoarthritic phenotypes was assessed by two blinded observers using the OARSI semi-quantitative scoring system (Table 2.16) (224). Four compartments including medial femoral condyle (MFC), medial tibial plateau (MTP), lateral femoral condyle (LFC) and lateral tibial plateau (LTP) were scored separately. The severity was expressed as the maximal score of selected 15 sections for each compartment and entire knee joint. The higher score defines more severe cartilage degradation.

*Table 2.16 OARSI semi-quantitative scoring system. This scoring system was proposed for histologic scoring of osteoarthritis in mice. Adapted from (224).*

<b>Grade</b>	<b>Grade Osteoarthritic damage</b>
<b>0</b>	Normal
<b>0.5</b>	Loss of Safranin-O without structural changes
<b>1</b>	Small fibrillations without loss of cartilage
<b>2</b>	Vertical clefts down to the layer immediately below the superficial layer and some loss of surface lamina
<b>3</b>	Vertical clefts/erosion to the calcified cartilage extending to <25% of the articular surface
<b>4</b>	Vertical clefts/erosion to the calcified cartilage extending to 25-50% of the articular surface
<b>5</b>	Vertical clefts/erosion to the calcified cartilage extending to 50-75% of the articular surface
<b>6</b>	Vertical clefts/erosion to the calcified cartilage extending >75% of the articular surface

## 2.24 Statistical analysis

The constitutively expressed housekeeping reference 18S rRNA is used for normalization of the relative expression level of mRNAs, whilst U6 small nuclear RNA (snRNA) was used for miRNAs. Assuming that the efficiencies of amplifications are equal, the  $2^{-\Delta Ct}$  method is applied for comparative qRT-PCR, where  $\Delta Ct = Ct_{\text{target gene}} - Ct_{\text{reference gene}}$ .(225, 226)

Acquired images were processed and analysed by the Image J software and Microsoft PowerPoint 2016.

Statistical analysis was performed with Microsoft Excel 2016, IBM SPSS version 23.0 and GraphPad Prism 8. Data were shown as mean  $\pm$  standard error of the mean (SEM) for at least 3 independent repeated experiments. The differences between groups were analysed mainly by two-tailed Student's t-test or one-way ANOVA with Dunnett's or Tukey's post hoc test for multiple comparisons in normally distributed dataset. Two-way ANOVA with Geisser-Greenhouse correction and Sidak's post hoc test was used when testing for an effect of 2 factors including treatment and time points. The correlation within groups was investigated using two-tailed Pearson correlation test. A p value  $< 0.05$  is taken as statistically significance. To analyse data of histologic assessment using OARSI scoring system, a non-parametric Kruskal–Wallis test with Dunn's post hoc test was performed.

RNA-seq raw data was quantified and analysed through Kallisto (227) and Sleuth (228). Significance corrected for multiple testing was shown as q-value, and the log2 fold change was presented as beta value, which was weighted based on gene abundance so that high fold changes at very low expression are penalized. A q value cut-off of 0.05 was applied.

# **Chapter 3 Optimizing of effective dosage and time of miR-3085-3p on ITGA5 in cell lines**

## **3.1 Introduction**

Crowe et al. have revealed that ITGA5 is a direct target of miR-3085-3p. QRT-PCR demonstrated a decrease in response to miR-3085-3p in human primary chondrocytes. A luciferase reporter was constructed with the 3'UTR of ITGA5 inserted downstream the firefly luciferase. This reporter was transiently transfected together with mimic of 3085 into SW1353. Luciferase activity reduced at the presence of miR-3085-3p. This was rescued by a mutation in seed sites for miR-3085-3p compared with wild type 3'UTR construct. In addition, western blot showed that miR3085 was as effective as an siRNA to ITGA5 in decreasing protein levels of ITGA5 in human primary chondrocytes.(206) In addition, there was a lot of variability in the concentrations of mimics and inhibitors, times of transfection etc both within the lab and in the literature (147, 190, 198, 208).

To further verify the effects of miR-3085-3p on regulating the expression of ITGA5, as well as identify optimum concentrations and times for each procedure that could be use across the laboratory to ensure more consistency. Experimental was executed applying different cell lines including DF1, SW1353, HeLa, C28/I2 and HAC, in the miR-3085-3p to ITGA5 system. Optimal working dosage and time were also determined in various experimental conditions.

## 3.2 Results

### 1.1.1 MiR-3085-3p is highly expressed in human osteoarthritic chondrocytes

In order to determine levels of miR-3085-3p in the cell lines under test, and compare with primary HAC, we measured the expression of miR-3085-3p. As shown in Figure 3.1, the expression level of miR-3085-3p was higher in HAC than that in any other cell lines ( $p < 0.0001$ ), while there were not significant differences within DF1, SW1353, HeLa and C28/I2 cells. Although ITGA5 showed an increased expression in HAC ( $p < 0.0001$ ) as well as SW1353 ( $p < 0.0001$ ) compared with DF1, HeLa and C28/I2, no correlation between the expression patterns of miR-3085 and ITGA5 was identified.

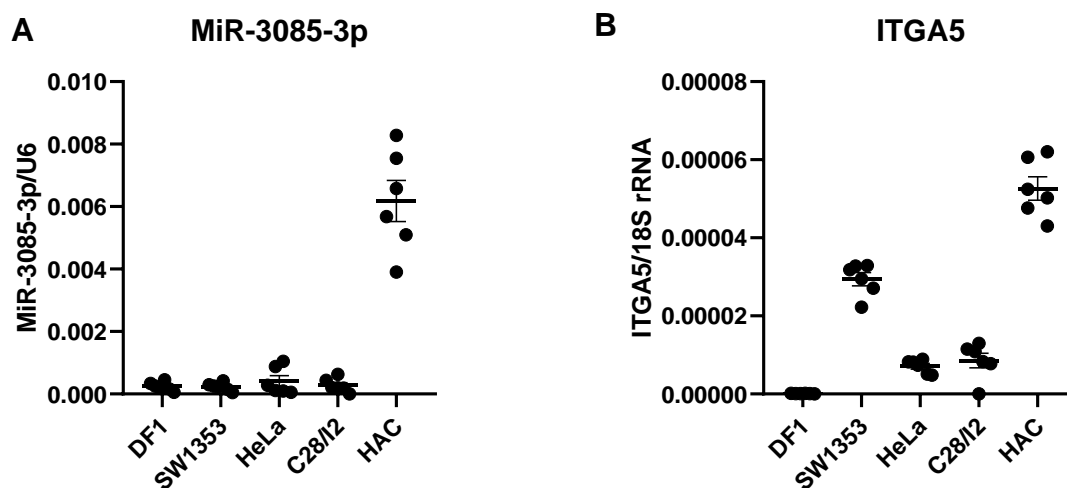


Figure 3.1 The relative expression levels of miR-3085-3p (A) and ITGA5 (B) in different cell lines. The expression level of ITGA5 mRNA was normalized by 18S rRNA, while miR-3085 by U6, and presented as the  $2^{-\Delta Ct}$  value, as mean  $\pm$  SEM,  $N=6$ . The expression of ITGA5 in DF1 was not detected, as chicken had different ITGA5 gene sequence from human.

### **1.1.2 Overexpression of miR-3085-3p decreases the expression of ITGA5 mRNA**

Results derived from qRT-PCR indicated a dose dependent effect of miR-3085-3p on expression of the ITGA5 gene (Figure 3.2), with significant efficacy observed at 25nM ( $p=0.0005$ ), 50nM ( $p=0.0003$ ) and 100nM ( $p=0.021$ ) in SW1353 (Figure 3.2A), overall repression in HeLa (5nM,  $p=0.04$ ; 10nM to 100nM,  $p<0.0001$ ) (Figure 3.2B), whilst the trend shifted to higher concentrations (100nM,  $p=0.017$ ) in C28/I2 cells (Figure 3.2C). In general, miR-3085-3p at 50nM achieved a maximal repression of ITGA5 mRNA in SW1353 and HeLa cells (Figure 3.2A and B).

Based on these data, at the fixed concentration of 50nM in SW1353 and HeLa, 100nM in C28/I2, the efficacy of miR-3085-3p was explored across a 72-hour time course. Significant decrease of ITGA5 was observed by 48h incubation after transfection in all cell lines (SW1353,  $p<0.0001$ ; HeLa,  $p<0.0001$ ; C28/I2,  $p=0.0089$ ) (Figure 3.3). A decreasing expression level of ITGA5 was identified in terms of time course, in SW1353 and HeLa (Figure 3.3A and B), but only at 48h after transfection in C28/I2 (Figure 3.3C).

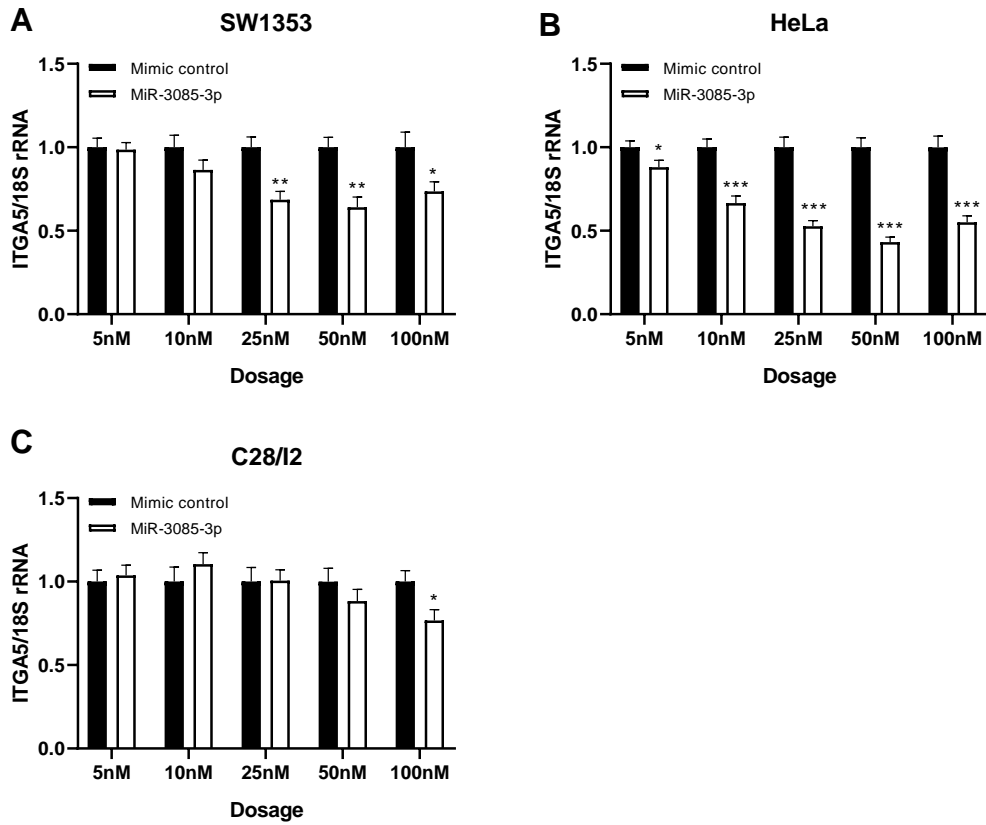


Figure 3.2 Dose dependent response in qRT-PCR. ITGA5 mRNA expression was shown 48 hours after cells transfected by mimic control and miR-3085-3p mimic in SW1353 (A), HeLa (B) and C28/12 (C). Comparative Ct method was applied and ITGA5 expression was normalized by 18S rRNA. Statistical analysis between control group and mimic group was performed using unpaired Student's *t*-test. Means of mimic control groups were set as the standard 1. Data were presented as mean  $\pm$  SEM, N=5. \*,  $P < 0.05$ ; \*\*,  $P < 0.01$ ; \*\*\*,  $P < 0.001$ .

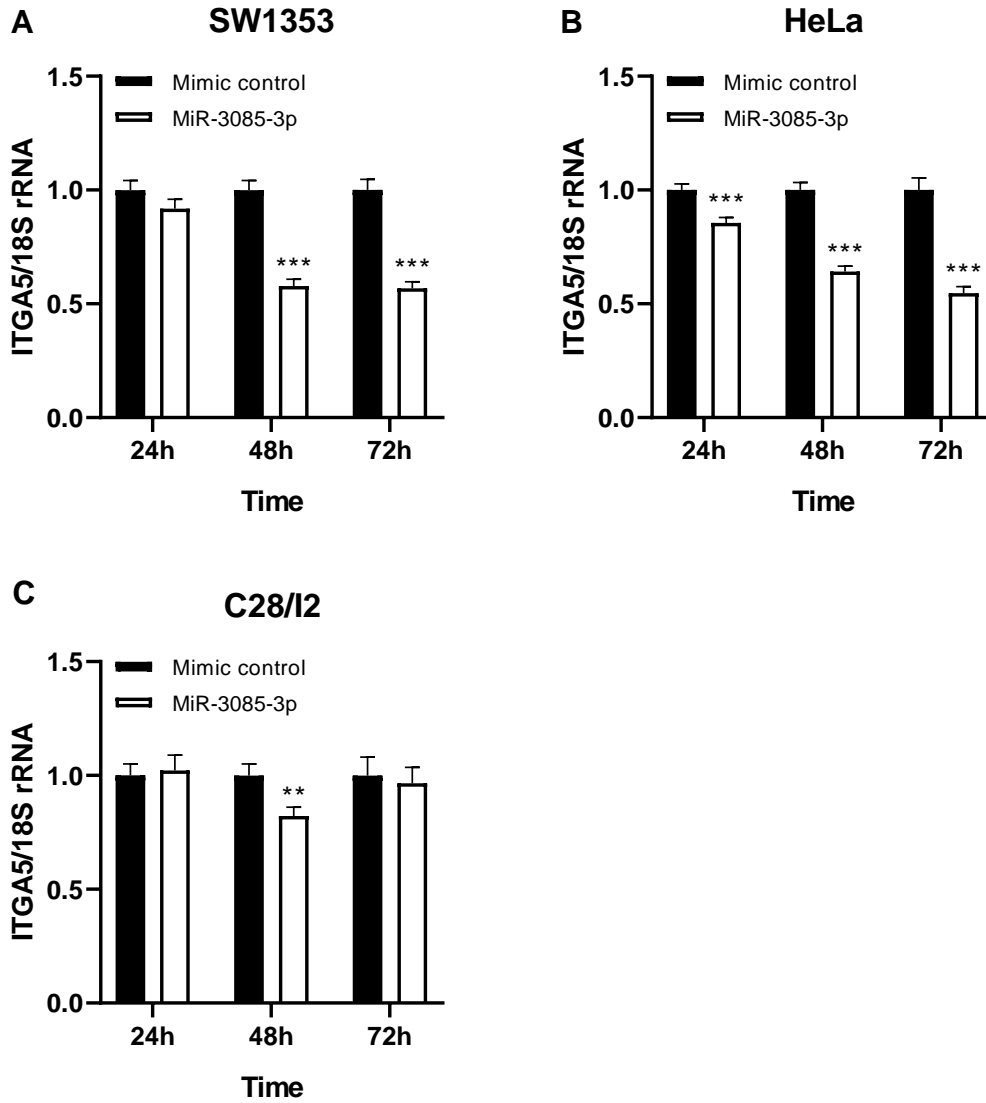


Figure 3.3 Time course investigation of ITGA5 mRNA via qRT-PCR. SW1353 (A) and HeLa (B) cells were transfected at a concentration of 50nM microRNA, while C28/I2 (C) at 100nM, according to the dose screening. Detection time points were 24 hours, 48 hours and 72 hours respectively after transfection. Comparative Ct method was applied and ITGA5 expression was normalized by 18S rRNA. Statistical analysis between control group and mimic group was performed using unpaired Student's *t*-test. Means of mimic control groups were set as the standard 1. Data were presented as mean  $\pm$  SEM, N=5. \*\*,  $P < 0.01$ ; \*\*\*,  $P < 0.001$ .

We further explored the role of miR-3085-3p in regulating ITGA5 in HAC. As shown in Figure 3.4A, the overexpression of miR-3085-3p did not reduce expression of ITGA5, indeed there was a trend to increased expression at lower concentrations. This might be because of high endogenous expression level of miR-3085-3p. An inhibitor of miR-3085-3p was therefore transfected and this gave increased ITGA5 levels even at low concentrations from 5nM ( $p=0.0032$ ) to 50nM ( $p=0.023$ ), with a maximum induction at 25nM ( $p=0.013$ ) (Figure 3.4B), reinforcing the hypothesis.

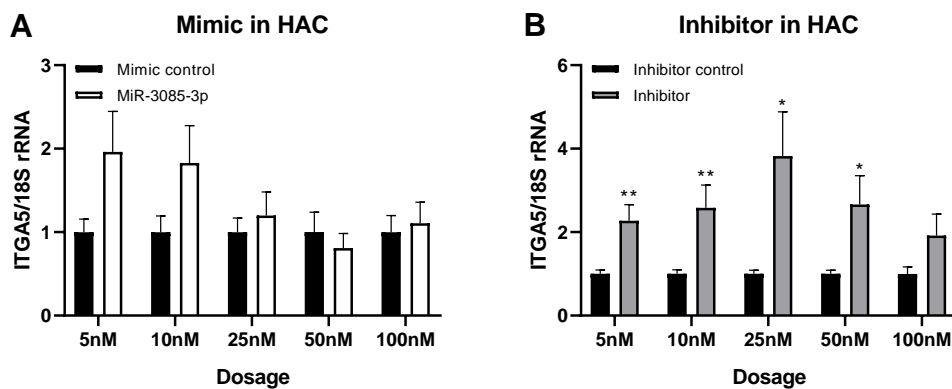


Figure 3.4 Expression level of ITGA5 is detected by qRT-PCR in primary chondrocytes. A illustrated the results when cells are transfected with mimic and control, while B presented results transfected with inhibitor and control, followed by incubation for 48 hours. Comparative Ct method was applied and ITGA5 expression was normalized by 18S rRNA. Statistical analysis between control group and mimic/inhibitor group was performed using unpaired Student's t-test. Means of control groups were set as the standard 1. Data were presented as mean  $\pm$  SEM, N=3. \*,  $P<0.05$ ; \*\*,  $P<0.01$ . HAC, human articular chondrocytes from knee osteoarthritic patients.

### **1.1.3 MiR-3085-3p suppresses ITGA5 by targeting seed sites within 3'UTR**

Dose and time course Luciferase assay were performed in DF1, SW1353, HeLa and C28/I2 cell lines. Significant downregulation of the luciferase activity can be seen in DF1, SW1353 and HeLa cells after treatment by miR-3085-3p mimic for 48h at all doses in DF1 (5nM,  $p=0.0001$ ; 10nM to 100nM,  $p<0.0001$ ) (Figure 3.7A) and from 5nM to 50nM in SW1353 (5nM,  $p=0.0013$ ; 10nM,  $p=0.036$ ; 25nM,  $p=0.0066$ ; 100nM,  $p=0.0018$ ) (Figure 3.7B) and HeLa (5nM,  $p=0.0002$ ; 10nM to 50nM,  $p<0.0001$ ) (Figure 3.7C), signifying the direct negative regulation of miR-3085-3p on ITGA5 mRNA expression by targeting its 3'UTR sequence. In C28/I2, slight decreases but with no more than 10% were observed at 5nM ( $p=0.039$ ) and 50nM ( $p=0.038$ ) (Figure 3.7D). Overall, there was not obvious dose dependent effect shown all over cell lines (Figure 3.7). We therefore chose the dose of 50nM as the optimal action dose, though this choice was influenced by prior experience the laboratory.

In terms of time course, as expected, there was a decreasing trend of luciferase activity in DF1 (Figure 3.8A), HeLa (Figure 3.8C) and C28/I2 (Figure 3.8D), particularly in HeLa cells with an approximately decline of 30% at 96 hours ( $p=0.0002$ ) compared to that at 24 hours ( $p<0.0001$ ) (Figure 3.8C). Even though, bigger standard errors were observed at the late time point (96h) in SW1353 ( $p=0.011$ ) and HeLa ( $p=0.0002$ ) (Figure 3.8B and C). The 96-hour time point in DF1 was discarded as cells were overconfluent and distinct cell detachment/death were observed. Taken as a whole, in luciferase assays, 50nM miR-3085-3p mimic and 72h incubation were recommended as optimal, at which the miR-3085-3p mimic exerted a more reliable effect in each cell line.

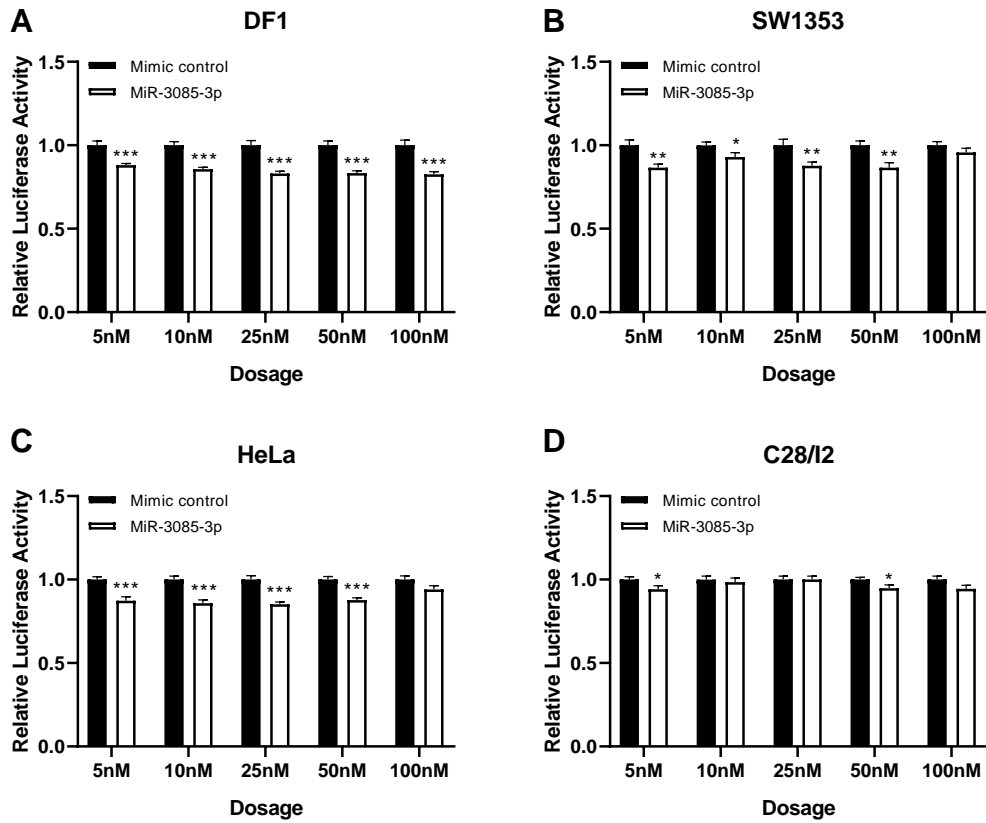


Figure 3.5 Dose dependent response in luciferase assay. Relative luciferase activities were shown at 48 hours after cells transfected by 100ng ITGA5 construct where the 3'UTR of ITGA5 inserted in the luciferase reporter (pmirGLO plasmid), following the transfection of non-targeting miRNA control or miR-3085-3p mimic at indicated concentrations. Luminescence was presented as the light units of Firefly luciferase normalized by those of Renilla luciferase. Statistical analysis between control group and mimic group was performed using unpaired Student's t-test. Means of mimic control groups were set as the standard 1. Data were presented as mean  $\pm$  SEM, N=5. \*,  $P < 0.05$ ; \*\*,  $P < 0.01$ ; \*\*\*,  $P < 0.001$ .

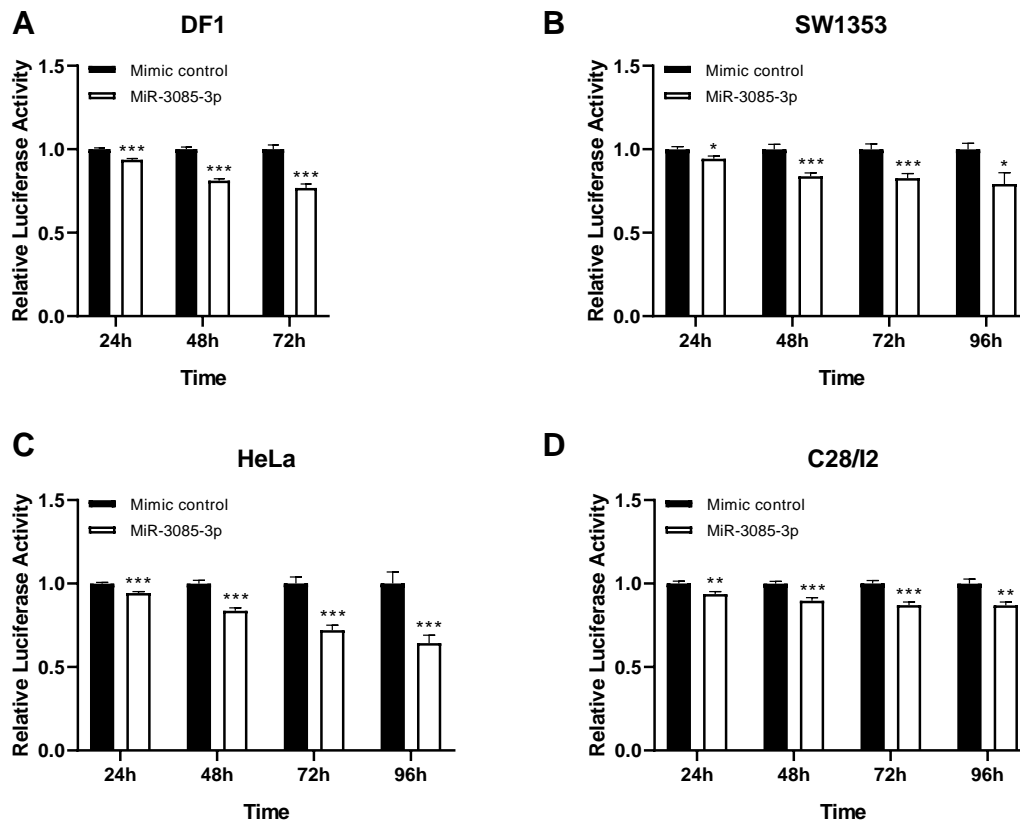


Figure 3.6 Time course in luciferase assay. DF1 (A), SW1353 (B), HeLa (C) and C28/I2 (D) were transfected with non-targeting miRNA mimic control or miR-3085-3p mimic at 50nM, followed by the transfection of 100ngITGA5 construct where the 3'UTR of ITGA5 inserted in the luciferase reporter (pmirGLO plasmid). Relative luciferase activities were shown at desired time points after transfection. Luminescence was presented as the light units of Firefly luciferase normalized by those of Renilla luciferase. Statistical analysis between control group and mimic group was performed using unpaired Student's *t*-test. Means of mimic control groups were set as the standard 1. Data were presented as mean  $\pm$  SEM, N=5. \*,  $P < 0.05$ ; \*\*,  $P < 0.01$ ; \*\*\*,  $P < 0.001$ .

### 1.1.4 ITGA5 protein is downregulated by miR-3085-3p

The protein level of ITGA5 appeared to decline in cells after transfected with miR-3085-3p mimic, when comparing to the non-targeting control group in western blot (Figure 3.5). After normalizing by the grey values of GAPDH and combining the results of three repeats, statistically significant differences were found at 100nM ( $p=0.038$ ) in SW1353 (Figure 3.5A), 50nM ( $p=0.021$ ) and 100nM ( $p=0.0025$ ) in HeLa (Figure 3.5B).

Furthermore, at the concentration of 100nM miR-3085-3p mimic, an incubation time of 72h after transfection led to significant decrease of ITGA5 protein in all cell lines (SW1353,  $p=0.020$ ; HeLa,  $p=0.029$ ; C28/I2,  $p=0.033$ ) (Figure 3.6). Taken together, 100nM and 72h were chosen as the optimal dose and time point for Western blotting.

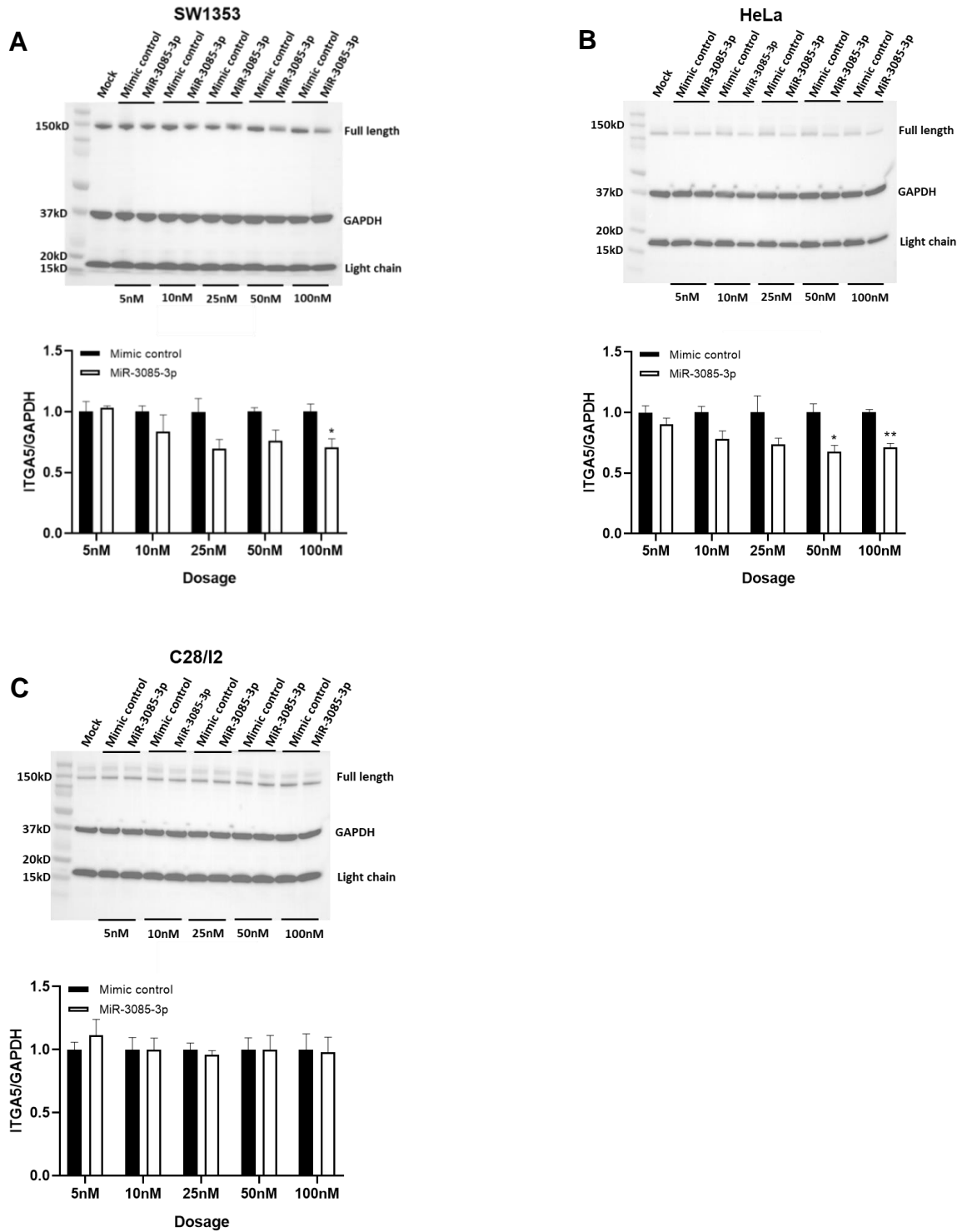


Figure 3.7 Western blot analysis was performed to determine the protein levels of ITGA5 at 72 hours after transfection of miR-3085-3p mimic at indicated concentrations. Representative western blots from three repeat experiment were shown, with ITGA5 (full length, 150kDa; light chain: 19kDa) and GAPDH (37kDa) indicated. Quantification of ITGA5 is normalised to GAPDH. Statistical analysis between control group and mimic group was performed using unpaired Student's t-test. Means of control groups were set as 1. Graphs were presented as mean  $\pm$  SEM, N=3. \*,  $P < 0.05$ ; \*\*,  $P < 0.01$ .

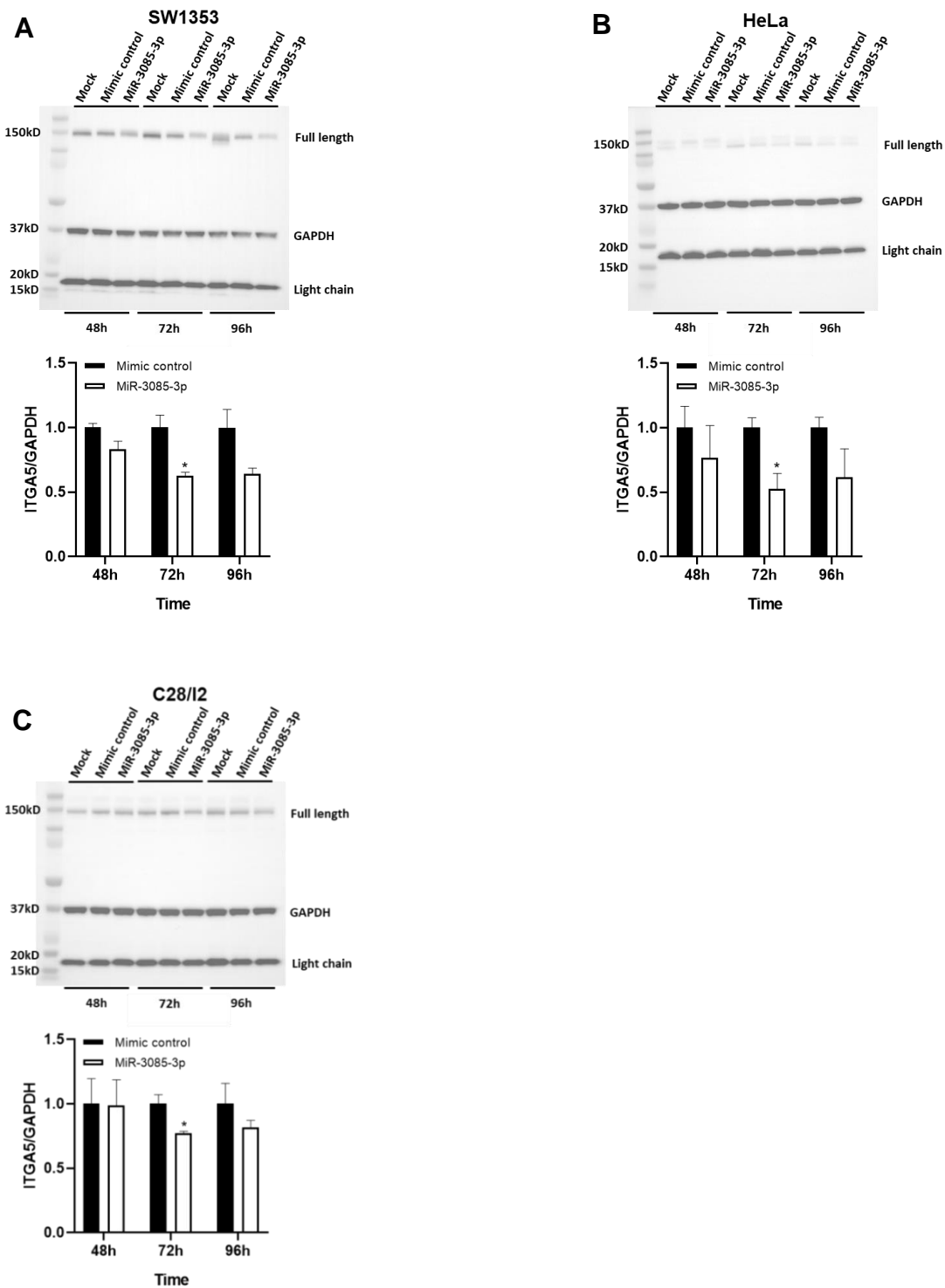


Figure 3.8 Time course investigation of ITGA5 protein using western blotting. SW1353 (A), HeLa (B) and C28/12 (C) cells were transfected at a concentration of 100nM microRNA according to the dose screening. Detection time points were 48 hours, 72 hours and 96 hours respectively after transfection. Representative western blots from three repeat experiment were shown with ITGA5 (full length, 150kDa; light chain: 19kDa) and GAPDH (37kDa) indicated. Quantification of ITGA5 is normalised to GAPDH. Statistical analysis between control group and mimic group was performed using unpaired Student's *t*-test. Means of control groups were set as 1. Graphs were presented as mean  $\pm$  SEM, N=3. \*,  $P < 0.05$ .

### 3.3 Discussion

In our qRT-PCR assays, ITGA5 is significantly decreased by miR-3085-3p at certain concentrations and incubation time in most cell lines. However, HACs demonstrate a low reliability without significant differences shown after transfecting with miR-3085-3p mimic. On one hand, HACs have higher expression of miR-3085-3p than other cell lines (Figure 3.1A), dose greater than 100nM are likely to be sufficient to reduce ITGA5 expression. On the other hand, the individual difference within patients plays a role to some extent. All the HAC are from the knee joints of different patients. Differential responses to miR-3085-3p in reducing ITGA5 are observed in individual HAC. In the 3 HACs, there was only one demonstrated slight repression without significance in response to the overexpression of miR-3085-3p (data not shown). Many factors can exert an influence of the pathophysiology of the articular chondrocytes, such as different disease stages, diverse treatment received, age and sex of patients. Using HACs from the same patient might help to improve the reproducibility.

Our Western blotting data show that miR-3085-3p is effective at decreasing protein levels of ITGA5 at 100nM with incubation for 72h after transfection in both SW1353 and HeLa. Nevertheless, there is not significance suppression of ITGA5 by miR-3085-3p found in C28/I2. In addition, even though we have got statistically significant downregulation of ITGA5, the data isn't as compelling as when we did it previously (206). We don't have an exact explanation of what has changed. Many uncertain conditions such as diverse passages of cells, diverse batches of culture medium and experimental reagents can exert influence.

Luciferase assays demonstrate robust and reproducible outcomes in terms of our investigation of effects of miR-3085-3p on ITGA5. It is worthy to mention that liposomes have been reported to participate in or initiate cellular activity, leading to changes in gene expression and induce cytotoxicity (229). Lipofectamine 3000 is an advanced lipid nanoparticle developed and improved for transfection efficacy and cell viability. We still observe cell detachment/cell death after twice transfection with siRNAs and plasmid separately, which is worse when longer incubation time executed. This phenomenon might imply a dysregulated cellular viability, which might be as a consequence of a lipofectamine-induced stress response.

Overall, overexpression of miR-3085-3p gives rise to a decreasing expression of ITGA5 in DF1, SW1353, HeLa and C28/I2 in various assays including qRT-PCR, Western blotting and Luciferase assay. To make results generalized, for qRT-PCR, 50nM miR-3085-3p mimic and 48 hours incubation post transfection are recommended in either SW1353 or HeLa, whilst 100nM in C28/I2. For detection of ITGA5 proteins via western blotting, 100nM and 72h achieve an effective and reliable downregulation by miR-3085-3p, where C28/I2 is not an applicable cell line. For luciferase assay, 50nM and 72h are optimal all over cell lines.

# Chapter 4 Investigating roles of miR-3085-3p in chondrocyte function

## 4.1 Introduction

Based on the previous study in our lab, Dr Linh Le uncovered by qRT-PCR that COL2A1 and ACAN, two predominant structural genes of cartilage, had reduced expression at the presence of miR-3085-3p in HAC undergoing either micromass or monolayer cultures. What's more, IL-1 $\beta$  induced the expression of miR-3085-3p in HAC. Overexpression of miR-3085-3p increased the luciferase activity of an NF $\kappa$ B reporter. However, western blot looking at the fractionated cell extracts of SW1353 demonstrated that nuclear phospho-p65 and p65 were decreased, and cytoplasmic I $\kappa$ B $\alpha$  was increased by transfection of miR-3085-3p mimic and stimulated with IL-1-induced for 0.5h. Additionally, TGF $\beta$ 1 also induced miR-3085-3p. The protein levels of SMAD2, SMAD3 and SMAD4 were all suppressed by miR-3085-3p in both whole cell extracts and the nuclear fractions, with phospho-SMAD3 decreased in whole cell extracts. Similarly, miR-3085-3p reduced WNT3A-induced  $\beta$ -catenin and phospho- $\beta$ -catenin in either whole cell or nuclear extracts.(230)

What Dr. Linh Le found has signified that miR-3085-3p plays a part in cartilage homeostasis and various signalling pathways involved in chondrocyte function. Following her study, further exploration of functions of miR-3085-3p in chondrocytes were emphasized in this chapter.

## 4.2 Results

### 4.2.1 MicroRNA-3085-3p and extracellular matrix genes

To continue the evaluation of miR-3085-3p in regulating two predominant matrix genes, ACAN and COL2A1, luciferase assays were carried out. Overexpression of miR-3085-3p significantly decreased luciferase activities of the 3'UTR constructs of either ACAN ( $p=0.0003$ ) (Figure 4.1A) or COL2A1 ( $p<0.0001$ ) (Figure 4.1B), when compared with a negative mimic control. This downregulation was rescued by mutating seed sites seated in the 3'UTR of respective genes.

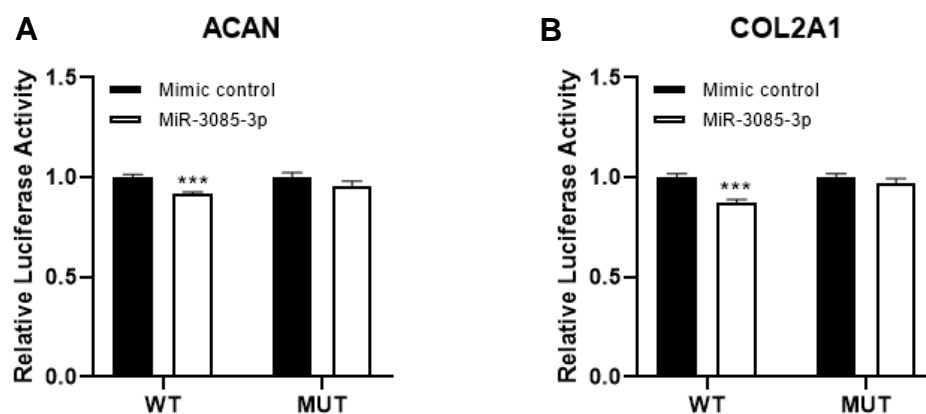


Figure 4.1 Luciferase assay of 3'utr constructs of ACAN and COL2A1. Relative luciferase activities were measured at 48 hours after SW1353 cells transfected with 50 $\mu$ M non-targeting miRNA control or miR-3085-3p mimic, followed by subsequent transfection of 100ng wild type (WT) or seed sites mutated (MUT) of ACAN (A) and COL2A1 (B). Luminescence was presented as the light units of Firefly luciferase normalized by those of Renilla luciferase. Statistical analysis between control group and mimic group was performed using unpaired Student's *t*-test. Mean of mimic control group was set as 1. Data were shown as mean  $\pm$  SEM,  $N=5$ . \*\*\*,  $P<0.001$ .

## 4.2.2 MicroRNA-3085-3p and NFκB signalling

MiR-3085-3p increased the expression of MMP13 mRNA induced by IL-1β for 8h in HACs (p=0.027) (Figure 4.2A), which was not in line with (230). Effects of miR-3085-3p in regulating IL-1β-induced MMP13 expression were therefore investigated in time course. MMP13 didn't significantly increase till later stimulation time points at 6h (p=0.042) and 9h (p=0.043) (Figure 4.2B).

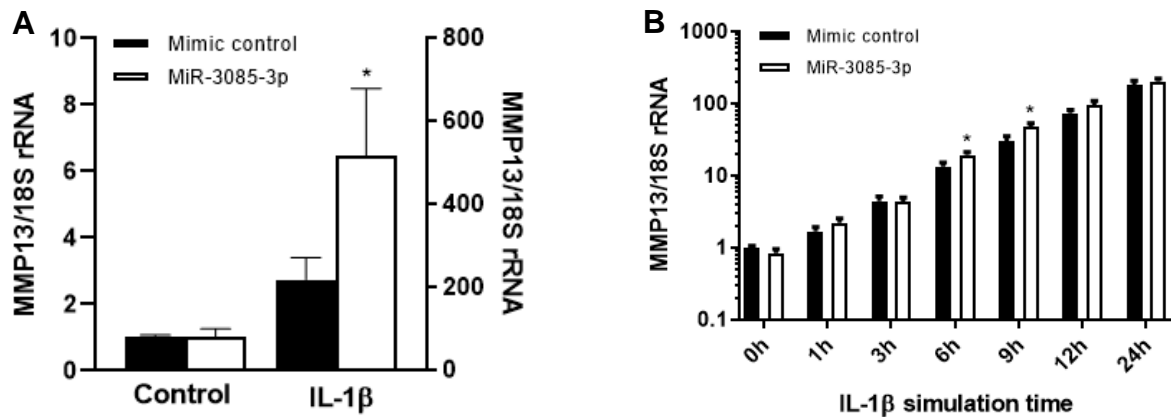
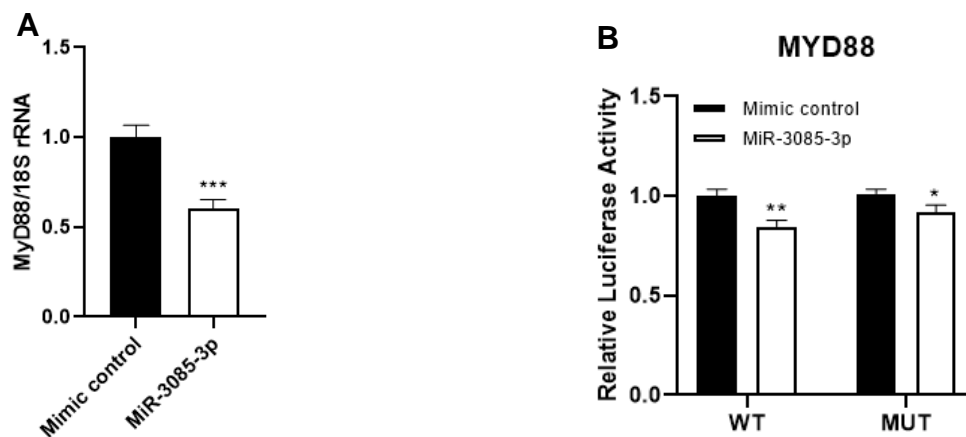


Figure 4.2 Regulation of miR-3085-3p in IL-1β-induced MMP13 in HACs. 50μM miR-3085-3p mimic or mimic control were transfected into HACs from 3 patients using lipofectamine 3000, followed by serum starvation for 24 hours and subsequent IL-1β stimulation at 5μg/L for 8 hours (A) and indicated stimulation time (B). RNAs were then extracted and reversely transcribed using Cell to cDNA kits. QRT-PCR were performed to detect the relative expression of MMP13 at indicated time points. Comparative Ct method was applied, and gene expression was normalized by 18S rRNA. Statistical analysis between control group and mimic group was performed using unpaired Student's t-test(A) and two-way ANOVA with Sidak's post hoc test (B). The mean of negative mimic control group was set as 1. Data were presented as mean ± SEM, N=3. \*, P<0.05.

It has been reported that MYD88, a universal adaptor for TLRs or IL-1R, mediates the activation of NF- $\kappa$ B (76, 231-234), and promote subsequent synthesis of MMP13 (92, 235). Besides, overexpression of miR-3085-3p repressed MYD88 mRNA in HACs ( $p < 0.0001$ ) (Figure 4.3A). Luciferase activity controlled by the 3'UTR of MYD88 was significantly reduced at the presence of miR-3085-3p ( $p = 0.0028$ ), but partial rescue was achieved by the mutation of seed sites of miR-3085-3p ( $p = 0.035$ ) (Figure 4.3B).



**Figure 4.3 Regulation of MYD88 by miR-3085-3p.** (A) 50 $\mu$ M miR-3085-3p mimic or mimic control were transfected into HACs from 3 patients using lipofectamine 3000 and incubated for 48 hours. RNAs were then extracted and reversely transcribed using Cell to cDNA kits. QRT-PCR were performed to detect the relative expression of MMP13. Comparative Ct method was applied, and gene expression was normalized by 18S rRNA. (B) Relative luciferase activities of 3'utr constructs of MYD88 were measured at 48 hours after SW1353 transfected with 100ng wild type (WT) or seed sites mutated (MUT) pmirGLO, following the transfection of 50 $\mu$ M non-targeting miRNA control or miR-3085-3p mimic. Luminescence was presented as the light units of Firefly luciferase normalized by those of Renilla luciferase. Statistical analysis between control group and mimic group was performed using unpaired Student's *t*-test. The mean of negative mimic control group was set as 1. Values were mean  $\pm$  SEM,  $N=3$ . \*,  $P < 0.05$ ; \*\*,  $P < 0.01$ ; \*\*\*,  $P < 0.001$ .

### 4.2.3 MicroRNA-3085-3p and TGF $\beta$ signalling

CAGA<sub>12</sub>-Luc reporter, a SMADs dependent responsive luciferase reporter, didn't show significant response to miR-3085-3p (Figure 4.4A). A few genes relevant to ECM such as COL1A2 (236), serpin family E member 1 (SERPINE1) (237), and TIMP metalloproteinase inhibitor 3 (TIMP3) (238) have been reported as inducible targets by TGF $\beta$ /SMAD cascades. Whereas expression of COL1A1 was not effectively stimulated by TGF $\beta$ 1 (data not shown). Seed sites of miR-3085-3p were found in the 3'UTR of both SERPINE1 and TIMP3, suggesting that they are potential direct targets of miR-3085-3p and not applicable to demonstrate the regulation of TGF $\beta$ /SMAD signalling pathway by miR-3085-3p. We therefore selected inhibitor of DNA binding 1, HLH protein (ID1) as a responsive gene of TGF $\beta$ /SMAD signalling (116, 239) in this study. As shown in Figure 4.4B, overexpression of miR-3085-3p reduced the expression of ID1 ( $p=0.0005$ ).

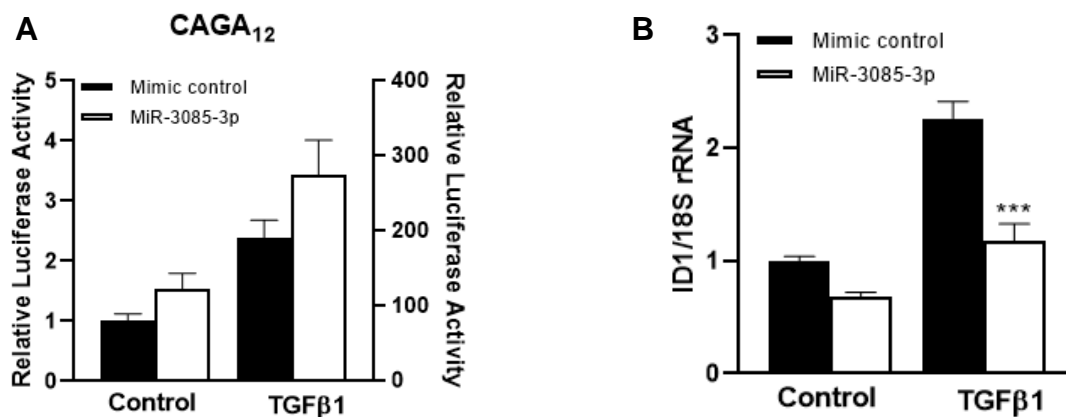


Figure 4.4 Regulation of TGF $\beta$ /SMAD signalling by miR-3085-3p. (A) Cotransfection of 100ng CAGA<sub>12</sub> luciferase reporter and 50 $\mu$ M miR-3085-3p mimic or control were performed in SW1353 and incubated for 24 hours, followed by 24-hour serum starvation and subsequently stimulated by TGF $\beta$ 1 at 4 $\mu$ g/L for 8 hours. Relative luciferase activity was measured and presented as the light units of Firefly luciferase normalized by those of Renilla luciferase. (B) 50 $\mu$ M miR-3085-3p mimic or mimic control were transfected into HACs and incubated for 824 hours, followed by 24-hour serum starvation and subsequent TGF $\beta$ 1 stimulation at 4 $\mu$ g/L for 8 hours. RNAs were then extracted and reversely transcribed. QRT-PCR were performed to detect the relative expression of ID1. Comparative Ct method was applied, and gene expression was normalized by 18S rRNA. Statistical analysis between control group and mimic group was performed using unpaired Student's t-test. The mean of negative mimic control group was set as 1. Data were shown as mean  $\pm$  SEM, N=3. \*\*\*,  $P<0.001$ .

In luciferase assays, 3'UTR constructs of SMAD2 ( $p < 0.0001$ ), SMAD3 ( $p < 0.0001$ ) and SMAD4 ( $p < 0.0001$ ) were all decreased by miR-3085-3p, and this was rescued by seed sites mutation in SMAD3 ( $p = 0.078$ ) and SMAD4 ( $p = 0.053$ ) except SMAD2 ( $p < 0.0001$ ) (Figure 4.5).

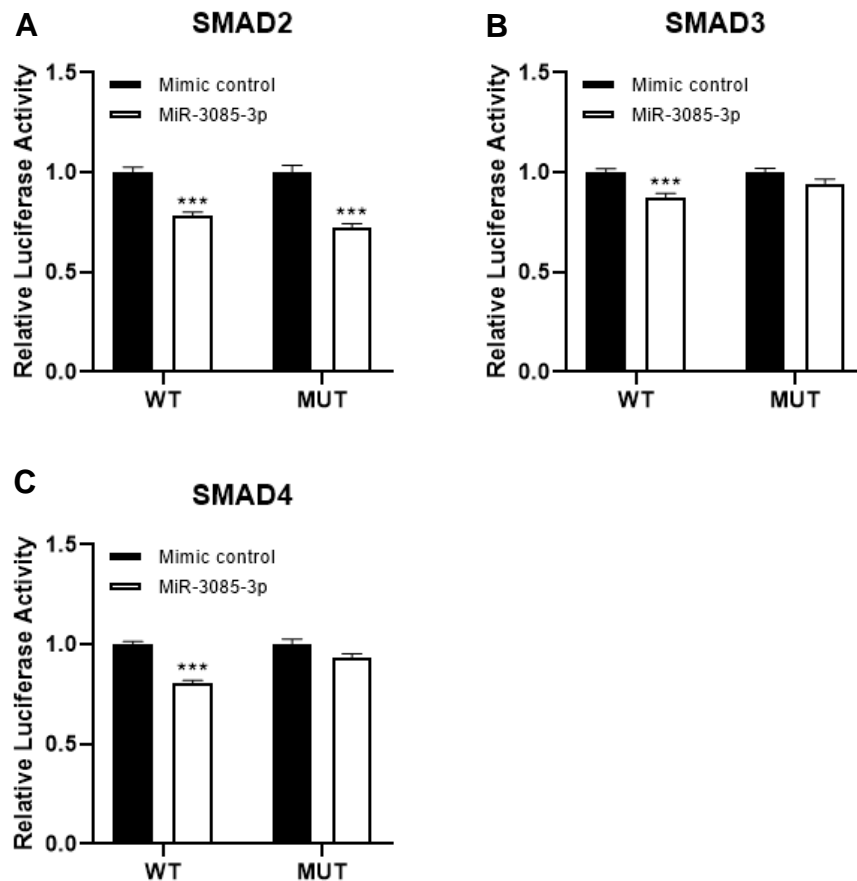


Figure 4.5 Regulation of miR-3085-3p on SMADs. Relative luciferase activities of 3'utr constructs of SMAD2 (A), SMAD3 (B) and SMAD4 (C) were measured at 48 hours after SW1353 cells transfected with 100ng wild type (WT) or seed sites mutated (MUT) pmirGLO reporters, following the transfection of 50  $\mu$ M non-targeting miRNA control or miR-3085-3p mimic. Luminescence was presented as the light units of Firefly luciferase normalized by those of Renilla luciferase. Statistical analysis between control group and mimic group was performed using unpaired Student's *t*-test. The mean of negative mimic control group was set as 1. Values were mean  $\pm$  SEM, N=3. \*\*\*,  $P < 0.001$ .

#### 4.2.4 MicroRNA-3085-3p and WNT signalling

MiR-3085-3p effectively increased the expression of WNT3A-induced AXIN2 ( $p=0.035$ ) (Figure 4.6B) as well as the luciferase activity of WNT3A-induced TOPFLASH reporter ( $p<0.0001$ ) (Figure 4.6A), showing a promotive effect in activating the canonical WNT signalling pathway.

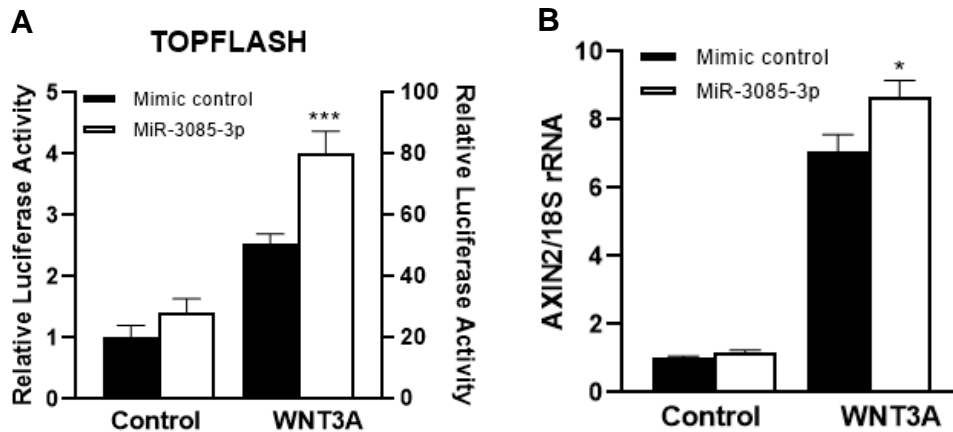


Figure 4.6 Regulation of miR-3085-3p on WNT3A signalling. (A) Cotransfection of 100ng TOPFLASH luciferase reporter and 50  $\mu$ M miR-3085-3p mimic or control were performed in SW1353 and incubated for 24 hours, followed by 24-hour serum starvation and subsequently stimulated by WNT3A at 100 $\mu$ g/l for 8 hours. Relative luciferase activity was measured and presented as the light units of Firefly luciferase normalized by those of Renilla luciferase. (B) 50  $\mu$ M miR-3085-3p mimic or mimic control were transfected into HACs and incubated for 824 hours, followed by 24-hour serum starvation and WNT3A stimulation at 100 $\mu$ g/l for 8 hours. RNAs were then extracted and reversely transcribed. QRT-PCR were performed to detect the relative expression of ID1. Comparative Ct method was applied, and gene expression was normalized by 18S rRNA. Statistical analysis between control group and mimic group was performed using unpaired Student's t-test. Mean of negative mimic control group was set as 1. Data were shown as mean  $\pm$  SEM, N=3. \*,  $P<0.05$ ; \*\*\*,  $P<0.001$ .

### 4.3 Discussion

ACAN and COL2A1 are predominantly expressed by chondrocytes and essential in maintaining normal structure and function of extracellular matrix in articular cartilage. In this project, miR-3085-3p were found to efficiently decrease the expression of both ACAN and COL2A1. These genes were further proved to be direct targets of miR-3085-3p, indicating that miR-3085-3p closely gets involved in the progress of cartilage degradation.

IL-1 $\beta$  is reported to initiate the activation of NF $\kappa$ B signalling pathway (240). Induction of NF $\kappa$ B signalling pathway triggers the production of matrix-degrading enzymes including MMPs and ADAMTs (81, 241). In our study, Dr Linh Le (230) revealed that IL-1 $\beta$  induced the expression of miR-3085-3p and this upregulation can be diminished by an NF $\kappa$ B inhibitor (JSH-23). In turn, miR-3085-3p induced the luciferase activity of NF $\kappa$ B reporter. Consistently, IL-1 $\beta$ -induced MMP13 was highly expressed at the presence of miR-3085-3p suggesting that miR-3085-3p interacts with NF $\kappa$ B signalling pathway. MYD88, known as a dependant adapter that mediates cytokines through Toll-like receptor and IL-1 receptor, can activate NF $\kappa$ B (76, 231-234) and lead to an increased expression of MMP13 in chondrocytes (92, 235), and it is also predicted to be a target gene of miR-3085-3p. We thereby explored miR-3085-3p's effects on the MyD88-dependant NF $\kappa$ B pathway. Our results demonstrated a negative regulation of miR-3085-3p in the expression of MYD88 at both mRNA and protein level. Taking together with Dr Linh Le's western blots where nuclear phospho-p65 and p65 were decreased by miR-3085-3p for 30min IL-1 $\beta$  induction (230), we deduce that miR-3085-3p transiently hampers NF $\kappa$ B signalling pathway by directly repressing MYD88 at early time point. This repression then subsides and is overcome by other miR-3085-3p regulating mechanism, contributing to the subsequent activation of NF $\kappa$ B signalling.

TGF $\beta$ /SMAD signalling is also a key pathway involved in osteoarthritis development and progression (119, 242). Our data showed that miR-3085-3p decreased ID1 which acts as a TGF $\beta$  signalling responsive gene (243), though exerted no significant influence on the SMAD dependant reporter. Previous study reported transiently transfected MMP13-promoter reporter did not show the IL-1-induced activity consistent with the responsive genes, where stably transfected promoter showed

strongly inducible activity (244). In consistence, our SMAD-responsive reporter didn't demonstrate TGF $\beta$  induced activity, suggesting that a stable integration into DNA might be needed to observe TGF $\beta$  signalling. Furthermore, SMAD2, SMAD3 and SMAD4, acting as central nodes of TGF $\beta$  signalling, were all downregulated by miR-3085-3p. MiR-3085-3p has an overall inhibition of TGF $\beta$ /SMAD signalling pathway.

Canonical WNT/ $\beta$ -catenin signalling is another crucial pathway that tightly modulates the homeostasis and degeneration of articular cartilage (105, 245, 246). MiR-3085-3p demonstrated a further upregulation of the canonical WNT target gene AXIN2 as well as the induction of WNT3A-induced TOPFLASH reporter. On contrary, miR-3085-3p overexpression decreased both WNT3A-induced  $\beta$ -catenin and phospho- $\beta$ -catenin protein at 30 minutes (data not shown). This could be explained by the fact that miR-3085-3p targeted seed site are held in the 3'UTR of one of its transcript variants (NCBI Reference Sequence: NM\_001330729.2, Ensemble transcript ID: ENST00000349496.11), so that translation for  $\beta$ -catenin is likely to be suppressed by miR-3085-3p resulting in a decrease in both basal and phosphorylated  $\beta$ -catenin protein at early stage of WNT3A stimulation. Subsequently, this reduction is possibly compensated by the expression of other transcript variants. This inference is needed to be further verified through detection of the WNT-induced  $\beta$ -catenin in time course. In addition to the canonical WNT signalling pathway, the non-canonical WNT signalling pathway also closely participate in the development and progression of OA (104, 110-112, 157). Several studies have reported that WNT3A was capable of inducing both canonical and the Ca<sup>2+</sup>/CAMKII non-canonical WNT signalling pathways (247-249). It is speculated that miR-3085-3p could repress the non-canonical WNT signalling which gives rise to the relatively upregulated canonical WNT/ $\beta$ -catenin signalling by WNT3A.

In summary, some potential interaction of miR-3085-3p with predominant signalling pathways related to chondrocyte functions were investigated in our study. Our data reveal that miR-3085-3p could effectively decrease the expression of chondrocyte marker, ACAN and COL2A1. This microRNA leads to a comprehensive dynamic regulation of NF $\kappa$ B signalling and WNT signalling, and repression of TGF $\beta$ /SMAD signalling. These strongly suggest that miR-3085-3p is closely involved in the regulation of cartilage homeostasis, chondrocyte function and progression of osteoarthritis.

# Chapter 5 Exploring effects of miR-3085-3p on human bone marrow mesenchymal stem cell differentiation

## 5.1 Introduction

Mesenchymal stem cells (MSCs) are stromal cells that have capacity of self-renewal and multiple differentiation. Experiencing proliferation, commitment, MSCs can differentiate into chondrocytes, osteoblasts, adipocytes and so on, and further generate tissues such as cartilage, bone, adipose. What's interesting, In fact, many of the biologic changes that occur during the development and progression of OA mimic a differentiation pattern characteristic of fetal skeletogenesis (250, 251). This includes changes not only in cellular phenotypes and in anabolic and catabolic events but also in other basic mechanisms such as matrix calcification, apoptosis, and proliferation. But just as in a jigsaw puzzle, the assembly is the challenge. Identification of marker genes and mechanisms during chondrogenesis as well as skeletal development may contribute to the molecular context and cellular behaviour in osteoarthritic chondrocytes (252, 253).

MiR-3085-3p has shown a cartilage-specific expression pattern (206). In chapter 4, functions of miR-3075-3p were explored. It showed that miR-3085-3p effectively suppressed the expression of extracellular matrix genes. MiR-3085-3p also induced the IL-1/NF $\kappa$ B signalling and WNT signalling, inhibited TGF $\beta$ /SMAD signalling, strongly suggesting that it participates in the regulation of chondrocyte function and OA progression. However, roles of miR-3085-3p during the process of skeletal development as well as cartilage generation and degradation have not been defined. Taking advantage of the potential of self-renewal and plural differentiation of human MSCs, biological functions and mechanisms of miR-3085-3p during chondrogenesis, osteogenesis and adipogenesis were investigated.

## 5.2 Results

### 5.2.1 Differential expression of miR-3085-3p during human BMMSC differentiation.

Human bone marrow mesenchymal stem cells (hBMMSCs) were differentiated to chondrocytes (14 days), adipocytes (14 days) or osteoblasts (4 days) and expression levels of miR-3085-3p measured. There was an overall increase during adipogenesis with fluctuation at day 7 and day 14. Human MSCs had a dramatic decrease of miR-3085-3p in the very beginning of osteogenic induction. MiR-3085-3p slightly increased in the late stage of chondrogenesis from day 7 but not significantly. (Figure 5.1)

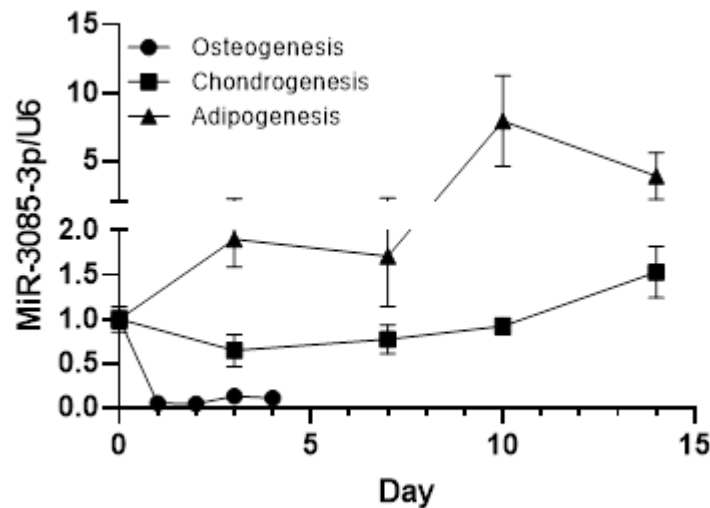


Figure 5.1 The relative expression of miR-3085-3p during human MSC differentiation. MiR-3085-3p expression was normalized to U6 snRNA, and the mean of that at day 0 was set as 1 in osteogenesis, chondrogenesis and adipogenesis, respectively. MiRNAs at desired time points were extracted from MSCs of 3 donors, followed by MiRCURY LNA Universal cDNA synthesis and qRT-PCR. Data show Mean  $\pm$  SEM, N=3.

## 5.2.2 MiR-3085-3p suppresses human BMMSC chondrogenesis.

Marker genes, ACAN, COL2A1, COL10A1 and SOX9 for chondrocytes were detected using qRT-PCR. As shown in Figure 5.2, all markers increased over time, indicating hBMMSCs were induced to chondrogenic differentiation successfully.

In order to explore the impact of miR-3085-3p on chondrogenesis, a mimic of miR-3085-3p in parallel with a negative control was transiently transfected into hBMMSCs using Lipofectamine 3000 prior to the induction of differentiation. Compared with negative control, overexpression of miR-3085-3p predominantly downregulated ACAN ( $p=0.027$ ) (Figure 5.3A) until day 3, COL2A1 (Figure 5.3B) from day 10 (day 10,  $p=0.015$ ; day 14,  $p=0.006$ ), COL10A1 (Figure 5.3C) and SOX9 (Figure 5.3D) at day 3 (COL10A1,  $p=0.0098$ ; SOX9,  $p=0.037$ ) and day 14 (COL10A1,  $p=0.024$ ; SOX9,  $p=0.035$ ). Nonetheless, miR-3085-3p inhibitor exerted no significant effect on chondrogenesis. (Figure 5.4)

GAG assay for sulphated glycosaminoglycans quantification demonstrated a decrease in the level of GAGs in the presence of miR-3085-3p mimic at day 3 ( $p=0.0068$ ) (Figure 5.5A), but no significant effect from inhibitor on chondrogenesis was observed (Figure 5.5B). This was in line with the morphology of Alcian Blue stained chondrogenic pellets. After transfection with mimic, differentiated cells had delayed spheroid formation with obviously rough and less compact outer edge until day 2, which recovered at day 3. (Figure 5.6)

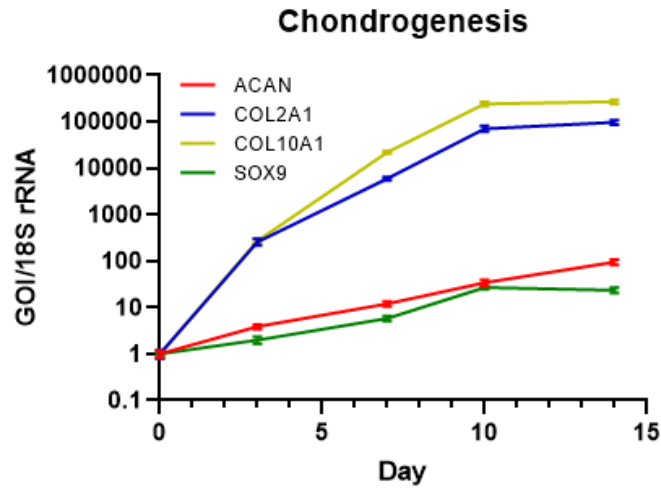


Figure 5.2 Expression of marker genes for chondrocytes during chondrogenesis. RNAs were extracted from MSCs of 3 donors and reverse transcribed via Cells to cDNA at indicated time points. Expression of ACAN, COL2A1, COL10A1 and SOX9 were measured by qRT-PCR. Gene expression was normalized by 18S rRNA, and the mean at day 0 was set as 1 to necessitate the combination of data from different donors. Values show mean  $\pm$  SEM, N=3.

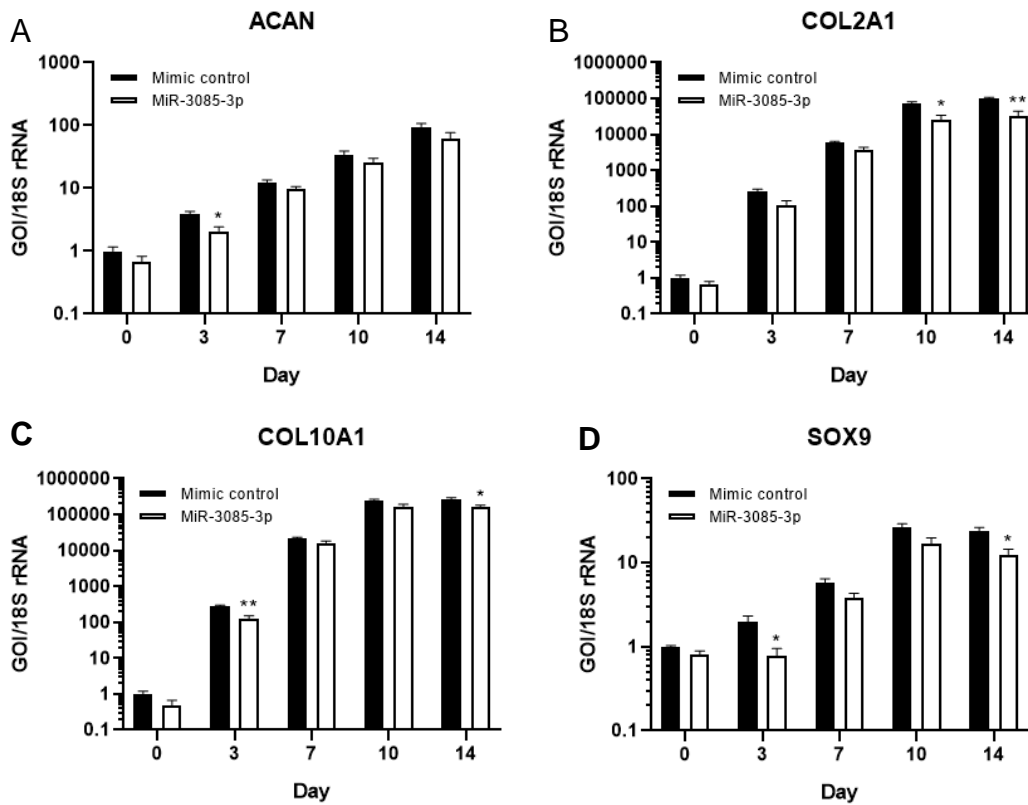


Figure 5.3 Regulation of marker genes by miR-3085-3p mimic throughout chondrogenesis. MSCs from 3 donor were transiently transfected with miR-3085-3p mimic (100  $\mu$ M) or inhibitor control prior to chondrogenic differentiation. RNAs were extracted and reverse transcribed via Cells to cDNA method at desired time points, detected by qRT-PCR. Gene expression was normalized by 18S rRNA. Mean at day 0 was set as 1. Statistical analysis between control group and mimic group was performed using two-way ANOVA with Sidak's post hoc test. Data are presented as mean  $\pm$  SEM, N=3. \*,  $P < 0.05$ ; \*\*,  $P < 0.01$ .

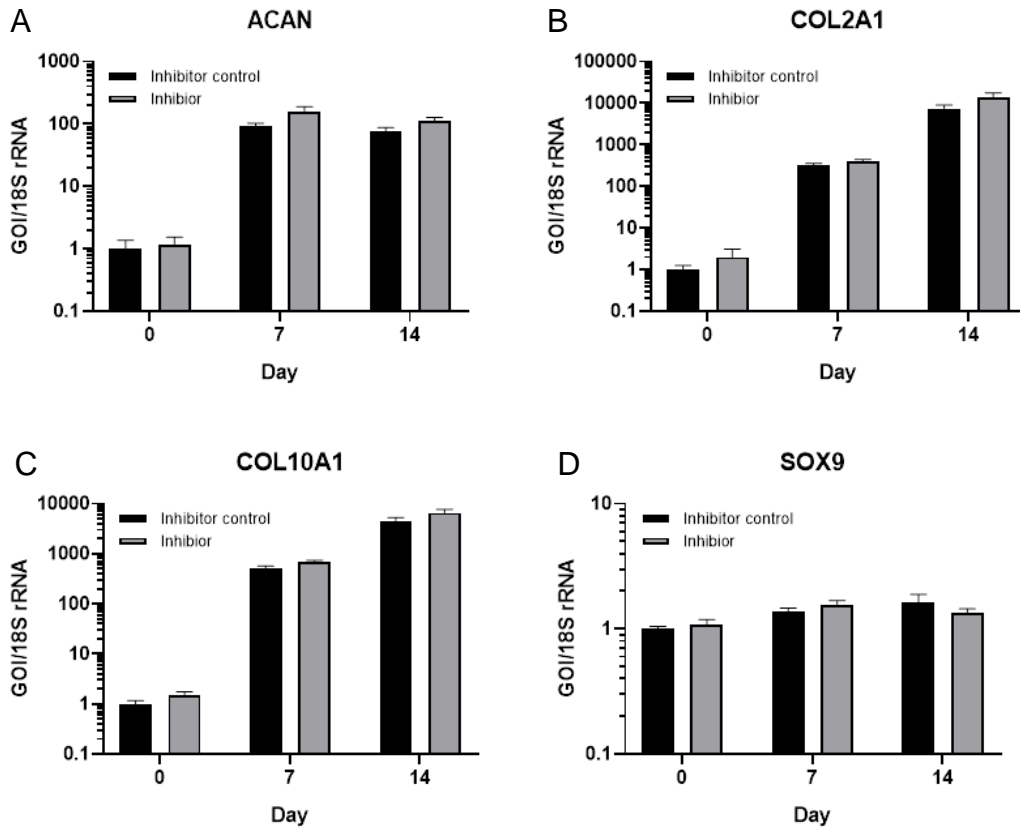


Figure 5.4 Regulation of marker genes by miR-3085-3p inhibitor throughout chondrogenesis. MSCs from 3 donor were transiently transfected with miR-3085-3p inhibitor (50  $\mu$ M) or inhibitor control prior to chondrogenic differentiation. RNAs were extracted and reverse transcribed via Cells to cDNA method at desired time points, detected by qRT-PCR. Gene expression was normalized by 18S rRNA. Statistical analysis between control group and inhibitor group was performed using two-way ANOVA with Sidak's post hoc test. Mean at day 0 was set as 1. Data are presented as mean  $\pm$  SEM, N=3.

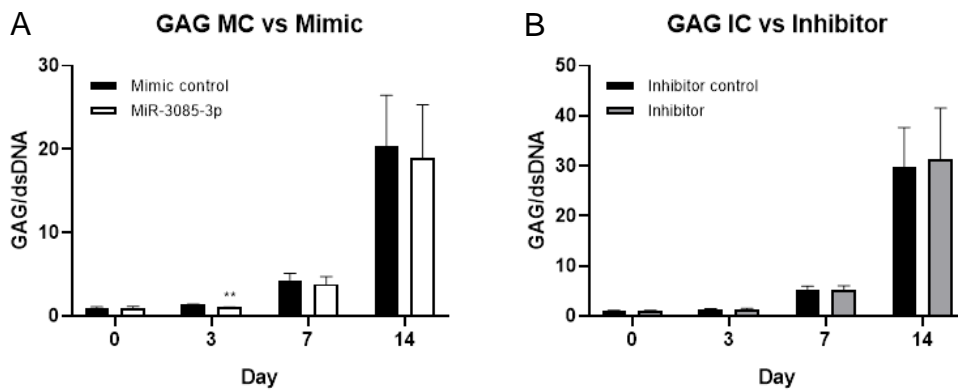


Figure 5.5 Sulphated glycosaminoglycans contents of chondrogenic pellets. MSCs were transfected with miR-3085-3p mimic (A) or inhibitor (B) versus negative controls, and then induced into chondrogenesis. Chondrogenic pellets were papain-digested and assessed by DMMB assay. Concentrations of GAG were normalized to those of dsDNAs. Statistical analysis between control group and mimic/inhibitor group was performed using two-way ANOVA with Sidak's post hoc test. Values are mean  $\pm$  SEM, N=3. \*\*,  $P < 0.01$ .

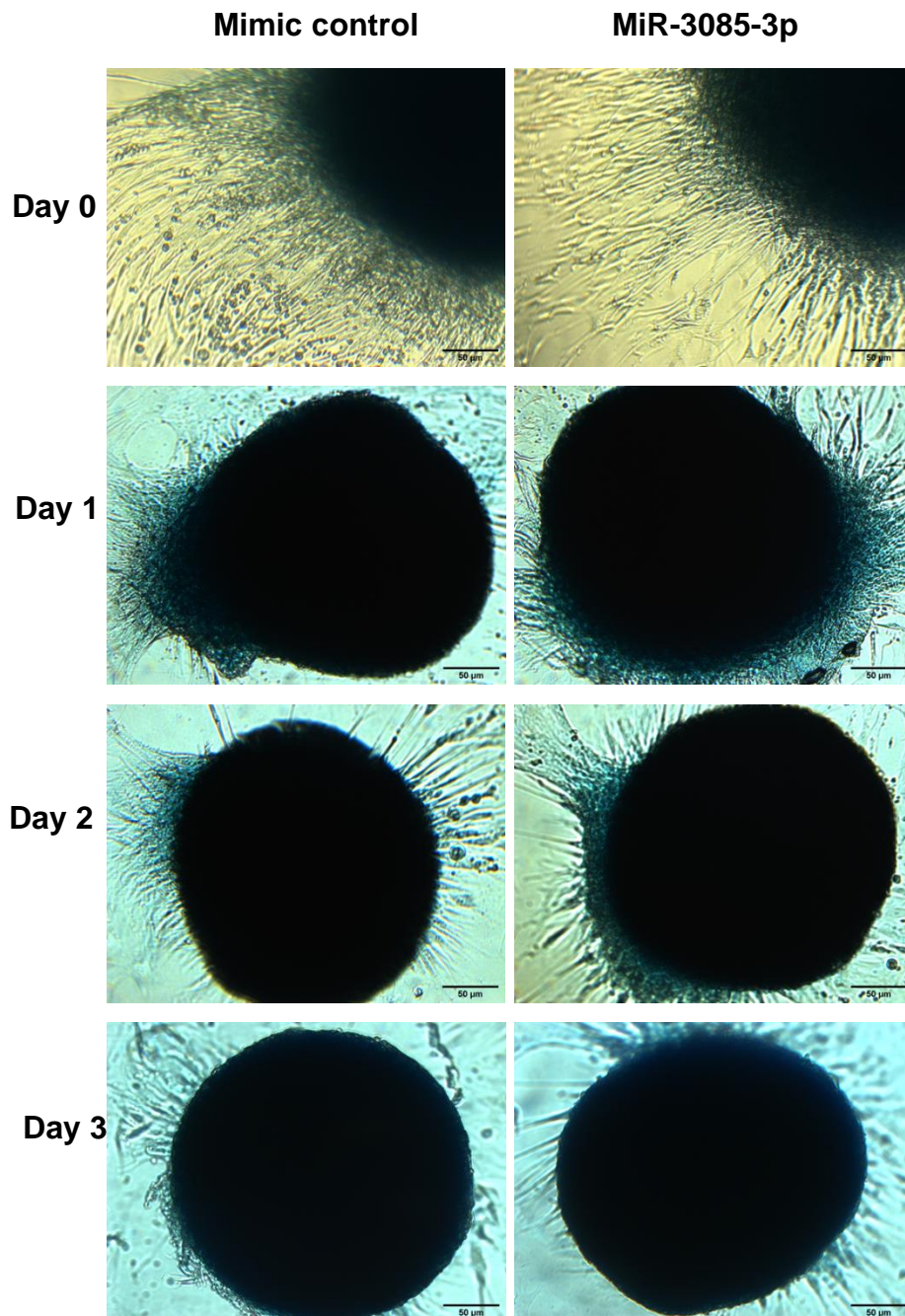


Figure 5.6 Representative chondrogenic pellets stained with Alcian Blue. At day 0, 1, 2 and 3 of chondrogenesis, chondrogenic pellets were harvested, fixed and stained with Alcian Blue. Pictures show representative stained pellets transfected with miR-3085-3p mimic (right column) or mimic control (left column) at indicated time points. Scale bar = 50 $\mu$ m.

### **5.2.3 JUN and FOS are potential target genes of miR-3085-3p in human chondrocytes.**

By comparing gene (mRNA) expression levels from a microarray dataset where the mRNA expression changes at day 0 and day 14 of hBMMSC chondrogenesis were annotated, (kindly given by Dr Matt Barter in Newcastle University), and a microarray dataset where either miR-3085-3p mimic or inhibitor against negative controls were transfected in human primary articular chondrocytes (HACs), potential target genes of miR-3085-3p were identified. Firstly, three criteria were taken into consideration, where a gene was (1) downregulated by miR-3085-3p mimic, (2) upregulated by inhibitor and (3) altered during chondrogenesis. Among increased genes across chondrogenesis, there were 1508 downregulated by mimic only, 1149 upregulated by inhibitor only, 1149 simultaneously downregulated by mimic and upregulated by inhibitor. In contrast, among decreased genes during chondrogenesis, 1596 were downregulated by mimic only, 1329 were increased by inhibitor only, and 1278 were both downregulated by mimic and upregulated by inhibitor (Figure 5.7A). Overlapped genes which ranked in the top 20 of each criterion and held at least one of four common types of miR-3085-3p seed sequences (6mer: AGCCAG; 7merA1: AGCCAGA; 7mer8: CAGCCAG; 8mer:CAGCCAGA) within the 3'UTR (254) were regarded as candidate targets and passed onto subsequent experimental validation (Figure 5.7B and Table 5.1).

To validate the selected genes experimentally, qRT-PCR was firstly performed using HACs. Figure 5.8 demonstrated that the expression of JUN ( $p=0.0025$ ;  $p<0.0001$ ), FOS ( $p=0.021$ ;  $p=0.0002$ ) and KLF6 ( $p=0.0024$ ;  $p=0.0059$ ) were decreased by miR-3085-3p mimic and increased by inhibitor, compared with negative controls. It is known that JUN could interact with FOS through leucine zipper to form the heterodimeric AP-1 (activator protein-1) transcription factor complex which binds to the TPA responsive element of target genes including MMP1, MMP2, MMP9, and MMP13 (255-259). Kruppel like factor 6 (KLF6) is a zinc finger transcription factor that regulates its target genes through the combination with GC box (260). KLF6 has been found reduced or mutated in various carcinomas and acts as a tumour suppressor by participating in cell proliferation inhibition and apoptosis induction (261, 262).

SCIN ( $p=0.0011$ ), EFNA1 ( $p<0.0001$ ), CHST3 ( $p<0.0001$ ) and PLEKHF1 ( $p=0.011$ ) were decreased by mimic only but did not significantly alter in the presence of miR-3085-3p inhibitor (Figure 5.9). Scinderin (SCIN) is a  $Ca^{2+}$ -dependent filamentous actin (F-actin) cleavage protein, firstly found in chromaffin cells (263). It takes an important part in regulating cytoskeleton remodelling, thereby effecting cells migration and movement (264). Ephrin A1 (EFNA1) belongs to a Eph family receptors interacting proteins which are ligands for erythropoietin producing human hepatocellular carcinoma receptors (Eph receptors) (265). EFNA1 was discovered to bind to extracellular ligand binding domain of EphA2 and then activate tyrosine kinases, leading to the autophosphorylation and the phosphorylation of downstream molecules, hereby initiating growth, migration and differentiation of tumour cells (265, 266). Carbohydrate Sulfotransferase 3 (CHST3) transfers the sulphate in 3'-phosphoadenosine 5'-phosphosulfate (PAPS) to the sulphation sites of chondroitin sulphate (CS), specifically the position 6 of N-acetylgalactosamine (GalNAc) residue (267). The catalysis of CHST3 on CS sulfation significantly affects the development and function of cartilage. Clinic studies have reported that the mutation of CHST3 gene can cause a variety of skeletal recessive genetic diseases including chondrodysplasia (268), humerospinal dysostosis (269), and Spondyloepiphyseal dysplasia (270, 271). Pleckstrin homology and FYVE domain containing 1 (PLEKHF1) is a lysosomal-related apoptosis-inducing protein, which can recruit phospho-p53 to lysosome and initiate the caspase-independent apoptosis (272, 273).

ACAN ( $p<0.001$ ;  $p=0.016$ ), TGFBR3 ( $p=0.001$ ;  $p=0.0005$ ), SCARA3 ( $p<0.0001$ ;  $p<0.0001$ ), DAB2 ( $p=0.0012$ ;  $p<0.0001$ ), CD248 ( $p=0.0003$ ;  $p=0.0065$ ) and RAB3IL1 ( $p=0.0016$ ;  $p<0.0001$ ) were downregulated by both miR-3085-3p mimic and inhibitor (Figure 5.10). ACAN is the predominant component of cartilage ECM (18, 19). TGF $\beta$  receptor 3 (TGFBR3) together with TGFBR1 and TGFBR2 compose the TGF $\beta$  receptor family, playing an essential role in the TGF $\beta$  signal transduction (274). Scavenger receptor class A member 3 (SCARA3) are mainly expressed on the plasma membrane and endoplasmic reticulum membrane, which can be upregulated in response to cellular stress such as UV radiation and reactive oxygen species (275). SCARA3 was reduced in prostate cancer (276) and associated with adipogenesis in metabolic disorders (277). Disabled homolog 2 adapter protein (DAB2) is known as a

tumour suppressor, the downregulation of which has been widely observed in ovarian (278), colorectal (279), prostate (280), esophageal squamous (281), bladder (282) cancer cells and so on. It has been demonstrated that DAB2 negatively modulates WNT/ $\beta$ -catenin signalling (283), NF $\kappa$ B signalling (284), and TGF $\beta$  signalling (285) pathways. CD248 is one cell surface transmembrane glycoprotein that was identified in perivascular and fibroblast-like synovial cells (286, 287). In vivo study reported that, in collagen antibody induced arthritis, the CD248 knockout mice presented less severe arthritis characterized by suppressed synovial hyperplasia, reduced leukocyte influx and decreased cytokines in the inflamed synovium, suggesting that CD248 is a putative target in alleviating inflammation in rheumatoid arthritis and psoriatic arthritis (288). RAB3A interacting protein like 1 (RAB3IL1), also known as guanine nucleotide exchange factor for Rab3A (GRAB), can catalyse the exchange of GTP to GDP on Ras-related protein RAB3A, thereby taking part in exocytosis and secretion (289).

To further validate whether JUN and FOS are direct target of miR-3085-3p, luciferase reporters with the wild type and mutated 3'UTR of c-JUN and c-FOS respectively were constructed. All seed sites of miR-3085-3p within the inserted 3'UTR were mutated into desired restriction enzyme sites in the mutated 3'UTR constructs. MiR-3085-3p reduced the relative luciferase activity controlled by 3'UTR of JUN and FOS, however, this suppression was not rescued by the mutation of seed sites (Figure 5.11) and so these do not appear to be direct targets for miR-3085-3p.

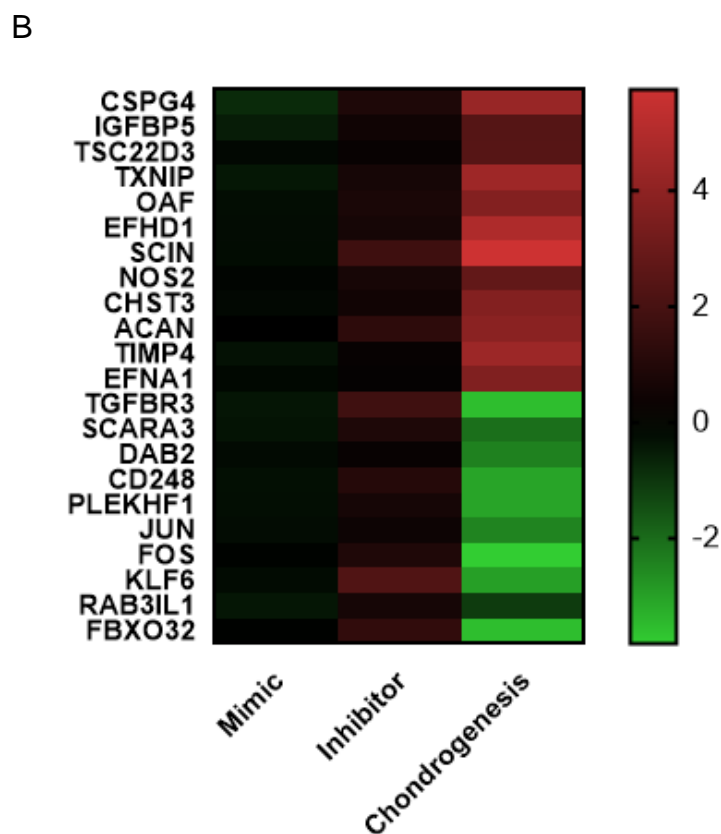
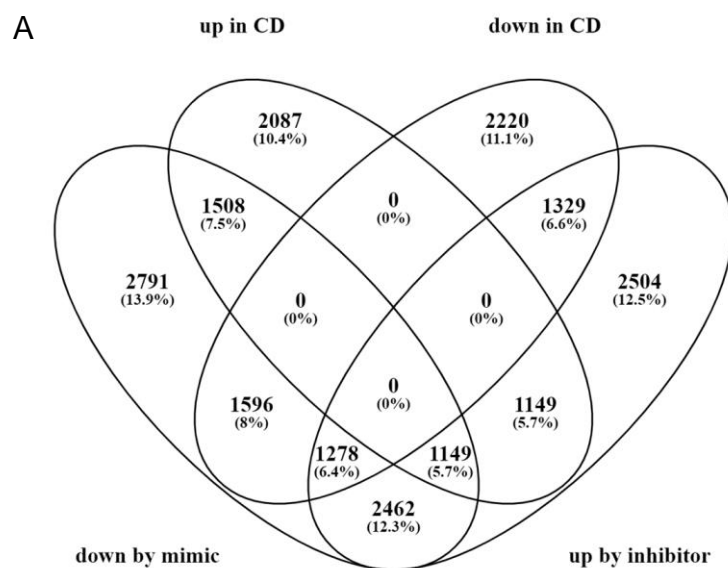


Figure 5.7 Profile of candidate target genes of miR-3085-3p during chondrogenesis. Based on the comparison of chondrogenesis microarray dataset and HAC microarray dataset, (A) a Venn diagram demonstrates the summary of differential expressed genes that changed during chondrogenesis, decreased with miR-3085-3p mimic and/or increased with inhibitor. (B) Heat map represents the  $\log_{10}(\text{fold change})$  of top candidate targets regulated by miR-3085-3p mimic and/or inhibitor against negative control during chondrogenesis. CD, chondrogenic differentiation.

Table 5.1 Summary of seed sites of miR-3085-3p seating within the 3'UTR of candidate target genes during chondrogenesis.

Gene symbol	Gene name	Seed site of miR-3085-3p				
		6mer	7mer-m8	7mer-A1	8mer	Total
<b>CSPG4</b>	chondroitin sulphate proteoglycan 4	1	2	0	0	3
<b>IGFBP5</b>	insulin like growth factor binding protein 5	4	4	1	1	10
<b>TSC22D3</b>	TSC22 domain family member 3	1	0	0	0	1
<b>TXNIP</b>	thioredoxin interacting protein	0	1	0	1	2
<b>OAF</b>	out at first homolog	2	0	0	0	2
<b>EFHD1</b>	EF-hand domain family member D1	2	0	1	0	3
<b>SCIN</b>	scinderin	1	0	0	0	1
<b>NOS2</b>	nitric oxide synthase 2	1	0	0	0	1
<b>CHST3</b>	carbohydrate sulfotransferase 3	1	4	1	1	7
<b>ACAN</b>	aggrecan	1	0	0	0	1
<b>TIMP4</b>	TIMP metalloproteinase inhibitor 4	0	1	0	1	2
<b>EFNA1</b>	ephrin A1	0	1	0	1	2
<b>TGFBR3</b>	transforming growth factor beta receptor 3	0	0	2	0	2
<b>SCARA3</b>	cavenger receptor class A member 3	1	0	0	0	1
<b>DAB2</b>	DAB adaptor protein 2	0	0	1	0	1
<b>CD248</b>	CD248 molecule	0	1	0	0	1
<b>PLEKHF1</b>	pleckstrin homology and FYVE domain containing 1	1	0	0	1	2

<b>JUN</b>	Jun proto-oncogene, AP-1 transcription factor subunit	1	0	0	0	1
<b>FOS</b>	Fos proto-oncogene, AP-1 transcription factor subunit	1	0	0	0	1
<b>KLF6</b>	Kruppel like factor 6	1	1	0	0	2
<b>RAB3IL1</b>	RAB3A interacting protein like 1	2	1	1	0	4
<b>FBXO32</b>	F-box protein 32	0	1	0	0	1

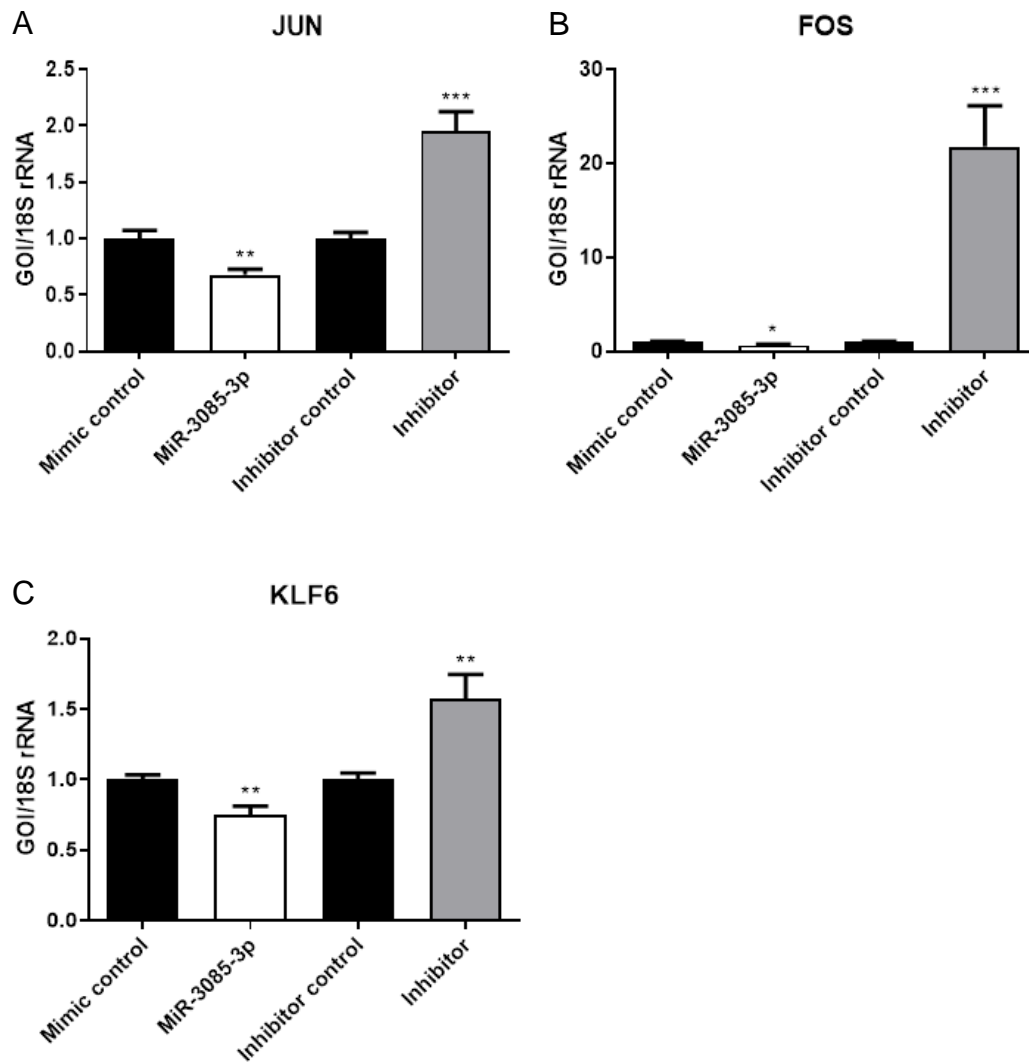


Figure 5.8 Expression of candidate genes of miR-3085-3p that downregulated by mimic and upregulated by inhibitor in HACs. MiR-3085-3p mimic (50  $\mu$ M) or inhibitor (25  $\mu$ M) were transfected into HACs from 3 patients using lipofectamine 3000 and incubated for 48 hours, RNAs were then extracted and reversely transcribed using Cell to cDNA kits. JUN (A), FOS (B) and KLF6 (C) were validated by qRT-PCR. Comparative Ct method was applied, and gene expression was normalized by 18S rRNA. Statistical analysis between control group and mimic/inhibitor group was performed using unpaired Student's t-test. The mean of respective negative control group was set as 1. Values are mean  $\pm$  SEM, N=3. \*,  $P < 0.05$ ; \*\*,  $P < 0.01$ ; \*\*\*,  $P < 0.001$ .

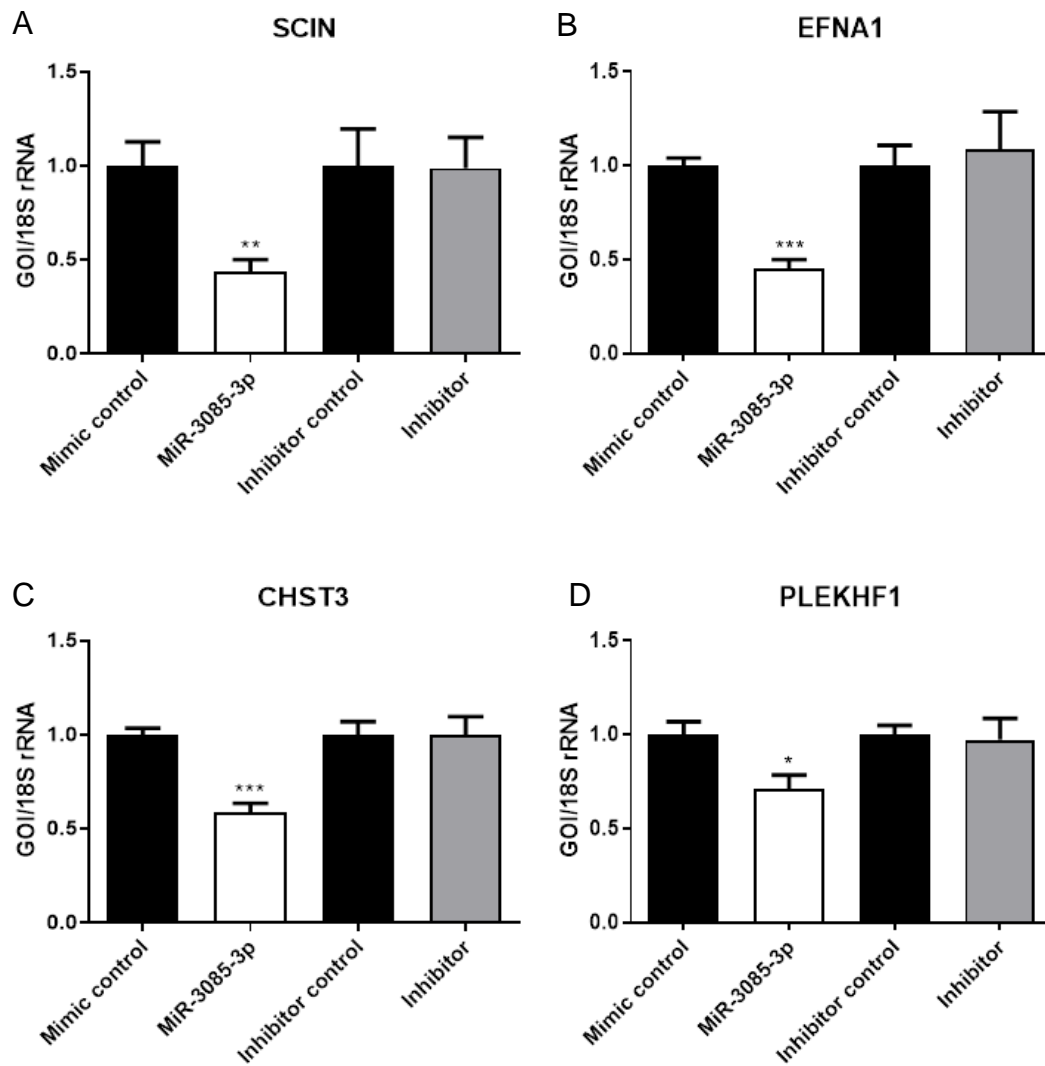


Figure 5.9 Expression of candidate genes of miR-3085-3p that downregulated by mimic alone in HACs. MiR-3085-3p mimic (50  $\mu$ m) or inhibitor (25  $\mu$ m) were transfected into HACs from 3 patients using lipofectamine 3000 and incubated for 48 hours, RNAs were then extracted and reversely transcribed using Cell to cDNA kits. SCIN (A), EFNA1 (B), CHST3 (C) and OLEKHF1 (D) were validated by qRT-PCR. Comparative Ct method was applied, and gene expression was normalized by 18S rRNA. Statistical analysis between control group and mimic/inhibitor group was performed using unpaired Student's *t*-test. The mean of respective negative control group was set as 1. Values are mean  $\pm$  SEM, N=3. \*, *P*<0.05; \*\*, *P*<0.01; \*\*\*, *P*<0.001.

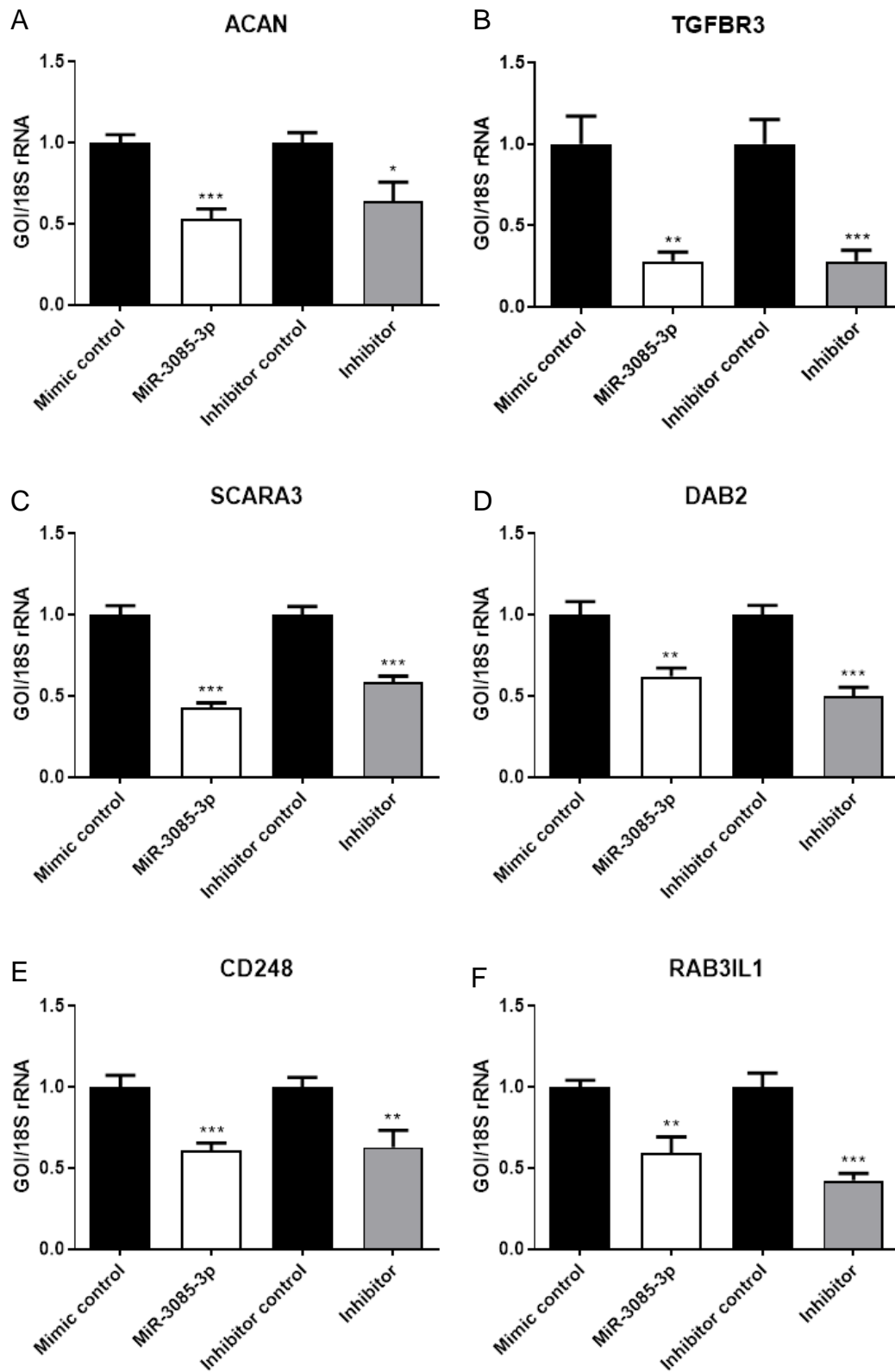


Figure 5.10 Expression of candidate genes of miR-3085-3p that downregulated by both mimic and inhibitor in HACs. ACAN (A), TGFBR3 (B), SCARA3 (C), DAB2 (D), CD248 (E), and RAB3IL1 (F) were validated by qRT-PCR. Comparative Ct method was applied, and gene expression was normalized by 18S rRNA. Statistical analysis between control group and mimic/inhibitor group was performed using unpaired Student's t-test. The mean of respective negative control group was set as 1. Values are mean  $\pm$  SEM, N=3. \*, P<0.05; \*\*, P<0.01; \*\*\*, P<0.001.

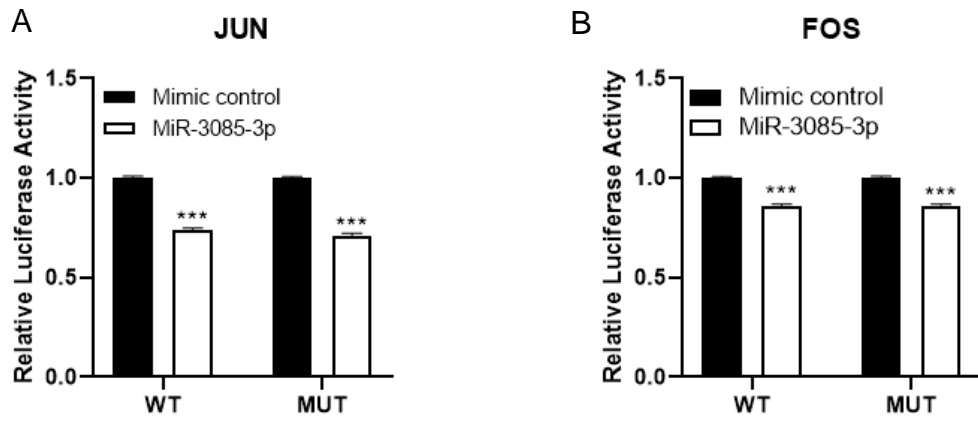


Figure 5.11 Luciferase assay of 3'utr constructs of JUN and FOS. Relative luciferase activities were measured at 48 hours after SW1353 cells transfected with 100 ng wild type (WT) or seed sites mutated (MUT) pmir-GLO plasmid (3'UTR constructs) of JUN (A) and FOS (B), followed by subsequent transfection of 50  $\mu$ M non-targeting miRNA control or miR-3085-3p mimic. Luminescence was presented as the light units of Firefly luciferase normalized by those of Renilla luciferase. Statistical analysis between control group and mimic group was performed using unpaired Student's *t*-test. Mean of mimic control groups was set at 1. Data were shown as mean  $\pm$  SEM, N=3. \*\*\*, *P*<0.001

#### **5.2.4 MiR-3085-3p contributes to IL-1 $\beta$ -induced MMP-13 expression by activating JNK/AP-1 pathway.**

AP-1 binding site has been identified in the promotor region of MMP13 gene, suggesting its role in modulation the expression of MMP13 (257, 290). One major upstream signal transductor of AP-1 is JNK, involved in the mitogen-activated protein kinase (MAPK) signalling cassettes (291). We therefore verified that the regulation of MMP13 by JUN/FOS. In a time course in response to IL-1 $\beta$ , both JUN and FOS were upregulated by miR-3085-3p in the first hour after stimulation and descended afterwards (Figure 5.12A and B), whilst MMP13 significantly increased at later time points at 6 hours and 9 hours (Figure 5.12C). Western blot revealed that IL-1 $\beta$  triggered a transient increase of phospho-JNK at 30 minutes after stimulation. In parallel, overexpression of miR-3085-3p reduced the IL-1 induced phosphor-JNK at 30 minutes but increased that at 1 hour. (Figure 5.12D).

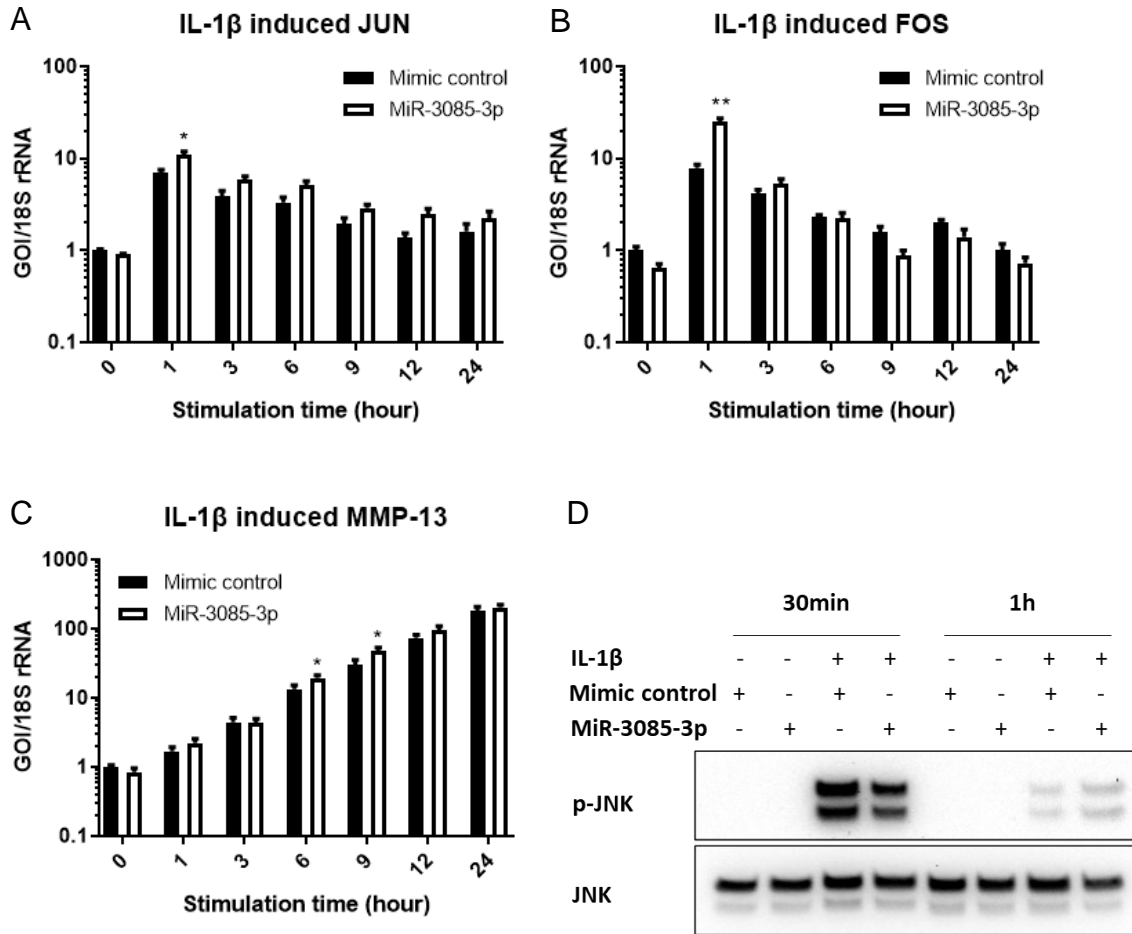


Figure 5.12 Time course of IL-1 induced JUN, FOS and MMP-13 mRNA expression and JNK protein level in HACs. 50 $\mu$ M miR-3085-3p mimic or mimic control were transfected into HACs from 3 patients using lipofectamine 3000 and incubated for 24 hours, followed by IL-1 $\beta$  stimulation at 5 $\mu$ g/l and incubation for 48 hours. RNAs were then extracted and reversely transcribed using Cell to cDNA kits. QRT-PCR were performed to detect the relative expression of JUN (A), FOS (B) and MMP-13 (C) at indicated time points. Comparative Ct method was applied, and gene expression was normalized by 18S rRNA. Statistical analysis between control group and mimic group was performed using two-way ANOVA with Sidak's post hoc test. The mean of negative control group at day 0 was set as 1. Values are mean  $\pm$  SEM, N=3. \*, P<0.05. (D) Representative Western blot of whole cell extracts from HACs demonstrated phospho-JNK and JNK protein expression at 30 minutes and 1 hour after IL-1 $\beta$  stimulation.

### 5.2.5 MiR-3085-3p inhibits human BMMSC adipogenesis.

To confirm the induction of hBMMSC through adipogenesis, CCAAT enhancer-binding protein  $\alpha$  (CEBP $\alpha$ ) and peroxisome proliferator activated receptor  $\gamma$  (PPAR $\gamma$ ), marker genes for adipocytes were measured by qRT-PCR (Figure 5.13). MiR-3085-3p repressed both markers all over the process (Figure 5.14A and B). However, unexpectedly, inhibition of miR-3085-3p also restrained expression of CEBP $\alpha$  and PPAR $\gamma$  (Figure 5.14C and D).

After adipogenic induction, less and smaller lipid droplets formed in cells transfected with miR-3085-3p mimic as well as inhibitor (Figure 5.15A). Besides, throughout adipogenesis, cytoplasmic triacylglycerol stained with Oil Red O was reduced by miR-3085-3p mimic at day 21 ( $p=0.0012$ ) (Figure 5.15B), whilst reduced by inhibitor at day 7 ( $p=0.0001$ ), day 14 ( $p<0.0001$ ) and day 21 ( $p=0.0004$ ) (Figure 5.15C) according to the spectrophotometric quantification derived from eluates.

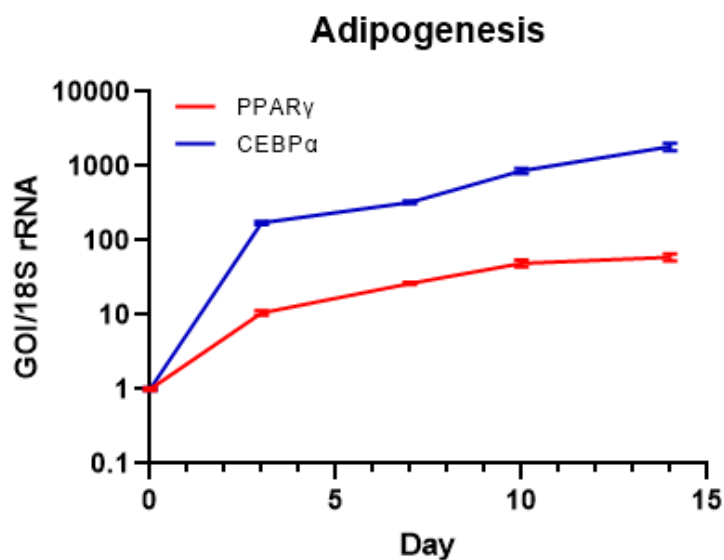


Figure 5.13 Regulation of marker genes for adipocytes during adipogenesis. RNAs were extracted from MSCs of 3 donors and reversely transcribed via Cells to cDNA method at indicated time points, followed by qRT-PCR to measure CEBP $\alpha$  and PPAR $\gamma$ . Gene expression was normalized by 18S rRNA. Mean at day 0 was set as 1. Data show mean  $\pm$  SEM, N=3.

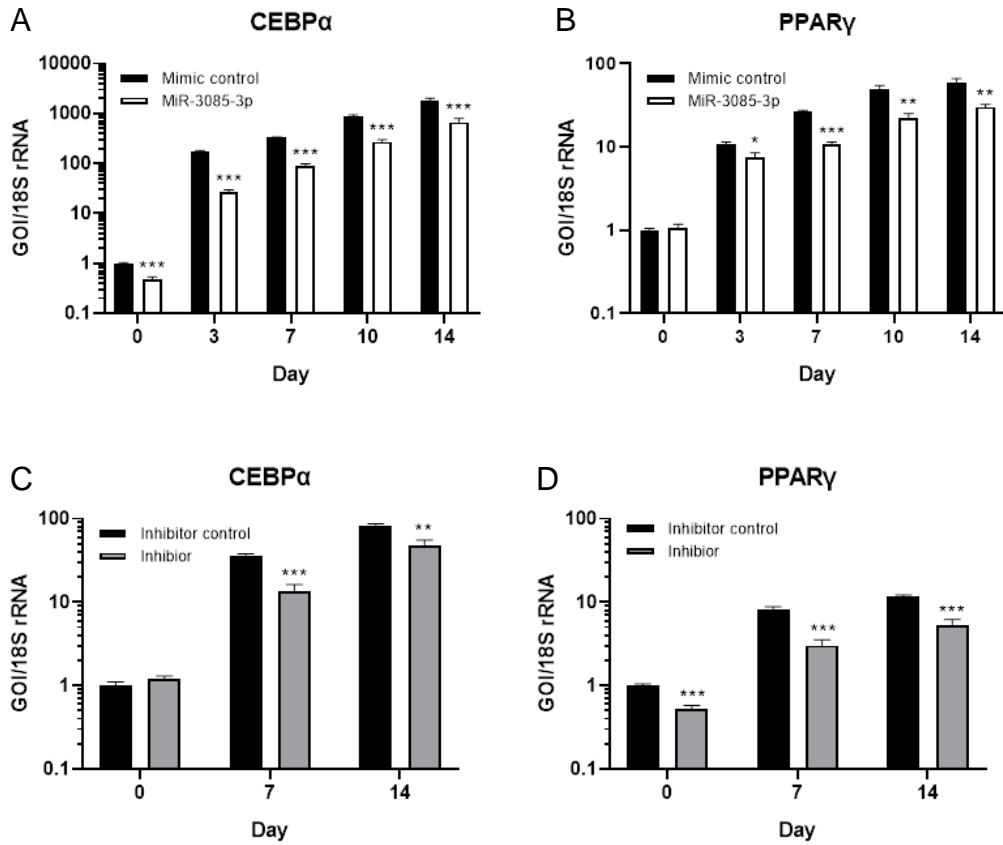


Figure 5.14 Regulation of marker genes by miR-3085-3p mimic and inhibitor across adipogenesis. MSCs from 3 donors were transfected with 50  $\mu$ M miR-3085-3p mimic or 25  $\mu$ M inhibitor against negative controls using lipofectamine 3000 prior to adipogenesis. RNAs were extracted and reversely transcribed via Cells to cDNA method at indicated time points. QRT-PCR was performed to detect mRNA levels of CEBP $\alpha$  (A and C) and PPAR $\gamma$  (B and D). Gene expression was normalized by 18S rRNA. Statistical analysis between control group and mimic/inhibitor group was performed using two-way ANOVA with Sidak's post hoc test. Mean at day 0 was set as 1. Data show mean  $\pm$  SEM, N=3. \*,  $P < 0.05$ ; \*\*,  $P < 0.01$ ; \*\*\*,  $P < 0.001$ .

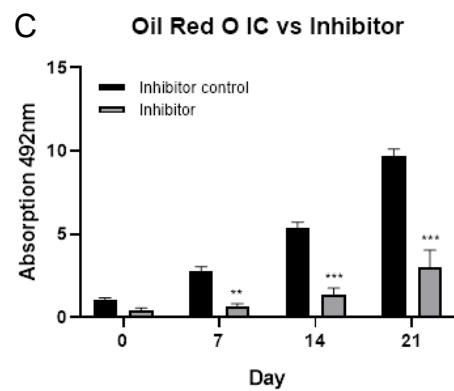
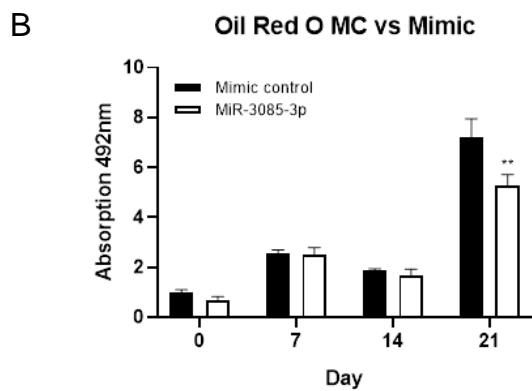
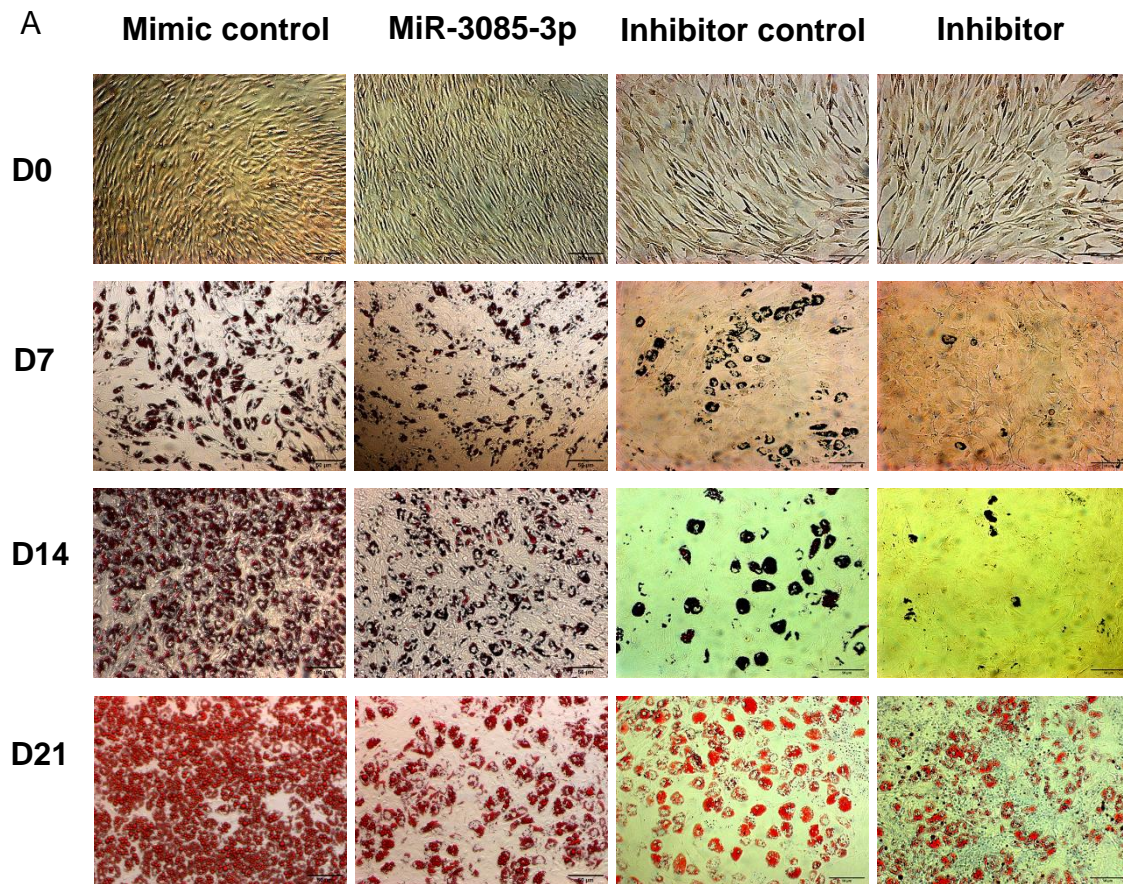


Figure 5.15 Oil Red O staining for cytoplasmic triacylglycerol of adipocytes. MSCs were transfected with 50  $\mu$ M miR-3085-3p mimic (B) or 25  $\mu$ M inhibitor (C) versus negative controls, and then induced into adipogenesis. After staining cells with Oil Red O (A) and elution, absorption of eluates was measured at 492 nm at desired time points. Statistical analysis between control group and mimic/inhibitor group was performed using two-way ANOVA with Sidak's post hoc test. Scale bar = 50  $\mu$ m. Values are mean  $\pm$  SEM, N=3. \*\*,  $P < 0.01$ ; \*\*\*,  $P < 0.001$ . MC, mimic control; IC, inhibitor control.

### 5.2.6 MiR-3085-3p enhances human BMMSC osteogenesis.

In order to confirm osteogenic differentiation from hBMMSC, the expression of osteoblast markers was measured by qRT-PCR. The expression of COL1A1, COL1A2 and ALPL was increased throughout osteogenic differentiation (Figure 5.16). Overexpression of miR-3085-3p significantly upregulated these markers from day 1 (COL1A1,  $p=0.005$ ; COL1A2,  $p=0.018$ ; ALPL,  $p=0.0066$ ) (Figure 5.17A, C, and E), whilst suppression of miR-3085-3p dramatically reduced their expression at day 2 (COL1A1,  $p<0.0001$ ; COL1A2,  $p<0.0001$ ; ALPL,  $p=0.0023$ ) and day 4 (COL1A1,  $p=0.002$ ; COL1A2,  $p=0.0004$ ; ALPL,  $p=0.0005$ ) (Figure 5.17B, D and F). Consistently, comparing with negative control group, a higher level of mineralization in osteogenic differentiation was observed in the group transfected with miR-3085-3p mimic, as shown by early occurred, widely branched, and darker red mineralized nodules (Figure 5.18A), as well as the quantification of absorption in eluates (day 5,  $p=0.044$ ; day 5.5,  $p=0.0003$ ) (Figure 5.18B). In contrast, Alizarin Red S staining also demonstrated repression of mineralization by miR-3085-3p inhibitor (day 5 and 5.5,  $p<0.0001$ ) (Figure 5.18A and C).

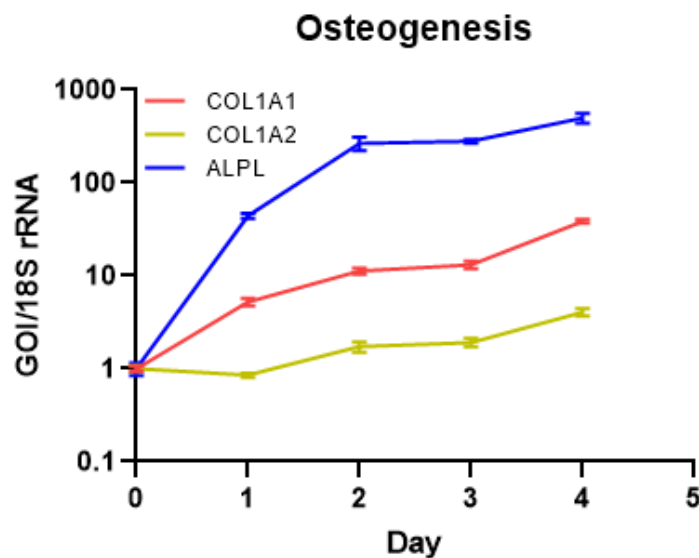


Figure 5.16 Regulation of marker genes for osteoblast during osteogenesis. RNAs were extracted from MSCs of 3 donors and reverse transcribed via Cells to cDNA at indicated time points. Expression of COL1A1, COL1A2 and ALPL were measured by qRT-PCR. Gene expression was normalized by 18S rRNA. Means at day 0 were set as 1. Data were presented as mean  $\pm$  SEM, N=3.

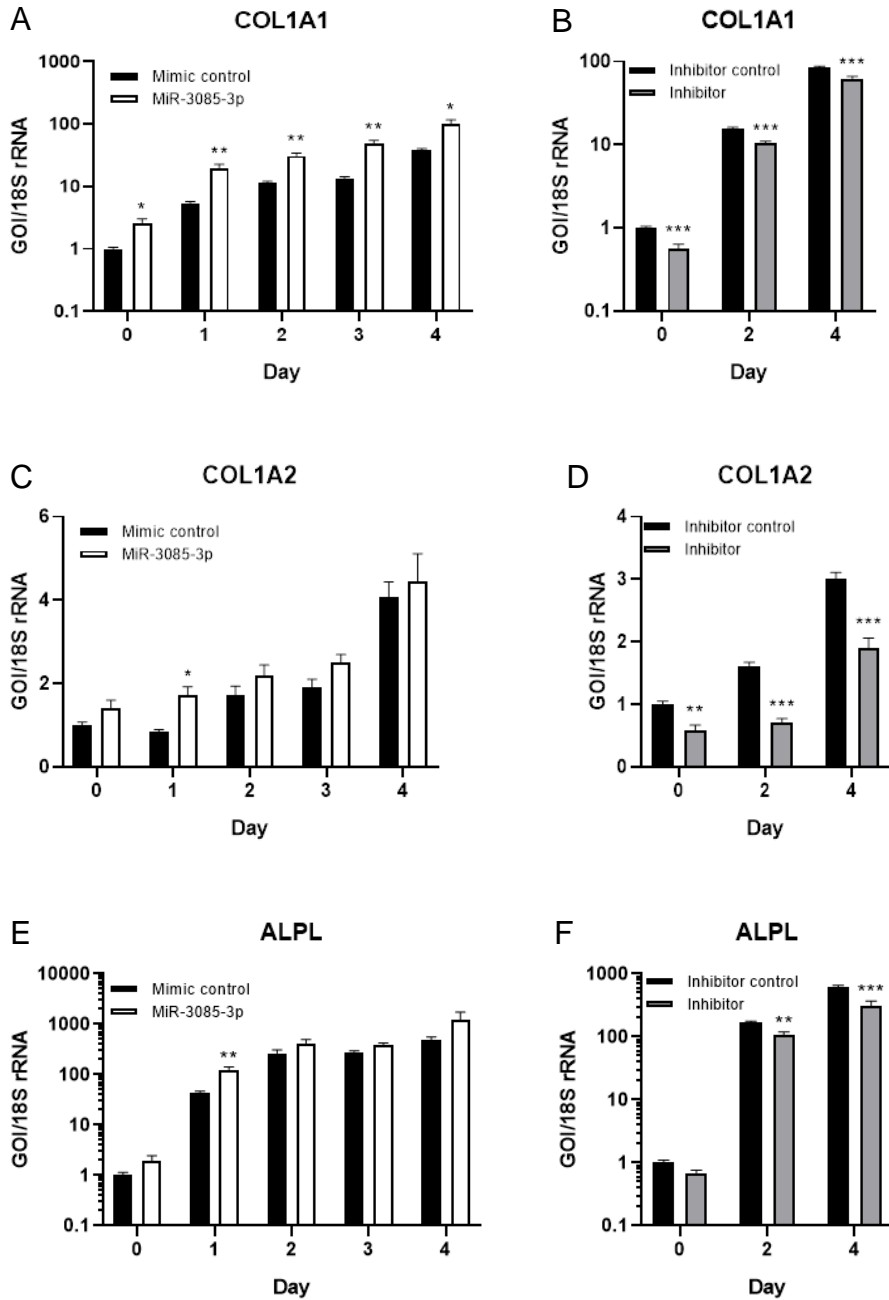


Figure 5.17 Regulation of marker genes by miR-3085-3p mimic and inhibitor across osteogenesis. MSCs from 3 donors were transfected with 50 $\mu$ M miR-3085-3p mimic or 25 $\mu$ M inhibitor against negative controls using lipofectamine 3000 prior to adipogenesis. RNAs were extracted and reversely transcribed via Cells to cDNA method at indicated time points. QRT-PCR was performed to measure mRNA levels of COL1A1 (A and B), COL1A2 (C and D) and ALPL (E and F). Gene expression was normalized by 18S rRNA. Statistical analysis between control group and mimic/inhibitor group was performed using two-way ANOVA with Sidak's post hoc test. Mean at day 0 was set as 1. Data show mean  $\pm$  SEM, N=3. \*,  $P < 0.05$ ; \*\*,  $P < 0.01$ ; \*\*\*,  $P < 0.001$ .

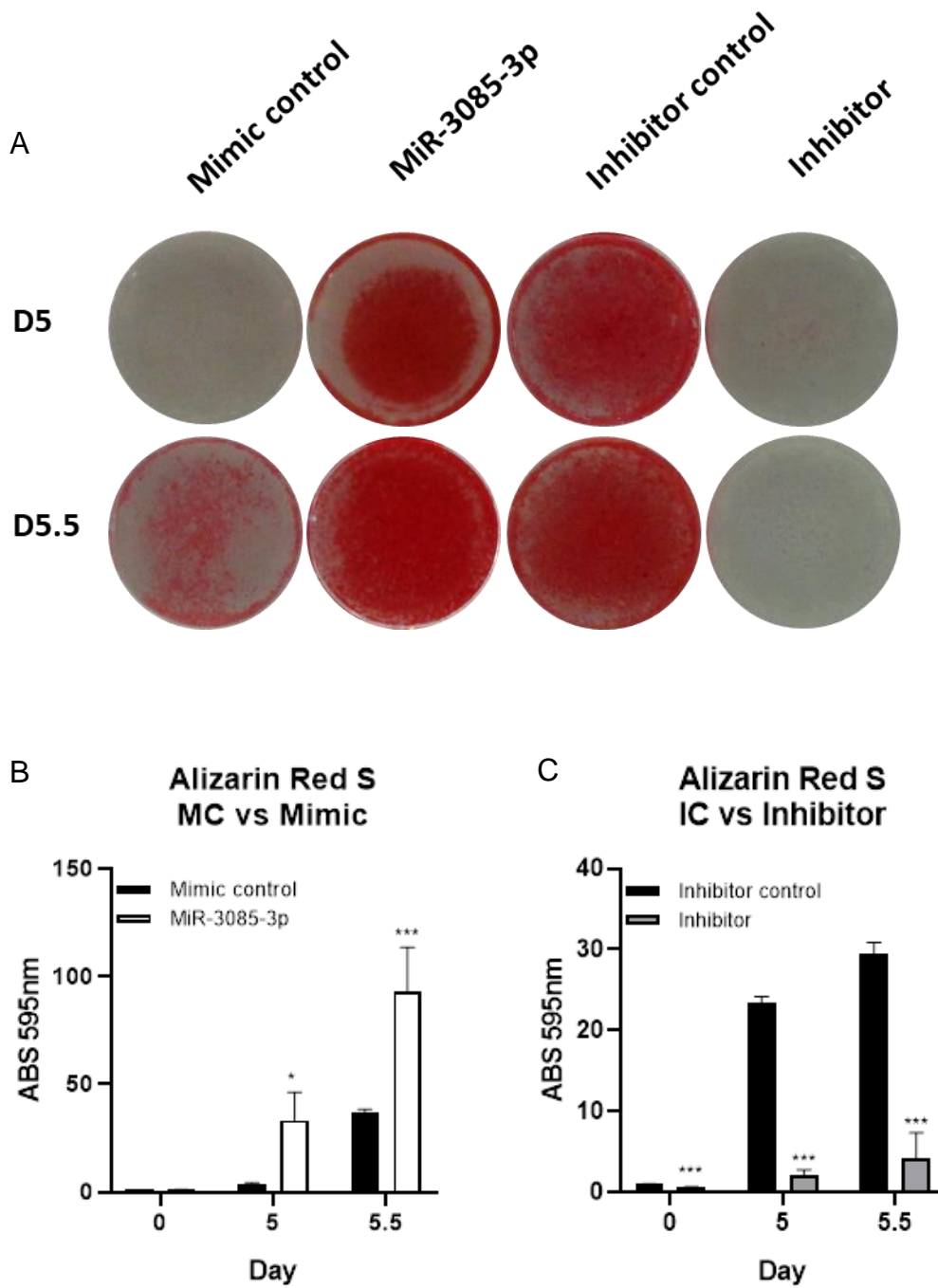


Figure 5.18 Alizarin Red S staining for calcification across osteogenesis. MSCs were transfected with 50 $\mu$ M miR-3085-3p mimic (B) or 25 $\mu$ M inhibitor (C) versus negative controls prior to osteogenic induction. Cells were stained by Alizarin Red S. (A) Representative pictures showed the whole view of each plate well. (B) Absorption of eluates was measured at 595 nm. Statistical analysis between control group and mimic/inhibitor group was performed using two-way ANOVA with Sidak's post hoc test. Values are mean  $\pm$  SEM, N=3. \*,  $P < 0.05$ ; \*\*\*,  $P < 0.001$ . MC, mimic control; IC, inhibitor control.

### **5.2.7 CMTM3, CTDSP2 and LBH are target genes of miR-3085-3p during osteogenesis.**

As shown in Figure 5.1, miR-3085-3p greatly decreased in the early osteogenesis. Genes that had increasing expression during the same period were predicted to be possible targets of miR-3085-3p. For exploring differentially regulated genes by miR-3085-3p, expression of mRNAs during first two days of hBMMSCs osteogenic differentiation was profiled by RNA-Seq. After comparing with the HACs RNA-seq dataset, among 700 upregulated genes in the early 2 days of osteogenesis when miR-3085-3p expression decreased, 184 genes were regulated by both miR-3085-3p mimic and inhibitor, 126 genes only decreased with mimic, 148 genes increased with inhibitor alone (Figure 5.19A). Further prediction was performed by searching seed sites of miR-3085-3p within 3'UTR. Overlapping genes which were upregulated in early osteogenesis and the top 10 genes either downregulated by mimic or upregulated by inhibitor in HACs were chosen as candidate targets of miR-3085-3p in osteogenic differentiation (Figure 5.19B and Table 5.2)

Validating qRT-PCR in HACs verified that, among these candidates, CTDSP2 ( $p < 0.0001$ ), CMTM3 ( $p < 0.0001$ ) and LBH ( $p = 0.049$ ) were predominantly decreased by miR-3085-3p (Figure 5.20A-C). Additionally, CMTM3 ( $p < 0.0001$ ) and LBH ( $p = 0.023$ ) were increased by miR-3085-3p inhibitor (Figure 5.20A and B). It is known that the CKLF like MARVEL transmembrane domain containing 3 (CMTM3) belongs to the CMTM family consisting of chemokine-like factor (CLKF) and CMTM 1-8 which share a conserved MAL and related proteins for vesicle trafficking and membrane link (MARVEL) domain (292, 293). CMTM3 is highly expressed in human testis, leukocytes and spleen, but can be silence by CpG methylation in gastrointestinal cancer, playing roles in reproductive system and immune system as well as the proliferation and migration of cancer cells (292, 294-297). Limb bud and heart (LBH) is a transcription cofactor, functioning as transcription activator and corepressor and participating in embryogenesis in mammalian, particularly in the development of limb and heart (298). RNA polymerase II C-terminal domain small phosphatase 2 (CTDSP2), as termed, is capable of dephosphorylating the C-terminal domain of RNA polymerase II, thereby mediating gene transcription (299).

GLDN ( $p < 0.0001$ ) and TNIP1 ( $p = 0.024$ ) were only downregulated by miR-3085-3p mimic (Figure 5.20D and E). Gliomedin (GLDN) gene is mainly expressed by myelinating Schwann cells and encodes a secreted glial ligand related to cell adhesion and the formation of Ranvier nodes in the peripheral nervous system (300). The TNF $\alpha$ -induced protein 3 interacting protein 1 (TNIP1) is found to interact with certain signalling transducers such as TNF $\alpha$ -induced protein 3 (TNFAIP3) (301), PPARs (302), extracellular signal regulated kinase 2 (ERK2) (303) to dampen NF $\kappa$ B, PPAR and MAPK pathways.

To further validate CMTM3, LBH and CTDSP2 as the direct targets of miR-3085-3p, corresponding 3'UTR luciferase reporters were constructed, and Luciferase assay was performed. As shown in Figure 5.21A and B, luciferase constructs controlled by corresponding 3'UTRs of CMTM3 ( $p < 0.0001$ ) and LBH ( $p < 0.0001$ ) demonstrated lower luciferase activities in the presence of miR-3085-3p. These were rescued by the mutation of seed sites in CMTM3 ( $p = 0.1$ ) and LBH ( $p = 0.25$ ), demonstrating that these are direct targets for miR-3085-3p. CTDSP2 has an approximate 3.6kb 3'UTR which is difficult to be entirely cloned into the pmirGLO vector. We therefore constructed 2 separate plasmids containing a 350bp (CTDSP2.1) and 1.5kb (CTDSP2.2) fragment of the 3'UTR of CTDSP2 which covers 1 seed site and 7 seed sites of miR-3085-3p respectively. Neither miR-3085-3p mimic nor inhibitor had effects on the luciferase activity of CTDSP2.1 (Figure 5.21C). This suggests that the only 1 seed site of miR-3085-2p is not sufficient in suppression of CTDSP2 expression. CTDSP2.2 construct presented reduced luciferase activities ( $p < 0.0001$ ). Nonetheless, its mutant demonstrated partial rescue ( $p = 0.0001$ ), indicating that CTDSP2 might be a direct target of miR-3085-3p but one or more cryptic target sites could exist. (Figure 5.21D)

Tracking the expression of candidate targets during osteogenesis, CMTM3 (Figure 5.22A), LBH (Figure 5.22B) and CTDSP2 (Figure 5.22C) increased until day 2 and decreased gradually from then. In parallel, overexpression of miR-3085-3p downregulated the expression of CMTM3 and CTDSP2 (Figure 5.22A and C), whilst upregulated that of LBH after induction of osteogenesis (Figure 5.22B).

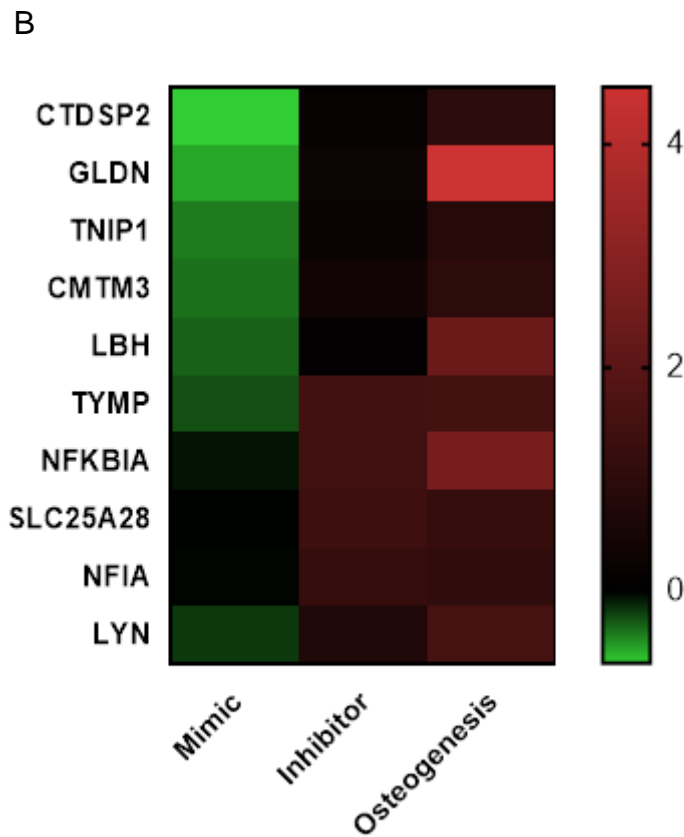
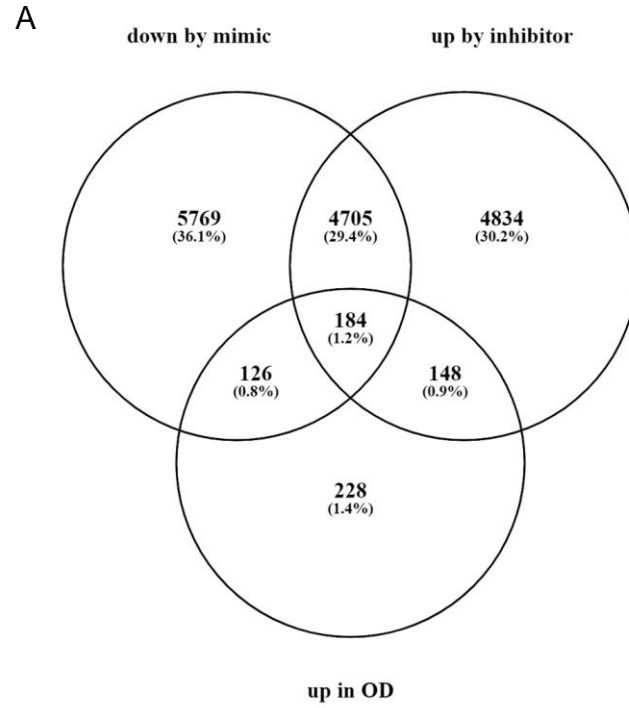


Figure 5.19 Profile of candidate target genes of miR-3085-3p across osteogenesis. Taking advantage of osteogenesis and HACs RNA-seq dataset, (A) Venn diagram demonstrate the summary of differential expressed genes that changed during osteogenesis, decreased with miR-3085-3p mimic and/or increased with inhibitor. (B) Heat map represents the  $\log_{10}(\text{fold change})$  of top 10 candidate targets regulated by miR-3085-3p mimic and/or inhibitor against negative controls during osteogenesis. OD, osteogenic differentiation.

Table 5.2 Summary of seed sites of miR-3085-3p seating within the 3'UTR of candidate targets during osteogenesis.

Gene symbol	Gene name	Seed site of miR-3085-3p				
		6mer	7mer-m8	7mer-A1	8mer	Total
<b>CTDSP2</b>	CTD small phosphatase 2	4	3	1	0	8
<b>GLDN</b>	gliomedin	2	1	0	1	4
<b>TNIP1</b>	TNFAIP3 interacting protein 1	1	1	0	0	2
<b>CMTM3</b>	CKLF like MARVEL transmembrane domain containing 3	0	1	2	0	3
<b>LBH</b>	limb bud and heart development	3	2	0	0	5
<b>TYMP</b>	thymidine phosphorylase	1	0	0	0	1
<b>NFKBIA</b>	NFKB inhibitor alpha	0	1	0	1	2
<b>SLC25A28</b>	solute carrier family 25 member 28	1	0	0	0	1
<b>NFIA</b>	nuclear factor I A	1	1	0	1	3
<b>LYN</b>	LYN proto-oncogene, Src family tyrosine kinase	2	1	0	0	3

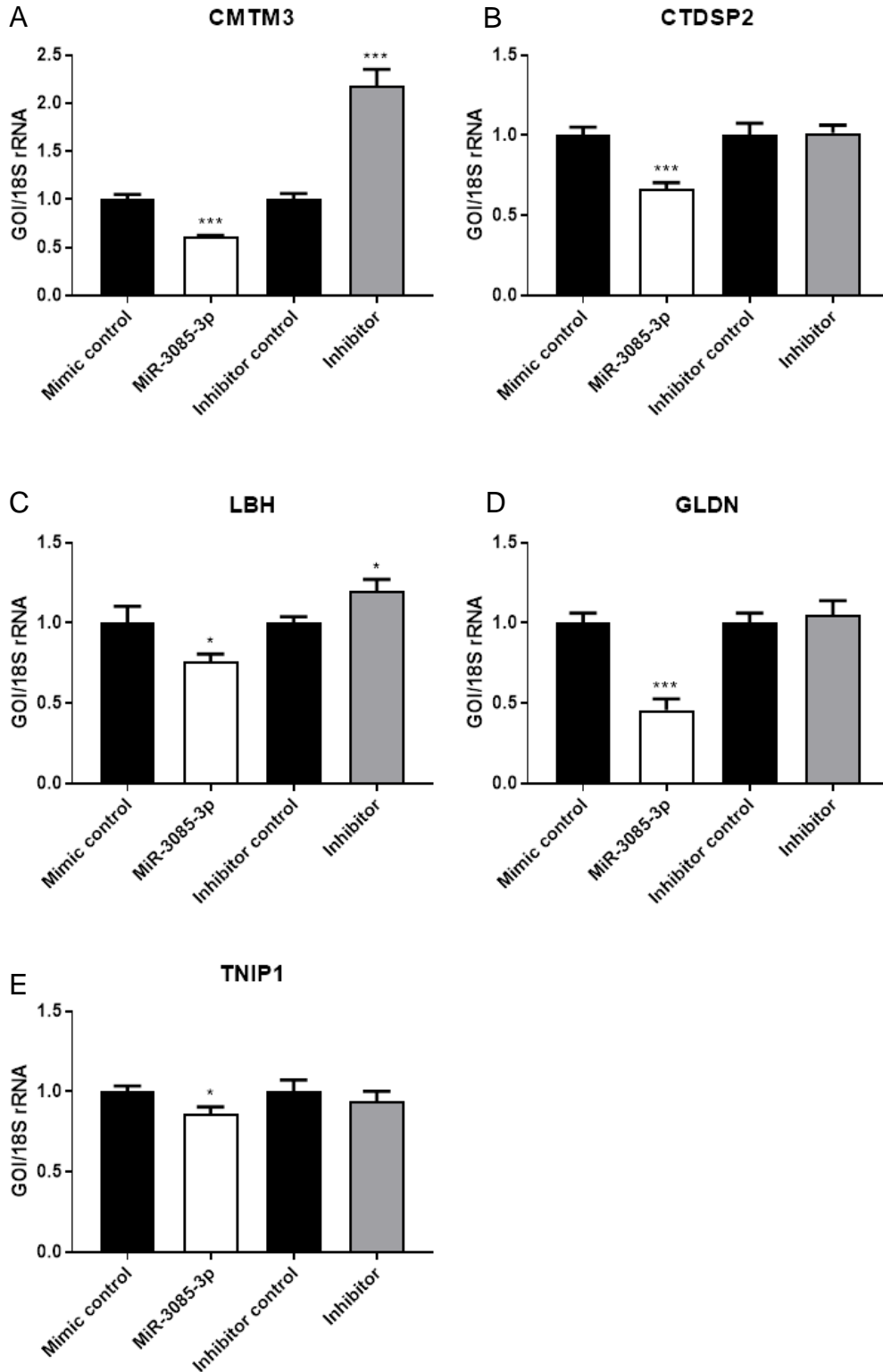


Figure 5.20 Expression of candidate genes of miR-3085-3p that downregulated by mimic and upregulated by inhibitor in HACs. MiR-3085-3p mimic (50  $\mu$ M) or inhibitor (25  $\mu$ M) were transfected into HACs from 3 patients using lipofectamine 3000 and incubated for 48 hours, RNAs were then extracted and reversely transcribed using Cell to cDNA kits. CMTM3 (A), CTDSP2 (B), LBH (C), GLDN (D) and TNIP1 (D) were validated by qRT-PCR. Comparative Ct method was applied, and gene expression was normalized by 18S rRNA. The mean of respective negative control group was set as 1. Statistical analysis between control group and mimic/inhibitor group was performed using unpaired Student's t-test. Values are mean  $\pm$  SEM, N=3. \*, P<0.05; \*\*\*, P<0.001.

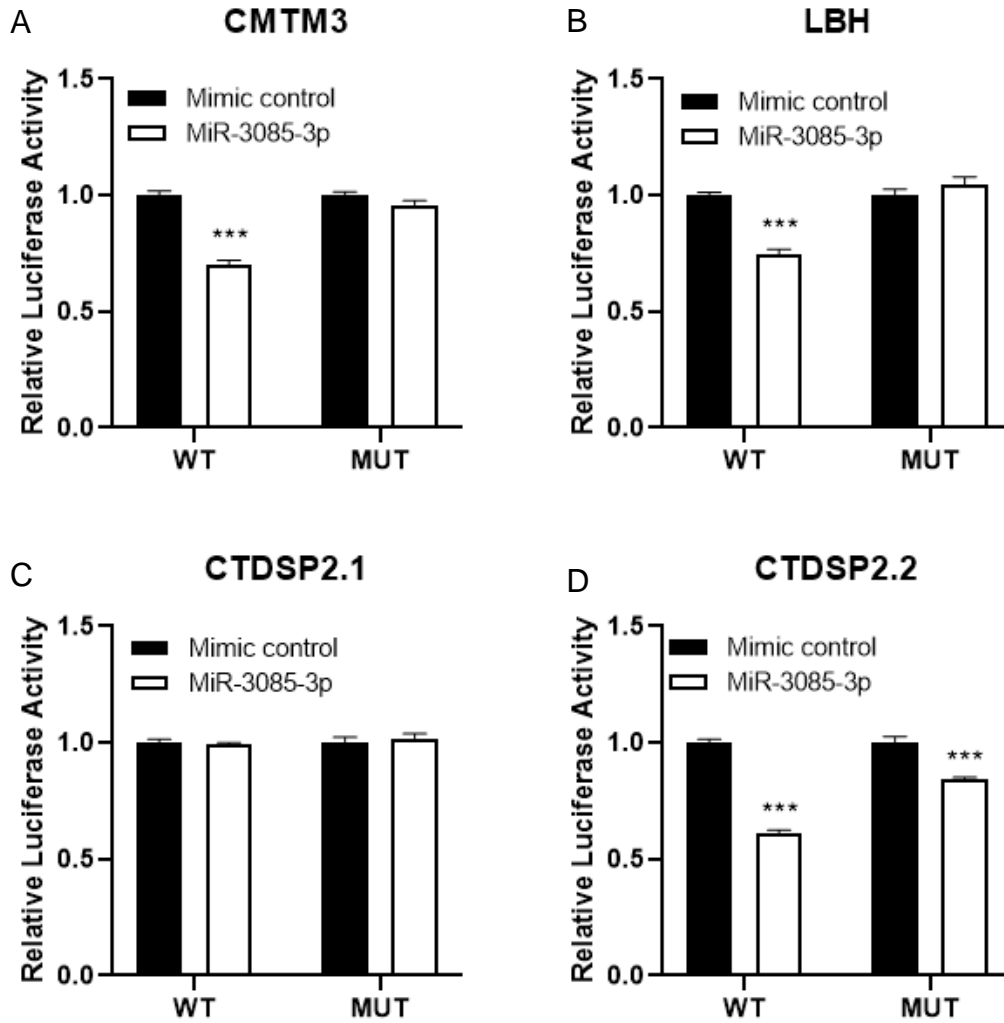


Figure 5.21 Luciferase assay of 3'UTR constructs of CMTM3, CTDSP2 and LBH. Relative luciferase activities were measured at 48 hours after SW1353 cells transfected with 100ng wild type (WT) or seed sites mutated (MUT) 3'UTR constructs of CMTM3 (A), LBH (B) and CTDSP2 (C and D), followed by subsequent transfection of 50  $\mu$ M non-targeting miRNA control or miR-3085-3p mimic. The 3'UTR of CTDSP2 mRNA is around 3.6 kb so that it was split into 2 regions to necessitate the construction of 3'UTR luciferase reporter. CTDSP2.1 contains 350bp region of 3'UTR and 1 seed site of miR-3085-3p. CTDSP2.2 covers 1.5 kb region and 7 seed sites. Luminescence was presented as the light units of Firefly luciferase normalized by those of Renilla luciferase. Mean of UTR group where cells were transfected with 3'UTR constructs only was set at 1. Statistical analysis between control group and mimic group was performed using unpaired Student's t-test. Data were shown as mean  $\pm$  SEM, N=3. \*\*\*,  $P < 0.001$ .

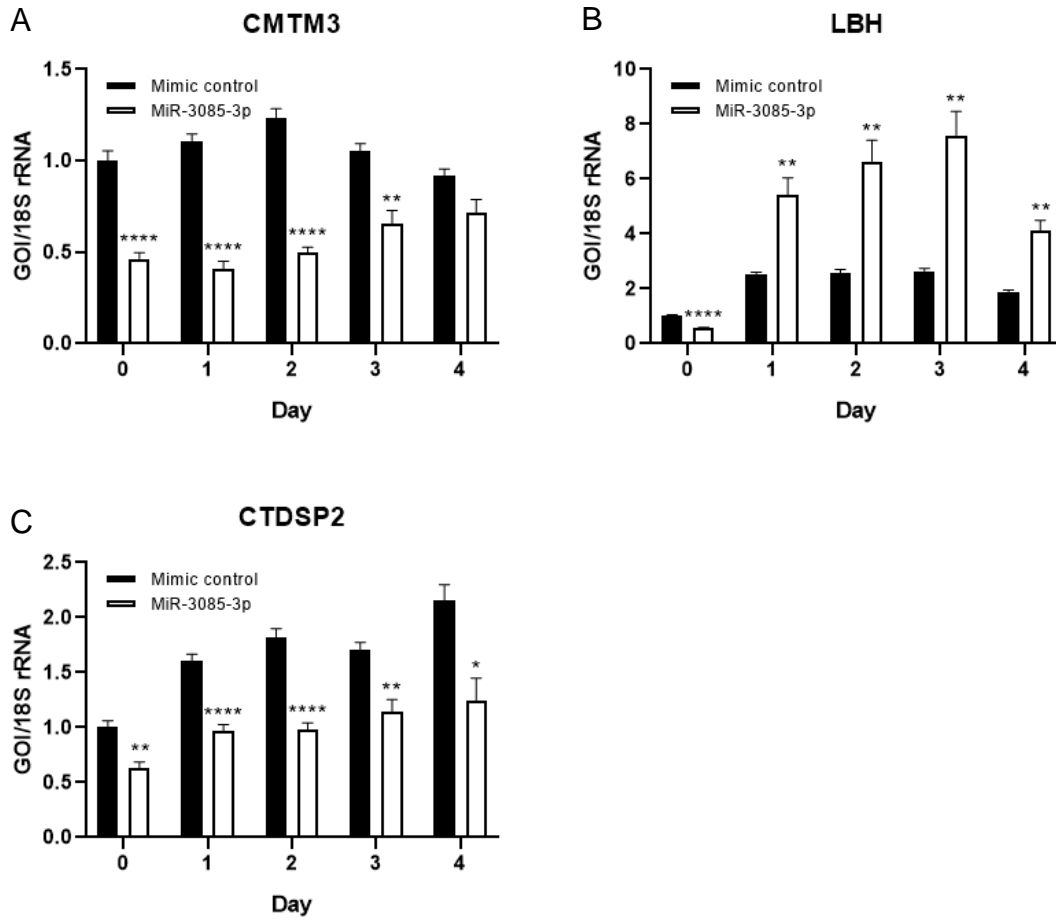


Figure 5.22 Expression of candidate targets of miR-3085-3p across osteogenesis. MSCs from 3 donors were transfected with 50  $\mu$ M miR-3085-3p mimic against negative controls using lipofectamine 3000 prior to adipogenesis. RNAs were extracted and reversely transcribed via Cells to cDNA method at indicated time points. QRT-PCR was performed to measure mRNA levels of CMTM3 (A), LBH (B) and CTDSP2 (C). Gene expression was normalized by 18S rRNA. Statistical analysis between control group and mimic group was performed using two-way ANOVA with Sidak's post hoc test. Mean at day 0 was set as 1. Data show mean  $\pm$  SEM, N=3. \*,  $P < 0.05$ ; \*\*,  $P < 0.01$ ; \*\*\*,  $P < 0.001$ .

### **5.2.8 Depletion of CMTM3, CTDSP2 and LBH promotes human MSC osteogenesis.**

To investigate the influence of miR-3085-3p on its target genes across osteogenesis, siRNA against CTDSP2 (siCTDSP2), CMTM3 (siCMTM3) and LBH (siLBH) were transfected into hMSCs. Similar to Figure 5.22, a transient increase of CMTM3 (Figure 5.23D), LBH (Figure 5.23E) or CTDSP2 (Figure 5.13F) at the early stage of osteogenic was observed in the negative control group, followed by reduction afterwards. All siRNAs efficiently suppressed the expression of their targets (Figure 5.23D-F). Increased expression of COL1A1 were found resulted from suppression of either LBH or CTDSP2 from day 1 to day 3 (Figure 5.23A). COL1A2 was also upregulated by silencing LBH and CTDSP2 at day 1 and day 2 (Figure 5.23B). The expression of ALP was enhanced across osteogenesis by knocking down CTDSP2 (Figure 5.23C). Consistently, Alizarin Red S staining showed that knockdown of CMTM3, LBH and CTDSP2 respectively all boosted osteogenic differentiation (Figure 5.24). Pearson correlation test demonstrated that there was close correlation between CMTM3, LBH, CTDSP2 and miR-3085-3p in the influence on osteogenesis (Table 5.3).

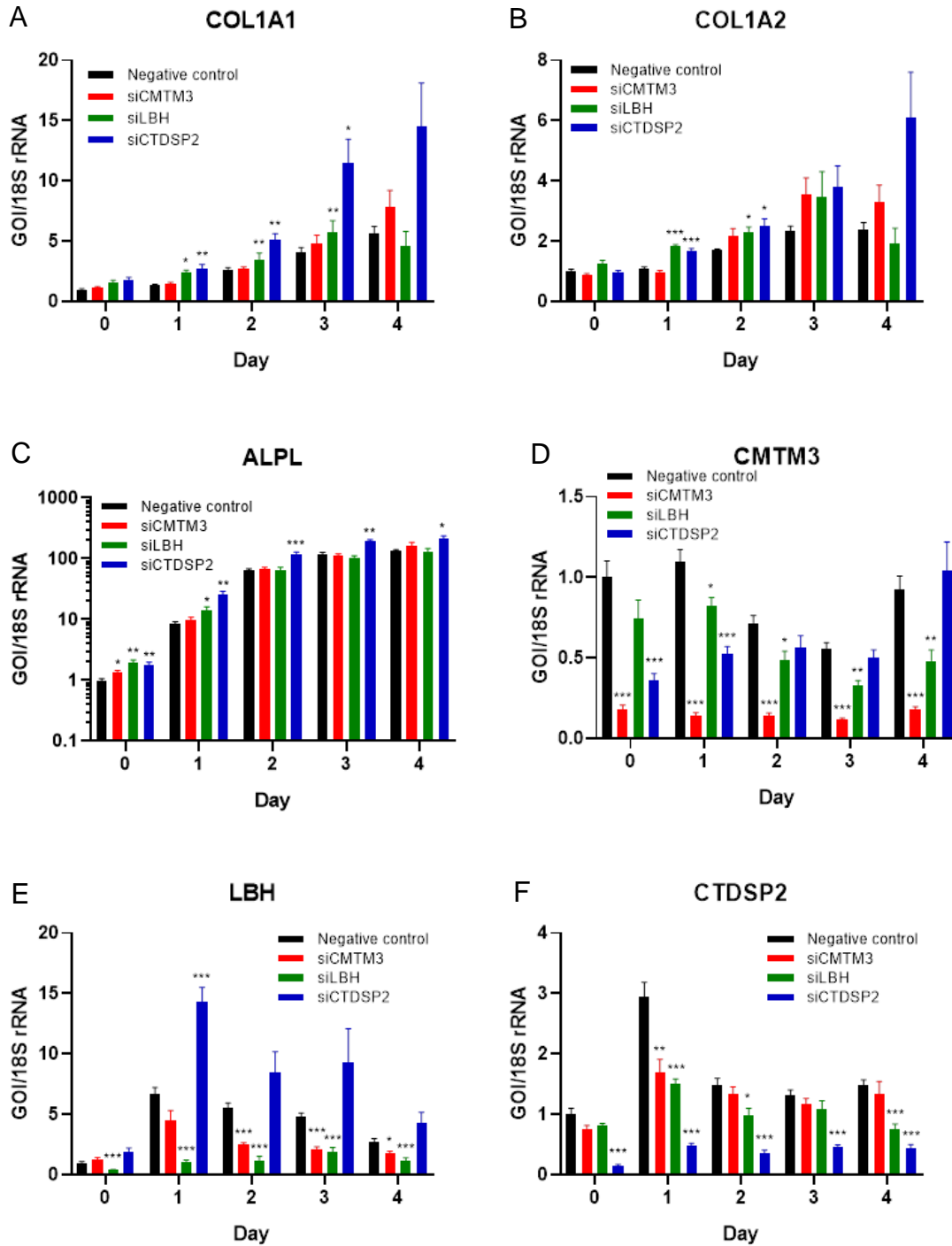


Figure 5.23 Expression of markers and candidate targets of miR-3085-3p that regulated by siRNAs during osteogenesis. SiRNAs (50 $\mu$ m) against negative control (50  $\mu$ m) were transfected into MSCs from 3 donors using lipofectamine 3000 and incubated for 72 hours prior to osteogenesis induction. RNAs were then extracted and reversely transcribed using Cell to cDNA kits. QRT-PCR was performed at indicated time points to detect mRNA level of COL1A1 (A), COL1A2 (B), ALPL (C), CMTM3 (D), LBH (E) and CTDSP2 (F). Comparative Ct method was applied, and gene expression was normalized by 18S rRNA. Statistical analysis between control group and siRNA group was performed using two-way ANOVA with Sidak's post hoc test. The mean of respective negative control group was set as 1. Values are mean  $\pm$  SEM, N=3. \*, P<0.05; \*\*, P<0.01; \*\*\*, P<0.001.

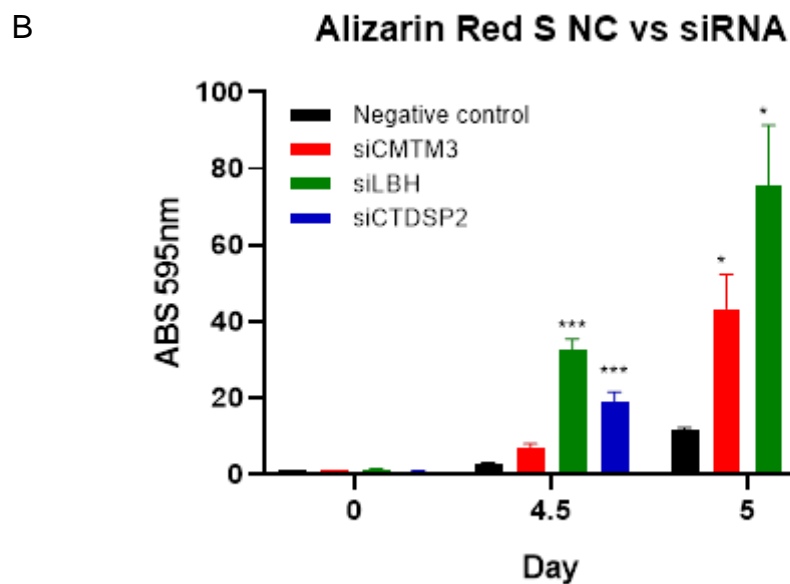
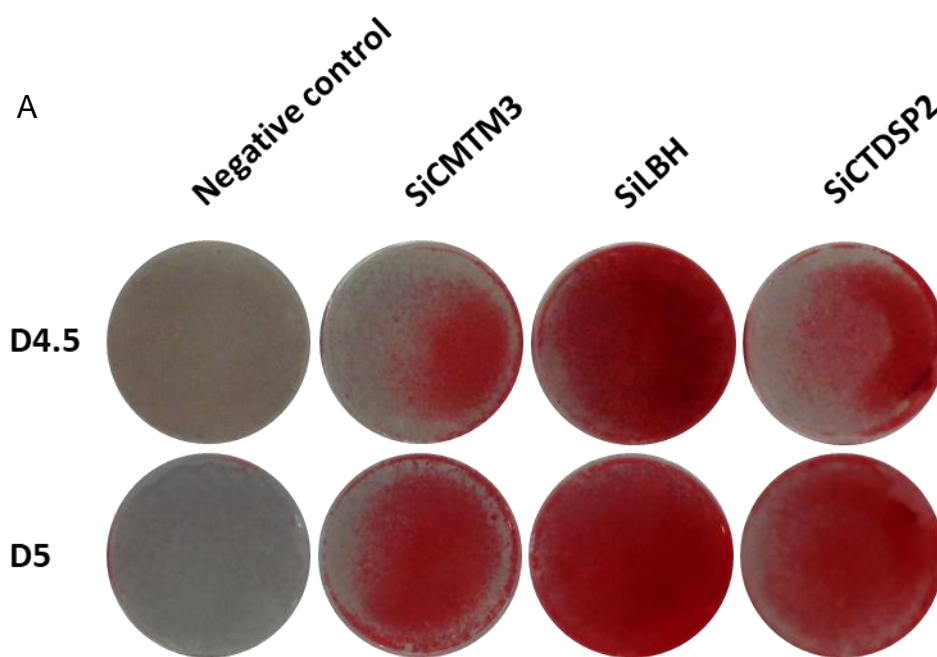


Figure 5.24 Alizarin Red S staining for calcification across osteogenesis under effects of siRNAs. CMTM3, LBH and CTDSP2 were silenced by transfection with 50 $\mu$ M siRNA into MSCs. After incubation for 72 hours, MSCs were induced to osteogenesis and then analysed by Alizarin Red S staining at desired time. (A) Representative pictures showed the whole view of each plate well. (B) Absorption of eluates was measured at 595nm. Statistical analysis between control group and siRNA group was performed using two-way ANOVA with Sidak's post hoc test. Values are mean  $\pm$  SEM, N=3. \*, P<0.05; \*\*\*, P<0.001. NC, negative control; siCMTM3, siRNA against CMTM3; siLBH, siRNA against LBH; siCTDSP2, siRNA against CTDSP2.

Table 5.3 Results of Pearson correlation test between influence of siRNAs and miR-3085-3p on osteogenesis.

Pearson r / p-value	MiR-3085-3p		
	COL1A1	COL1A2	ALPL
siCMTM3	0.984 / 0.003 **	0.759 / 0.136	0.915 / 0.029 *
siCTDSP2	0.937 / 0.019 *	0.979 / 0.004 **	0.820 / 0.089
siLBH	0.718 / 0.172	0.194 / 0.754	0.873 / 0.053

N=3. \*, P<0.05; \*\*, P<0.01. siCMTM3, siRNA against CMTM3; siLBH, siRNA against LBH; siCTDSP2, siRNA against CTDSP2.

It is interesting that knock down of LBH and CTDSP2 decreased CMTM3 (Figure 5.23D). Correspondingly, repression of CMTM3 downregulated LBH (Figure 5.23E). Moreover, knock down of CMTM3 and LBH gave rise to lower expression of CTDSP2 to some extent (Figure 5.23F). Surprisingly, silence of CTDSP2 gave rise to an increase of LBH, similar to that of miR-3085-3p (Figure 5.22B and 5.23E). These indicate that CMTM3, CTDSP2 and LBH play mutual roles in regulating osteogenesis, and miR-3085-3p regulates osteogenesis by targeting CTDSP2.

## 5.3 Discussion

MSCs are characterized by their self-renewal capacity and multipotential differentiation into chondrocytes, adipocytes and osteoblasts. MiRNAs have multiple target genes which participate in diverse regulatory processes required for MSC differentiation. In this study, potential roles of miR-3085-3p in MSC differentiation were revealed.

Chondrogenesis was inhibited by miR-3085-3p which effectively decreased ACAN and COL2A1 expression, potentially by directly targeting seed sites within 3'UTR. Other marker genes for chondrocytes including COL10A1 and SOX9 were also suppressed by miR-3085-3p, even though there were no seed sites found in their 3'UTR, suggesting that miR-3085-3p could take effects via functional sites in the CDS and 5'UTR (304-307). Moreover, miRNAs exert their effects on quite a few targets. Except direct repression, this downregulation possibly resulted from other mechanisms that regulated by miR-3085-3p. Additionally, miR-3085-3p led to less sulphated glycosaminoglycan content in extracellular matrix of chondrogenic pellets. The chondrogenic pellets had lower density at the presence of miR-3085-3p mimic at early stage of chondrogenesis. It is known that ITGA5 is essential in cell adhesion (55) and a direct target of miR-3085-3p (206). We speculate that this process could be disrupted by the decrease of ITGA5 as a consequence of overexpressing miR-3085-3p.

AP-1 dimers are known as transcription factor complexes composed of JUN, FOS, ATF or MAF protein families (291, 308), involved in multiple biological processes such as cell proliferation, differentiation, apoptosis and transformation(309, 310).In the JNK cascade, AP-1 function can be induced by phosphorylated c-JUN which was activated by the phosphorylation of JNK (311-313). It has been demonstrated that the MAPK/JNK pathway is crucial for AP-1 activity and MMP-13 expression in rheumatoid arthritis (314).Other studies have reported that MMP-13 responds to IL-1 depending on interaction between c-JUN/c-FOS with RUNX2 through MAPK/JNK pathway by two hours after IL-1 induction in chondrocytes and SW1353 cells (244, 313, 315).According to our data, miR-3085-3p reduced c-JUN and c-FOS in human primary chondrocytes, but induced c-JUN/c-FOS at an early stage (30 minutes) of IL-1

induction and subsequent MMP-13. MiR-3085-3p also resulted in a transient activation of the phosphorylation of JNK, indicating that miR-3085-3p possibly promotes IL-1 induced MMP-13 through activating the JNK/AP-1 signalling pathway.

The induction of CEBP $\alpha$  and PPAR $\gamma$  contributes to mitotic clonal expansion dependent for adipogenesis, and maintenance of the terminal differentiation (171, 316-318). We found overexpression of miR-3085-3p significantly downregulated both CEBP $\alpha$  and PPAR $\gamma$ . Nevertheless, suppression of miR-3085-3p also decreased the expression of these two marker genes during adipogenesis. It indicates that miR-3085-3p plays a vital role in the adipogenic differentiation, but the regulation is unknown in our study.

Different from chondrogenesis and adipogenesis, miR-3085-3p enhanced COL1A1, COL1A2 and ALPL known as marker genes for osteoblasts (319, 320). Moreover, miR-3085-3p accelerated the mineralization of osteogenic cells. Collectively, overexpression of miR-3085-3p contributed to the promotion of hBMMSC osteogenesis.

Taking advantage of two novel RNA sequencing datasets, one was derived from osteogenic cells at day 0 and day 2, the other one was from primary HACs where miR-3085-3p mimic or inhibitor was transfected, we thereby screened out a list of potential target genes of miR-3085. These selected targets were then validated by qRT-PCR and luciferase assay. CMTM3, LBH and CTDSP2 were identified as direct targets of miR-3085-3p, with expression in HACs decreased and luciferase activities of 3'UTR declined by mimic. The mutation of seed sites of miR-3085-3p in the 3'UTR construct of CTDSP2 cannot rescue the downregulation, suggesting that the central seed mutation is not essential for miR-3085-3p function. Noncanonical target sites or flexible seed:target pairing probably contribute to the mutant still being reduced by miR-3085-3p mimic (254, 321-325). During osteogenesis, qRT-PCR demonstrated that CMTM3, LBH and CTDSP2 had a transient upregulation which correlated with the decline of miR-3085-3p resulting from the initiation of osteogenic differentiation, in agreement with our RNA-seq dataset. This suggests that miR-3085-3p plays an important role in maintenance of the expression of CMTM3, LBH and CTDSP2 as well as the undifferentiating status of hBMMSCs.

To directly investigate the regulation of miR-3085-3p on these genes during osteogenesis, miR-3085-3p was overexpressed and inhibited in hBMSCs before osteogenic differentiation. Expression of CMTM3, CTDSP2 and LBH were all decreased by miR-3085-3p. Furthermore, knock down of these genes by siRNA silence respectively shared the same pattern as miR-3085-3p overexpression in promoting osteogenesis.

A recent study reported that, in CMTM3 KO mice, greater bone density and strength were observed. In vitro experiments in this study revealed that suppression of CMTM3 promoted osteogenesis through activation of the phosphorylation of Erk1/2 and vice versa (326). Consistently, in our study, siRNA against CMTM3 enhanced hMSC osteogenic differentiation. Taken these together, miR-3085-3p possibly contributed to the promotion of osteogenesis by directly targeting CMTM3 leading to the activation of Erk1/2 signalling pathway.

Previously, LBH was found predominantly expressed in late hypertrophic chondrocytes and osteoblasts (327). Overexpressing LBH gave rise to delayed chondrocyte hypertrophy and osteoblast maturation in chicken wings (327).

It is known that the BMP-SMAD1/5/8 signalling pathway is closely associated with the activation of gene transcription involved in osteogenesis, skeletal development and bone formation (328, 329). CTDSP1-3 are essential enzymes to dephosphorylate the C-terminal domain of RNA polymerase II. Knockaert et al. identified that CTDSP2 mediated dephosphorylation and degradation of phospho-SMAD1 (330). Loss of function of CTDSP2 individually or co-suppression with CTDSP1 promoted phosphorylation of BMP-induced SMAD1 (330). We thereby deduce that miR-3085-3p is capable to enhancing hMSC osteogenesis through the BMP/SMAD1 pathway by downregulating CTDSP2.

Interestingly, knock down of CMTM3, LBH or CTDSP2 individually demonstrated a synergistic reduction on the expression level of other two. Except that inhibition of CTDSP2 led to increasing LBH, which was surprisingly analogous to the overexpression of miR-3085-3p, further confirming that CTDSP2 is a direct target of miR-3085-3p. (Figure 5.25)

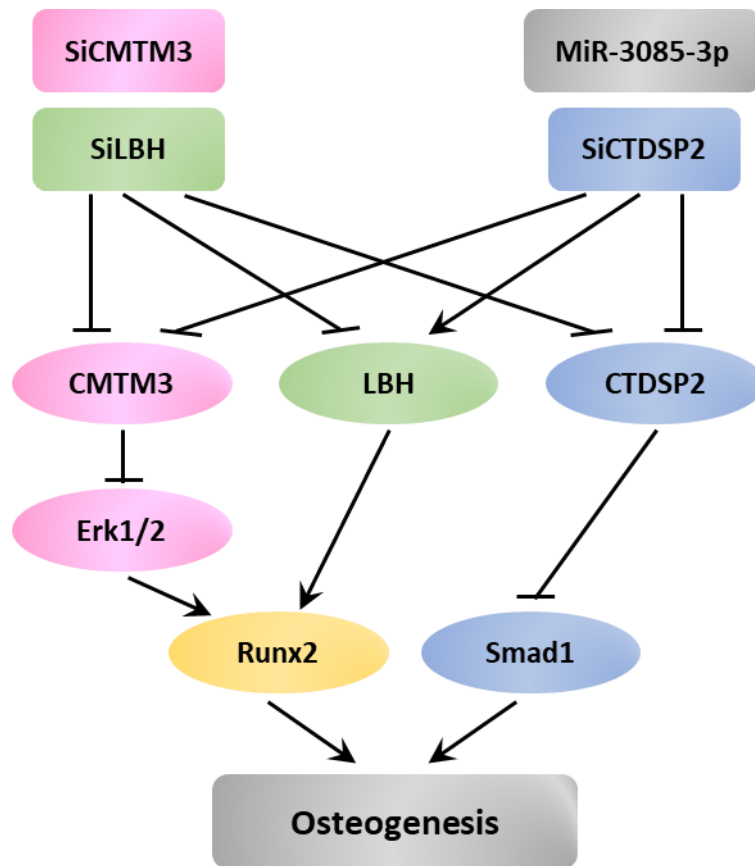


Figure 5.25 Schematic overview of regulation of miR-3085-3p, siRNAs on target genes and downstream pathways involved in osteogenesis. Arrows indicate the activation processes, while bars indicate the inhibition.

In summary, miR-3085-3p is closely involved in hBMMSC differentiation. It could depress chondrogenesis and boost IL-1 induced MMP-13 via JNK/AP-1 pathway in primary HACs. It also negatively regulates adipogenesis by targeting adipogenic marker genes - CEBP $\alpha$  and PPAR $\gamma$ . In contrast, miR-3085-3p enhances osteogenesis by inhibition of CMTM3 and LBH, especially CTDSP2.

# Chapter 6 Phenotyping the ITGA5 cartilage-specific knockout mice

## 6.1 Lethality of miR-3085-3p null mice

Taking advantage of CRISPR-Cas9 technology, 4 genetically altered (GA) mice were generated with deletion of 50-73bp segment, substitution and insertion of miR-3085. All were heterozygotes. Among them, founder #1 and #2 held gross deletion of 50bp and 73bp in the miR-3085 region in one allele respectively (Figure 6.1). They were thereby selected to breed forward with a wild-type C57BL/6, intending to get more heterozygotes in F1. Unfortunately, only five litters were given with a relatively small number of pups, most of which are found perinatally dead and all turned out to be wild type (Figure 6.2 and Table 6.1), strongly suggesting that full mir3085 knockout is lethal.

Due to feeble reproduction and aging of founders, we resorted to rederivation by embryo transfer to improve founders' fertility and expected to transmit their gene modifications into germline. Frustratingly, there were no embryos at all in founder #1 just the cumulus cloud and only 2 embryos in founder #2. Of the embryos that were present, one was misshapen and the other one divided incorrectly. Both were not viable.

As founder #1 and #2 cannot breed anymore, we then considered founder #11 where modification of +3/-2bp together with a substitution T>C occurred (Figure 6.1). Genotypes of offspring generated by founder #11 were identified by genotyping PCR using specific primers, and further confirmed by sequencing. Frustratingly, when verifying the expression of miR-3085-3p across tissues, there was no decrease observed in the miR-3085-3p<sup>-/-</sup> (Figure 6.3). The genetic alteration of founder #11 had nothing to do with the expression of miR-3085-3p. Eventually, we had to accept that we did not have success in generating miR-3085-3p null mice.

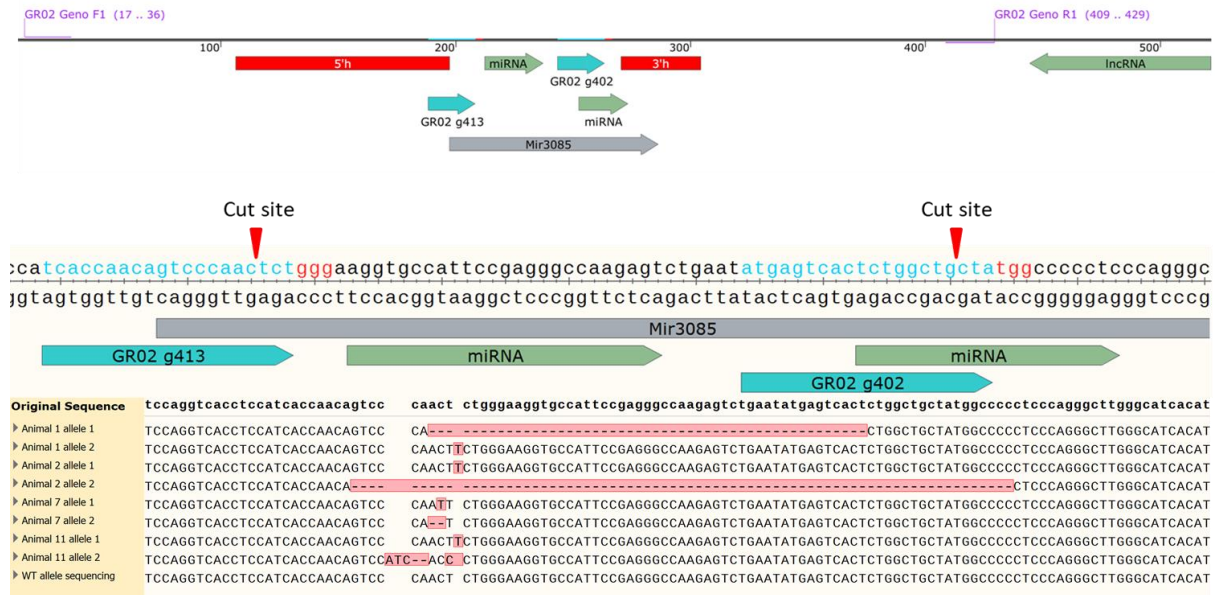


Figure 6.1 Picture illustrated the sequence of alleles from selective genetically altered founders heterozygous mice. Two CRISPR guides (g413 and g402) are indicated in red, and a ssDNA asymmetric HDR repair template for which homology arms are indicated in red rectangle. The alterations of miR-3085-3p gene are highlighted in pink.

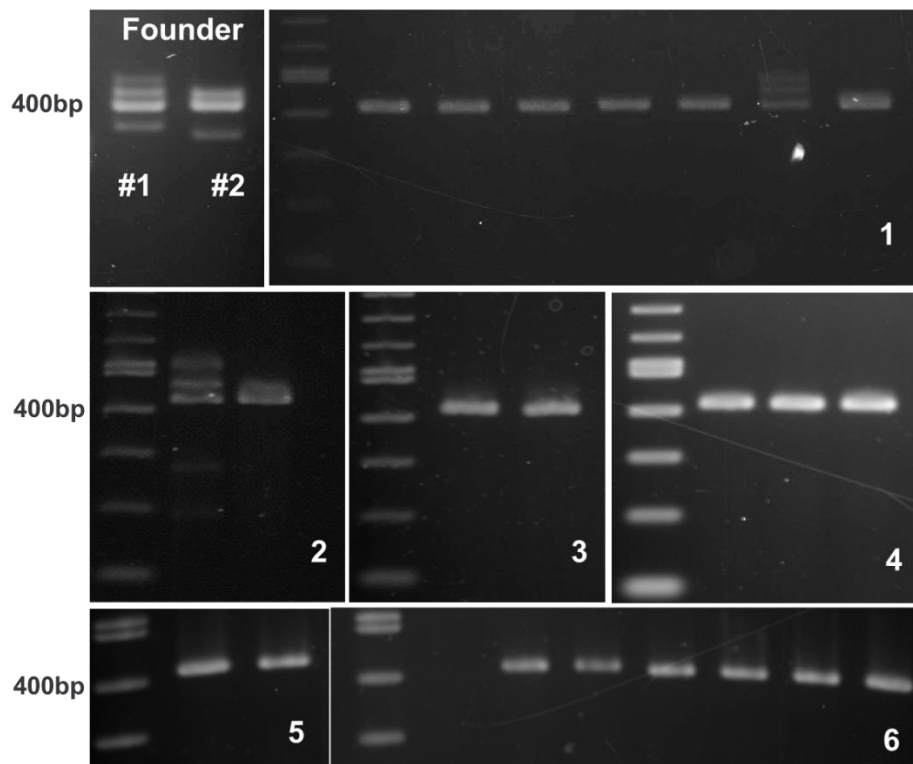


Figure 6.2 Genotyping images of miR-3085-3p null strain. #1 and #2 are two founders held gross deletion of 50bp and 73bp in the miR-3085 region in one allele respectively, shown on top left. 1-6 represent the outcome of genotype for litter 1-6. a 428bp wild-type band and 378bp/355bp null band were presented. The larger bands are not necessarily large insertions, but instead changes in DNA migration patterns due heterodimerised DNA hybrids.

Table 6.1 Information of pups from F1 litters of miR-3085-3p null strain.

Litter No.	Founder	Litter size	Genotype	Status
1	#1	7	WT	Perinatal dead
2	#1	2	WT	Perinatal dead
3	#2	2	WT	Alive
4	#2	3	WT	Alive
5	#2	3	WT	Alive
6	#2	6	WT	Alive

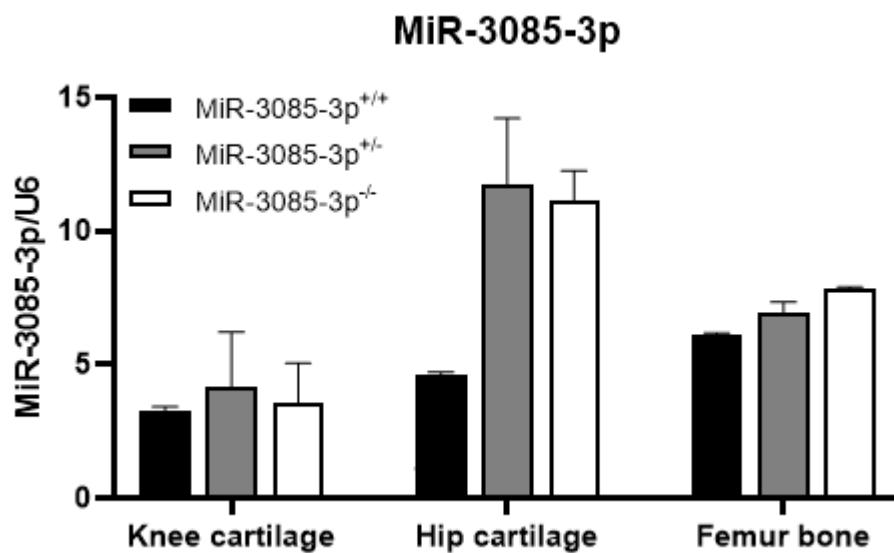


Figure 6.3 Expression of miR-3085-3p in offspring generated by founder #11. RNAs were extracted by Trizol and reverse transcribed via MiRCURY LNA Universal cDNA synthesis kit. Expression of miR-3085-3p was measured by qRT-PCR and normalized by U6. Statistical analysis was performed using unpaired Student's *t*-test. Values show mean  $\pm$  SEM, N=3.

## 6.2 Rationale for the generation of ITGA5 cartilage-specific knockout mice

ITGA5 has been reported to be involved in various processes during postgastrulation stages including mesoderm formation (331), mesodermal cells derivation (332) and vasculature remodelling (221). It is also one of the integrin dimers primarily expressed in chondrocytes, which can recognize fibronectin (59), playing vital roles in mechanotransduction, cellular adherence, proliferation and differentiation of articular chondrocytes (57, 58). A previous study has reported that, ITGA5 conditional knockout mice line achieved by GDF5-Cre system didn't show obvious abnormalities compared with controls. Whereas this conditional ablation of ITGA5 demonstrated stronger resistance to surgically induced osteoarthritis with less cartilage erosion and synovial changes. These suggest that ITGA5 may not be crucial for synovial joint formation, but it has a protective effect on the pathogenesis of osteoarthritis.(73) However, GDF5, which is known as a member of BMP family and a marker of synovial joint formation, is widely expressed in the developing joint area including articular cartilage, ligaments and synovium, but not cartilage specific.(333) More importantly, ITGA5 has been verified to be a direct target of miR-3085-3p (230). We thereby hypothesize that ITGA5 gets involved in the skeletal development as well as the occurrence and pathogenesis of osteoarthritis, which could also imply the regulation of miR-3085-3p in skeletal development and osteoarthritis by interfering ITGA5. ITGA5 cartilage-specific knockout mice was hence generated, using the COL2A1Cre tool mice, where a cre recombinase is driven by the promoter of COL2A1 (220), and ITGA5<sup>F1/F1</sup> mice with the first exon of ITGA5 is flanked by loxp (221).

## 6.3 Results

### 6.3.1 Decreased ITGA5 expression across a tissue panel in the ITGA5 cartilage-specific knockout mice

In order to determine the efficiency of cre recombinase in knocking out ITGA5 in cartilage, 3-month-old ITGA5<sup>Col2a1Cre</sup> and their littermate control ITGA5<sup>Fl</sup> were sacrificed. Various tissues were harvested, followed by RNA extraction, reverse transcription and qRT-PCR. The expression of ITGA5 mRNA was significantly reduced by 70% in cartilaginous tissues of ITGA5<sup>Col2a1Cre</sup> (hip,  $p=0.0037$ ; knee,  $p=0.0018$ ; xphoid;  $p=0.011$ ). Interestingly, other non-cartilaginous tissues also had a relative decreased expression of ITGA5, especially in heart ( $p=0.014$ ) and kidney ( $p=0.035$ ). (Figure 6.4)

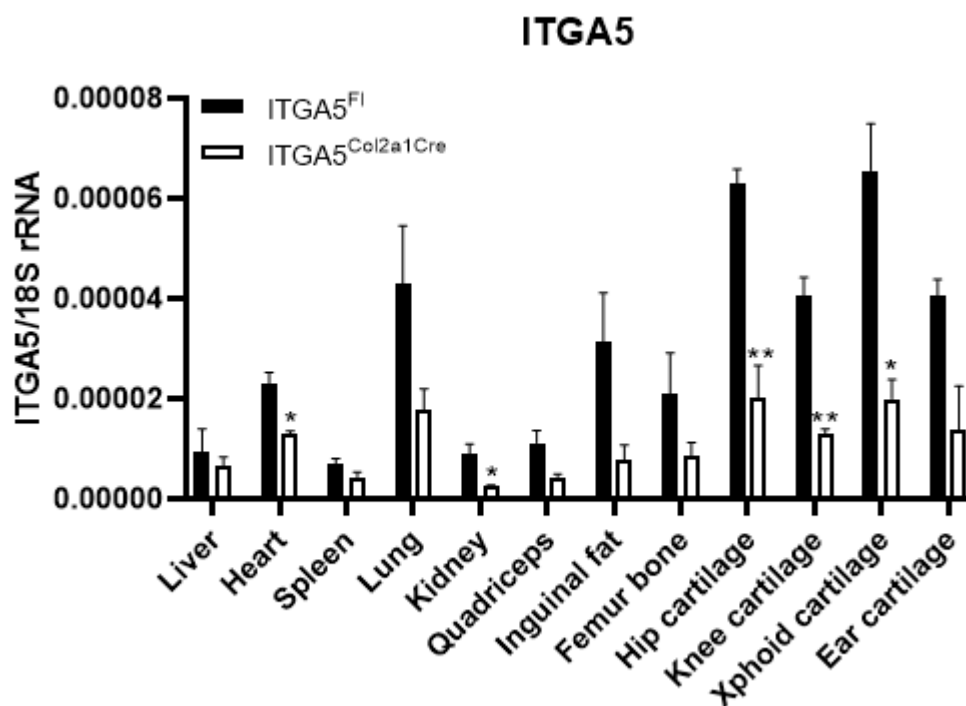


Figure 6.4 Expression of ITGA5 in a tissue panel of ITGA5 cartilage-specific knockout strain. RNAs were extracted by Trizol and reverse transcribed via SuperScript II. Expression of ITGA5 was measured by qRT-PCR. Gene expression was normalized by 18S rRNA. Statistical analysis was performed using unpaired Student's t-test. Values show mean  $\pm$  SEM, N=3, \*,  $P<0.05$ ; \*\*,  $P<0.01$ .

### **6.3.2 Embryonic defects in the ITGA5 cartilage-specific knockout mice**

According to my record, ITGA5<sup>Col2a1Cre</sup> demonstrated extremely low birth rate at 1/141. Most of the ITGA5 deficient mutants died shortly after birth indicating a significant incidence of embryonic lethality. Embryos from E15.5-E17.5 were further investigated. Consistently, defects were observed across embryonic development.

From E12.5 to E13.0, there was physiological umbilical hernia occurred, where the midgut ring protruded through the abdominal wall from the navel. At E15.5, the intestinal tract began to return to the abdominal cavity, and the body wall was then closed at E16.5 with only the umbilical cord left at the umbilicus.(334) As shown in figure 6.5, in sagittal sections, ITGA5<sup>Col2a1Cre</sup> presented strikingly large omphalocele at E15.5 and E16.5, when compared with the littermate control ITGA5<sup>Fl</sup> controls. At E17.5, extensive defects including swelling, subcutaneous haemorrhage inner organ/tissue degradation (Figure 6.5). Specifically, there was significant malformation of the heart of ITGA5<sup>Col2a1Cre</sup> mutants, characterized by apparent disorganization and hypertrophy of cardiomyocytes. ITGA5<sup>Col2a1Cre</sup> also demonstrated a dysplasia of bronchiole and alveoli in lung, and cancellous layers of the diaphragm muscle. (Figure 6.6)

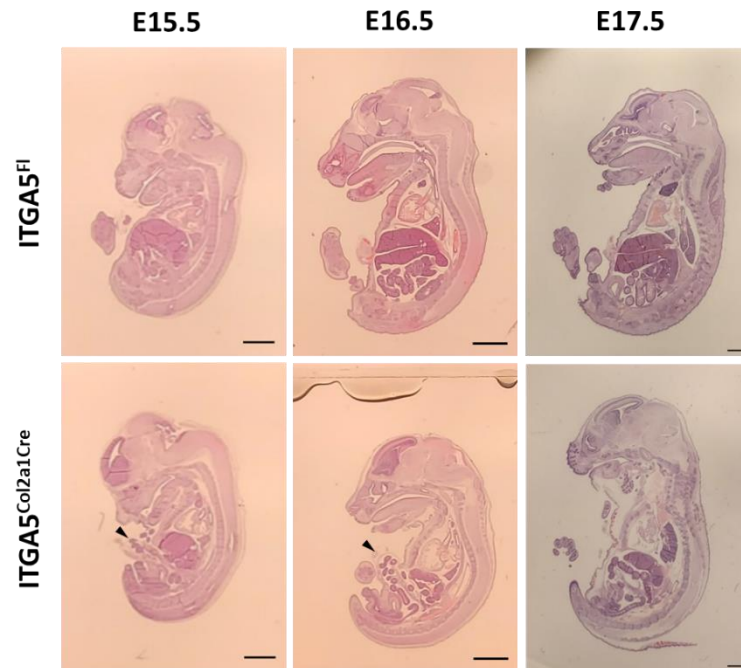


Figure 6.5 Sagittal sections from embryos of *ITGA5* cartilage-specific knockout mice. Embryos were fixed in formalin, processed and sagittally embedded in paraffin, and sectioned in 5 $\mu$ m. Sections were stained using Haematoxylin/Eosin. Omphalocele (arrowheads) were observed in *ITGA5*<sup>Col2a1Cre</sup> at E15.5 and E16.5 comparing with *ITGA5*<sup>Fl</sup> controls. At E17.5, global tissue degradation observed in *ITGA5*<sup>Col2a1Cre</sup>. Scale bar, 1mm.

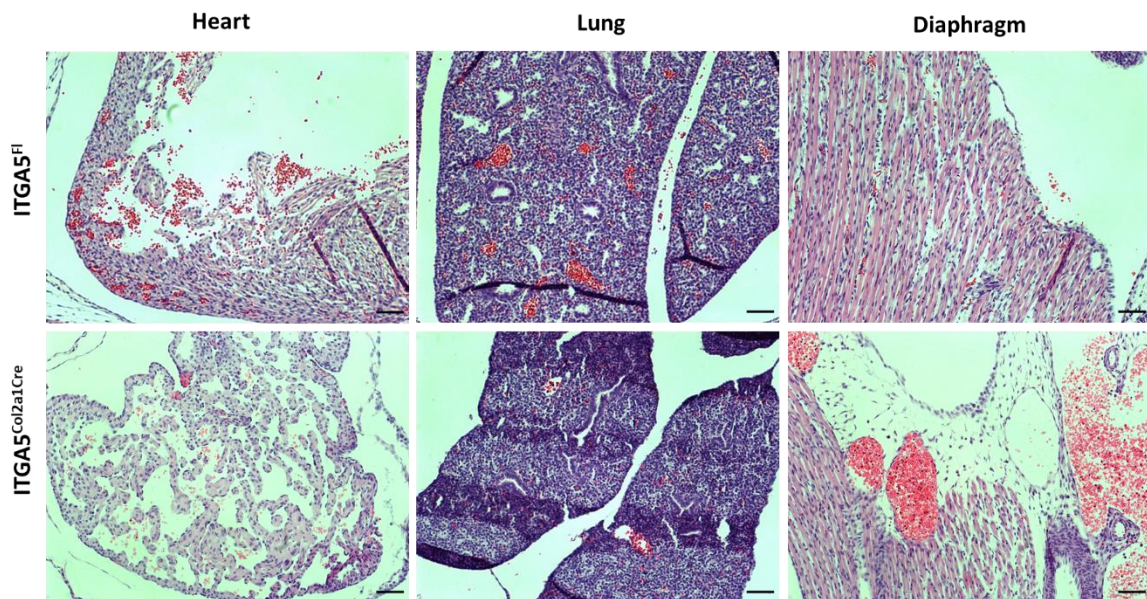


Figure 6.6 Sections from representative E17.5 embryo tissues. Embryos were fixed in formalin, processed and embedded in paraffin, and sectioned in 5 $\mu$ m. Sections were stained using Haematoxylin/Eosin. Scale bar, 100 $\mu$ m. Deficient skeletal development in the *ITGA5* cartilage-specific knockout mice

Whole mount skeletal staining was performed in embryos from E16.5 to E18.5, demonstrating that  $ITGA5^{Col2a1Cre}$  mutants had smaller skeleton size as a whole (Figure 6.7A) and explicitly shorter limb bones (Figure 6.7B) than the  $ITGA5^{Fl}$  controls. Additionally, lengths of humerus (E16.5,  $p=0.017$ ; E17.5,  $p=0.0046$ ; E18.5,  $p=0.031$ ), ulna (E16.5,  $p=0.017$ ; E17.5,  $p=0.024$ ; E18.5,  $p=0.0092$ ), femur (E16.5,  $p=0.037$ ; E17.5,  $p=0.008$ ; E18.5,  $p=0.023$ ) and tibia (E16.5,  $p=0.037$ ; E17.5,  $p=0.0063$ ; E18.5,  $p=0.013$ ) were measured and analysed in quantity. Significantly shorter length was observed in all investigated long bones of  $ITGA5^{Col2a1Cre}$  mutants (Figure 6.8).

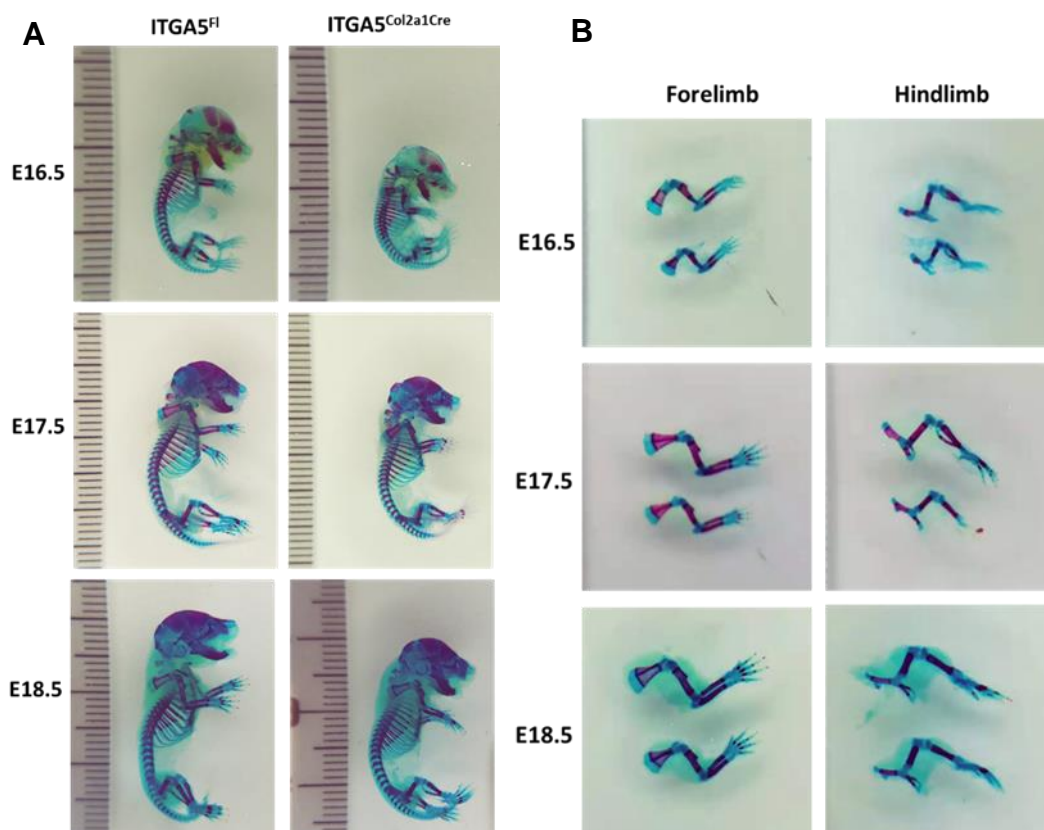


Figure 6.7 Whole mount skeletal preparation of embryos of  $ITGA5$  cartilage-specific knockout mice. Skeleton from embryos at indicated stages were processed and stained by Alcian Blue/ Alizarin Red S. (A) Overview of the embryo skeleton.  $ITGA5^{Col2a1Cre}$  mutants showed smaller size than  $ITGA5^{Fl}$  controls. (B) Comparison of Forelimb and hindlimb between  $ITGA5^{Col2a1Cre}$  mutants and  $ITGA5^{Fl}$  controls. The upper presented  $ITGA5^{Fl}$  control limbs, the lower presented  $ITGA5^{Col2a1Cre}$  mutant limbs. Lengths of limb bones of  $ITGA5^{Col2a1Cre}$  mutants were shorter than those of  $ITGA5^{Fl}$  controls.

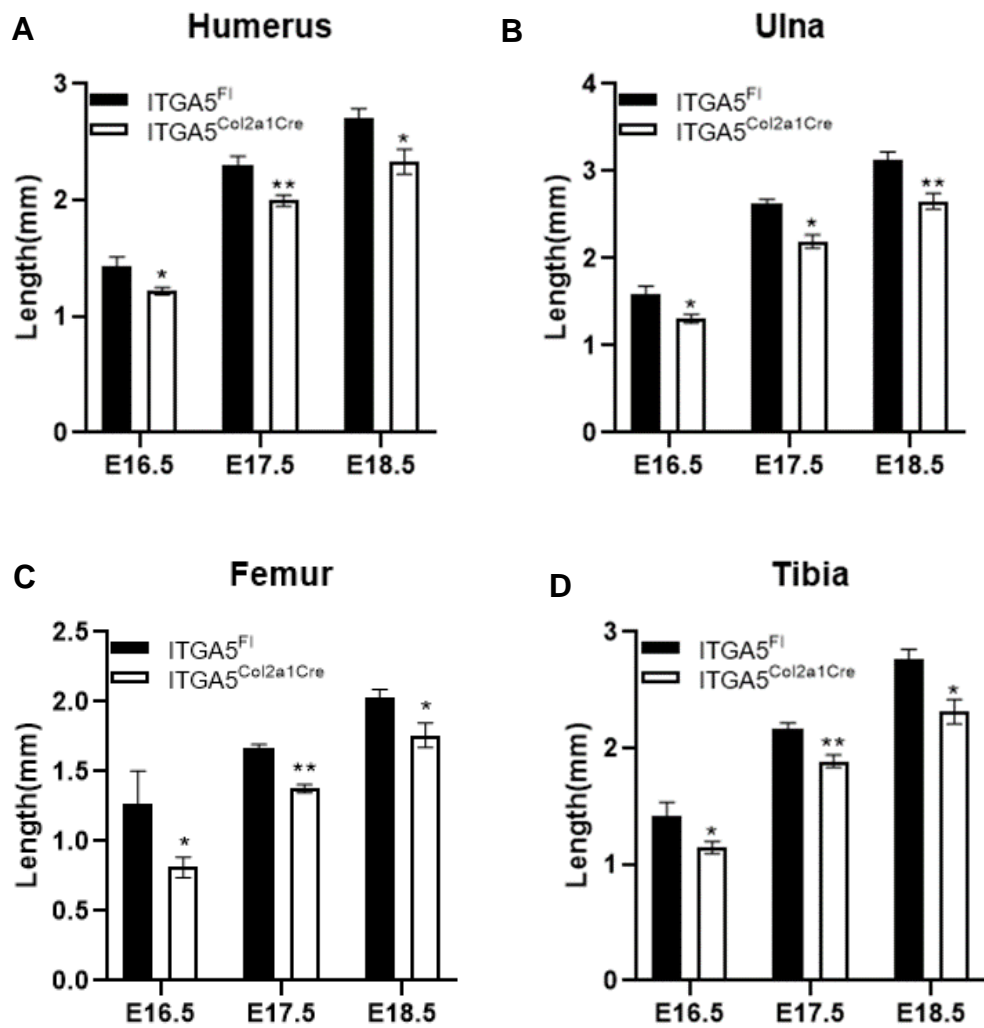


Figure 6.8 Quantification of the length of long bones of *ITGA5* cartilage-specific knockout mice. Embryos undergone skeletal staining with Alcian Blue/ Alizarin Red S. Limbs including humerus (A), ulna (B), femur (C) and tibia (D) were then carefully isolated from the skeleton and photographed. Lengths of desired bones were measure using ImageJ. Statistical analysis was performed using unpaired Student's t-test. Values show mean  $\pm$  SEM, N=5, \*,  $P < 0.05$ ; \*\*,  $P < 0.01$ .

### 6.3.3 Impaired postnatal development in the ITGA5 cartilage-specific knockout mice

In the line of ITGA5<sup>Col2a1Cre</sup> mutants that survived and was bred forwards, we analysed the growth plate at p21. Here, at p21, survival ITGA5<sup>Col2a1Cre</sup> mutants appeared to be smaller than ITGA5<sup>FL</sup> littermate controls (Figure 6.9A). Secondary ossification centre of proximal tibia turned out to be smaller and demonstrated thinner and more sparse trabecular bone in ITGA5<sup>Col2a1Cre</sup> mutants (Figure 6.9B). Looking at growth plates, there was not apparent disorganization of chondrocytes (Figure 6.9B). Surprisingly, the average area of proliferation zone increased ( $p=0.0443$ ), while the hypertrophic zone decreased significantly ( $p=0.0085$ ), implying the differentiation of proliferating cells towards the hypertrophic cells and terminal differentiation and calcification of the hypertrophic chondrocytes were possibly disrupted in the mutant tibia (Figure 6.9C).

Moreover, based on a weekly track of body weight, significantly smaller body mass (approximately 1.5g less than those of controls) was identified in ITGA5<sup>Col2a1Cre</sup> mutants until 10 weeks after birth, after which ITGA5<sup>FL</sup> controls were caught up gradually. (Figure 6.10)

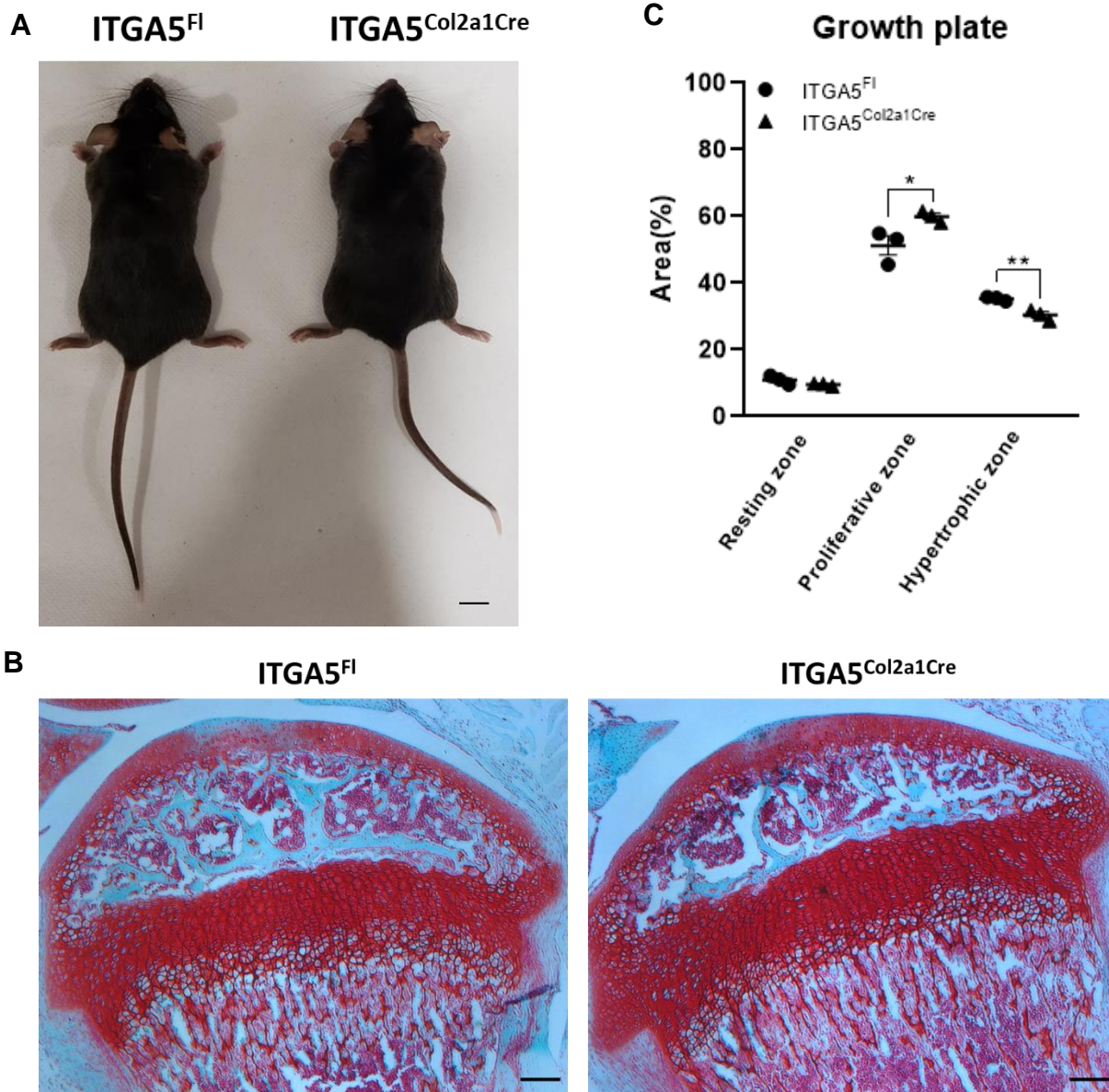


Figure 6.9 Growth plates ITGA5 cartilage-specific knockout mice at p21 were analysed in proximal heads of tibia. (A) Phenotypes of ITGA5<sup>Col2a1Cre</sup> mutants and ITGA5<sup>Fl</sup> littermate controls. Scale bar, 1cm. (B) Knees were harvested at p21, followed by fixation in formalin, processing and paraffin embedding in sagittal, and sectioned in 5µm. Sections were stained using Safranin O/Fast Green. Scale bar, 100µm. (C) Quantification of the area of resting zone, proliferative zone and hypertrophic zone of tibia growth plates at p21. Statistical analysis was performed using unpaired Student's t-test. Values show mean ± SEM, N=3, \*, P<0.05; \*\*, P<0.01.

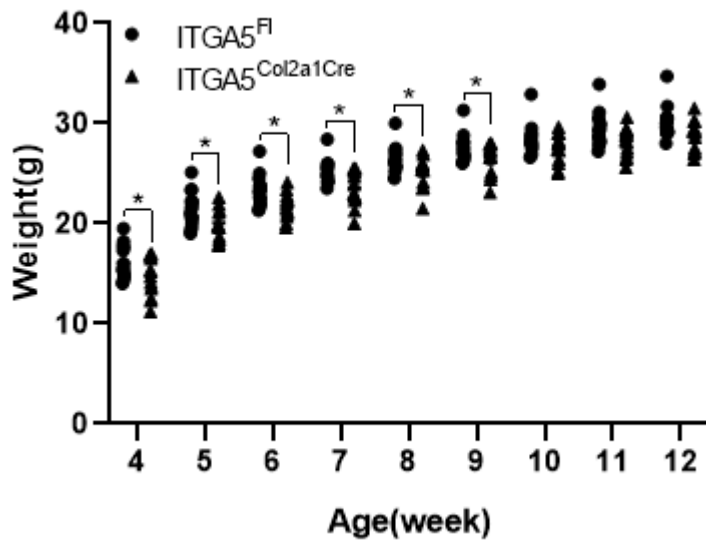


Figure 6.10 Mice weight monitoring. Born mice were weighed weekly from 4 weeks till 12 weeks. Statistical analysis was performed using unpaired Student's *t*-test. Values show mean  $\pm$  SEM, N=10, \*, *P*<0.05.

### 6.3.4 Accelerated osteoarthritis progression in the ITGA5 cartilage-specific knockout mice

DMM modelling surgery was performed on the right knee of 12 weeks old mice. A sham surgery without dissecting the medial meniscotibial ligament were carried out as a control. At 10 weeks post-surgery, histological analysis based on cartilage structure showed that OA like phenotypes, including loss of staining, fibrillation, cleavage and cartilage degeneration, were observed in DMM modelling mice compared with Sham mice, and deteriorated in ITGA5<sup>Col2a1Cre</sup> mutants. (Figure 6.11)

With regard to OARSI scores, higher grades were revealed in medial compartments ( $1.83 \pm 1.09$  to  $5.33 \pm 0.67$ ) of DMM induced knee joints, comparing with the lateral compartments ( $1.00 \pm 0.50$  to  $1.67 \pm 0.33$ ). However, OARSI scores didn't show any significance between ITGA5<sup>Col2a1Cre</sup> mutants and ITGA5<sup>Fl</sup> controls, rather an increased trend of cartilage degeneration in mutants, largely subject to the small number of experimental animals. (Figure 6.12)

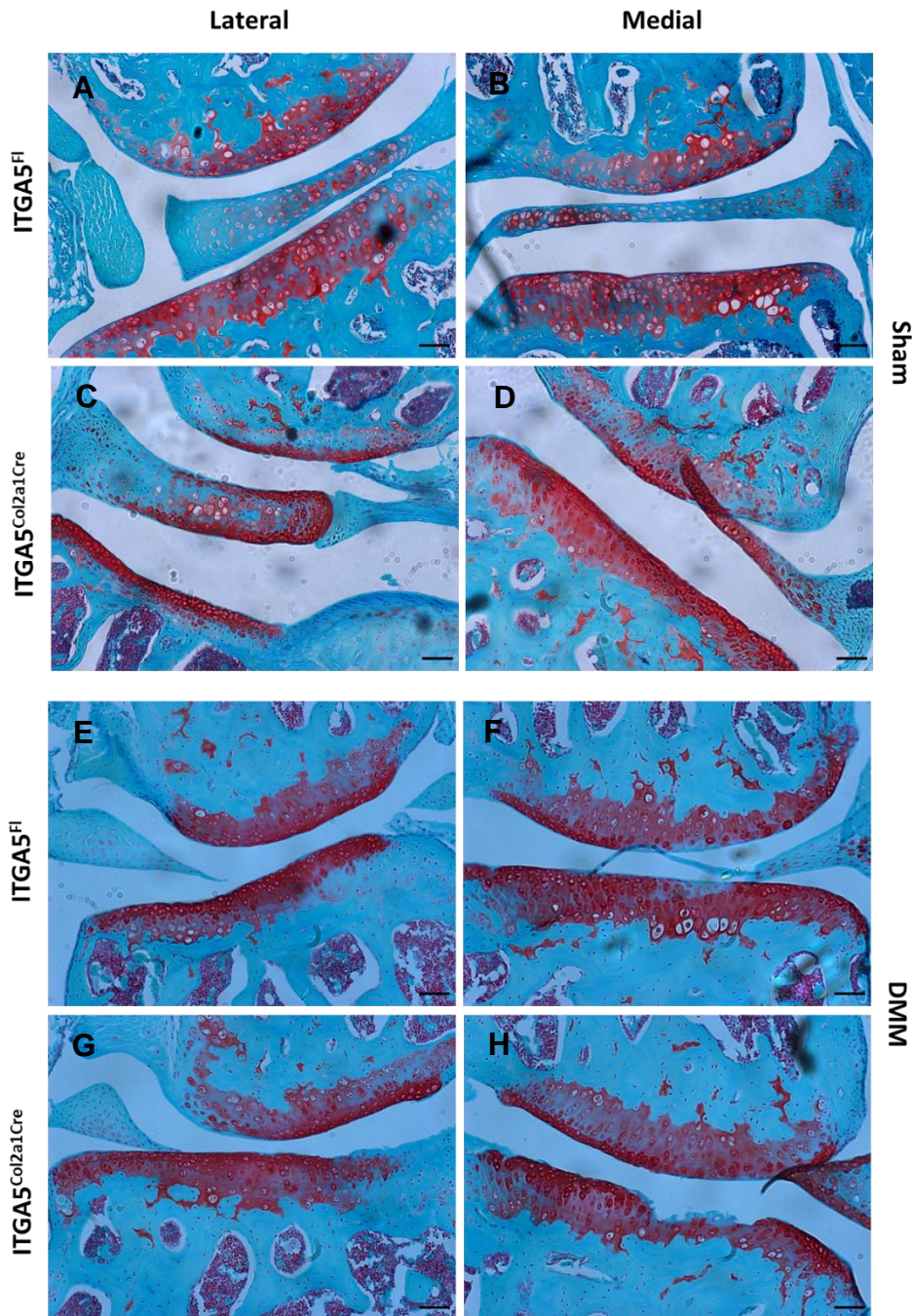


Figure 6.11 Representative images of knee joints of ITGA5 cartilage-specific knockout mice at 10 weeks following Sham or DMM surgery. Knees were harvested at 10 weeks after Sham (A-D) or DMM (E-H) surgery, followed by fixation in formalin, processing and paraffin embedding in frontal, and serially sectioned in 5 $\mu$ m. Sections were stained using Safranin O/Fast Green. Upper indicated femoral condyle and lower indicated tibial plateau. Loss of staining, fibrillation and cartilage erosion were featured on the medial tibial plateau and medial femoral condyle of DMM knees (F, H). Lesions were worsened in the ITGA5<sup>Col2a1Cre</sup> mutants (H). OARSI scoring system were applied to assess OA severity. First score represented femoral condyle, second score was tibial plateau; (A-E) 0, 0; (F) 0.5, 0.5; (G) 0, 0.5; (H) 0.5, 4. Scale bar, 100 $\mu$ m.

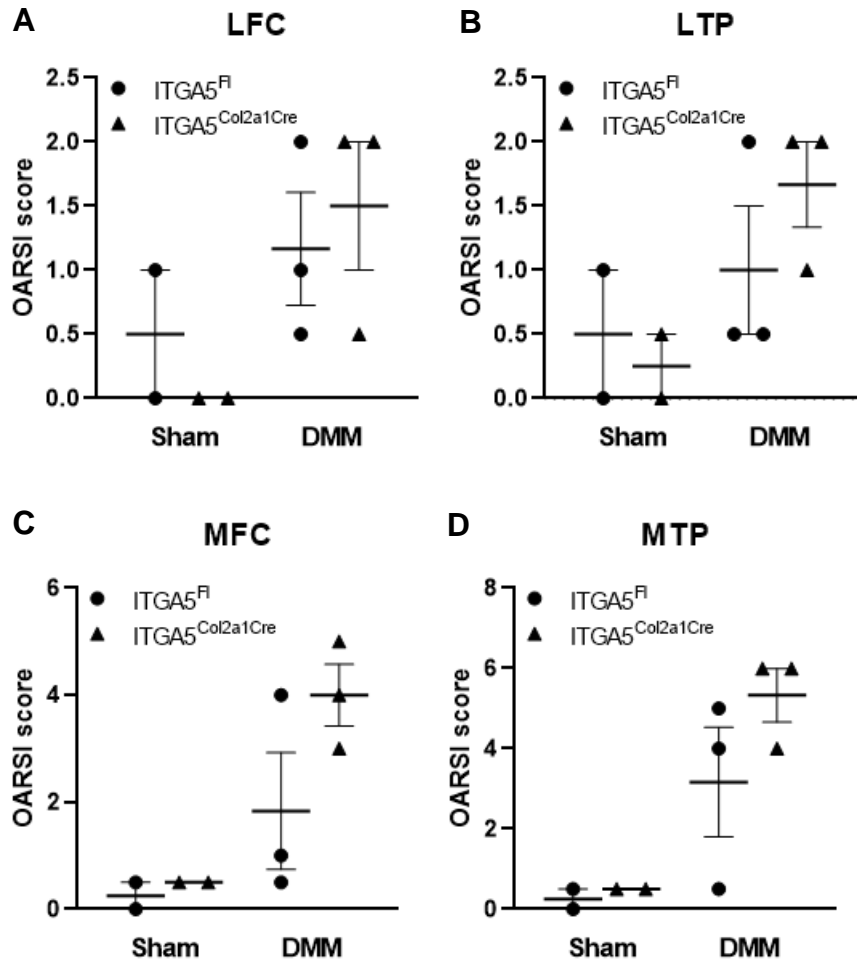


Figure 6.12 Histological analysis of four compartments of knees via OARSI scoring system. Knees were harvested at 10 weeks after DMM or Sham surgery, followed by fixation in formalin, processing and paraffin embedding in frontal, and serially sectioned in 5 $\mu$ m. For each knee, 15 sections with 25 $\mu$ m intervals were stained using Safranin O/Fast Green were scored. Scoring was applied to (A) LFC, lateral femoral condyle; (B) LTP, lateral tibial plateau; (C) MFC, medial femoral condyle and (D) MTP, medial tibial plateau separately. Statistical analysis was performed using a non-parametric Kruskal-Wallis test with Dunn's post hoc test. Values showed mean  $\pm$  SEM of maximal score for each knee. Sham, N=2; DMM, N=3.

## 6.4 Discussion

In this project, an ITGA5 cartilage-specific knockout transgenic mice line was successfully generated, with approximately 70% reduction of the ITGA5 expression in cartilaginous tissue. It has been known that ITGA5 null mice demonstrated lethal embryonic phenotype due to severe mesodermal defects (331, 332). Our ITGA5 conditional knock out mice was still featured with severe embryonic lethality. In embryos lacking both endothelial ITGA5 and ITGAV in their endothelial cells, remodelling of the vasculature impaired leading to embryonic death at E14.5(221). Even though COL2A1 is a key ECM molecule in cartilage, during development stage of mouse embryos between E9.3- E13.5, its transcripts are expressed and detected in various tissues including notochord, somatic mesoderm, otic capsule and fetal brain etc.(335, 336). Consistently, in Sakai et al.'s study where the COL2A1-Cre transgenic mice were firstly reported, transient Cre expression driven by the promoter of COL2A1 was found in hindbrain, notochord, developing eye and heart during E9.5- E11.5 (220). This is in agreement with our data showing the expression of Cre-excised ITGA5 in a tissue panel, where there was a significant reduction detected in heart and kidney. Consistently, according to a study of integrin  $\beta$ 1 conditional knockout mice using the same COL2A1-Cre mice, similar low survival ratio at 3 in 223 was reported (337). Despite we found strikingly developmental delay with omphalocele at E15.5 and E16.5, followed by extensive defects all over the embryos at E17.5, we haven't found out the cause resulting in the embryonic lethality yet. As there existed a transient Cre positive activity in non-cartilaginous tissues at the early stage of embryo development in the COL2A1-Cre mice (220), we highly suspected that the expression of Cre out of cartilaginous tissue resulting in unexpected deletion of ITGA5. This is in line with our data in the tissue screening for ITGA5 expression. Besides, malformation of cardiovascular and respiratory system was observed in E17.5 ITGA5<sup>Col2a1Cre</sup> mutants, this developmental failure could be one of the reasons for death.

The onset of chondrogenesis is primarily featured with intercellular space shrinkage and MSC condensation, degenerating the morphogenesis of developing limb bones in embryogenesis (338, 339). Early in vitro studies have revealed that ITGA5 was present in the cartilage nodules and perichondrium that were differentiated from the niche of mouse limb bud mesenchymal cells during the early stage of chondrogenesis

(338, 340). Unanimously, in human fetal knees, ITGA5 was strongly and ubiquitously expressed in cartilaginous tissues including articular, epiphyseal, growth plate and meniscal cartilage (341). These indicate the essential roles of ITGA5 in the early stage of skeletal development. Moreover, in the research of Aszodi et al.(337), the ablation of integrin  $\beta 1$  resulted in severe chondrodysplasia and progressively dwarfism in mice at both embryonic (E14.5-E17.5) and postnatal (6 weeks) development stages. Additionally, the study revealed that the integrin  $\beta 1$  cartilage-specific knockouts mutant was characterized with reduced hypertrophic chondrocytes, delayed mineralization and vascularization, disorganization of growth plate, demonstrating impaired chondrocyte differentiation and defective endochondral bone formation. Using isolated primary chondrocytes from the  $\beta 1$  mutants, reduced ability of adhesion to fibronectin ligand was also observed. Interestingly, in this study, FACS analysis of primary rib chondrocytes isolated from the  $\beta 1$  knockout mice demonstrated the absence of integrin  $\beta 1$  was correlated with a decrease of other integrin subunits including ITGA5. As ITGA5 forms dimers with  $\beta 1$  in chondrocytes and can recognize fibronectin (59). We hypothesize that ITGA5 is essential in the endochondral bone formation, and the absence of ITGA5 can trigger similar phenotype as that of  $\beta 1$ . As expected, ITGA5<sup>Col2a1Cre</sup> mutants turned to have less body mass than ITGA5<sup>Fl</sup> controls. Significantly shorter length of limb bones of mutant embryos, as well as relatively longer length of proliferative zone and shorter hypertrophic zone of the growth plates of ITGA5<sup>Col2a1Cre</sup> mutants, was also observed. These findings signify ITGA5 is involved in skeletal development.

However, as we only characterized certain phenotypes using basic histologic molecular staining on structure of embryos tissues and skeletons as well as the growth plate at p21. More investigation is worthy to do. To further confirm the Cre activity and ITGA5 expression in ITGA5 cartilage-specific knockout stain, immunohistochemistry (IHC), in situ hybridization (ISH) can be applied. R26R reporter mice can also be crossed with ITGA5 cartilage-specific knockout stain, where the expression of lacZ can be induced by Cre recombinase, enabling to detect Cre activity by X-gal staining.(342) Structures of growth plates can be characterized by detecting specific marker genes of different zones, for instance, COL2A1 used for defining proliferative zone and COL10A1 for hypertrophic zone. For functional investigation on chondrocytes lacking

ITGA5, primary chondrocytes can be isolated from ITGA5<sup>Col2a1Cre</sup> mutants for cell migration, adhesion and downstream pathways such as ERK and PI3K/Akt signalling.(65, 343)

To explore the effects of ITGA5 in pathogenesis and progression of osteoarthritis, we surgically induced osteoarthritis by destabilization of the medial meniscus on 12-week-old mice and scoring according to the structural changes of articular cartilage was performed at 10 weeks post-surgery. In despite of tendentious higher OARSI scores and worse cartilage damage in ITGA5<sup>Col2a1Cre</sup> mutants, no statistical significance found, subject to limited number of experiment mice. It is desperate to recruit more mice to supplement. Moreover, to better investigate the progression of DMM-induced osteoarthritis in our ITGA5 cartilage-specific knockout strain, assessment is interesting to be performed at serial harvest time such as 4 weeks, 8 weeks and 12 weeks post-surgery. The scoring system we applied is the OARSI recommended semiquantitative grading scheme(224), which composed of 8 grades (0-6, Table 2.14). Frankly speaking, the rank is narrow in assessment for small animals like mice. McNulty et al. (344) has developed a comprehensive and quantitative grading system consisting of both measurements and semiquantitative scores, supposed to be more reliable and applicable. It is composed of more grades (0-12) than grades (0-6) of the OARSI scoring system (224). Besides the scores of articular cartilage structure, the developed system includes fifteen parameters based on the area and thickness of articular cartilage and subchondral bone, area of chondrocyte death, area of menisci, size of osteophytes and loss of Safranin O staining. This improvement endues increased accuracy and specificity in the histological assessment of OA lesions in mice.

In a nutshell, we discovered significant developmental defects in skeletal development and possible accelerated progression of osteoarthritis in ITGA5 cartilage-specific knockout mice, strongly suggesting that ITGA5 is crucial in these processes. In other words, miR-3085-3p potentially has a negative influence on skeletal development and osteoarthritis by targeting ITGA5.

## Chapter 7 General discussion and future direction

Osteoarthritis is a common, skeletal disease characterized by articular cartilage degeneration and joint inflammation(345). The main clinical symptoms are chronic pain and joint dysfunction, which seriously affect the quality of life of patients. The disease is more common in middle-aged and elderly people, and about 80% of people aged $\geq$ 60 years have osteoarthritis (346). Osteoarthritis is caused by mechanical, genetic and environmental factors. Factors such as age hormones, diet, infection, trauma, alcohol intake and exposure to tobacco smoke, etc., will increase the risk of developing OA (347). Chondrocytes are the only cells in articular cartilage. The degradation of extracellular matrix, chondrocyte apoptosis and the production of cytokines are critical to the pathological progress of OA (31).

MicroRNAs are closely involved in skeletal development and progression of OA. By examining the growth plates, reduced proliferation but enhanced differentiation of chondrocytes is observed in cartilage specific Dicer null mice, implying that microRNAs as a class of molecules are important in skeletogenesis. As mentioned above, Dicer is closely involved in the biogenesis of miRNAs, the abnormal developing pattern of chondrocyte along with reduced expression level of miRNAs due to the deficiency of Dicer implies a vital impact of miRNAs in chondrogenesis and skeletal development (348). The expression of miR-140 was further investigated and confirmed to be specifically expressed in cartilaginous tissues during the skeletal development of mouse embryos (349). Taking advantage of miR-140 knock out mice, short stature and age-related osteoarthritic manifestations with loss of proteoglycan and fibrosis of the articular cartilage were observed, attributed to increased expression of ADAMTS-5. On the contrary, mice characterized by overexpression of miR-140 exhibited resistance to antigen-induced OA. Moreover, miR-140 directly targets the insulin-like growth factor binding protein (IGFBP)-5 which leads to an increased IGF-1 level and thereby a release of cartilage damage (350). Taken as a whole, miRNA-140 gets involved in the cartilage development and homeostasis, showing a crucial effect during the progression of OA.

## 7.1 Validation and optimization

MiR-3085-3p was a novel microRNA found by next generation deep sequencing in our lab, which had a cartilage-specific expression pattern. ITGA5 was also shown to be a direct target of miR-3085-3p.

To validate a direct target of microRNA, analogues or antagonist are commonly used to overexpress or repress the miRNA level. qRT-PCR is applied to detect the mRNA expression of target genes after interfering the level of microRNA. Western blot is used for testing the target genes at protein level. While in Luciferase assay, luciferase reporters are constructed where the luciferase activity are controlled by the 3'UTR of potential target genes, enabling researchers to investigate whether a microRNA repress the putative genes by targeting the seed sites within its 3'UTR. However, there was a lot of variability in the concentrations of mimics and inhibitors, times of transfection etc. So, we used ITGA5, a validated target gene of miR-3085-3p to optimize the working dosage and time points across cell lines and assays. In Chapter 3, it was confirmed that ITGA5 mRNA can be downregulated by overexpression of miR-3085-3p in cell lines except HACs where no repression by miR-3085-3p mimic was observed. Whilst an inhibitor of miR-3085-3p significantly increased ITGA5 mRNA just at a low concentration, 5nM. Taking consideration of the high basal expression level of miR-3085-3p in HACs, optimal working dose of miR-3085-3p mimic should be out of our indicated range (5nM-100nM). Using higher dosage in HACs from the same patient might be of help to improve the reproducibility. Besides, C28/I2, the human chondrocyte cell line did not positively respond as well. According to Goldring MB et al.'s (351) suggestion, culture strategies including culturing in high density and serum-free medium, suspending over agarose or polyhydroxyethylmethacrylate (polyHEMA), or within scaffolds could keep the proliferative capacity and avoid loss of phenotype of chondrocyte cell lines.

## 7.2 MiR-3085-3p in cartilage homeostasis and chondrocyte function

We then moved forward to the exploration of roles of miR-3085-3p in cartilage homeostasis and chondrocyte function. MicroRNAs can regulate the expression of extracellular matrix genes and cartilage degradation-related enzymes, by which exert

effects on the cartilage homeostasis and OA pathology (352, 353). Moreover, microRNAs participate in the regulation of inflammatory transmitters, vascular endothelial growth factor and nerve growth factor through multiple signalling pathways to promote or inhibit the progression of OA (354). Chapter 4 demonstrated that miR-3085-3p efficiently decrease the expression of both ACAN and COL2A1. ACAN and COL2A1 are predominantly expressed by chondrocytes and essential in maintaining normal structure and function of extracellular matrix in articular cartilage. In this project, miR-3085-3p were found to efficiently decrease the expression of both ACAN and COL2A1, implying that it could induce the ECM generation and homeostasis in cartilage. IL-1 $\beta$ -induced MMP13 was highly expressed at the presence of miR-3085-3p, whilst MYD88, a key TLR/ILR adaptor that could induce downstream expression of MMP13, was downregulated by overexpression of miR-3085-3p at 8h after IL-1 $\beta$  stimulation. Meanwhile, decreased phospho-p65 and p65 was observed at early stage of stimulation (30 minutes). In addition, IL-1 is able to induce MMP13 through different signalling pathways such as p38 MAPK and JNK (244) and STAT pathways (355). We suspect that miR-3085-3p transiently hampers NF $\kappa$ B signalling pathway by directly repressing MYD88 at early time point, which is compensated by activation of other signalling pathways. Our data also showed that miR-3085-3p decreased SMAD2, SMAD3 and SMAD4, known as the essential transducers for TGF $\beta$  signal. PAI1 and TIMP3 are two commonly used TGF $\beta$  responsive genes, but not applicable in this context as their 3'UTR contain seed sites of miR-3085-3p. Similar to the NF $\kappa$ B signalling, miR-3085-3p demonstrated an upregulation of the canonical WNT target gene AXIN2 but decreased both  $\beta$ -catenin and phospho- $\beta$ -catenin. There are 4 major transcript variants of  $\beta$ -catenin. One of them have the seed site of miR-3085-3p in its 3'UTR. So, the downregulation of  $\beta$ -catenin by miR-3085-3p could be transient as well. Time course detection on the protein level is necessary to verify our suggestion. Besides, our experiments here was subjected to the shortage of HAC resource, some are done using SW1353 cell line, which was a limitation.

In addition to the pathways we studied in this project, other signalling such as non-canonical WNT pathway, MAPK pathway, Notch pathway and Hedgehog pathway also take a crucial part in OA and worth being explored in the future.

### 7.3 MiR-3085-3p in human BMMSC differentiation

In order to investigate the influence of miR-3085-3p on hBMMSC differentiation predominantly on chondrogenesis and osteogenesis. During differentiation, we found that overexpression of miR-3085-3p inhibited chondrogenesis and adipogenesis, but promote osteogenesis, confirmed by the expression of corresponding marker gene and molecular staining. These indicate that miR-3085-3p did participate in the regulation of these processes. We then further identified putative target genes of miR-3085-3p that altered during hBMMSC differentiation. We compared two RNA sequencing datasets, one was from primary HACs where miR-3085-3p mimic or inhibitor was transfected and one was from chondrogenic MSCs. Top 20 overlapped genes were screened out as putative targets, which decreased with miR-3085-3p mimic, increased with miR-3085-3p inhibitor and changed during chondrogenesis. Validation was done in HACs using qRT-PCR and subsequent in SW1353 cells using luciferase assay. Interestingly, miR-3085-3p reduced c-JUN and c-FOS, two members of AP-1 family. AP-1 can be induced by phosphorylated c-JUN which activated by the phosphorylation of JNK (244, 311). Other studies reported that, through IL-1 stimulated MAPK/JNK pathway, MMP13 can be induced by the interaction between c-JUN/c-FOS with RUNX2 (313, 315). Our data showed overexpression of miR-3085-3p increased IL-1 $\beta$ -induced c-JUN/c-FOS at an early stage (30 minutes) and subsequent MMP-13. MiR-3085-3p also resulted in a transient activation of the phosphorylation of JNK. Taken together, miR-3085-3p could promote IL-1 induced MMP-13 through activating the JNK/AP-1 signalling pathway.

In the same way, we found CMTM3, LBH and CTDSP2 were direct targets of miR-3085-3p. Furthermore, knock down of these genes by siRNA silence respectively enhanced osteogenesis, in accordance with the promotion of osteogenesis by miR-3085-3p overexpression. suppression of CMTM3 promoted osteogenesis through activation of the phosphorylation of Erk1/2 in CMTM3 KO mice (326). MiR-3085-3p possibly contributed to the promotion of osteogenesis by directly targeting CMTM3 leading to the activation of Erk1/2 signalling pathway. Previously, LBH was found predominantly expressed in late hypertrophic chondrocytes and osteoblasts. Overexpressing LBH gave rise to delayed chondrocyte hypertrophy and osteoblast maturation in chicken wings (327). This indicate miR-3085-3p possibly get involved in

the terminal differentiation of chondrocytes and skeletal formation. What's more, CTDSP2 was reported to mediate the dephosphorylation and degradation of phospho-SMAD1. Loss of function of CTDSP2 individually or co-suppression with CTDSP1 promoted phosphorylation of BMP-induced SMAD1 (330). BMP-SMAD1/5/8 signalling pathway is correlated with the activation of gene transcription involved in osteogenesis, skeletal development and bone formation (329). We thereby deduce that miR-3085-3p is capable to enhancing hBMMSC osteogenesis through the BMP/SMAD1 pathway by downregulating CTDSP2.

However, we had limitations in the study of hBMMSCs differentiation. The BMMSCs we used were derived from bone marrow monocytes from 3 donors, showing different response to the differentiation induction in terms of proliferation rate and differentiation potential, making data analysis difficult. This can be figured out by increasing repeat numbers of experiment. Of the 2 RNA sequencing data for screening potential target gene of miR-3085-3p during osteogenesis, one was from HACs transfected with miR-3085-3p mimic or inhibitor, not osteoblast or BMMSCs, which could have distinct gene expression profiles. Subsequent validation experiments were carried out in HACs and SW1353 cells. Our data will be more convincing if primary osteoblast or osteoblast cell lines such as SaOS-2 are used.

## 7.4 ITGA5 cartilage-specific knockout mice

In the in vivo session of this project. We did not successfully generate the miR-3085-3p null mice, as a consequence of embryonic lethality. In the ITGA5 cartilage-specific knockout mice, embryonic lethality was also observed. In the ITGA5<sup>Col2a1Cre</sup> mutants, we found significant developmental delay at E15.5 and E16.5, followed by extensive defects at E17.5. the deletion of ITGA5 in cartilaginous tissue is likely to cause dysfunction and structural malformation in, for instance, the thorax, leading to respiratory and heart failure. Besides, it has been reported that a transient Cre positive activity in non-cartilaginous tissues such as hindbrain and notochord was observed at the early stage of embryo development in the COL2A1-Cre mice (220). the ITGA5<sup>Col2a1Cre</sup> mutants are possible die from the early Cre activity in the developmental stage for major organs or tissues. We found significant impaired pre- and post-natal development in the ITGA5 cartilage-specific knockout mice characterized with shorter limb bones in late-stage embryos and shorter hypertrophic zone at p21. In the surgical-induced OA model, the ITGA5<sup>Col2a1Cre</sup> mutants didn't show any statistically significance compared to the ITGA5<sup>Fl</sup> controls, but an increasing tendency of the severity of cartilage deterioration. Theses demonstrated developmental defects in skeletal development and possible accelerated progression of osteoarthritis in ITGA5 cartilage-specific knockout mice. In other words, as ITGA5 is a verified target of miR-3085-3p, miR-3085-3p has the potential in repressing skeletal development and exacerbating OA progression. Subject to restricted access to animal facility and control of animal numbers, we need to supplement the study using surgery induced OA modelling. Besides, we only measured the expression of ITGA5 using qRT-PCR. Other experiments such as in situ hybridization or immunohistochemistry should be carried out to detect and confirm the expression ITGA5 and Cre activity. The R26R mouse could also be used to cross with ITGA5<sup>Col2a1Cre</sup> mice, where Cre can activate the LacZ gene by excising the floxed neomycin gene, enabling X-gal staining and visualization the Cre activity (342). As ITGA5 is essential in mediating cell adhesion and mechanotransduction, chondrocytes could also be isolated from ITGA5<sup>Col2a1Cre</sup> mice to test their function involving cell proliferation, apoptosis, adhesion and response to mechanical stress in the absence of ITGA5. Furthermore, due to the frustration in generating miR-3085-3p null mice, we could knockout miR-3085-3p in cells using

CRISPR-CAS9 system to explore the effect of a stable deletion of miR-3085-3p. Overexpression of miR-3085-3p in vivo by delivering mimic or gene knock-in is promising to be involved in the research of miR-3085-3p and OA.

In a nutshell, this project was largely accomplished by addressing the hypothesis that miR-3085-3p takes an active part in skeletal development and OA pathogenesis, and provide insight into the in vivo study of miR-3085-3p.

## Reference

1. Kloppenburg M, Berenbaum F. Osteoarthritis year in review 2019: epidemiology and therapy. *Osteoarthritis and cartilage*. 2020;28(3):242-8.
2. Arthritis V. State of musculoskeletal health 2019. 2019.
3. James SL, Abate D, Abate KH, Abay SM, Abbafati C, Abbasi N, et al. Global, regional, and national incidence, prevalence, and years lived with disability for 354 diseases and injuries for 195 countries and territories, 1990–2017: a systematic analysis for the Global Burden of Disease Study 2017. *The Lancet*. 2018;392(10159):1789-858.
4. Bijlsma JW, Berenbaum F, Lafeber FP. Osteoarthritis: an update with relevance for clinical practice. *The Lancet*. 2011;377(9783):2115-26.
5. Drake R, Vogl AW, Mitchell AW. *Gray's Anatomy for Students E-Book*: Elsevier Health Sciences; 2009.
6. Glyn-Jones S, Palmer AJR, Agricola R, Price AJ, Vincent TL, Weinans H, et al. Osteoarthritis. *The Lancet*. 2015;386(9991):376-87.
7. Aigner T, Van der Kraan P, Van den Berg W. Osteoarthritis and inflammation-inflammatory changes in osteoarthritic synoviopathy. *BIOMEDICAL AND HEALTH RESEARCH-COMMISSION OF THE EUROPEAN COMMUNITIES THEN IOS PRESS*. 2007;70:219.
8. Day J, Ding M, Van Der Linden J, Hvid I, Sumner D, Weinans H. A decreased subchondral trabecular bone tissue elastic modulus is associated with pre-arthritic cartilage damage. *Journal of orthopaedic research*. 2001;19(5):914-8.
9. van der Kraan PM, van den Berg WB. Osteophytes: relevance and biology. *Osteoarthritis and cartilage*. 2007;15(3):237-44.
10. Goldring SR. Role of bone in osteoarthritis pathogenesis. *Medical Clinics of North America*. 2009;93(1):25-35.
11. Eyre D. Articular cartilage and changes in arthritis: collagen of articular cartilage. *Arthritis Research & Therapy*. 2001;4(1):30.

12. Bekhouche M, Colige A. The procollagen N-proteinases ADAMTS2, 3 and 14 in pathophysiology. *Matrix Biology*. 2015;44:46-53.
13. Vaughan L, Mendler M, Huber S, Bruckner P, Winterhalter KH, Irwin MI, et al. D-periodic distribution of collagen type IX along cartilage fibrils. *The Journal of cell biology*. 1988;106(3):991-7.
14. Eyre DR, Pietka T, Weis MA, Wu J-J. Covalent cross-linking of the NC1 domain of collagen type IX to collagen type II in cartilage. *Journal of Biological Chemistry*. 2004;279(4):2568-74.
15. Kadler KE, Hill A, Canty-Laird EG. Collagen fibrillogenesis: fibronectin, integrins, and minor collagens as organizers and nucleators. *Current opinion in cell biology*. 2008;20(5):495-501.
16. Mecham RP, Birk DE. *Extracellular matrix assembly and structure*: Academic Press; 2013.
17. Fässler R, Schnegelsberg P, Dausman J, Shinya T, Muragaki Y, McCarthy MT, et al. Mice lacking alpha 1 (IX) collagen develop noninflammatory degenerative joint disease. *Proceedings of the National Academy of Sciences*. 1994;91(11):5070-4.
18. Stubendorff J, Lammentausta E, Struglics A, Lindberg L, Heinegård D, Dahlberg L. Is cartilage sGAG content related to early changes in cartilage disease? Implications for interpretation of dGEMRIC. *Osteoarthritis and cartilage*. 2012;20(5):396-404.
19. Lorenzo P, Bayliss MT, Heinegård D. Altered patterns and synthesis of extracellular matrix macromolecules in early osteoarthritis. *Matrix Biology*. 2004;23(6):381-91.
20. Hochberg M, Silman AJ, Smolen J, Weinblatt M, Weisman M. *Rheumatology*: Mosby Ltd.; 2014. 1976 p.
21. Humphries M, Travis M, Clark K, Mould A. *Mechanisms of integration of cells and extracellular matrices by integrins*. Portland Press Limited; 2004.
22. Garcíadiego-Cázares D, Aguirre-Sánchez HI, Abarca-Buis RF, Kouri JB, Velasquillo C, Ibarra C. Regulation of  $\alpha 5$  and  $\alpha V$  Integrin Expression by GDF-5 and BMP-7 in Chondrocyte Differentiation and Osteoarthritis. *PLoS one*. 2015;10(5):e0127166.

23. Xu L, Peng H, Wu D, Hu K, Goldring MB, Olsen BR, et al. Activation of the discoidin domain receptor 2 induces expression of matrix metalloproteinase 13 associated with osteoarthritis in mice. *Journal of Biological Chemistry*. 2005;280(1):548-55.
24. Haglund L, Tillgren V, Önnarfjord P, Heinegård D. The C-terminal peptide of chondroadherin modulates cellular activity by selectively binding to heparan sulfate chains. *Journal of Biological Chemistry*. 2013;288(2):995-1008.
25. Knudson CB, Knudson W. Hyaluronan and CD44: modulators of chondrocyte metabolism. *Clinical orthopaedics and related research*. 2004;427:S152-S62.
26. Nedvetzki S, Gonen E, Assayag N, Reich R, Williams RO, Thurmond RL, et al. RHAMM, a receptor for hyaluronan-mediated motility, compensates for CD44 in inflamed CD44-knockout mice: a different interpretation of redundancy. *Proceedings of the National Academy of Sciences*. 2004;101(52):18081-6.
27. Shoham AB, Rot C, Stern T, Krief S, Akiva A, Dadosh T, et al. Deposition of collagen type I onto skeletal endothelium reveals a new role for blood vessels in regulating bone morphology. *Development*. 2016;143(21):3933-43.
28. Hendriks M, Ramasamy SK. Blood Vessels and Vascular Niches in Bone Development and Physiological Remodeling. *Frontiers in Cell and Developmental Biology*. 2020;8.
29. Mackie E, Ahmed Y, Tatarczuch L, Chen K-S, Mirams M. Endochondral ossification: how cartilage is converted into bone in the developing skeleton. *The international journal of biochemistry & cell biology*. 2008;40(1):46-62.
30. De Crombrughe B, Lefebvre V, Behringer RR, Bi W, Murakami S, Huang W. Transcriptional mechanisms of chondrocyte differentiation. *Matrix Biology*. 2000;19(5):389-94.
31. Aigner T, Söder S, Gebhard PM, McAlinden A, Haag J. Mechanisms of disease: role of chondrocytes in the pathogenesis of osteoarthritis—structure, chaos and senescence. *Nature Clinical Practice Rheumatology*. 2007;3(7):391-9.

32. Brew C, Andrew J, Boot-Handford R, Hardingham T. Late osteoarthritic cartilage shows down regulation of SOX9 and aggrecan expression but little evidence of chondrocyte hypertrophy. *Trans Orthop Res Soc.* 2004;50:938.
33. Tew SR, Li Y, Pothacharoen P, Tweats LM, Hawkins RE, Hardingham TE. Retroviral transduction with SOX9 enhances re-expression of the chondrocyte phenotype in passaged osteoarthritic human articular chondrocytes. *Osteoarthritis and cartilage.* 2005;13(1):80-9.
34. Li Y, Tew SR, Russell AM, Gonzalez KR, Hardingham TE, Hawkins RE. Transduction of passaged human articular chondrocytes with adenoviral, retroviral, and lentiviral vectors and the effects of enhanced expression of SOX9. *Tissue engineering.* 2004;10(3-4):575-84.
35. Stöcker W, Bode W. Structural features of a superfamily of zinc-endopeptidases: the metzincins. *Current opinion in structural biology.* 1995;5(3):383-90.
36. Gomis-Rüth FX. Structural aspects of the metzincin clan of metalloendopeptidases. *Molecular biotechnology.* 2003;24(2):157-202.
37. Porter S, Clark IM, Kevorkian L, Edwards DR. The ADAMTS metalloproteinases. *Biochemical Journal.* 2005;386(1):15-27.
38. Nagase H, Visse R, Murphy G. Structure and function of matrix metalloproteinases and TIMPs. *Cardiovascular research.* 2006;69(3):562-73.
39. Kelwick R, Desanlis I, Wheeler GN, Edwards DR. The ADAMTS (A Disintegrin and Metalloproteinase with Thrombospondin motifs) family. *Genome biology.* 2015;16(1):1-16.
40. Baker AH, Edwards DR, Murphy G. Metalloproteinase inhibitors: biological actions and therapeutic opportunities. *Journal of cell science.* 2002;115(19):3719-27.
41. Tang BL. ADAMTS: a novel family of extracellular matrix proteases. *The international journal of biochemistry & cell biology.* 2001;33(1):33-44.

42. Stamenkovic I. Extracellular matrix remodelling: the role of matrix metalloproteinases. *The journal of Pathology: a Journal of the Pathological Society of Great Britain and Ireland*. 2003;200(4):448-64.
43. Bonnans C, Chou J, Werb Z. Remodelling the extracellular matrix in development and disease. *Nature reviews Molecular cell biology*. 2014;15(12):786-801.
44. Glasson SS, Askew R, Sheppard B, Carito B, Blanchet T, Ma H-L, et al. Deletion of active ADAMTS5 prevents cartilage degradation in a murine model of osteoarthritis. *Nature*. 2007;446(7131):102-.
45. Song RH, Tortorella M, Malfait AM, Alston JT, Yang Z, Arner EC, et al. Aggrecan degradation in human articular cartilage explants is mediated by both ADAMTS-4 and ADAMTS-5. *Arthritis & Rheumatology*. 2007;56(2):575-85.
46. Fosang AJ, Last K, Knäuper V, Murphy G, Neame PJ. Degradation of cartilage aggrecan by collagenase-3 (MMP-13). *FEBS letters*. 1996;380(1-2):17-20.
47. Stanton H, Rogerson FM, East CJ, Golub SB, Lawlor KE, Meeker CT, et al. ADAMTS5 is the major aggrecanase in mouse cartilage in vivo and in vitro. *Nature*. 2005;434(7033):648-52.
48. Martel-Pelletier J, McCollum R, Fujimoto N, Obata Ki, Cloutier J-M, Pelletier J-P. Excess of metalloproteases over tissue inhibitor of metalloprotease may contribute to cartilage degradation in osteoarthritis and rheumatoid arthritis. *Laboratory investigation; a journal of technical methods and pathology*. 1994;70(6):807-15.
49. Kevorkian L, Young DA, Darrah C, Donell ST, Shepstone L, Porter S, et al. Expression profiling of metalloproteinases and their inhibitors in cartilage. *Arthritis & Rheumatism: Official Journal of the American College of Rheumatology*. 2004;50(1):131-41.
50. Burrage PS, Mix KS, Brinckerhoff CE. Matrix metalloproteinases: role in arthritis. *Front Biosci*. 2006;11(1):529-43.
51. Malemud CJ. Matrix metalloproteinases (MMPs) in health and disease: an overview. *Frontiers in bioscience: a journal and virtual library*. 2006;11:1696-701.

52. Akkiraju H, Nohe A. Role of Chondrocytes in Cartilage Formation, Progression of Osteoarthritis and Cartilage Regeneration. *Journal of Developmental Biology*. 2015;3(4):177-92.
53. Takada Y, Ye X, Simon S. The integrins. *Genome biology*. 2007;8(5):1-9.
54. Luo B-H, Carman CV, Springer TA. Structural basis of integrin regulation and signaling. *Annu Rev Immunol*. 2007;25:619-47.
55. Barczyk M, Carracedo S, Gullberg D. Integrins. *Cell and Tissue Research*. 2009;339(1):269.
56. Takagi J, Petre BM, Walz T, Springer TA. Global conformational rearrangements in integrin extracellular domains in outside-in and inside-out signaling. *Cell*. 2002;110(5):599-611.
57. Ramage L, Nuki G, Salter D. Signalling cascades in mechanotransduction: cell–matrix interactions and mechanical loading. *Scandinavian journal of medicine & science in sports*. 2009;19(4):457-69.
58. Loeser RF. Integrins and chondrocyte–matrix interactions in articular cartilage. *Matrix Biology*. 2014;39:11-6.
59. Wright M, Nishida K, Bavington C, Godolphin J, Dunne E, Walmsley S, et al. Hyperpolarisation of cultured human chondrocytes following cyclical pressure-induced strain: Evidence of a role for  $\alpha 5\beta 1$  integrin as a chondrocyte mechanoreceptor. *Journal of orthopaedic research*. 1997;15(5):742-7.
60. Johnson A, Smith R, Saxne T, Hickery M, Heinegård D. Fibronectin fragments cause release and degradation of collagen-binding molecules from equine explant cultures. *Osteoarthritis and cartilage*. 2004;12(2):149-59.
61. Homandberg G, Kang Y, Zhang J, Cole A, Williams J. A single injection of fibronectin fragments into rabbit knee joints enhances catabolism in the articular cartilage followed by reparative responses but also induces systemic effects in the non-injected knee joints. *Osteoarthritis and Cartilage*. 2001;9(8):673-83.

62. Xia M, Zhu Y. Fibronectin fragment activation of ERK increasing integrin  $\alpha 5$  and  $\beta 1$  subunit expression to degenerate nucleus pulposus cells. *Journal of Orthopaedic Research*. 2011;29(4):556-61.
63. Pal S, Kumar Ganguly K, Moulik S, Chatterjee A. Modulation of MMPs by cell surface integrin receptor  $\alpha 5\beta 1$ . *Anti-Cancer Agents in Medicinal Chemistry (Formerly Current Medicinal Chemistry-Anti-Cancer Agents)*. 2012;12(7):726-32.
64. Tanaka K, Yokosaki Y, Higashikawa F, Saito Y, Eboshida A, Ochi M. The integrin  $\alpha 5\beta 1$  regulates chondrocyte hypertrophic differentiation induced by GTP-bound transglutaminase 2. *Matrix biology*. 2007;26(6):409-18.
65. Tanaka N, Ikeda Y, Yamaguchi T, Furukawa H, Mitomi H, Nakagawa T, et al.  $\alpha 5\beta 1$  integrin induces the expression of noncartilaginous procollagen gene expression in articular chondrocytes cultured in monolayers. *Arthritis research & therapy*. 2013;15(5):1-13.
66. Garciadiego-Cázares D, Rosales C, Katoh M, Chimal-Monroy J. Coordination of chondrocyte differentiation and joint formation by  $\alpha 5\beta 1$  integrin in the developing appendicular skeleton. *Development*. 2004;131(19):4735-42.
67. Wright M, Jobanputra P, Bavington C, Salter DM, Nuki G. Effects of intermittent pressure-induced strain on the electrophysiology of cultured human chondrocytes: evidence for the presence of stretch-activated membrane ion channels. *Clinical Science*. 1996;90(1):61-71.
68. Millward-Sadler S, Wright M, Lee H-S, Nishida K, Caldwell H, Nuki G, et al. Integrin-regulated secretion of interleukin 4: a novel pathway of mechanotransduction in human articular chondrocytes. *The Journal of cell biology*. 1999;145(1):183-9.
69. Nemoto O, Yamada H, Kikuchi T, Shinmei M, Obata Ki, Sato H, et al. Suppression of matrix metalloproteinase-3 synthesis by interleukin-4 in human articular chondrocytes. *The Journal of rheumatology*. 1997;24(9):1774-9.

70. Shingu M, Miyauchi S, Nagai Y, Yasutake C, Horie K. The role of IL-4 and IL-6 in IL-1-dependent cartilage matrix degradation. *Rheumatology*. 1995;34(2):101-6.
71. Millward-Sadler S, Wright M, Lee H-S, Caldwell H, Nuki G, Salter D. Altered electrophysiological responses to mechanical stimulation and abnormal signalling through  $\alpha 5\beta 1$  integrin in chondrocytes from osteoarthritic cartilage. *Osteoarthritis and cartilage*. 2000;8(4):272-8.
72. Friedland JC, Lee MH, Boettiger D. Mechanically activated integrin switch controls  $\alpha 5\beta 1$  function. *Science*. 2009;323(5914):642-4.
73. Candela ME, Wang C, Gunawardena AT, Zhang K, Cantley L, Yasuhara R, et al. Alpha 5 integrin mediates osteoarthritic changes in mouse knee joints. *PloS one*. 2016;11(6):e0156783.
74. Kim HA, Cho ML, Choi HY, Yoon CS, Jhun JY, Oh HJ, et al. The catabolic pathway mediated by Toll-like receptors in human osteoarthritic chondrocytes. *Arthritis & Rheumatology*. 2006;54(7):2152-63.
75. Shinohara H, Inoue A, Toyama-Sorimachi N, Nagai Y, Yasuda T, Suzuki H, et al. Dok-1 and Dok-2 are negative regulators of lipopolysaccharide-induced signaling. *Journal of Experimental Medicine*. 2005;201(3):333-9.
76. Husa M, Zhao X, Yao H, June R, Terkeltaub R, Liu-Bryan R. MYD88-dependent TLR-2/4 signaling in osteoarthritis: protective or not? *Osteoarthritis and Cartilage*. 2012;20:S234.
77. Liu-Bryan R, Terkeltaub R. Chondrocyte innate immune myeloid differentiation factor 88-dependent signaling drives pro-catabolic effects of the endogenous toll-like receptor 2/toll-like receptor 4 ligands low molecular weight hyaluronan and high mobility group box chromosomal protein 1 in mice. *Arthritis & Rheumatology*. 2010;62(7):2004-12.
78. Hwang HS, Park SJ, Cheon EJ, Lee MH, Kim HA. Fibronectin fragment-induced expression of matrix metalloproteinases is mediated by MyD88-dependent TLR-2 signaling pathway in human chondrocytes. *Arthritis Research & Therapy*. 2015;17:320.

79. Robinson WH, Lepus CM, Wang Q, Raghu H, Mao R, Lindstrom TM, et al. Low-grade inflammation as a key mediator of the pathogenesis of osteoarthritis. *Nature Reviews Rheumatology*. 2016.
80. Zheng C, Yin Q, Wu H. Structural studies of NF- $\kappa$ B signaling. *Cell research*. 2011;21(1):183-95.
81. Rigoglou S, Papavassiliou AG. The NF- $\kappa$ B signalling pathway in osteoarthritis. *The international journal of biochemistry & cell biology*. 2013;45(11):2580-4.
82. Kapoor M, Martel-Pelletier J, Lajeunesse D, Pelletier J-P, Fahmi H. Role of proinflammatory cytokines in the pathophysiology of osteoarthritis. *Nature Reviews Rheumatology*. 2011;7(1):33.
83. Goldring MB, Marcu KB. Cartilage homeostasis in health and rheumatic diseases. *Arthritis research & therapy*. 2009;11(3):1-16.
84. B Marcu K, Otero M, Olivotto E, Maria Borzi R, B Goldring M. NF- $\kappa$ B signaling: multiple angles to target OA. *Current drug targets*. 2010;11(5):599-613.
85. Yasuda T. Activation of Akt leading to NF- $\kappa$ B up-regulation in chondrocytes stimulated with fibronectin fragment. *Biomedical Research*. 2011;32(3):209-15.
86. Ijiri K, Zerbini LF, Peng H, Otu HH, Tsuchimochi K, Otero M, et al. Differential expression of GADD45 $\beta$  in normal and osteoarthritic cartilage: potential role in homeostasis of articular chondrocytes. *Arthritis & Rheumatism: Official Journal of the American College of Rheumatology*. 2008;58(7):2075-87.
87. Goldring MB, Otero M, Plumb DA, Dragomir C, Favero M, El Hachem K, et al. Roles of inflammatory and anabolic cytokines in cartilage metabolism: signals and multiple effectors converge upon MMP-13 regulation in osteoarthritis. *European cells & materials*. 2011;21:202.
88. Natarajan K, Singh S, Burke TR, Grunberger D, Aggarwal BB. Caffeic acid phenethyl ester is a potent and specific inhibitor of activation of nuclear transcription factor NF-kappa B. *Proceedings of the National Academy of Sciences*. 1996;93(17):9090-5.

89. Elmali N, Ayan Í, Türköz Y, Mizrak B, Germen B, Bora A. Effect of caffeic acid phenethyl ester on cartilage in experimental osteoarthritis. *Rheumatology international*. 2002;22(6):222-6.
90. Elmali N, Esenkaya I, Harma A, Ertem K, Turkoz Y, Mizrak B. Effect of resveratrol in experimental osteoarthritis in rabbits. *Inflammation research*. 2005;54(4):158-62.
91. Wang J, Gao J-S, Chen J-W, Li F, Tian J. Effect of resveratrol on cartilage protection and apoptosis inhibition in experimental osteoarthritis of rabbit. *Rheumatology international*. 2012;32(6):1541-8.
92. Gu H, Jiao Y, Yu X, Li X, Wang W, Ding L, et al. Resveratrol inhibits the IL-1 $\beta$ -induced expression of MMP-13 and IL-6 in human articular chondrocytes via TLR4/MyD88-dependent and-independent signaling cascades. *International journal of molecular medicine*. 2017;39(3):734-40.
93. Lianxu C, Hongti J, Changlong Y. NF- $\kappa$ Bp65-specific siRNA inhibits expression of genes of COX-2, NOS-2 and MMP-9 in rat IL-1 $\beta$ -induced and TNF- $\alpha$ -induced chondrocytes. *Osteoarthritis and Cartilage*. 2006;14(4):367-76.
94. Bondeson J, Lauder S, Wainwright S, Amos N, Evans A, Hughes C, et al. Adenoviral gene transfer of the endogenous inhibitor I $\kappa$ B $\alpha$  into human osteoarthritis synovial fibroblasts demonstrates that several matrix metalloproteinases and aggrecanases are nuclear factor-kappaB-dependent. *The Journal of rheumatology*. 2007;34(3):523-33.
95. Olarerin-George AO, Anton L, Hwang Y-C, Elovitz MA, Hogenesch JB. A functional genomics screen for microRNA regulators of NF-kappaB signaling. *BMC biology*. 2013;11(1):19.
96. Undi RB, Gutti U, Sahu I, Sarvothaman S, Pasupuleti SR, Kandi R, et al. Wnt signaling: role in regulation of haematopoiesis. *Indian Journal of Hematology and Blood Transfusion*. 2016;32(2):123-34.
97. Ozawa M, Baribault H, Kemler R. The cytoplasmic domain of the cell adhesion molecule uvomorulin associates with three independent

proteins structurally related in different species. *The EMBO journal*. 1989;8(6):1711-7.

98. Liu C, Li Y, Semenov M, Han C, Baeg G-H, Tan Y, et al. Control of  $\beta$ -catenin phosphorylation/degradation by a dual-kinase mechanism. *Cell*. 2002;108(6):837-47.

99. Slusarski DC, Corces VG, Moon RT. Interaction of Wnt and a Frizzled homologue triggers G-protein-linked phosphatidylinositol signalling. *Nature*. 1997;390(6658):410-3.

100. Slusarski DC, Yang-Snyder J, Busa WB, Moon RT. Modulation of embryonic intracellular  $ca^{2+}$  signaling by wnt-5a. *Developmental biology*. 1997;182(1):114-20.

101. Wang Y, Guo N, Nathans J. The role of Frizzled3 and Frizzled6 in neural tube closure and in the planar polarity of inner-ear sensory hair cells. *Journal of Neuroscience*. 2006;26(8):2147-56.

102. Simons M, Mlodzik M. Planar cell polarity signaling: from fly development to human disease. *Annual review of genetics*. 2008;42:517-40.

103. Patel S, Alam A, Pant R, Chattopadhyay S. Wnt signaling and its significance within the tumor microenvironment: novel therapeutic insights. *Frontiers in immunology*. 2019;10:2872.

104. Wang Y, Fan X, Xing L, Tian F. Wnt signaling: a promising target for osteoarthritis therapy. *Cell Communication and Signaling*. 2019;17(1):1-14.

105. Luyten FP, Tylzanowski P, Lories RJ. Wnt signaling and osteoarthritis. *Bone*. 2009;44(4):522-7.

106. Sassi N, Laadhar L, Allouche M, Zandieh-Doulabi B, Hamdoun M, Klein-Nulend J, et al. The roles of canonical and non-canonical Wnt signaling in human de-differentiated articular chondrocytes. *Biotechnic & Histochemistry*. 2014;89(1):53-65.

107. Surmann-Schmitt C, Widmann N, Dietz U, Saeger B, Eitzinger N, Nakamura Y, et al. Wif-1 is expressed at cartilage-mesenchyme interfaces and impedes Wnt3a-mediated inhibition of chondrogenesis. *Journal of cell science*. 2009;122(20):3627-37.

108. Gao SG, Zeng C, Liu JJ, Tian J, Cheng C, Zhang FJ, et al. Association between Wnt inhibitory factor-1 expression levels in articular cartilage and the disease severity of patients with osteoarthritis of the knee. *Experimental and therapeutic medicine*. 2016;11(4):1405-9.
109. Bougault C, Priam S, Houard X, Pigenet A, Sudre L, Lories RJ, et al. Protective role of frizzled-related protein B on matrix metalloproteinase induction in mouse chondrocytes. *Arthritis research & therapy*. 2014;16(4):1-8.
110. Sugimura R, Li L. Noncanonical Wnt signaling in vertebrate development, stem cells, and diseases. *Birth Defects Research Part C: Embryo Today: Reviews*. 2010;90(4):243-56.
111. Yang Y, Topol L, Lee H, Wu J. Wnt5a and Wnt5b exhibit distinct activities in coordinating chondrocyte proliferation and differentiation. 2003.
112. Huang G, Chubinskaya S, Liao W, Loeser R. Wnt5a induces catabolic signaling and matrix metalloproteinase production in human articular chondrocytes. *Osteoarthritis and cartilage*. 2017;25(9):1505-15.
113. Garcia AL, Udeh A, Kalahasty K, Hackam AS. A growing field: The regulation of axonal regeneration by Wnt signaling. *Neural regeneration research*. 2018;13(1):43.
114. De Caestecker M. The transforming growth factor- $\beta$  superfamily of receptors. *Cytokine & growth factor reviews*. 2004;15(1):1-11.
115. Finnsen KW, Parker WL, ten Dijke P, Thorikay M, Philip A. ALK1 opposes ALK5/Smad3 signaling and expression of extracellular matrix components in human chondrocytes. *Journal of bone and mineral research*. 2008;23(6):896-906.
116. Davidson ENB, Remst DF, Vitters EL, van Beuningen HM, Blom AB, Goumans M-J, et al. Increase in ALK1/ALK5 ratio as a cause for elevated MMP-13 expression in osteoarthritis in humans and mice. *The Journal of Immunology*. 2009;182(12):7937-45.

117. Javelaud D, Mauviel A. Mammalian transforming growth factor- $\beta$ s: Smad signaling and physio-pathological roles. *The international journal of biochemistry & cell biology*. 2004;36(7):1161-5.
118. Verrecchia F, Mauviel A. Transforming growth factor- $\beta$  signaling through the Smad pathway: role in extracellular matrix gene expression and regulation. *Journal of Investigative Dermatology*. 2002;118(2):211-5.
119. Hellingman CA, Davidson ENB, Koevoet W, Vitters EL, Van Den Berg WB, Van Osch GJ, et al. Smad signaling determines chondrogenic differentiation of bone-marrow-derived mesenchymal stem cells: inhibition of Smad1/5/8P prevents terminal differentiation and calcification. *Tissue engineering part A*. 2011;17(7-8):1157-67.
120. Horiki M, Imamura T, Okamoto M, Hayashi M, Murai J, Myoui A, et al. Smad6/Smurf1 overexpression in cartilage delays chondrocyte hypertrophy and causes dwarfism with osteopenia. *The Journal of cell biology*. 2004;165(3):433-45.
121. Wang Y-J, Shen M, Wang S, Wen X, Han X-R, Zhang Z-F, et al. Inhibition of the TGF- $\beta$ 1/Smad signaling pathway protects against cartilage injury and osteoarthritis in a rat model. *Life sciences*. 2017;189:106-13.
122. Yamada Y, Okuizumi H, Miyauchi A, Takagi Y, Ikeda K, Harada A. Association of transforming growth factor  $\beta$ 1 genotype with spinal osteophytosis in Japanese women. *Arthritis & Rheumatism: Official Journal of the American College of Rheumatology*. 2000;43(2):452-60.
123. Lau H, Ho A, Luk K, Kung A. Transforming growth factor- $\beta$ 1 gene polymorphisms and bone turnover, bone mineral density and fracture risk in southern Chinese women. *Calcified tissue international*. 2004;74(6):516-21.
124. Kinoshita A, Saito T, Tomita H-a, Makita Y, Yoshida K, Ghadami M, et al. Domain-specific mutations in TGFB1 result in Camurati-Engelmann disease. *Nature genetics*. 2000;26(1):19-20.
125. van de Laar IM, van der Linde D, Oei EH, Bos PK, Bessems JH, Bierma-Zeinstra SM, et al. Phenotypic spectrum of the SMAD3-related

- aneurysms–osteoarthritis syndrome. *Journal of medical genetics*. 2012;49(1):47-57.
126. Valdes AM, Spector TD, Tamm A, Kisand K, Doherty SA, Dennison EM, et al. Genetic variation in the SMAD3 gene is associated with hip and knee osteoarthritis. *Arthritis & Rheumatism*. 2010;62(8):2347-52.
127. van de Laar IM, Oldenburg RA, Pals G, Roos-Hesselink JW, de Graaf BM, Verhagen JM, et al. Mutations in SMAD3 cause a syndromic form of aortic aneurysms and dissections with early-onset osteoarthritis. *Nature genetics*. 2011;43(2):121-6.
128. Zhong L, Huang X, Marcel K, Janine P. The Regulatory Role of Signaling Crosstalk in Hypertrophy of MSCs and Human Articular Chondrocytes. *International Journal of Molecular Sciences*. 2015;16(8):19225-47.
129. Chen S, Liu S, Ma K, Zhao L, Lin H, Shao Z. TGF- $\beta$  signaling in intervertebral disc health and disease. *Osteoarthritis and cartilage*. 2019;27(8):1109-17.
130. Stergachis AB, Neph S, Sandstrom R, Haugen E, Reynolds AP, Zhang M, et al. Conservation of trans-acting circuitry during mammalian regulatory evolution. *Nature*. 2014;515(7527):365-70.
131. Mural RJ, Adams MD, Myers EW, Smith HO, Miklos GLG, Wides R, et al. A comparison of whole-genome shotgun-derived mouse chromosome 16 and the human genome. *Science*. 2002;296(5573):1661-71.
132. Lin S, Lin Y, Nery JR, Urich MA, Breschi A, Davis CA, et al. Comparison of the transcriptional landscapes between human and mouse tissues. *Proceedings of the National Academy of Sciences*. 2014;111(48):17224-9.
133. Lammel S, Steinberg EE, Földy C, Wall NR, Beier K, Luo L, et al. Diversity of transgenic mouse models for selective targeting of midbrain dopamine neurons. *Neuron*. 2015;85(2):429-38.
134. Ashraf S, Mapp PI, Burston J, Bennett AJ, Chapman V, Walsh DA. Augmented pain behavioural responses to intra-articular injection of

nerve growth factor in two animal models of osteoarthritis. *Annals of the rheumatic diseases*. 2014;73(9):1710-8.

135. Guzman RE, Evans MG, Bove S, Morenko B, Kilgore K. Mono-iodoacetate-induced histologic changes in subchondral bone and articular cartilage of rat femorotibial joints: an animal model of osteoarthritis. *Toxicologic Pathology*. 2003;31(6):619-24.

136. Botter S, Van Osch G, Waarsing J, Van der Linden J, Verhaar J, Pols H, et al. Cartilage damage pattern in relation to subchondral plate thickness in a collagenase-induced model of osteoarthritis. *Osteoarthritis and cartilage*. 2008;16(4):506-14.

137. Appleton CTG, McERLAIN DD, Henry JL, Holdsworth DW, Beier F. Molecular and histological analysis of a new rat model of experimental knee osteoarthritis. *Annals of the New York Academy of Sciences*. 2007;1117(1):165-74.

138. Malfait A, Ritchie J, Gil A, Austin J-S, Hartke J, Qin W, et al. ADAMTS-5 deficient mice do not develop mechanical allodynia associated with osteoarthritis following medial meniscal destabilization. *Osteoarthritis and cartilage*. 2010;18(4):572-80.

139. O'Neil KT, Hoess RH, Degrado WF. Design of DNA-binding peptides on the leucine zipper motif. *Science*. 1990;249(4970):774-8.

140. Henderson SN. Site-specific DNA recombination in mammalian cells by the Cre recombinase of bacteriophage P1. *Proceedings of the National Academy of Sciences*. 1988;85(14):5166-70.

141. Kim H, Kim M, Im S-K, Fang S. Mouse Cre-LoxP system: general principles to determine tissue-specific roles of target genes. *Laboratory animal research*. 2018;34(4):147-59.

142. Sorek R, Kunin V, Hugenholtz P. CRISPR—a widespread system that provides acquired resistance against phages in bacteria and archaea. *Nature Reviews Microbiology*. 2008;6(3):181-6.

143. Ding Y, Hong L, Chen LL, Xie K. Recent Advances in Genome Editing Using CRISPR/Cas9. *Frontiers in Plant Science*. 2016;7:703-.

144. Esquela-Kerscher A, Slack FJ. Oncomirs - microRNAs with a role in cancer. *Nat Rev Cancer*. 2006;6(4):259-69.

145. Stefani G, Slack FJ. Small non-coding RNAs in animal development. *Nature reviews Molecular cell biology*. 2008;9(3):219-30.
146. Bi WM, Jian M, Zhang ZP, Behringer RR, Crombrughe BD. Sox9 is required for cartilage formation. *Nature Genetics*. 1999;22(1):85.
147. Yang B, Guo H, Zhang Y, Chen L, Dong S. MicroRNA-145 Regulates Chondrogenic Differentiation of Mesenchymal Stem Cells by Targeting Sox9. *PLoS ONE*. 2011;6(7):e21679-.
148. Lee S, Yoon DS, Paik S, Lee KM, Jang Y, Lee JW. microRNA-495 Inhibits Chondrogenic Differentiation in Human Mesenchymal Stem Cells by Targeting Sox9. *Stem Cells & Development*. 2014;23(15):1798-808.
149. Zhou X, Wang J, Sun H, Qi Y, Xu W, Luo D, et al. MicroRNA-99a regulates early chondrogenic differentiation of rat mesenchymal stem cells by targeting the BMP2 gene. *Cell & Tissue Research*. 2016;366(1):1-11.
150. Hou C, Yang Z, Kang Y, Zhang Z, Fu M, He A, et al. MiR-193b regulates early chondrogenesis by inhibiting the TGF-beta2 signaling pathway. *FEBS Letters*. 2015;589(9):1040-7.
151. Zhong Q, Wang T, Lu P, Zhang R, Zou J, Yuan S. miR-193b promotes cell proliferation by targeting Smad3 in human glioma. *Journal of Neuroscience Research*. 2014;92(5):619-26.
152. Nalesso G, Thomas BL, Eldridge SE, Wagner K, Sherwood J, Bertrand J, et al. Wnt5a/CaMKII pathway is activated in osteoarthritis and promotes loss of chondrocyte phenotype. *Osteoarthritis and Cartilage*. 2013;21:S226.
153. Li Y, Xiao W, Sun M, Deng Z, Zeng C, Li H, et al. The Expression of Osteopontin and Wnt5a in Articular Cartilage of Patients with Knee Osteoarthritis and Its Correlation with Disease Severity. *Biomed Res Int*. 2016;2016:9561058.
154. Blom AB, Brockbank SM, van Lent PL, van Beuningen HM, Geurts J, Takahashi N, et al. Involvement of the Wnt signaling pathway in experimental and human osteoarthritis: prominent role of Wnt-

- induced signaling protein 1. *Arthritis & Rheumatism: Official Journal of the American College of Rheumatology*. 2009;60(2):501-12.
155. van den Bosch M, Blom A, Maeda A, Kiltz T, van den Berg W, Lafeber F, et al. SAT0034 WISP1 aggravates osteoarthritis by modulation of TGF- $\beta$  signaling and positive regulation of canonical WNT signaling. *BMJ Publishing Group Ltd*; 2015.
156. Zhang Y, Huang X, Yuan Y. MicroRNA-410 promotes chondrogenic differentiation of human bone marrow mesenchymal stem cells through down-regulating Wnt3a. *American Journal of Translational Research*. 2017;9(1):136.
157. Mao G, Zhang Z, Hu S, Zhang Z, Chang Z, Huang Z, et al. Exosomes derived from miR-92a-3p-overexpressing human mesenchymal stem cells enhance chondrogenesis and suppress cartilage degradation via targeting WNT5A. *Stem Cell Research & Therapy*. 2018;9(1):247.
158. Carbonare LD, Innamorati G, Valenti MT. Transcription Factor Runx2 and its Application to Bone Tissue Engineering. *Stem Cell Reviews & Reports*. 2012;8(3):891-7.
159. Vimalraj S, Arumugam B, Miranda PJ, Selvamurugan N. Runx2: Structure, Function, and Phosphorylation in Osteoblast Differentiation. *International journal of biological macromolecules*. 2015;78:202-8.
160. Li Z, Hassan MQ, Volinia S, van Wijnen AJ, Stein JL, Croce CM, et al. A microRNA signature for a BMP2-induced osteoblast lineage commitment program. *Proceedings of the National Academy of Sciences*. 2008;105(37):13906-11.
161. Deng L, Hu G, Jin L, Wang C, Niu H. Involvement of microRNA-23b in TNF- $\alpha$ -reduced BMSC osteogenic differentiation via targeting runx2. *Journal of Bone and Mineral Metabolism*. 2017;36(6):1-13.
162. Li W, Chen Z, Cai C, Li G, Wang X, Shi Z. MicroRNA-505 is involved in the regulation of osteogenic differentiation of MC3T3-E1 cells partially by targeting RUNX2. *Journal of Orthopaedic Surgery and Research*. 2020;15(1):143.

163. Wang C-G, Liao Z, Xiao H, Liu H, Hu Y-H, Liao Q-D, et al. LncRNA KCNQ1OT1 promoted BMP2 expression to regulate osteogenic differentiation by sponging miRNA-214. *Experimental and Molecular Pathology*. 2019;107:77-84.
164. Long H, Sun B, Cheng L, Zhao S, Zhu Y, Zhao R, et al. miR-139-5p represses BMSC osteogenesis via targeting Wnt/ $\beta$ -catenin signaling pathway. *DNA and cell biology*. 2017;36(8):715-24.
165. Hu H, Zhao C, Zhang P, Liu Y, Jiang Y, Wu E, et al. miR-26b modulates OA induced BMSC osteogenesis through regulating GSK3 $\beta$ / $\beta$ -catenin pathway. *Experimental and Molecular Pathology*. 2019;107:158-64.
166. Conrozier T, Chappuis-Cellier C, Richard M, Mathieu P, Richard S, Vignon E. Increased serum C-reactive protein levels by immunonephelometry in patients with rapidly destructive hip osteoarthritis. *Revue du rhumatisme (English ed)*. 1998;65(12):759-65.
167. Blagojevic M, Jinks C, Jeffery A, Jordan K. Risk factors for onset of osteoarthritis of the knee in older adults: a systematic review and meta-analysis. *Osteoarthritis and cartilage*. 2010;18(1):24-33.
168. Collins KH, Lenz KL, Pollitt EN, Ferguson D, Hutson I, Springer LE, et al. Adipose tissue is a critical regulator of osteoarthritis. *Proceedings of the National Academy of Sciences*. 2021;118(1).
169. Zapata-Linares N, Eymard F, Berenbaum F, Houard X. Role of adipose tissues in osteoarthritis. *Current Opinion in Rheumatology*. 2021;33(1):84-93.
170. Murphy JM, Dixon K, Beck S, Fabian D, Feldman A, Barry F. Reduced chondrogenic and adipogenic activity of mesenchymal stem cells from patients with advanced osteoarthritis. *Arthritis & Rheumatism*. 2002;46(3):704-13.
171. Chen L, Song J, Cui J, Hou J, Zheng X, Li C, et al. microRNAs regulate adipocyte differentiation. *Cell biology international*. 2013;37(6):533-46.
172. Kim SY, Kim AY, Lee HW, Son YH, Lee GY, Lee J-W, et al. miR-27a is a negative regulator of adipocyte differentiation via suppressing

- PPAR $\gamma$  expression. *Biochemical and biophysical research communications*. 2010;392(3):323-8.
173. Lin Q, Gao Z, Alarcon RM, Ye J, Yun Z. A role of miR-27 in the regulation of adipogenesis. *The FEBS journal*. 2009;276(8):2348-58.
174. Karbiener M, Fischer C, Nowitsch S, Opriessnig P, Papak C, Ailhaud G, et al. microRNA miR-27b impairs human adipocyte differentiation and targets PPAR $\gamma$ . *Biochem Biophys Res Commun*. 2009;390(2):247-51.
175. Zhang G, Zhou Y, Su M, Yang X, Zeng B. Inhibition of microRNA-27b-3p relieves osteoarthritis pain via regulation of KDM4B-dependent DLX5. *Biofactors*. 2020;46(5):788-802.
176. Li Y, Yang F, Gao M, Gong R, Jin M, Liu T, et al. miR-149-3p regulates the switch between adipogenic and osteogenic differentiation of BMSCs by targeting FTO. *Molecular Therapy-Nucleic Acids*. 2019;17:590-600.
177. Iliopoulos D, Malizos KN, Oikonomou P, Tsezou A. Integrative microRNA and proteomic approaches identify novel osteoarthritis genes and their collaborative metabolic and inflammatory networks. *PloS one*. 2008;3(11):e3740.
178. Jones S, Watkins G, Le Good N, Roberts S, Murphy C, Brockbank S, et al. The identification of differentially expressed microRNA in osteoarthritic tissue that modulate the production of TNF- $\alpha$  and MMP13. *Osteoarthritis and cartilage*. 2009;17(4):464-72.
179. Díaz-Prado S, Cicione C, Muiños-López E, Hermida-Gómez T, Oreiro N, Fernández-López C, et al. Characterization of microRNA expression profiles in normal and osteoarthritic human chondrocytes. *BMC musculoskeletal disorders*. 2012;13(1):144.
180. de Almeida RC, Ramos YF, Mahfouz A, den Hollander W, Lakenberg N, Houtman E, et al. RNA sequencing data integration reveals an miRNA interactome of osteoarthritis cartilage. *Annals of the rheumatic diseases*. 2019;78(2):270-7.
181. Díaz-Prado S, Cicione C, Muiños-López E, Hermida-Gómez T, Oreiro N, Fernández-López C, et al. Characterization of microRNA

- expression profiles in normal and osteoarthritic human chondrocytes. *BMC musculoskeletal disorders*. 2012;13(1):1-14.
182. Wang M, Sampson ER, Jin H, Jia L, Di C. MMP13 is a critical target gene during the progression of osteoarthritis. *Arthritis research & therapy*. 2013;15(1):R5.
183. Mitchell PG, Magna HA, Reeves LM, Lopresti-Morrow LL, Hambor JE. Cloning, expression, and type II collagenolytic activity of matrix metalloproteinase-13 from human osteoarthritic cartilage. *Journal of Clinical Investigation*. 1996;97(3):761.
184. Fushimi K, Troeberg L, Nakamura H, Lim NH, Nagase H. Functional Differences of the Catalytic and Non-catalytic Domains in Human ADAMTS-4 and ADAMTS-5 in Aggrecanolytic Activity. *Journal of Biological Chemistry*. 2008;283(11):6706-16.
185. Bondeson J, Wainwright S, Hughes C, Caterson B. The regulation of the ADAMTS4 and ADAMTS5 aggrecanases in osteoarthritis: a review. *Clinical & Experimental Rheumatology*. 2008;26(1):139-45.
186. Etich J, Holzer T, Pitzler L, Bluhm B, Brachvogel B. MiR-26a modulates extracellular matrix homeostasis in cartilage. *Matrix Biology*. 2015;43:27-34.
187. Yin X, Wang JQ, Yan SY. Reduced miR-26a and miR-26b expression contributes to the pathogenesis of osteoarthritis via the promotion of p65 translocation. *Molecular Medicine Reports*. 2017;15(2):551-8.
188. Hu J, Wang Z, Pan Y, Ma J, Miao X, Qi X, et al. MiR-26a and miR-26b mediate osteoarthritis progression by targeting FUT4 via NF- $\kappa$ B signaling pathway. *The International Journal of Biochemistry & Cell Biology*. 2018;94:79-88.
189. Mao G, Wu P, Zhang Z, Zhang Z, Liao W, Li Y, et al. MicroRNA-92a-3p regulates aggrecanase-1 and aggrecanase-2 expression in chondrogenesis and IL-1 $\beta$ -induced catabolism in human articular chondrocytes. *Cellular Physiology and Biochemistry*. 2017;44(1):38-52.
190. Mao G, Zhang Z, Huang Z, Chen W, Huang G, Meng F, et al. MicroRNA-92a-3p regulates the expression of cartilage-specific genes

by directly targeting histone deacetylase 2 in chondrogenesis and degradation. *Osteoarthritis and Cartilage*. 2017;25(4):521-32.

191. Choi W-S, Lee G, Song W-H, Koh J-T, Yang J, Kwak J-S, et al. The CH25H–CYP7B1–ROR $\alpha$  axis of cholesterol metabolism regulates osteoarthritis. *Nature*. 2019;566(7743):254-8.

192. Li X, Zhang L, Shi X, Liao T, Zhang N, Gao Y, et al. MicroRNA-10a-3p Improves Cartilage Degeneration by Regulating CH25H-CYP7B1-ROR $\alpha$  Mediated Cholesterol Metabolism in Knee Osteoarthritis Rats. *Frontiers in Pharmacology*. 2021;12(1407).

193. Bai Y, Chen K, Zhan J, Wu M. miR-122/SIRT1 axis regulates chondrocyte extracellular matrix degradation in osteoarthritis. *Bioscience Reports*. 2020;40(6).

194. Goldring MB. Chondrogenesis, chondrocyte differentiation, and articular cartilage metabolism in health and osteoarthritis. *Ther Adv Musculoskelet Dis*. 2012;4(4):269-85.

195. Chen L, Li Q, Wang J, Jin S, Zheng H, Lin J, et al. MiR-29b-3p promotes chondrocyte apoptosis and facilitates the occurrence and development of osteoarthritis by targeting PGRN. *Journal of Cellular and Molecular Medicine*,21,12(2017-06-13). 2017.

196. Dou P, He Y, Yu B, Duan J. Downregulation of microRNA-29b by DNMT3B decelerates chondrocyte apoptosis and the progression of osteoarthritis via PTHLH/CDK4/RUNX2 axis. *Aging (Albany NY)*. 2021;13(5):7676.

197. Shi J, Guo K, Su S, Li J, Li C. miR-486-5p is upregulated in osteoarthritis and inhibits chondrocyte proliferation and migration by suppressing SMAD2. *Molecular Medicine Reports*. 2018;18(1).

198. He W, Ye C. Inhibition of miR-20 promotes proliferation and autophagy in articular chondrocytes by PI3K/AKT/mTOR signaling pathway. *Retour Au Numéro*. 2018;97:607.

199. Zhang W, Peichun H, Zhong B, Shang G, Chi Z, Wang Y, et al. MiR-34a Enhances Chondrocyte Apoptosis, Senescence and Facilitates Development of Osteoarthritis by Targeting DLL1 and Regulating PI3K/AKT Pathway. *Cellular Physiology and Biochemistry*. 2018;48:1304-16.

200. Wei ZJ, Liu J, Qin J. miR-138 suppressed the progression of osteoarthritis mainly through targeting p65. *European Review for Medical & Pharmacological Sciences*. 2017;21(9):2177.
201. Xu W, Gao P, Zhang Y, Piao L, Dong D. microRNA-138 induces cell survival and reduces WNT/ $\beta$ -catenin signaling of osteoarthritis chondrocytes through NEK2. *IUBMB life*. 2019;71(9):1355-66.
202. Nakamura A, Rampersaud YR, Nakamura S, Sharma A, Zeng F, Rossomacha E, et al. microRNA-181a-5p antisense oligonucleotides attenuate osteoarthritis in facet and knee joints. *Annals of the rheumatic diseases*. 2019;78(1):111-21.
203. Xue H, Tu Y, Ma T, Wen T, Yang T, Xue L, et al. miR-93-5p attenuates IL-1 $\beta$ -induced chondrocyte apoptosis and cartilage degradation in osteoarthritis partially by targeting TCF4. *Bone*. 2019;123:129-36.
204. Geng Y, Chen J, Alahdal M, Chang C, Duan L, Zhu W, et al. Intra-articular injection of hUC-MSCs expressing miR-140-5p induces cartilage self-repairing in the rat osteoarthritis. *Journal of Bone and Mineral Metabolism*. 2020;38(3):277-88.
205. Wang J, Wang X, Ding X, Huang T, Song D, Tao H. EZH2 is associated with cartilage degeneration in osteoarthritis by promoting SDC1 expression via histone methylation of the microRNA-138 promoter. *Laboratory Investigation*. 2021;101(5):600-11.
206. Crowe N, Swingler T, Le L, Barter M, Wheeler G, Pais H, et al. Detecting new microRNAs in human osteoarthritic chondrocytes identifies miR-3085 as a human, chondrocyte-selective, microRNA. *Osteoarthritis and cartilage*. 2016;24(3):534-43.
207. Culley KL, Hui W, Barter MJ, Davidson RK, Swingler TE, Destrumont AP, et al. Class I histone deacetylase inhibition modulates metalloproteinase expression and blocks cytokine-induced cartilage degradation. *Arthritis & Rheumatism*. 2013;65(7):1822-30.
208. Barter MJ, Tselepi M, Gómez R, Woods S, Hui W, Smith GR, et al. Genome-wide MicroRNA and gene analysis of mesenchymal stem cell chondrogenesis identifies an essential role and multiple targets for miR-140-5p. *Stem Cells*. 2015;33(11):3266-80.

209. Takara Bio USA Inc. NucleoSpin Gel and PCR Clean-up User Manual 2017 [Available from: [https://www.takarabio.com/documents/User%20Manual/NucleoSpin%20Gel%20and%20PCR%20Clean/NucleoSpin%20Gel%20and%20PCR%20Clean-up%20User%20Manual\\_Rev\\_04.pdf](https://www.takarabio.com/documents/User%20Manual/NucleoSpin%20Gel%20and%20PCR%20Clean/NucleoSpin%20Gel%20and%20PCR%20Clean-up%20User%20Manual_Rev_04.pdf)].
210. Thermo Fisher Scientific Inc. GeneJET RNA Purification Kit User Guide 2014 [Available from: [https://www.thermofisher.com/document-connect/document-connect.html?url=https%3A%2F%2Fassets.thermofisher.com%2FTFS-Assets%2FLSG%2Fmanuals%2FMAN0012664\\_GeneJET\\_RNA\\_Purification\\_UG.pdf](https://www.thermofisher.com/document-connect/document-connect.html?url=https%3A%2F%2Fassets.thermofisher.com%2FTFS-Assets%2FLSG%2Fmanuals%2FMAN0012664_GeneJET_RNA_Purification_UG.pdf)].
211. Thermo Fisher Scientific Inc. TRIzol Reagent User Guide: Thermo Fisher Scientific Inc.; 2020 [Available from: [https://assets.thermofisher.com/TFS-Assets/LSG/manuals/trizol\\_reagent.pdf](https://assets.thermofisher.com/TFS-Assets/LSG/manuals/trizol_reagent.pdf)].
212. Bio-Rad Laboratories I. Experion™ RNA StdSens and HighSens Analysis Kits Instruction Manual 2010 [Available from: <https://www.bio-rad.com/sites/default/files/webroot/web/pdf/lsr/literature/10000976C.pdf>].
213. QIAGEN. miRCURY LNA miRNA SYBR Green PCR Handbook 2019 [Available from: [file:///ueahome/eressci8/tyq17cwu/data/Downloads/HB-2431-002\\_HB\\_miRC\\_LNA\\_miRNA\\_PCR\\_1019\\_WW.pdf](file:///ueahome/eressci8/tyq17cwu/data/Downloads/HB-2431-002_HB_miRC_LNA_miRNA_PCR_1019_WW.pdf)].
214. Bio-Rad Laboratories I. Instruction Manual, Bio-Rad Protein Assay, Rev C. 2013.
215. Bradford MM. A rapid and sensitive method for the quantitation of microgram quantities of protein utilizing the principle of protein-dye binding. *Analytical biochemistry*. 1976;72(1-2):248-54.
216. Thermo Fisher Scientific Inc. SuperSignal™ West Pico PLUS Chemiluminescent Substrate User Guide 2021 [Available from: <https://www.thermofisher.com/document-connect/document-connect.html?url=https%3A%2F%2Fassets.thermofisher.com%2FTFS->

217. Farndale RW, Sayers CA, Barrett AJ. A direct spectrophotometric microassay for sulfated glycosaminoglycans in cartilage cultures. *Connective tissue research*. 1982;9(4):247-8.
218. Billington CJ. Cartilage proteoglycan release assay. *Matrix Metalloproteinase Protocols*: Springer; 2001. p. 451-6.
219. Leggate J, Allain R, Isaac L, Blais BW. Microplate fluorescence assay for the quantification of double stranded DNA using SYBR Green I dye. *Biotechnology letters*. 2006;28(19):1587-94.
220. Sakai K, Hiripi L, Glumoff V, Brandau O, Eerola R, Vuorio E, et al. Stage-and tissue-specific expression of a Col2a1-Cre fusion gene in transgenic mice. *Matrix Biology*. 2001;19(8):761-7.
221. van der Flier A, Badu-Nkansah K, Whittaker CA, Crowley D, Bronson RT, Lacy-Hulbert A, et al. Endothelial  $\alpha 5$  and  $\alpha v$  integrins cooperate in remodeling of the vasculature during development. *Development*. 2010;137(14):2439-49.
222. Blease A, Das Neves Borges P, Curtinha M, Javaheri B, von Loga IS, Parisi I, et al. Studying osteoarthritis pathogenesis in mice. *Current protocols in mouse biology*. 2018;8(4):e50.
223. Rigueur D, Lyons KM. Whole-mount skeletal staining. *Skeletal Development and Repair*: Springer; 2014. p. 113-21.
224. Glasson S, Chambers M, Van Den Berg W, Little C. The OARSI histopathology initiative—recommendations for histological assessments of osteoarthritis in the mouse. *Osteoarthritis and cartilage*. 2010;18:S17-S23.
225. Winer J, Jung CKS, Shackel I, Williams PM. Development and Validation of Real-Time Quantitative Reverse Transcriptase–Polymerase Chain Reaction for Monitoring Gene Expression in Cardiac Myocytes in Vitro. *Analytical Biochemistry*. 1999;270(1):41-9.
226. Livak KJ, Schmittgen TD. Analysis of Relative Gene Expression Data Using Real-Time Quantitative PCR and the  $2^{-\Delta\Delta CT}$  Method. *Methods*. 2001;25(4):402-8.

227. Bray NL, Pimentel H, Melsted P, Pachter L. Near-optimal probabilistic RNA-seq quantification. *Nature biotechnology*. 2016;34(5):525-7.
228. Pimentel H, Bray NL, Puente S, Melsted P, Pachter L. Differential analysis of RNA-seq incorporating quantification uncertainty. *Nature methods*. 2017;14(7):687-90.
229. Zhong Y, Wei J, Fu Y, Shao J, Liang Y, Lin Y, et al. Toxicity of cationic liposome Lipofectamine 2000 in human pancreatic cancer Capan-2 cells. *Nan fang yi ke da xue xue bao= Journal of Southern Medical University*. 2008;28(11):1981-4.
230. Le L, Niu L, Barter MJ, Young DA, Dalmay T, Clark IM, et al. The role of microRNA-3085 in chondrocyte function. *Scientific Reports*. 2020;10(1):1-10.
231. Sugiyama K, Muroi M, Kinoshita M, Hamada O, Minai Y, Sugita-Konishi Y, et al. NF- $\kappa$ B activation via MyD88-dependent Toll-like receptor signaling is inhibited by trichothecene mycotoxin deoxynivalenol. *J Toxicol Sci*. 2016;41(2):273-9.
232. Davis CN, Mann E, Behrens MM, Gaidarova S, Rebek M, Rebek J, et al. MyD88-dependent and-independent signaling by IL-1 in neurons probed by bifunctional Toll/IL-1 receptor domain/BB-loop mimetics. *Proceedings of the National Academy of Sciences*. 2006;103(8):2953-8.
233. Deguine J, Barton GM. MyD88: a central player in innate immune signaling. *F1000prime reports*. 2014;6.
234. Medzhitov R, Preston-Hurlburt P, Kopp E, Stadlen A, Chen C, Ghosh S, et al. MyD88 is an adaptor protein in the hToll/IL-1 receptor family signaling pathways. *Molecular cell*. 1998;2(2):253-8.
235. Ellman MB, Kim J-S, An HS, Chen D, Ranjan K, An J, et al. Toll-like receptor adaptor signaling molecule MyD88 on intervertebral disk homeostasis: in vitro, ex vivo studies. *Gene*. 2012;505(2):283-90.
236. Chen S-J, Yuan W, Mori Y, Levenson A, Varga J, Trojanowska M. Stimulation of type I collagen transcription in human skin fibroblasts by TGF- $\beta$ : involvement of Smad 3. *Journal of Investigative Dermatology*. 1999;112(1):49-57.

237. Dennler S, Itoh S, Vivien D, ten Dijke P, Huet S, Gauthier JM. Direct binding of Smad3 and Smad4 to critical TGF $\beta$ -inducible elements in the promoter of human plasminogen activator inhibitor-type 1 gene. *The EMBO journal*. 1998;17(11):3091-100.
238. Verrecchia F, Chu M-L, Mauviel A. Identification of novel TGF- $\beta$ /Smad gene targets in dermal fibroblasts using a combined cDNA microarray/promoter transactivation approach. *Journal of Biological Chemistry*. 2001;276(20):17058-62.
239. Lebrin F, Goumans MJ, Jonker L, Carvalho RL, Valdimarsdottir G, Thorikay M, et al. Endoglin promotes endothelial cell proliferation and TGF- $\beta$ /ALK1 signal transduction. *The EMBO journal*. 2004;23(20):4018-28.
240. Dinarello CA, Gatti S, Bartfai T. Fever: links with an ancient receptor. *Current biology*. 1999;9(4):R143-R6.
241. Ge X-P, Gan Y-H, Zhang C-G, Zhou C-Y, Ma K-T, Meng J-H, et al. Requirement of the NF- $\kappa$ B pathway for induction of Wnt-5A by interleukin-1 $\beta$  in condylar chondrocytes of the temporomandibular joint: functional crosstalk between the Wnt-5A and NF- $\kappa$ B signaling pathways. *Osteoarthritis and cartilage*. 2011;19(1):111-7.
242. Shen J, Li S, Chen D. TGF- $\beta$  signaling and the development of osteoarthritis. *Bone research*. 2014;2(1):1-7.
243. Wiercinska E, Wickert L, Denecke B, Said HM, Hamzavi J, Gressner A, et al. Id1 is a critical mediator in TGF- $\beta$ -induced transdifferentiation of rat hepatic stellate cells. *Hepatology*. 2006;43(5):1032-41.
244. Mengshol JA, Vincenti MP, Brinckerhoff CE. IL-1 induces collagenase-3 (MMP-13) promoter activity in stably transfected chondrocytic cells: requirement for Runx-2 and activation by p38 MAPK and JNK pathways. *Nucleic acids research*. 2001;29(21):4361-72.
245. Corr M. Wnt- $\beta$ -catenin signaling in the pathogenesis of osteoarthritis. *Nature Clinical Practice Rheumatology*. 2008;4(10):550-6.

246. Schett G, Zwerina J, David J-P. The role of Wnt proteins in arthritis. *Nature Clinical Practice Rheumatology*. 2008;4(9):473-80.
247. Nalesso G, Sherwood J, Bertrand J, Pap T, Ramachandran M, De Bari C, et al. WNT-3A modulates articular chondrocyte phenotype by activating both canonical and noncanonical pathways. *Journal of Cell Biology*. 2011;193(3):551-64.
248. Qu F, Wang J, Xu N, Liu C, Li S, Wang N, et al. WNT3A modulates chondrogenesis via canonical and non-canonical Wnt pathways in MSCs. *Frontiers in bioscience (Landmark edition)*. 2013;18:493-503.
249. Xie Z, Khair M, Shaukat I, Netter P, Mainard D, Barré L, et al. Non-canonical Wnt induces chondrocyte de-differentiation through Frizzled 6 and DVL-2/B-raf/CaMKII $\alpha$ /syndecan 4 axis. *Cell Death & Differentiation*. 2018;25(8):1442-56.
250. Kawaguchi H. Endochondral ossification signals in cartilage degradation during osteoarthritis progression in experimental mouse models. *Molecules & Cells*. 2008;25(1):1-6.
251. Xiao ZF, Su GY, Hou Y, Chen SD, Lin DK. Cartilage degradation in osteoarthritis: A process of endochondral remodeling resembles the endochondral ossification in growth plate? *Medical Hypotheses*. 2018;121:183-7.
252. Yagi R, McBurney D, Laverty D, Weiner S, Horton WE. Intrajoint comparisons of gene expression patterns in human osteoarthritis suggest a change in chondrocyte phenotype. *Journal of orthopaedic research*. 2005;23(5):1128-38.
253. Wuelling M, Vortkamp A. Chondrocyte proliferation and differentiation. *Endocr Dev*. 2011;21(21):1-11.
254. Saito T, Saetrom P. MicroRNAs—targeting and target prediction. *New biotechnology*. 2010;27(3):243-9.
255. de Groot RP, Kruyt F, van der Saag PT, Kruijer W. Ectopic expression of c-jun leads to differentiation of P19 embryonal carcinoma cells. *The EMBO Journal*. 1990;9(6):1831-7.
256. O'Shea EK, Rutkowski R, Kim PS. Mechanism of specificity in the Fos-Jun oncoprotein heterodimer. *Cell*. 1992;68(4):699-708.

257. Chakraborti S, Mandal M, Das S, Mandal A, Chakraborti T. Regulation of matrix metalloproteinases: an overview. *Molecular and cellular biochemistry*. 2003;253(1):269-85.
258. Motomura H, Seki S, Shiozawa S, Aikawa Y, Nogami M, Kimura T. A selective c-Fos/AP-1 inhibitor prevents cartilage destruction and subsequent osteophyte formation. *Biochemical and biophysical research communications*. 2018;497(2):756-61.
259. Chinenov Y, Kerppola TK. Close encounters of many kinds: Fos-Jun interactions that mediate transcription regulatory specificity. *Oncogene*. 2001;20(19):2438-52.
260. Ratziu V, Lalazar A, Wong L, Dang Q, Collins C, Shaulian E, et al. Zf9, a Kruppel-like transcription factor up-regulated in vivo during early hepatic fibrosis. *Proceedings of the National Academy of Sciences*. 1998;95(16):9500-5.
261. Narla G, Heath KE, Reeves HL, Li D, Giono LE, Kimmelman AC, et al. KLF6, a candidate tumor suppressor gene mutated in prostate cancer. *Science*. 2001;294(5551):2563-6.
262. Ito G, Uchiyama M, Kondo M, Mori S, Usami N, Maeda O, et al. Krüppel-like factor 6 is frequently down-regulated and induces apoptosis in non-small cell lung cancer cells. *Cancer research*. 2004;64(11):3838-43.
263. Rodriguez Del Castillo A, Lemaire S, Tchakarov L, Jeyapragasan M, Doucet J, Vitale M, et al. Chromaffin cell scinderin, a novel calcium-dependent actin filament-severing protein. *The EMBO Journal*. 1990;9(1):43-52.
264. Del Castillo AR, Vitale M, Tchakarov L, Trifaro J. Human platelets contain scinderin, a Ca<sup>2+</sup>-dependent actin filament-severing protein. *Thrombosis and haemostasis*. 1992;67(02):248-51.
265. Wykosky J, Debinski W. The EphA2 receptor and ephrinA1 ligand in solid tumors: function and therapeutic targeting. *Molecular Cancer Research*. 2008;6(12):1795-806.
266. Pasquale EB. Eph receptors and ephrins in cancer: bidirectional signalling and beyond. *Nature Reviews Cancer*. 2010;10(3):165-80.

267. Honke K, Taniguchi N. Sulfotransferases and sulfated oligosaccharides. *Medicinal research reviews*. 2002;22(6):637-54.
268. Thiele H, Sakano M, Kitagawa H, Sugahara K, Rajab A, Höhne W, et al. Loss of chondroitin 6-O-sulfotransferase-1 function results in severe human chondrodysplasia with progressive spinal involvement. *Proceedings of the National Academy of Sciences*. 2004;101(27):10155-60.
269. Unger S, Lausch E, Rossi A, Mégarbané A, Sillence D, Alcausin M, et al. Phenotypic features of carbohydrate sulfotransferase 3 (CHST3) deficiency in 24 patients: congenital dislocations and vertebral changes as principal diagnostic features. *American journal of medical genetics Part A*. 2010;152(10):2543-9.
270. Rajab A, Kunze J, Mundlos S. Spondyloepiphyseal dysplasia Omani type: a new recessive type of SED with progressive spinal involvement. *American Journal of Medical Genetics Part A*. 2004;126(4):413-9.
271. Tuysuz B, Mizumoto S, Sugahara K, Celebi A, Mundlos S, Turkmen S. Omani-type spondyloepiphyseal dysplasia with cardiac involvement caused by a missense mutation in CHST3. *Clinical genetics*. 2009;75(4):375-83.
272. Lin WJ, Yang CY, Li LL, Yi YH, Chen KW, Lin YC, et al. Lysosomal targeting of phafin1 mediated by Rab7 induces autophagosome formation. *Biochem Biophys Res Commun*. 2012;417(1):35-42.
273. Li N, Zheng Y, Chen W, Wang C, Liu X, He W, et al. Adaptor protein LAPF recruits phosphorylated p53 to lysosomes and triggers lysosomal destabilization in apoptosis. *Cancer research*. 2007;67(23):11176-85.
274. López-Casillas F, Wrana JL, Massagué J. Betaglycan presents ligand to the TGF $\beta$  signaling receptor. *Cell*. 1993;73(7):1435-44.
275. Han H-J, Tokino T, Nakamura Y. CSR, a scavenger receptor-like protein with a protective role against cellular damage caused by UV irradiation and oxidative stress. *Human molecular genetics*. 1998;7(6):1039-46.

276. Yu G, Tseng GC, Yu YP, Gavel T, Nelson J, Wells A, et al. CSR1 suppresses tumor growth and metastasis of prostate cancer. *The American journal of pathology*. 2006;168(2):597-607.
277. Peng H, Guo Q, Su T, Xiao Y, Li C-J, Huang Y, et al. Identification of SCARA3 with potential roles in metabolic disorders. *Aging (Albany NY)*. 2021;13(2):2149.
278. Mok SC, Wong K-K, Chan RK, Lau CC, Tsao S-W, Knapp RC, et al. Molecular cloning of differentially expressed genes in human epithelial ovarian cancer. *Gynecologic oncology*. 1994;52(2):247-52.
279. Kleeff J, Huang Y, Mok SC, Zimmermann A, Friess H, Büchler MW. Down-regulation of DOC-2 in colorectal cancer points to its role as a tumor suppressor in this malignancy. *Diseases of the colon & rectum*. 2002;45(9):1242-8.
280. Zhou J, Scholes J, Hsieh J-T. Characterization of a novel negative regulator (DOC-2/DAB2) of c-Src in normal prostatic epithelium and cancer. *Journal of Biological Chemistry*. 2003;278(9):6936-41.
281. Anupam K, Tusharkant C, Gupta SD, Ranju R. Loss of disabled-2 expression is an early event in esophageal squamous tumorigenesis. *World journal of gastroenterology: WJG*. 2006;12(37):6041.
282. Karam JA, Shariat SF, Huang H-Y, Pong R-C, Ashfaq R, Shapiro E, et al. Decreased DOC-2/DAB2 expression in urothelial carcinoma of the bladder. *Clinical Cancer Research*. 2007;13(15):4400-6.
283. Jiang Y, He X, Howe PH. Disabled-2 (Dab2) inhibits Wnt/ $\beta$ -catenin signalling by binding LRP6 and promoting its internalization through clathrin. *The EMBO journal*. 2012;31(10):2336-49.
284. Adamson SE, Griffiths R, Moravec R, Senthivinayagam S, Montgomery G, Chen W, et al. Disabled homolog 2 controls macrophage phenotypic polarization and adipose tissue inflammation. *The Journal of clinical investigation*. 2016;126(4):1311-22.
285. Finkielstein CV, Capelluto DG. Disabled-2: A modular scaffold protein with multifaceted functions in signaling. *Bioessays*. 2016;38:S45-S55.

286. Rettig WJ, Garin-Chesa P, Healey JH, Su SL, Jaffe EA, Old LJ. Identification of endosialin, a cell surface glycoprotein of vascular endothelial cells in human cancer. *Proceedings of the National Academy of Sciences*. 1992;89(22):10832-6.
287. MacFadyen JR, Haworth O, Roberston D, Hardie D, Webster M-T, Morris HR, et al. Endosialin (TEM1, CD248) is a marker of stromal fibroblasts and is not selectively expressed on tumour endothelium. *FEBS letters*. 2005;579(12):2569-75.
288. Maia M, de Vriese A, Janssens T, Moons M, Van Landuyt K, Tavernier J, et al. CD248 and its cytoplasmic domain: a therapeutic target for arthritis. *Arthritis & Rheumatism*. 2010;62(12):3595-606.
289. Luo HR, Saiardi A, Nagata E, Ye K, Yu H, Jung TS, et al. GRAB: a physiologic guanine nucleotide exchange factor for Rab3A, which interacts with inositol hexakisphosphate kinase. *Neuron*. 2001;31(3):439-51.
290. Westermarck J, Kähäri VM. Regulation of matrix metalloproteinase expression in tumor invasion. *The FASEB journal*. 1999;13(8):781-92.
291. Hess J, Angel P, Schorpp-Kistner M. AP-1 subunits: quarrel and harmony among siblings. *Journal of cell science*. 2004;117(25):5965-73.
292. Han W, Ding P, Xu M, Wang L, Rui M, Shi S, et al. Identification of eight genes encoding chemokine-like factor superfamily members 1–8 (CKLFSF1–8) by in silico cloning and experimental validation. *Genomics*. 2003;81(6):609-17.
293. Zhong J, Wang Y, Qiu X, Mo X, Liu Y, Li T, et al. Characterization and expression profile of CMTM3/CKLFSF3. *BMB Reports*. 2006;39(5):537-45.
294. Wang Y, Li J, Cui Y, Li T, Ng KM, Geng H, et al. CMTM3, located at the critical tumor suppressor locus 16q22. 1, is silenced by CpG methylation in carcinomas and inhibits tumor cell growth through inducing apoptosis. *Cancer research*. 2009;69(12):5194-201.

295. Su Y, Lin Y, Zhang L, Liu B, Yuan W, Mo X, et al. CMTM3 inhibits cell migration and invasion and correlates with favorable prognosis in gastric cancer. *Cancer science*. 2014;105(1):26-34.
296. Zhang H, Zhang J, Nan X, Li X, Qu J, Hong Y, et al. CMTM3 inhibits cell growth and migration and predicts favorable survival in oral squamous cell carcinoma. *Tumor Biology*. 2015;36(10):7849-58.
297. Li J, Chen C, Bi X, Zhou C, Huang T, Ni C, et al. DNA methylation of CMTM3, SSTR2, and MDFI genes in colorectal cancer. *Gene*. 2017;630:1-7.
298. Briegel KJ, Joyner AL. Identification and characterization of Lbh, a novel conserved nuclear protein expressed during early limb and heart development. *Developmental biology*. 2001;233(2):291-304.
299. Yeo M, Lee S-K, Lee B, Ruiz EC, Pfaff SL, Gill GN. Small CTD phosphatases function in silencing neuronal gene expression. *Science*. 2005;307(5709):596-600.
300. Eshed Y, Feinberg K, Poliak S, Sabanay H, Sarig-Nadir O, Spiegel I, et al. Gliomedin mediates Schwann cell-axon interaction and the molecular assembly of the nodes of Ranvier. *Neuron*. 2005;47(2):215-29.
301. Heyninck K, De Valck D, Berghe WV, Van Crielinge W, Contreras R, Fiers W, et al. The zinc finger protein A20 inhibits TNF-induced NF- $\kappa$ B-dependent gene expression by interfering with an RIP-or TRAF2-mediated transactivation signal and directly binds to a novel NF- $\kappa$ B-inhibiting protein ABIN. *The Journal of cell biology*. 1999;145(7):1471-82.
302. Flores AM, Gurevich I, Zhang C, Ramirez VP, Devens TR, Aneskievich BJ. TNIP1 is a corepressor of agonist-bound PPARs. *Archives of biochemistry and biophysics*. 2011;516(1):58-66.
303. Zhang S, Fukushi M, Hashimoto S, Gao C, Huang L, Fukuyo Y, et al. A new ERK2 binding protein, Naf1, attenuates the EGF/ERK2 nuclear signaling. *Biochemical and biophysical research communications*. 2002;297(1):17-23.

304. Tay Y, Zhang J, Thomson AM, Lim B, Rigoutsos I. MicroRNAs to Nanog, Oct4 and Sox2 coding regions modulate embryonic stem cell differentiation. *Nature*. 2008;455(7216):1124-8.
305. Lee I, Ajay SS, Yook JI, Kim HS, Hong SH, Kim NH, et al. New class of microRNA targets containing simultaneous 5'-UTR and 3'-UTR interaction sites. *Genome research*. 2009;19(7):1175-83.
306. Ørom UA, Nielsen FC, Lund AH. MicroRNA-10a binds the 5' UTR of ribosomal protein mRNAs and enhances their translation. *Molecular cell*. 2008;30(4):460-71.
307. Jin Y, Wang C, Liu X, Mu W, Chen Z, Yu D, et al. Molecular characterization of the microRNA-138-Fos-like antigen 1 (FOSL1) regulatory module in squamous cell carcinoma. *Journal of Biological Chemistry*. 2011;286(46):40104-9.
308. Shaulian E, Karin M. AP-1 as a regulator of cell life and death. *Nature cell biology*. 2002;4(5):E131-E6.
309. Angel P, Karin M. The role of Jun, Fos and the AP-1 complex in cell-proliferation and transformation. *Biochimica et Biophysica Acta (BBA)-Reviews on Cancer*. 1991;1072(2-3):129-57.
310. Jochum W, Passegué E, Wagner EF. AP-1 in mouse development and tumorigenesis. *Oncogene*. 2001;20(19):2401-12.
311. Grynberg K, Ma FY, Nikolic-Paterson DJ. The JNK signaling pathway in renal fibrosis. *Frontiers in physiology*. 2017;8:829.
312. Karin M, Liu Z-g, Zandi E. AP-1 function and regulation. *Current opinion in cell biology*. 1997;9(2):240-6.
313. Mengshol JA, Vincenti MP, Coon CI, Barchowsky A, Brinckerhoff CE. Interleukin-1 induction of collagenase 3 (matrix metalloproteinase 13) gene expression in chondrocytes requires p38, c-Jun N-terminal kinase, and nuclear factor  $\kappa$ B: differential regulation of collagenase 1 and collagenase 3. *Arthritis & Rheumatism: Official Journal of the American College of Rheumatology*. 2000;43(4):801-11.
314. Han Z, Boyle DL, Chang L, Bennett B, Karin M, Yang L, et al. c-Jun N-terminal kinase is required for metalloproteinase expression and joint destruction in inflammatory arthritis. *The Journal of clinical investigation*. 2001;108(1):73-81.

315. D'Alonzo RC, Selvamurugan N, Karsenty G, Partridge NC. Physical interaction of the activator protein-1 factors c-Fos and c-Jun with Cbfa1 for collagenase-3 promoter activation. *Journal of Biological Chemistry*. 2002;277(1):816-22.
316. Tang Q-Q, Otto TC, Lane MD. Mitotic clonal expansion: a synchronous process required for adipogenesis. *Proceedings of the National Academy of Sciences*. 2003;100(1):44-9.
317. Tang Q-Q, Otto TC, Lane MD. CCAAT/enhancer-binding protein  $\beta$  is required for mitotic clonal expansion during adipogenesis. *Proceedings of the National Academy of Sciences*. 2003;100(3):850-5.
318. Payne VA, Au W-S, Gray SL, Dalla Nora E, Rahman SM, Sanders R, et al. Sequential regulation of diacylglycerol acyltransferase 2 expression by CAAT/enhancer-binding protein  $\beta$  (C/EBP $\beta$ ) and C/EBP $\alpha$  during adipogenesis. *Journal of biological chemistry*. 2007;282(29):21005-14.
319. Jikko A, Harris SE, Chen D, Mendrick DL, Damsky CH. Collagen integrin receptors regulate early osteoblast differentiation induced by BMP-2. *Journal of bone and mineral research*. 1999;14(7):1075-83.
320. Jaiswal N, Haynesworth SE, Caplan AI, Bruder SP. Osteogenic differentiation of purified, culture-expanded human mesenchymal stem cells in vitro. *Journal of cellular biochemistry*. 1997;64(2):295-312.
321. Zhang H, Artiles KL, Fire AZ. Functional relevance of “seed” and “non-seed” sequences in microRNA-mediated promotion of *C. elegans* developmental progression. *Rna*. 2015;21(11):1980-92.
322. Zhang L, Hammell M, Kudlow BA, Ambros V, Han M. Systematic analysis of dynamic miRNA-target interactions during *C. elegans* development. *Development*. 2009;136(18):3043-55.
323. Zisoulis DG, Lovci MT, Wilbert ML, Hutt KR, Liang TY, Pasquinelli AE, et al. Comprehensive discovery of endogenous Argonaute binding sites in *Caenorhabditis elegans*. *Nature structural & molecular biology*. 2010;17(2):173.
324. Jovanovic M, Reiter L, Clark A, Weiss M, Picotti P, Rehrauer H, et al. RIP-chip-SRM—a new combinatorial large-scale approach identifies

- a set of translationally regulated bantam/miR-58 targets in *C. elegans*. *Genome research*. 2012;22(7):1360-71.
325. Grimson A, Farh KK-H, Johnston WK, Garrett-Engele P, Lim LP, Bartel DP. MicroRNA targeting specificity in mammals: determinants beyond seed pairing. *Molecular cell*. 2007;27(1):91-105.
326. Fan D, Fan D, Yuan W. CMTM3 suppresses bone formation and osteogenic differentiation of mesenchymal stem cells through inhibiting Erk1/2 and RUNX2 pathways. *Genes & Diseases*. 2020.
327. Conen K, Nishimori S, Provot S, Kronenberg H. The transcriptional cofactor Lbh regulates angiogenesis and endochondral bone formation during fetal bone development. *Developmental biology*. 2009;333(2):348-58.
328. Wu M, Chen G, Li Y-P. TGF- $\beta$  and BMP signaling in osteoblast, skeletal development, and bone formation, homeostasis and disease. *Bone research*. 2016;4(1):1-21.
329. Retting KN, Song B, Yoon BS, Lyons KM. BMP canonical Smad signaling through Smad1 and Smad5 is required for endochondral bone formation. *Development*. 2009;136(7):1093-104.
330. Knockaert M, Sapkota G, Alarcón C, Massagué J, Brivanlou AH. Unique players in the BMP pathway: small C-terminal domain phosphatases dephosphorylate Smad1 to attenuate BMP signaling. *Proceedings of the National Academy of Sciences*. 2006;103(32):11940-5.
331. Yang JT, Rayburn H, Hynes RO. Embryonic mesodermal defects in alpha 5 integrin-deficient mice. *Development*. 1993;119(4):1093-105.
332. Goh KL, Yang JT, Hynes RO. Mesodermal defects and cranial neural crest apoptosis in alpha5 integrin-null embryos. *Development*. 1997;124(21):4309-19.
333. Rountree RB, Schoor M, Chen H, Marks ME, Harley V, Mishina Y, et al. BMP receptor signaling is required for postnatal maintenance of articular cartilage. *PLoS Biol*. 2004;2(11):e355.
334. Kaufman MH. *Atlas of mouse development*: Academic press; 1992.

335. Cheah K, Lau E, Au P, Tam P. Expression of the mouse alpha 1 (II) collagen gene is not restricted to cartilage during development. *Development*. 1991;111(4):945-53.
336. Ng LJ, Tam PP, Cheah KS. Preferential expression of alternatively spliced mRNAs encoding type II procollagen with a cysteine-rich amino-propeptide in differentiating cartilage and nonchondrogenic tissues during early mouse development. *Developmental biology*. 1993;159(2):403-17.
337. Aszodi A, Hunziker EB, Brakebusch C, Fässler R.  $\beta$ 1 integrins regulate chondrocyte rotation, G1 progression, and cytokinesis. *Genes & development*. 2003;17(19):2465-79.
338. Tavella S, Bellese G, Castagnola P, Martin I, Piccini D, Doliana R, et al. Regulated expression of fibronectin, laminin and related integrin receptors during the early chondrocyte differentiation. *Journal of cell science*. 1997;110(18):2261-70.
339. Maini P, Solursh M. Cellular mechanisms of pattern formation in the developing limb. *International review of cytology*. 1991;129:91-133.
340. Shakibaei M. Inhibition of Chondrogenesis by Integrin Antibody in Vitro. *Experimental cell research*. 1998;240(1):95-106.
341. Salter DM, Godolphin JL, Gourlay MS. Chondrocyte heterogeneity: immunohistologically defined variation of integrin expression at different sites in human fetal knees. *Journal of Histochemistry & Cytochemistry*. 1995;43(4):447-57.
342. Soriano P. Generalized lacZ expression with the ROSA26 Cre reporter strain. *Nature genetics*. 1999;21(1):70-1.
343. Neves-Carvalho A, Logarinho E, Freitas A, Duarte-Silva S, Costa MdC, Silva-Fernandes A, et al. Dominant negative effect of polyglutamine expansion perturbs normal function of ataxin-3 in neuronal cells. *Human molecular genetics*. 2015;24(1):100-17.
344. McNulty MA, Loeser RF, Davey C, Callahan MF, Ferguson CM, Carlson CS. A comprehensive histological assessment of osteoarthritis lesions in mice. *Cartilage*. 2011;2(4):354-63.

345. Rychel JK. Diagnosis and treatment of osteoarthritis. *Topics in Companion Animal Medicine*. 2010;25(1):20-5.
346. Fransen M, McConnell S, Harmer AR, Van der Esch M, Simic M, Bennell KL. Exercise for osteoarthritis of the knee: a Cochrane systematic review. *British journal of sports medicine*. 2015;49(24):1554-7.
347. Hong E, Reddi AH. MicroRNAs in chondrogenesis, articular cartilage, and osteoarthritis: implications for tissue engineering. *Tissue Engineering Part B: Reviews*. 2012;18(6):445-53.
348. Kobayashi T, Lu J, Cobb BS, Rodda SJ, McMahan AP, Schipani E, et al. Dicer-dependent pathways regulate chondrocyte proliferation and differentiation. *Proceedings of the National Academy of Sciences*. 2008;105(6):1949-54.
349. Tuddenham L, Wheeler G, Ntounia-Fousara S, Waters J, Hajihosseini MK, Clark I, et al. The cartilage specific microRNA-140 targets histone deacetylase 4 in mouse cells. *FEBS letters*. 2006;580(17):4214-7.
350. Miyaki S, Sato T, Inoue A, Otsuki S, Ito Y, Yokoyama S, et al. MicroRNA-140 plays dual roles in both cartilage development and homeostasis. *Genes & development*. 2010;24(11):1173-85.
351. Goldring MB. Culture of immortalized chondrocytes and their use as models of chondrocyte function. *Cartilage and Osteoarthritis: Springer*; 2004. p. 37-52.
352. Mobasheri A, Rayman MP, Gualillo O, Sellam J, Van Der Kraan P, Fearon U. The role of metabolism in the pathogenesis of osteoarthritis. *Nature Reviews Rheumatology*. 2017;13(5):302-11.
353. Tew SR, McDermott BT, Fentem RB, Peffers MJ, Clegg PD. Transcriptome-wide analysis of messenger RNA decay in normal and osteoarthritic human articular chondrocytes. *Arthritis & rheumatology*. 2014;66(11):3052-61.
354. Kapoor M, Martel-Pelletier J, Lajeunesse D, Pelletier J-P, Fahmi H. Role of proinflammatory cytokines in the pathophysiology of osteoarthritis. *Nature Reviews Rheumatology*. 2011;7(1):33-42.

355. Ahmad R, Qureshi H, El Mabrouk M, Sylvester J, Ahmad M, Zafarullah M. Inhibition of interleukin 1-induced matrix metalloproteinase 13 expression in human chondrocytes by interferon  $\gamma$ . *Annals of the rheumatic diseases*. 2007;66(6):782-9.
356. QIAGEN. miRCURY LNA miRNA Inhibitors and Target Site Blockers Handbook 2017 [Available from: file:///ueahome/eressci8/tyq17cwu/data/Downloads/HB-2443-001\_1107949\_HB\_miRC\_LNA\_miRNA\_Inhib\_TSB\_1017\_WW.pdf.
357. Thomson DW, Bracken CP, Szubert JM, Goodall GJ. On measuring miRNAs after transient transfection of mimics or antisense inhibitors. *PloS one*. 2013;8(1):e55214.

## Appendices

### *Appendix 1 Primers for pmirGLO construction*

Gene symbol	Primer	Sequence 5'-3'	Restriction enzyme sites
JUN	Forward	CTATAGAGCTCACAAAGTTGCGACGGAGAGAA	SacI
	Reverse	CTATAGTCGACAGCAAAGGCCATCTTTTTATCTAGG	Sall
FOS	Forward	CTATAGAGCTCAGGGAAGGGGAGGCAGC	SacI
	Reverse	CTATAGTCGAC TGGAACAATAAGCAAACAATGCT	Sall
CMTM3	Forward	TCCGCTCGAGAGGCCTGGCGGGTGCCTTG	XhoI
	Reverse	CCGCGTCGACAAATGGTAGTCAGATTTACGTGTATTTTTGC	Sall
LBH	Forward	TATACTCGAGTGTGGACTCCCATGGGTCAT	XhoI
	Reverse	TATAGTCGACGGCGGGAATCCATAGGTGAG	Sall
CTDSP2.1	Forward	TATACTCGAGGGGGGAGAAGCTGAAAGACC	XhoI
	Reverse	TATAGTCGACAAAAGGCCTATCCCAGGCAC	Sall
CTDSP2.2	Forward	TATACTCGAGAAGGGGAGAAGGACCCCATGT	XhoI
	Reverse	TATAGTCGACACGTTAAAAGAATGGGGCAGC	Sall

Appendix 2 Primers for QuikChange Lightning Multi Site-Directed Mutagenesis

Gene symbol	Primer	Sequence 5'-3'	Restriction enzyme sites
JUN	Site1	CAGGCGGCCGCTCCCGTCGACCACGCCAAGGGAGGG	Sall
FOS	Site1	CACAGACCCAGGCCGTCGACAACATGCTACTAACTACCAGCTCTCTG	Sall
CMTM3	Site1	CTTCCTAGAGCCCCTCGAGCAGGCAGGAGTTC	XhoI
CMTM3	Site2	TAGGCCTCACAAAAGCTCGAGAGTTCTGGACCCATG	XhoI
CMTM3	Site3	CCTGAAAAAAGCCATAATGAATTACTCGAGACTGACCACTTGC	XhoI
LBH	Site1	CCCATGGGTCATACCGGATCCCATCTGTTCTGAAC	BamHI
LBH	Site2	AGGAAGCTGCTTAGGAGCTCGGGGTTAGTGGG	SacI
LBH	Site3	GCAGAGAACTGCGGATCCGATGCGCTCAGC	BamHI
LBH	Site4	TTGGCTGCCTGCAAGAGCTCCTGGAGGTGAAG	SacI
LBH	Site5	GCTGTGGTAGGCTCACATGGATCCTGTGATCGGTTTTTAA	BamHI
CTDSP2.1	Site1	TCTGAAATCCTTCTCGCTAGCGCTGCTGCAGACAAAAG	NheI
CTDSP2.2	Site1	GTTGTTTAAACGAGCTCGCTGGATCCAAATATACTGTCTCTTG AAG	BamHI
CTDSP2.2	Site2	GCTCAGACTCTTAGCTCGAGCTGTGGCTTCGGAC	XhoI
CTDSP2.2	Site3	GCCGTCTAGGCCCGGATCCGCTTTTCTGACTA	BamHI
CTDSP2.2	Site4	CTACTCGGCCAAACCTCTCGAGGGTCTGTTCTTGT	XhoI
CTDSP2.2	Site5	CTGTTCTTGTGGACCAGCGGCCGCTAGTCATTATTTGCT	NotI
CTDSP2.2	Site6	TGGCACCCAGTGTCCCTGAGCTCGCCAAGTATATG	SacI
CTDSP2.2	Site7	TGGTAAATATTTACATTGCTAGCGGAAGAGGAGGCCAGAG	NheI

Appendix 3 Primers and probes for GOI qRT-PCR.

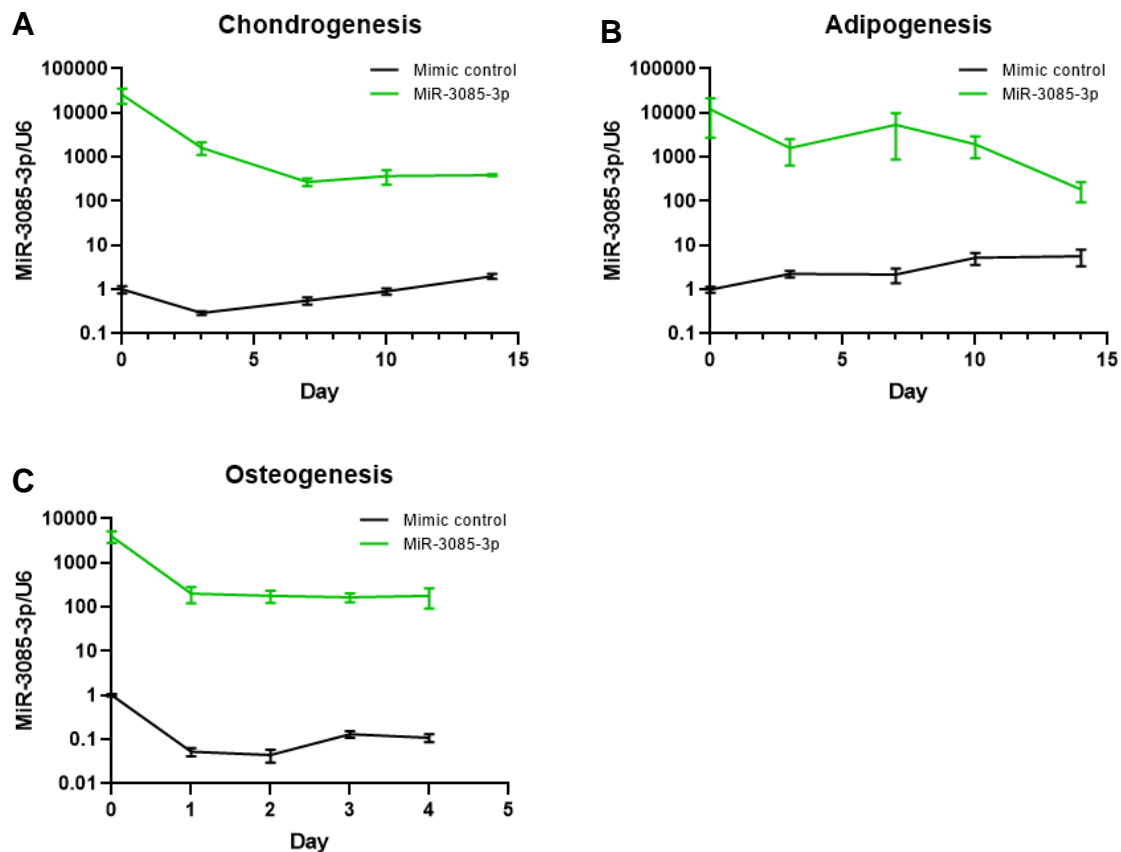
Gene symbol	Primer	Sequence 5'-3'	Probe
18S rRNA	Forward	GCCGCTAGAGGTGAAATTCTTG	6-FAM- ACCGGCGCAAGACGGA- TAMRA
	Reverse	CATTCTTGGCAAATGCTTTTCG	
ACAN	Forward	AAGCACTGGAGTTCTGTGAATCT	#1
	Reverse	CGGCATAGCACTTGTCCAG	
COL2A1	Forward	CCCTGGTCTTGGTGGAAAC	#65
	Reverse	TCCTTGCATTACTCCCAACTG	
COL10A1	Forward	CACCTTCTGCACTGCTCATC	#6
	Reverse	GGCAGCATATTCTCAGATGGA	
SOX9	Forward	GTACCCGCACTTGCACAAC	#61
	Reverse	TCTCGCTCTCGTTCAGAAGTC	
PPARG	Forward	TTGCTGTCATTATTCTCAGTGGA	#1
	Reverse	GAGGACTCAGGGTGGTTCAG	
CEBPA	Forward	GGAGCTGAGATCCCGACA	#18
	Reverse	TTCTAAGGACAGGCGTGGAG	
COL1A1	Forward	CCCAAGGCTTCCAAGGTC	#1
	Reverse	GGACGACCAGGTTTTCCAG	
COL1A2	Forward	GAGTCCGAGGACCTAATGGA	#54
	Reverse	AGGGGAACCAGGAAGACCT	
BMP2	Forward	GACTGCGGTCTCCTAAAGGTC	#49
	Reverse	GGAAGCAGCAACGCTAGAAG	
ALP	Forward	AACACCACCCAGGGGAAC	#58
	Reverse	GGTCACAATGCCACAGATT	
RUNX2	Forward	CAGTGACACCATGTCAGCAA	#41
	Reverse	GCTCACGTCGCTCATTTTG	
BGLAP	Forward	TGAGAGCCCTCACACTCCTC	#81
	Reverse	ACCTTTGCTGGACTCTGCAC	
SPP1	Forward	GAGGGCTTGGTTGTCAGC	#18
	Reverse	CAATTCTCATGGTAGTGAGTTTTCC	
ITGA5	Forward	TGCAAGGACTTGTACTCCACA	#55
	Reverse	CCCATTGAATTTGACAGCAA	
CRTAC1	Forward	CGGCATGTCCAGGATGTTA	#18
	Reverse	GGTGAAGTGCAGTGAACATGG	
CSPG4	Forward	CCAGCTGAGTGTGGTGGGA	#17

	Reverse	CGCTGGACCTCGTACTCAAT	
IGFBP5	Forward	ACTGAGGCCACGAGTCTT	#69
	Reverse	AGGGAGGATGCAGGGACT	
TSC22D3	Forward	CCATCCTGCTCTTCTCCAC	#36
	Reverse	TCAGATGATTCTTACCAGATCC	
TXNIP	Forward	ACGCTTCTTCTGGAAGACCA	#85
	Reverse	AAGCTCAAAGCCGAACTTGT	
OAF	Forward	CTTCACCGCCGACTTCAA	#24
	Reverse	GAGGGCCTGGAAGTACTCT	
EFHD1	Forward	GGCAAAGCTTTCTGAGATCG	#81
	Reverse	GATGACAAGGCTTGGACCTT	
SCIN	Forward	GACCTCACCCTACTGGAAACC	#41
	Reverse	GGGTGAACTCTCTGGAATCT	
EFNA	Forward	GAAGTTCCAGCGCTTACA	#61
	Reverse	TGGTGGATGGGTTTGGAG	
NOS	Forward	CAACGTGGAATCACTCAGC	#11
	Reverse	ATCGAAGCGGCCGACTT	
CHST3	Forward	CACACACACAGAAACATACATTCG	#80
	Reverse	TTGCCCTTCTGATTGTTAAA	
TIMP4	Forward	TTGGTGCAGAGGGAAAGTCT	#5
	Reverse	GGTACTGTGTAGCAGGTGGTGA	
LPAR4	Forward	TCAGCACATTCTCTCATCTAGCA	#40
	Reverse	TCTTCTGTCACCCATGGACTT	
TGFBR3	Forward	CGACCTGAAATCGTGGTGTT	#3
	Reverse	GCTCCATGTTGAAGGTGATG	
SCARA3	Forward	CCGGCTCCACTACAGCTC	#6
	Reverse	CCGACCTCACTTTCATGGTC	
DAB2	Forward	TTGAGTGCCTTTGCCAGTTA	#2
	Reverse	GCATCAAAGTCATCATGGTCTG	
CD248	Forward	CGTGATCGCAGCCAACTAT	#8
	Reverse	ACAGAGAGAATACCGGGTTGG	
SYNC	Forward	CCGGGAAGTGCTGACTACA	#6
	Reverse	TTCTGCTTCTGATAGGCATCC	
PLEKHF1	Forward	GCTACTGCGGTGTGGACTC	#23
	Reverse	GGTCCACCATCGTCTCCA	
JUN	Forward	CCAAAGGATAGTGCGATGTTT	#75
	Reverse	CTGTCCCTCTCCACTGCAAC	
KLF6	Forward	GCACGAGACCGGCTACTTC	#25

	Reverse	CCAGCTCTAGGCAGGTCTGTT	
FOS	Forward	CTACCACTCACCCGCAGACT	#67
	Reverse	AGGTCCGTGCAGAAATCCT	
FBXO32	Forward	GAGCAAGGGGCCATGATA	#3
	Reverse	TGTTTGCTGAGTGAATTCAAGG	
RAB3IL	Forward	CAGAACAAGCCGACACACAG	#1
	Reverse	TGTCTGTCCATCCATTCTGC	
CTDSP2	Forward	AAGGAGGAAGCAAACACCATT	#47
	Reverse	TCCCTGGGATCTGGTAGAACT	
NFKBIA	Forward	GTC AAGGAGCTGCAGGAGAT	#38
	Reverse	GATGGCCAAGTGCAGGAA	
TNIP1	Forward	GAAGCAGCGTGACTTTGACC	#63
	Reverse	TGCTCCTTGTCGGTCTCC	
GLDN	Forward	CAAAGGGGGTTCTAATACCCTAGT	#72
	Reverse	CATTTTCAAGCTTCAGAGTTTGG	
CMTM3	Forward	GGCTTTCCTCTGCTCTCTCA	#18
	Reverse	GAGGACGCCACATAGCAGATA	
LBH	Forward	CTCAGCACGAAGGTCTCTCC	#74
	Reverse	ACTCCATCTCGGGAGCAAG	
TYMP	Forward	CAAGGTCAGCCTGGTCCTC	#5
	Reverse	CCACGTCCGCTGATCATT	
NFIA	Forward	TCGATTTATATTTGGCATACTTTGTG	#20
	Reverse	GGTCCTTAATGTCAGCGTCAC	
LYN	Forward	AGGTTCAAGCGTTTCTGTTC	#2
	Reverse	CATCATGTGATACAGAAGTTTCCA	
SLC25A28	Forward	CCATCGACTGCGTCAAGA	#65
	Reverse	CCATAGGCCCTCCGTTCT	

Appendix 4 Primer sets for genotyping PCR.

Strain	Primer	Sequence 5'-3'
MiR-3085-null	Forward	TCCTTCTCCAAGTCAAGGGC
	Reverse	TGACTGTCCTCCTGAAGTTGG
MiR-3085-null #11 WT	Forward	CCATCACCAACAGTCCCAACT
MiR-3085-null #11 MUT	Forward	TCCATCACCAACAGTCCATC
	Reverse	TGACTGTCCTCCTGAAGTTGG
Col2a1Cre	Forward	TCTGGTGTAGCTGATGATCCG
	Reverse	TATGTCCACACCAAATTCCTG
ITGA5	Forward	GCAGGATTTTACTCTGTGGGC
	Reverse 1	TCCTCTGGCGTCCGGCCAA
	Reverse 2	GAGGTTCTTCCACTGCCTCCTA



miR-3085-3p expression was normalized to U6 snRNA, and the mean of that at day 0 was set as 1 in chondrogenesis (A), adipogenesis (B) and osteogenesis (C), respectively. MiRNAs at desired time points were extracted from MSCs of 3 donors, followed by MiRCURY LNA Universal cDNA synthesis and qRT-PCR. Data show Mean  $\pm$  SEM, N=3.

The effect of miR-3085-3p mimic in knocking down the miR-3085-3p level are shown in Appendix 5. QRT-PCR results demonstrated dramatically increased miR-3085-3p by transfecting mimic into hBMMSCs. This upregulation endured across chondrogenesis, adipogenesis and osteogenesis. However, we observed a slight increase rather than decrease of miR-3085-3p by inhibitor (data not shown). On the basis of the designation of the inhibitors we used (356), the inhibitors are locked nucleic acid (LNA) modified antisense oligonucleotides complimentary to miR-3085-3p. Instead of directly degrading miR-3085-3p, the inhibitor has high affinity to and forms stable complex with miR-3085-3p so that the combination of miR-3085-3p to its target mRNAs is impeded. Nonetheless, the complex of miR-3085-3p and inhibitor leads to an accumulation of miRNA as a result of restrained turnover of miR-3085-3p, confounding the PCR reaction for detection of the functional miRNA. It is therefore recommended that measurement of the expression level of miRNA's

putative target genes can be applicable to assess the effect of miRNA inhibitor(356, 357). In our study, ITGA5, a validated direct target of miR-3085-3p (206), was significantly increased after transient transfection of miR-3085-3p inhibitor in HACs (Figure 3.4B), verifying that the inhibitor is effective in interfering the function of miR-3085-3p.

## **Publications**

1. Swingler T, Niu L, Smith P, Paddy P, Le L, Barter M, et al. The function of microRNAs in cartilage and osteoarthritis. *Clinical and experimental rheumatology*. 2019;37(5):40-7.
2. Le L, Niu L, Barter MJ, Young DA, Dalmay T, Clark IM, et al. The role of microRNA-3085 in chondrocyte function. *Scientific reports*. 2020;10(1):1-10.
3. Swingler TE, Niu L, Pontifex MG, Vauzour D, Clark IM. The microRNA-455 Null Mouse Has Memory Deficit and Increased Anxiety, Targeting Key Genes Involved in Alzheimer's Disease. *International Journal of Molecular Sciences*. 2022;23(1):554.



OPEN

## The role of microRNA-3085 in chondrocyte function

Linh Le<sup>1,3,4</sup>, Lingzi Niu<sup>1,4</sup>, Matthew J. Barter<sup>2</sup>, David A. Young<sup>2</sup>, Tamas Dalmay<sup>1</sup>, Ian M. Clark<sup>1,5</sup>✉ & Tracey E. Swingler<sup>1,5</sup>

MicroRNAs have been shown to play a role in cartilage development, homeostasis and breakdown during osteoarthritis. We previously identified miR-3085 in humans as a chondrocyte-selective microRNA, however it could not be detected by Northern blot. The aim of the current study was to prove that miR-3085 is a microRNA and to investigate the function of miR-3085 in signaling pathways relevant to cartilage homeostasis and osteoarthritis. Here, we confirm that miR-3085 is a microRNA and not another class of small RNA using (1) a pre-miR hairpin maturation assay, (2) expression levels in a Dicer null cell line, and (3) Ago2 pulldown. MicroRNA-3085-3p is expressed more highly in micromass than monolayer cultured chondrocytes. Transfection of miR-3085-3p into chondrocytes decreases expression of *COL2A1* and *ACAN*, both of which are validated as direct targets of miR-3085-3p. Interleukin-1 induces the expression of miR-3085-3p, at least in part via NFκB. In a feed-forward mechanism, miR-3085-3p then potentiates NFκB signaling. However, at early time points after transfection, its action appears to be inhibitory. MyD88 has been shown to be a direct target of miR-3085-3p and may be responsible for the early inhibition of NFκB signaling. However, at later time points, MyD88 knockdown remains inhibitory and so other functions of miR-3085-3p are clearly dominant. TGFβ1 also induces the expression of miR-3085-3p, but in this instance, it exerts a feedback inhibition on signaling with *SMAD3* and *SMAD4* shown to be direct targets. This *in vitro* analysis shows that miR-3085-3p functions in chondrocytes to induce IL-1-signaling, reduce TGFβ1 signaling, and inhibit expression of matrix genes. These data suggest that miR-3085-3p has a role in chondrocyte function and could contribute to the process of osteoarthritis.

Osteoarthritis (OA) is a degenerative disease of the articular joint, involving degradation of the articular cartilage, subchondral bone sclerosis and the formation of osteophytes<sup>1,2</sup>. Several factors (genetic, developmental, biochemical and biomechanical) impact upon the etiology of OA<sup>1</sup>. Cartilage homeostasis is dependent on the expression of appropriate genes by resident chondrocytes and this is aberrant in OA<sup>3</sup>.

One class of small non-coding RNAs known as microRNAs (miRNAs) have a key role in the regulation of gene expression in human cells. MiRNAs are transcribed as primary transcripts (pri-miRNA) and processed to short stem-loop structures (pre-miRNA) in the nucleus. The pre-miRNA is then processed by the ribonuclease, Dicer, forming two complementary short RNA strands. One of these, the guide strand, is integrated into the RNA-induced silencing complex (RISC), the other, the passenger strand, is degraded<sup>4</sup>. After integration into RISC, miRNAs base pair with their complementary mRNA targets, usually in the 3'UTR<sup>5</sup> to degrade mRNA or repress translation.

The miRNA pathway has a major role in skeletal development. The conditional knockout of Dicer in limb mesenchyme early in embryonic development leads to the formation of a smaller limb<sup>6</sup>. Dicer-null growth plates show diminished chondrocyte proliferation, with enhanced differentiation to postmitotic hypertrophic chondrocytes. Conditional knockout of Dicer in chondrocytes results in defects in skeletal growth and premature death<sup>7</sup>.

Many miRNAs are regulated during cartilage development, with a number of miRNAs regulated by the key cartilage-specifying transcription factor Sox9 (e.g. miR-140 and miR-455), or regulating Sox9 expression (e.g. miR-675 and miR-145 (see<sup>8</sup>)).

MicroRNAs are dysregulated in OA and have a functional effect on disease progression in models of disease<sup>8,9</sup>. Studies comparing expression of miRNAs in normal vs osteoarthritic human cartilage show little congruity, likely

<sup>1</sup>Biomedical Research Centre, School of Biological Sciences, Norwich Research Park, University of East Anglia, Norwich NR4 7TJ, Norfolk, UK. <sup>2</sup>Institute of Genetic Medicine, Newcastle University, Newcastle-upon-Tyne, UK. <sup>3</sup>Biotechnology Department, Ho Chi Minh City Open University, Ho Chi Minh City, Vietnam. <sup>4</sup>These authors contributed equally: Linh Le and Lingzi Niu. <sup>5</sup>These authors jointly supervised this work: Ian M. Clark and Tracey E. Swingler. ✉email: i.clark@uea.ac.uk

because of varying sample groups and this makes interpretation difficult. However, understanding the roles of miRNAs in OA is important and may lead to novel therapy<sup>8</sup>.

MicroRNA-140 is the most studied miRNA to date in cartilage and osteoarthritis. Universal knockout of miR-140 leads to mild dwarfism, probably as a result of impaired chondrocyte proliferation<sup>10,11</sup>. Such deletion of miR-140 in mice predisposed them to the development of age-related OA-like changes and increased cartilage destruction in surgically-induced OA, possibly through direct targeting of Adamts<sup>10,11</sup>. A number of other targets have been identified and validated in vitro which have the potential to be involved in chondrocyte development and/or cartilage homeostasis<sup>12</sup>.

We recently identified a miRNA in humans, previously sequenced (but uncharacterised) in mice and rats, microRNA-3085. We went on to demonstrate that miR-3085 was expressed selectively in cartilage compared to other tissues and its expression rapidly decreased upon chondrocyte isolation and passage in monolayer culture<sup>13</sup>. MicroRNA-3085 is genomically located within an intron of cartilage acidic protein 1 (CRTAC1, previously called CEP-68), the function of which is unknown<sup>14</sup>. CRTAC1 is expressed in both cartilage and bone tissue, but rapidly lost from osteoblasts on culture<sup>14</sup> and like miR-3085, its expression is also markedly decreased when chondrocytes are digested from cartilage<sup>15</sup>. CRTAC1 is also reported to be increased in expression in arrays of human OA cartilage (e.g.<sup>16</sup>).

The purpose of the current study was to: (1) prove that miR-3085 was a microRNA and not another type of small RNA; (2) investigate the function of miR-3085 in signaling pathways relevant to cartilage homeostasis and osteoarthritis.

## Materials and methods

**Cell culture.** SW1353 chondrosarcoma cells were from the American Type Culture Collection, parental and DLD-1 Dicer null cell lines were from Horizon Discovery and originated from a colorectal adenocarcinoma. Cells were cultured in Dulbecco's modified Eagle's medium (DMEM, Thermo Fisher Scientific) with GlutaMAX containing 10% (v/v) fetal bovine serum (Sigma Aldrich), 100 IU/ml penicillin and 100 µg/ml streptomycin, 37 °C, 5% (v/v) CO<sub>2</sub> under normoxia, as described<sup>17</sup>.

Primary human articular chondrocytes (HACs) were isolated from cartilage of osteoarthritis patients as described<sup>18</sup> and cultured as above. All experimental protocols were approved by NRES Committee East of England (ref: 08/h0304/85 + 5). All tissue donors gave informed written consent. All methods were performed in accordance with relevant laboratory guidelines and institutional regulations for research using human tissues and body fluids.

For micromass culture<sup>19</sup>, primary HACs were grown in monolayer culture in DMEM high glucose, with GlutaMAX (Thermo Fisher Scientific), containing 10% (v/v) fetal bovine serum (Sigma Aldrich), 100 IU/ml penicillin and 100 µg/ml streptomycin (Thermo Fisher Scientific) (growth medium) at 37 °C, 5% (v/v) CO<sub>2</sub> until passage two. Confluent cells were then trypsinised and resuspended at a density of  $2 \times 10^7$  in growth medium. Micromass was obtained by pipetting 20 µl cell suspension into individual wells of 24-well plates and incubating for 3 h to attach. One ml growth medium was then added, and the micromass was incubated for 24 h. Growth medium was then replaced with DMEM high glucose, with GlutaMax (Thermo Fisher Scientific) containing  $1 \times$  insulin-transferrin-selenium (Thermo Fisher Scientific) and 0.5% (v/v) fetal bovine serum (Sigma Aldrich), with or without recombinant human TGFβ1 (4 ng/ml) (R&D Systems) or IL-1β (5 ng/ml) (First Link (UK) Ltd) for 24 h. Inhibition of NFκB was achieved using JSH-23 at 10 µM (Calbiochem). JSH-23 was added 1 h before adding IL-1β and was kept in culture media for another 24 h.

**Transient transfection.** The 3'UTR of mRNAs containing the predicted binding site of miR-3085-3p were subcloned into pmirGLO (Promega), using QuikChange II XL site-directed mutagenesis kit (Agilent) to introduce mutations. Constructs were sequence verified (Source Bioscience). SW1353 cells were seeded into 96-well plate wells at  $5 \times 10^4$  cells/ml in 100 µl medium overnight and transiently transfected with 100 ng reporter plasmid, 50 nM miR-3085-3p mimic (Qiagen) or non-targeting control (Negative Control miRCURY LNA miRNA Mimic, Qiagen) using Lipofectamine 3000 (Thermo Fisher Scientific), according to manufacturer's instructions for either 24 h or 48 h (see<sup>20</sup>). Cell lysates were assayed for luciferase using the Dual Luciferase Reporter Assay Kit (Promega), read with an EnVision 2103 Multilabel plate reader (Perkin Elmer). Relative luciferase activity was the ratio of firefly luciferase to Renilla luciferase activity<sup>20</sup>.

Signalling pathways were measured using p(CAGA)<sub>12</sub>-luc (Smad2/3)<sup>21</sup>; κB-luc (NFκB)<sup>22</sup>; TOPFlash (canonical Wnt) reporters<sup>23</sup>. 100 ng of the plasmid and 10 ng of constitutive Renilla plasmid were co-transfected into SW1353 cells with 50 nM miR-3085-3p mimic or non-targeting control. After serum starvation for 24 h, cells were treated with either TGFβ1 (4 ng/ml) (R&D Systems) or IL-1β (5 ng/ml) (First Link (UK) Ltd) for 6 h. Luciferase activity and data analysis were as described above.

HACs were plated in 96-well plate wells at a density of  $7 \times 10^4$  cells/ml in 100 µl, and grown to 80%-90% confluence. MicroRNA-3085-3p mimic (50 nM), non-targeting control (50 nM), MyD88 siRNA (50 nM) and negative control siRNA (50 nM) (AllStars Negative Control siRNA, Qiagen) were transfected as described above and<sup>20</sup>. Cells were then incubated at 37 °C in 5% CO<sub>2</sub> for 48 h. After serum starvation for 24 h, cells were treated with recombinant human TGFβ1 (4 ng/ml) (R&D Systems), IL-1β (5 ng/ml) (First Link (UK) Ltd) for another 8 h<sup>20</sup>, followed by RNA isolation.

**RNA isolation and qRT-PCR.** Trizol reagent (Thermo Fisher Scientific) was used to isolate total RNA from cultured cells according to manufacturer's instructions. The miRCURY LNA Universal cDNA synthesis kit (Exiqon) and miRNA-specific LNA primers (Exiqon) was used for quantification of mature miRNA transcripts by qRT-PCR. Data were normalized to U6 as the housekeeping gene. For mRNA, Ambion Cells-to-cDNA II Kit

(Life Technologies) or SuperScript II RT (Thermo Fisher Scientific) was used with data normalised to expression of 18S rRNA ribosomal RNA. Only samples where the housekeeping genes are expressed within median  $\pm$  1 Ct are included in analyses. Primer sequences are listed in Supplementary Table 1. Both miRNA and mRNA relative quantifications were calculated using the  $\Delta\Delta$ CT method. Fluorescence for each cycle was analysed by the real-time PCR 7500 system (Applied Biosystems)<sup>20</sup>.

**Western blot.** SW1353 cells were plated in 6-well plate wells at  $1.5 \times 10^5$  cells/well and left to adhere overnight. Cells were transiently transfected with 50 nM miR-3085-3p mimic (Qiagen), siRNA (Qiagen) or non-targeting controls (Qiagen) for 48 h. After serum starvation for another 24 h, cells were stimulated with IL-1 $\beta$  (5 ng/ml) (First Link (UK) Ltd) for 30 min or TGF $\beta$ 1 (4 ng/ml) (R&D Systems) for 2 h and washed twice in ice-cold phosphate buffered saline (PBS). Whole cell lysates were harvested into ice cold RIPA buffer (50 mM Tris-HCl pH7.6, 150 mM NaCl, 1% (v/v) Triton x-100, 1% (w/v) sodium deoxycholate, 0.1% (w/v) SDS, 10 mM NaF, 2 mM Na<sub>3</sub>VO<sub>4</sub>, 1  $\times$  protease inhibitor cocktail III (Thermo Fisher Scientific)). Samples were separated on reducing SDS-PAGE, transferred to PVDF membrane and probed overnight at 4 °C. The p65 (#8242), phospho-p65 (#3033), I $\kappa$ B $\alpha$  (#4814), phospho-I $\kappa$ B $\alpha$  (#2859), SMADs (#3103, #9513, #38,454), phospho-SMADs (#9523), MyD88 (#4283),  $\beta$ -catenin (#9582), phospho- $\beta$ -catenin (#9561) and GAPDH (#2118) (all from Cell Signaling Technology, used at recommended concentrations) were detected using HRP-conjugated secondary antibodies (DAKO), visualised using Pierce ECL Western Blotting Substrate (Thermo Fisher Scientific), and imaged by ChemiDoc MP Imaging System (Biorad)<sup>13</sup>.

**Cellular fractionation.** SW1353 cells were plated in 60-mm culture dishes at  $3.5 \times 10^5$  cells/dish overnight. The cells were then transiently transfected with either miR-3085-3p mimic (Qiagen) or non-targeting control (Qiagen), serum starved, and treated with IL-1 $\beta$  or TGF $\beta$ 1 as described above. Nuclear and cytosolic fractions were purified using the Nuclear and Cytoplasmic Extraction kit (Thermo Fisher Scientific) according to manufacturer's instructions, using 1  $\times$  protease inhibitor cocktail III (Thermo Fisher Scientific), 1  $\times$  phosphatase inhibitor cocktail 2 (Sigma Aldrich), and 1  $\times$  phosphatase inhibitor cocktail 3 (Sigma Aldrich).

**Hairpin maturation assay.** An approximately 500 bp region containing the precursor of miR-140 or miR-3085 sequences was sub-cloned into pcDNA3.0. Primers for sub-cloning miR-3085 were.

5'-ATGCAAGCTTAGGATCAAGAGCAGGATTGG-3',  
5'-ATGCAAGCTTCTGGCCTCAGAGAAGACTGG-3' and for miR-140 were  
5'-ATGCAAGCTTAGAGAGAGAGAGCGCTGTGG-3',  
5'-ATGCAAGCTTGCAACTCTTGCACCTTGC-3'.

SW1353 cells were transiently transfected using Lipofectamine 3000 (Thermo Fisher Scientific) according to manufacturer's instructions) with expression constructs for either precursor miR-140 or precursor miR-3085 compared to an empty vector and cultured for 48 h. RNA was isolated and miRCURY LNA Universal cDNA synthesis kit (Exiqon) and miRNA-specific LNA primers (Exiqon) for U6, miR-3085-3p and miR-140-5p were used for quantification of mature miRNA transcripts by qRT-PCR.

**Agonate pulldown.** SW1353 cells were transiently transfected with either precursor miR-140 or precursor miR-3085 for 48 h as above. Cell lysates were harvested with 0.5% (v/v) NP40, 150 mM KCl, 25 mM Tris-glycine pH7.5, 2 mM EDTA, 0.5 mM DTT, and 1  $\times$  protease inhibitor cocktail III (Thermo Fisher Scientific). Samples were pulled down with Ago2 antibody (MABE253, Sigma Aldrich) using Dynabeads Protein G (Thermo Fisher Scientific) and DynaMag Magnet at 4 °C, overnight. In order to quantify miRNA expression, targeted Ago2 was eluted with Cells-to-cDNA II lysis buffer (Thermo Fisher Scientific) and the miRCURY LNA Universal cDNA synthesis kit (Exiqon, Denmark) and miRNA-specific LNA primers (Exiqon, Denmark) for miR-140-3p, miR-29b-3p, and miR-3085-3p were used for quantification of mature miRNA transcripts by qRT-PCR.

**Statistical analysis.** Data were tested for normal distribution and analysed using Student's *t*-test to compare between two samples, or one-way ANOVA with post-hoc Tukey's test to compare between multiple samples using GraphPad Prism version 6. Experiments were performed on three independent replicates ( $n = 3$ ); for primary human chondrocytes, three different patient isolates were used.

## Results

**MicroRNA-3085 is a microRNA.** Northern blot of chondrocyte RNA probed for miR-3085 failed to show a signal<sup>13</sup>. In order to verify the identity of this RNA as a microRNA, an expression construct of the presumed pre-miR-3085 hairpin sequence was transiently transfected into SW1353 cells. This led to a statistically significant increase in the mature miR-3085-3p ( $p < 0.001$ , Fig. 1A). As a positive control, the same increase in mature miR-140-3p was measured after transfection with pre-miR-140 expression construct (Fig. 1B). Furthermore, this increase in mature miR-3085-3p was significantly reduced in DLD-1 Dicer null cells compared to isogenic wild-type cells ( $p < 0.001$ , Fig. 1C). Finally, mature miR-3085-3p was immunoprecipitated with an anti-AGO2 antibody after transfection with pre-miR-3085 (but not pre-miR-140) and vice versa (Fig. 1D,E). Western blot of the immunoprecipitates with anti-AGO2 shows equal loading (Supplementary Fig. 1).

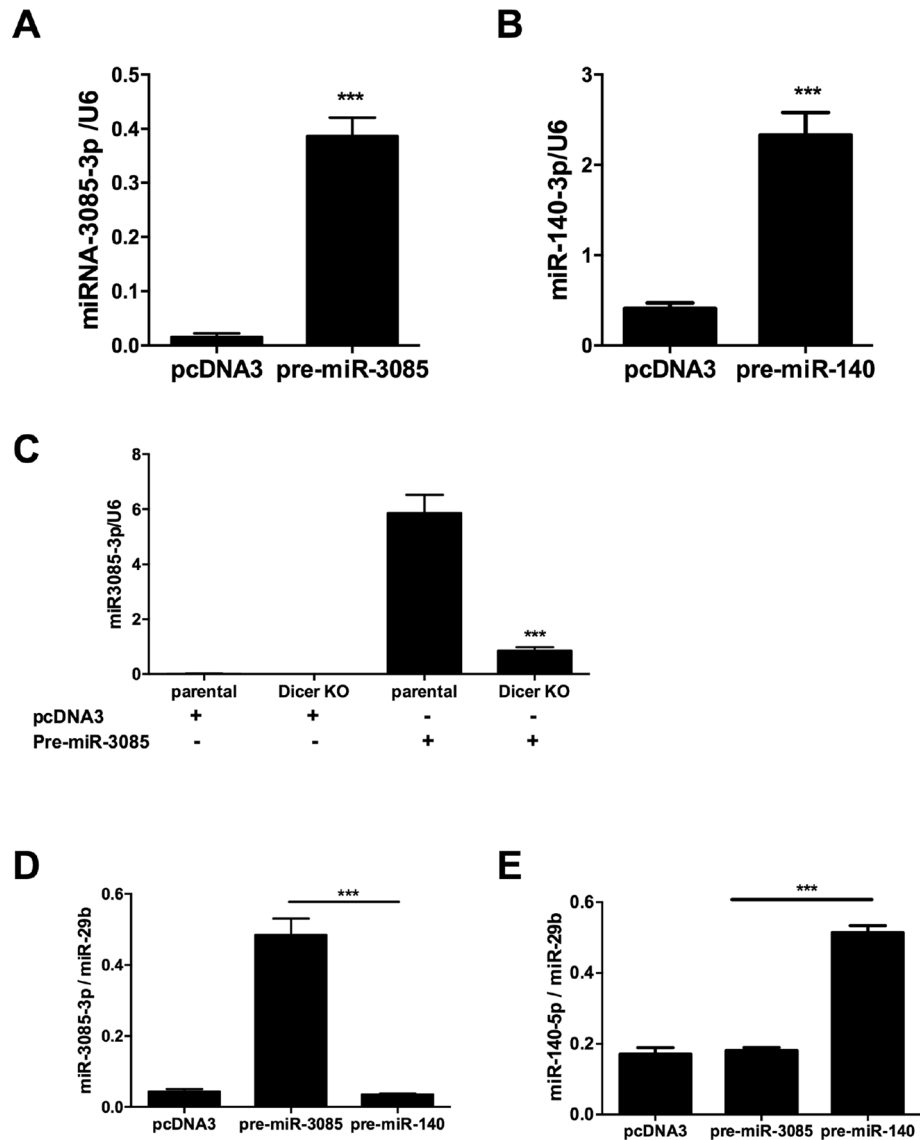


**Figure 1.** miR-3085 is a microRNA. (A) SW1353 chondrosarcoma cells were transiently transfected with expression plasmids for either (A), pre-miR-3085 hairpin or (B), pre-miR-140 hairpin and empty vector (pcDNA3) control and cultured for 48 h. Expression of mature miR-3085-3p or miR-140-3p was measured by qRT-PCR. (C) Parental DLD-1 cells or isogenic Dicer null (KO) cells were transiently transfected with expression plasmids for pre-miR-3085 hairpin and culture for 48 h. Expression of mature miR-3085-3p was measured by qRT-PCR. (D,E), SW1353 cells were transiently transfected with either pre-miR-3085 or pre-miR-140 for 48 h, cell lysates were immunoprecipitated using an Ago2 antibody; mature miR-3085-3p, miR-140-3p and miR-29b-3p were measured by qRT-PCR. Mean  $\pm$  SEM,  $n = 3$ ; (A,B) Student's t-test; (C-E), ANOVA with Tukey's post test; \*\* $p < 0.01$ ; \*\*\* $p < 0.001$ .

**MicroRNA-3085-3p modulates the expression of matrix genes.** The expression of miR-3085-3p is increased by micromass (three-dimensional) culture of human articular chondrocytes ( $p < 0.05$ , Fig. 2A), which significantly enhances expression of matrix genes<sup>19</sup>. However, the overexpression of miR-3085 represses the expression of both *COL2A1* ( $p < 0.001$ ) and *ACAN* ( $p < 0.01$ ), though *SOX9* expression shows a small increase ( $p < 0.05$ ) (Fig. 2B). Expression of luciferase controlled by the 3'UTR of either the *COL2A1* or *ACAN* gene shows that miR-3085-3p significantly reduces this expression and that this is rescued by mutation of the miR-3085-3p seed site in each UTR (Fig. 2C,D). This shows that these genes are direct targets of miR-3085-3p.

**MicroRNA-3085-3p and NF $\kappa$ B signaling.** Interleukin-1 and NF $\kappa$ B signaling are deemed key in OA<sup>1,24</sup>. Interleukin-1 $\beta$  induces expression of miR-3085-3p in primary human articular chondrocytes in either monolayer or micromass culture ( $p < 0.001$ , Fig. 3A, micromass) and this is in part dependent on NF $\kappa$ B signaling (Fig. 3B). IL-1-induced activation of an NF $\kappa$ B reporter, transiently transfected into SW1353 cells is further increased by co-transfection with miR-3085-3p ( $p < 0.01$ , Fig. 3C), with the same pattern seen for IL-1 induced

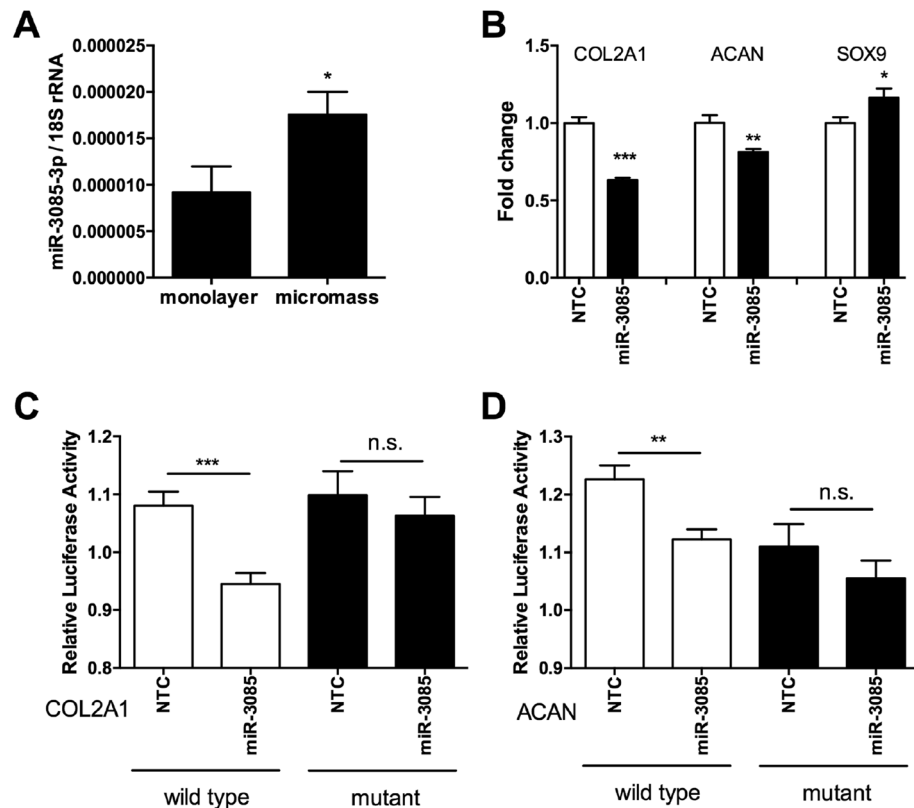


**Figure 2.** miR-3085 downregulates type II collagen and aggrecan expression. (A) Primary human articular chondrocytes were cultured in micromass culture for 48 h; miR-3085-3p was measured by qRT-PCR. (B) Micromass cultures of primary human articular chondrocytes transfected with miR-3085-3p mimic or non-targeting control (NTC) for 48 h; COL2A1 and ACAN were measured by qRT-PCR. SW1353 cells were transiently transfected with the (C). ACAN 3'UTR and (D). COL2A1 3'UTR subcloned into the pmirGLO vector (wild-type) or a construct with miR-3085-3p seed sites mutated (mutant) with miR-3085-3p mimic or non-targeting control (NTC) for 24 h. Firefly luciferase relative light units were normalised to Renilla relative light units to give overall relative light units. Mean  $\pm$  SEM,  $n = 3$ ; Student's t-test; \* $p < 0.05$ ; \*\* $p < 0.01$ ; \*\*\* $p < 0.001$ .

*MMP13* expression in HACs ( $p < 0.05$ , Fig. 3D), at 8 or 6 h of induction respectively. However, at an optimal early time point (30 min), miR-3085-3p mimic decreased nuclear levels of IL-1-induced p65 and phospho-p65 (Fig. 3E). Indeed, time course data from qRT-PCR of IL-1 induced *MMP13* expression did not show a response until 6 h of stimulation (Supplementary Fig. 2).

Since MyD88 is an adapter protein involved in IL-1 signalling<sup>25</sup> and *MyD88* is predicted to be a direct target of miR-3085-3p, we explored this further. MyD88 is experimentally shown to be a direct target of miR-3085-3p, though rescue by mutation of the seed site is partial rather than complete (Fig. 4A). Quantitative RT-PCR (Fig. 4B) and western blot (Fig. 4C) also demonstrates that overexpression of miR-3085-3p leads to a decrease in MyD88 mRNA ( $p < 0.001$ ) and protein. Treatment with siRNA against *MyD88* leads to a decrease in phospho-p65 (Fig. 4D) and it also decreases IL-1-induced *MMP13* expression ( $p < 0.05$ , Fig. 4E), so this is not the mechanism by which miR-3085-3p potentiates IL-1/ NF $\kappa$ B signaling.

**MicroRNA-3085-3p and Smad signaling.** TGF $\beta$ -signalling is also key in OA<sup>1,24</sup>. Similar to IL-1, TGF $\beta$ 1 also induces expression of miR-3085-3p ( $p < 0.05$ , Fig. 5A). In this instance, miR-3085-3p does not show a significant effect on TGF $\beta$ 1-induced luciferase from a Smad-responsive luciferase reporter (CAGA<sub>12</sub>) (Supplementary Fig. 3). TGF $\beta$ 1-induced expression of the inhibitor of DNA-binding 1 (*ID1*) gene is repressed by over-expression of miR-3085-3p ( $p < 0.01$ , Fig. 5B). *SMAD3* and *SMAD4* are direct targets for miR-3085-3p; a *SMAD2* 3' UTR construct is also repressed by miR-3085-3p, but this repression is not rescued by mutation of the seed site (Fig. 5C–E). In total cell extracts, miR-3085-3p reduced expression of SMAD2, SMAD3 and SMAD4 protein (Fig. 5F), whilst in fractionated cells these SMADs were decreased in the nuclear fraction (Fig. 5G) and phospho-SMAD3 was also reduced in whole cell extracts (Fig. 5H).

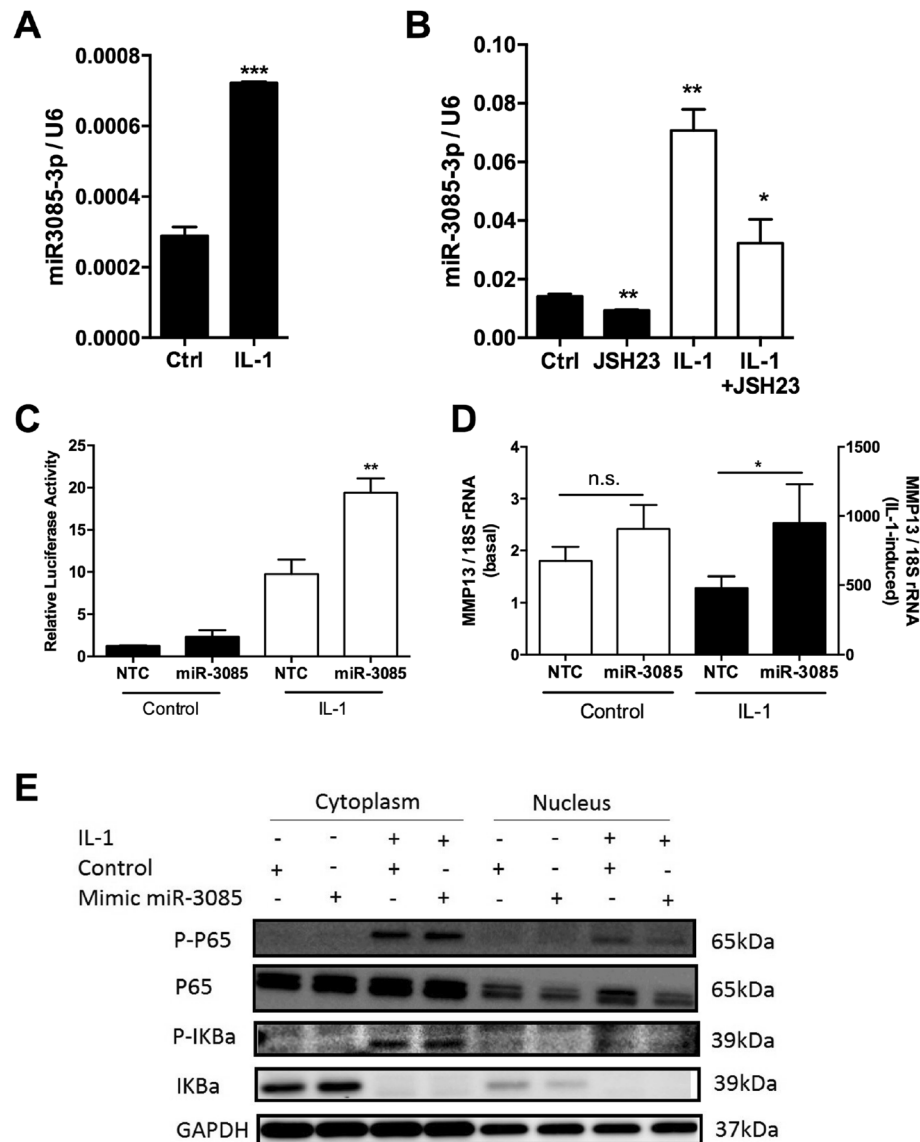


**Figure 3.** IL-1 induces miR-3085-3p which represses NF $\kappa$ B signaling. Primary human articular chondrocytes were cultured in micromass culture for 48 h. (A) cells were then treated with IL-1 $\beta$  (5 ng/ml) or control for 24 h; (B) cells were then treated with IL-1 $\beta$  (5 ng/ml) or control +/- an NF $\kappa$ B inhibitor JSH-23 (10  $\mu$ M) or vehicle 24 h; miR-3085-3p was measured by qRT-PCR. (C) SW1353 cells were transfected with an NF $\kappa$ B luciferase reporter +/- miR-3085-3p mimic or non-targeting control (NTC) for 24 h prior to stimulation with IL-1 $\beta$  (5 ng/ml) or control for 8 h. (D) Primary human articular chondrocytes were grown in monolayer culture and transiently transfected with miR-3085-3p or a non-targeting control (NTC) for 24 h prior to stimulation with IL-1 $\beta$  (5 ng/ml) or control for 6 h; *MMP13* was measured by qRT-PCR. Mean  $\pm$  SEM, n = 3; Student's t-test; \* $p$  < 0.05; \*\* $p$  < 0.01; \*\*\* $p$  < 0.001. (E) SW1353 cells were grown in monolayer culture and transiently transfected with miR-3085-3p or a non-targeting control for 48 h, serum starved for 24 h and stimulated with IL-1 $\beta$  (5 ng/ml) or control for 30 min, fractionation and western blot analysis. Full-length blots are presented in Supplementary data.

## Discussion

MicroRNA-3085 was identified in humans during a small RNA-Seq experiment in primary human articular chondrocytes from osteoarthritis patients<sup>13</sup> where it was shown to be genomically located in the final intron for CRTAC1, a gene expressed in cartilage. It had previously been identified in mouse and rat genomes, but was intergenic in these, though new annotation now shows it also overlaps with CRTAC1 in the rat genome (Ensembl Release 92, data not shown).

In northern blot experiments in RNA purified from cells, expression was undetectable<sup>13</sup>. It has previously been noted that poorly expressed microRNAs require validation via more sensitive methodologies<sup>26</sup>. We therefore looked at its identity as a miRNA using three experiments: transient transfection of an expression plasmid for the hairpin precursor sequence and measuring the mature miR-3085-3p<sup>27,28</sup>; an identical experiment comparing

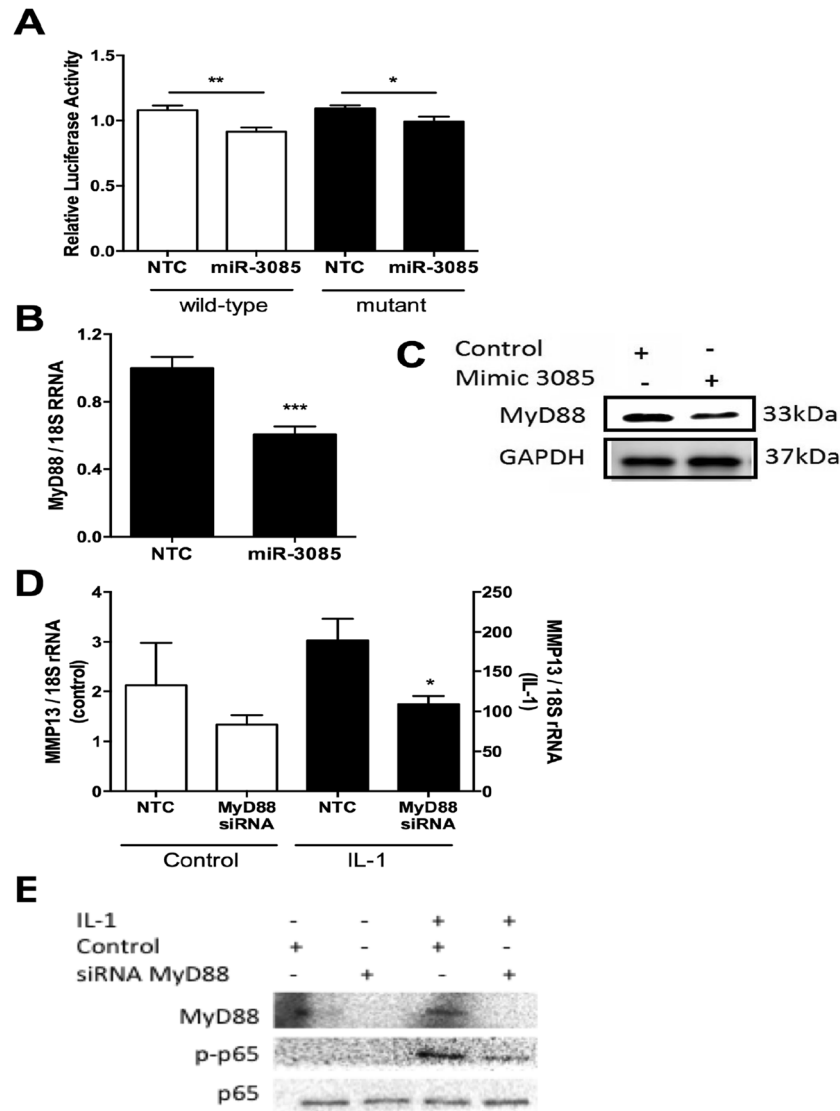


**Figure 4.** MyD88 is a direct target of miR-3085-3p. (A) SW1353 cells were transiently transfected with the MyD88 3'UTR subcloned into the pmirGLO vector (wild-type) or a construct with miR-3085-3p seed sites mutated (mutant) with miR-3085-3p mimic or non-targeting control (NTC) for 24 h. Firefly luciferase relative light units were normalised to Renilla relative light units to give overall relative light units. (B) Primary human articular chondrocytes were grown in monolayer culture and transiently transfected with miR-3085-3p or a non-targeting control (NTC) for 48 h; *MyD88* was measured by (B) qRT-PCR and (C) SW1353 cells were transfected with miR-3085-3p or a non-targeting control (NTC) for 48 h, *MyD88* protein level were measured by western blot. (D) Primary human articular chondrocytes were grown in monolayer culture and transiently transfected with *MyD88* siRNA or a non-targeting control (NTC) for 24 h prior to stimulation with IL-1 $\beta$  (5 ng/ml) or control for 6 h; *MMP13* was measured by qRT-PCR. Mean  $\pm$  SEM,  $n = 3$ . Student's t-test; \* $p < 0.05$ ; \*\* $p < 0.01$ ; \*\*\* $p < 0.001$ . (E) SW1353 cells were grown in monolayer culture and transiently transfected with *MyD88* siRNA or a non-targeting control (NTC) for 24 h prior to stimulation with IL-1 $\beta$  (5 ng/ml) or control for 30 min prior to western blot analysis. Full-length blots are presented in Supplementary data; N.B. the full blot for *MyD88* in (C) is over saturated.

isogenic cell lines which are wild-type or Dicer null<sup>29</sup>; pull down with anti-Argonaute antibody<sup>30</sup>. In each case, miR-3085 behaved in an identical manner to a miR-140 control, providing strong evidence that it is a miRNA rather than any other species of small RNA.

Expression of miR-3085-3p increases when cells are grown in micromass culture compared to monolayer. This is a similar pattern to CRTAC-1 itself<sup>31</sup>, suggesting that they may be regulated by the same promoter. However, overexpression of Sox9, the master regulator of the chondrocyte phenotype, significantly induces *CRTAC1* expression but has a lesser effect on miR-3085-3p expression (data not shown). MicroRNA-3085-3p increases expression of *SOX9* in primary HACs in micromass culture, but decreases expression of both *COL2A1* and *ACAN*

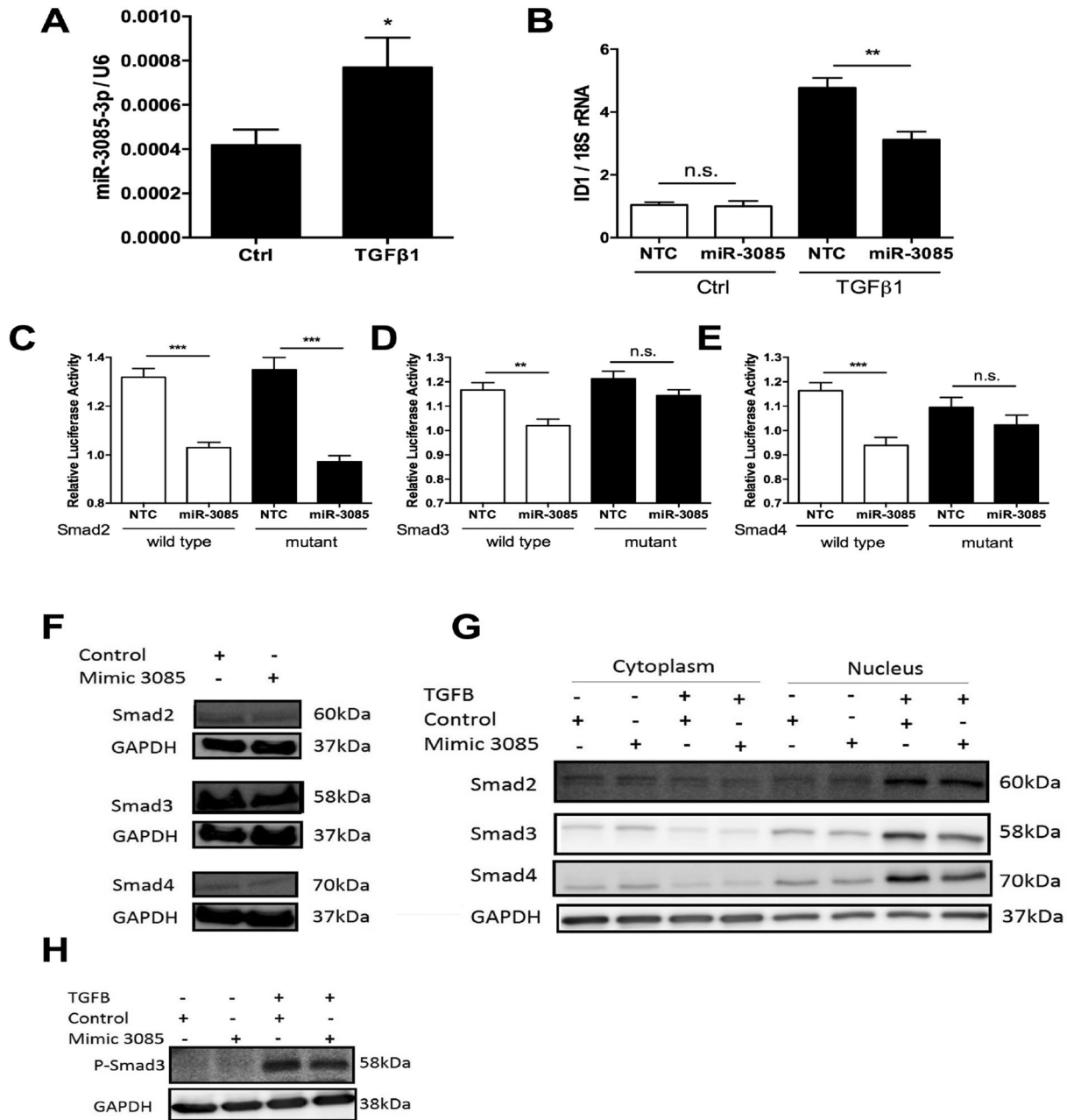


**Figure 5.** TGFβ induces miR-3085-3p which represses Smad signaling. Primary human articular chondrocytes were cultured in micromass culture for 48 h. (A) cells were then treated with TGFβ1 (4 ng/ml), or control for 24 h; miR-3085-3p was measured by qRT-PCR. (B) Primary human articular chondrocytes were grown in monolayer culture and transiently transfected with miR-3085-3p or a non-targeting control (NTC) for 24 h prior to stimulation with TGFβ1 (4 ng/ml), or control for 6 h; *ID1* was measured by qRT-PCR. (C–E) SW1353 cells were transiently transfected with the (C) Smad2, (D) Smad3, (E) Smad4. 3'UTR subcloned into the pmirGLO vector (wild-type) or a construct with miR-3085-3p seed sites mutated (mutant) with miR-3085-3p mimic or non-targeting control (NTC) for 24 h. Firefly luciferase relative light units were normalised to Renilla relative light units to give overall relative light units. Mean  $\pm$  SEM, n = 3; Student's t-test; \* $p < 0.05$ ; \*\* $p < 0.01$ ; \*\*\* $p < 0.001$ . (F) SW1353 cells were transiently transfected with miR-3085-3p or a non-targeting control for 48 h prior to western blot analysis. (G) SW1353 cells were grown in monolayer culture and transiently transfected with miR-3085-3p or a non-targeting control for 48 h prior to stimulation with TGFβ1 (4 ng/ml), or control for 2 h, fractionation and western blot analysis. (H) SW1353 cells were grown in monolayer culture and transiently transfected with miR-3085-3p or a non-targeting control for 48 h prior to stimulation with TGFβ1 (4 ng/ml), or control for 2 h and western blot analysis. Full-length blots are presented in Supplementary data.

genes. These genes are direct targets of miR-3085-3p and this direct effect appears to be dominant in regulating *COL2A1* and *ACAN* expression.

Interleukin-1 induces expression of miR-3085-3p and this is in part mediated by NF $\kappa$ B signaling. Interleukin-1 induction of an NF $\kappa$ B-induced luciferase reporter is further induced by overexpression of miR-3085-3p and this is reinforced by a similar effect on the IL-1-induced expression of the *MMP13* gene. Whilst we have identified MyD88 as a direct target of miR-3085-3p, we have excluded its role in the effect of the microRNA on IL-1 signaling. The direct target of miR-3085-3p responsible has not been identified either using prediction software or by experimental overexpression of miR-3085-3p followed by microarray<sup>13</sup>.

Transforming growth factor beta also induces expression of miR-3085-3p, however the miRNA has no significant effect on the (CAGA)<sub>12</sub> Smad sensitive reporter. This is difficult to explain, since miR-3085-3p clearly decreases expression of Smads 2–4 at both mRNA and protein level. However, the TGF $\beta$ 1-induced expression of *IDI1*, used as a model TGF $\beta$ 1-inducible gene, was repressed by the overexpression of miR-3085-3p. Interestingly, two other genes often used to demonstrate induction by TGF $\beta$ 1, *PAII* and *TIMP3*, are both predicted to be direct targets of miR-3085-3p and therefore not useful in this context.

The effect of miR-3085-3p on IL-1 signalling represents a feed-forward mechanism, whilst on TGF $\beta$ -signalling, it is feed-back. Both of these have been described for microRNAs previously<sup>32</sup>.

Some of the experiments reported have been performed in the SW1353 chondrosarcoma cell line and not in primary HACs. Whilst this is a limitation, the addition of exogenous miR-3085-3p to cell lines does demonstrate the impact of the miRNA on signaling pathways and their outcome. For experiments requiring transient transfection of plasmid DNA, we find that its efficiency in HACs is low and this restricts its utility to cell lines.

These data strongly suggest that miR-3085 functions in cartilage signaling and homeostasis. We have shown that it decreases matrix gene expression, enhances IL-1 signalling and decreases TGF $\beta$  signaling, suggesting that it acts to promote catabolism. However, since miRNAs regulate the expression of a number of genes and pathways, this would be best investigated in vivo. Whilst we were able to gain founder mice with deletions of miR-3085 using CrispR-Cas9, we could not breed these forwards to germline. We are not certain if this is simply a technical issue or whether the miRNA has a more critical function in development.

Received: 23 April 2020; Accepted: 23 November 2020

Published online: 14 December 2020

## References

- Goldring, S. R. & Goldring, M. B. Clinical aspects, pathology and pathophysiology of osteoarthritis. *J. Musculoskelet. Neuronal Interact.* **6**, 376–378 (2006).
- Hunter, D. J. & Bierma-Zeinstra, S. Osteoarthritis. *Lancet* **393**, 1745–1759. [https://doi.org/10.1016/S0140-6736\(19\)30417-9](https://doi.org/10.1016/S0140-6736(19)30417-9) (2019).
- Fisch, K. M. *et al.* Identification of transcription factors responsible for dysregulated networks in human osteoarthritis cartilage by global gene expression analysis. *Osteoarthr. Cartil.* **26**, 1531–1538. <https://doi.org/10.1016/j.joca.2018.07.012> (2018).
- O'Brien, J., Hayder, H., Zayed, Y. & Peng, C. Overview of MicroRNA biogenesis, mechanisms of actions, and circulation. *Front. Endocrinol. (Lausanne)* **9**, 402. <https://doi.org/10.3389/fendo.2018.00402> (2018).
- Winter, J., Jung, S., Keller, S., Gregory, R. I. & Diederichs, S. Many roads to maturity: microRNA biogenesis pathways and their regulation. *Nat. Cell Biol.* **11**, 228–234. <https://doi.org/10.1038/ncb0309-228> (2009).
- Harfe, B. D., McManus, M. T., Mansfield, J. H., Hornstein, E. & Tabin, C. J. The RNaseIII enzyme Dicer is required for morphogenesis but not patterning of the vertebrate limb. *Proc. Natl. Acad. Sci. USA* **102**, 10898–10903. <https://doi.org/10.1073/pnas.0504834102> (2005).
- Kobayashi, T. *et al.* Dicer-dependent pathways regulate chondrocyte proliferation and differentiation. *Proc. Natl. Acad. Sci. USA* **105**, 1949–1954. <https://doi.org/10.1073/pnas.0707900105> (2008).
- Swingler, T. E. *et al.* The function of microRNAs in cartilage and osteoarthritis. *Clin. Exp. Rheumatol.* **37**(Suppl 120), 40–47 (2019).
- Malemud, C. J. MicroRNAs and osteoarthritis. *Cells* **7**, 4. <https://doi.org/10.3390/cells7080092> (2018).
- Miyaki, S. *et al.* MicroRNA-140 plays dual roles in both cartilage development and homeostasis. *Genes Dev.* **24**, 1173–1185. <https://doi.org/10.1101/gad.1915510> (2010).
- Nakamura, Y., Inloes, J. B., Katagiri, T. & Kobayashi, T. Chondrocyte-specific microRNA-140 regulates endochondral bone development and targets Dnpep to modulate bone morphogenetic protein signaling. *Mol. Cell. Biol.* **31**, 3019–3028. <https://doi.org/10.1128/MCB.05178-11> (2011).
- Le, L. T., Swingler, T. E. & Clark, I. M. Review: the role of microRNAs in osteoarthritis and chondrogenesis. *Arthritis Rheum.* **65**, 1963–1974. <https://doi.org/10.1002/art.37990> (2013).
- Crowe, N. *et al.* Detecting new microRNAs in human osteoarthritic chondrocytes identifies miR-3085 as a human, chondrocyte-selective, microRNA. *Osteoarthr. Cartil.* **24**, 534–543. <https://doi.org/10.1016/j.joca.2015.10.002> (2016).
- Steck, E. *et al.* Chondrocyte expressed protein-68 (CEP-68), a novel human marker gene for cultured chondrocytes. *Biochem. J.* **353**, 169–174 (2001).
- Benz, K., Breit, S., Lukoschek, M., Mau, H. & Richter, W. Molecular analysis of expansion, differentiation, and growth factor treatment of human chondrocytes identifies differentiation markers and growth-related genes. *Biochem. Biophys. Res. Commun.* **293**, 284–292. [https://doi.org/10.1016/S0006-291X\(02\)00223-1](https://doi.org/10.1016/S0006-291X(02)00223-1) (2002).
- Ijiri, K. *et al.* Differential expression of GADD45beta in normal and osteoarthritic cartilage: potential role in homeostasis of articular chondrocytes. *Arthritis Rheum.* **58**, 2075–2087. <https://doi.org/10.1002/art.23504> (2008).
- Swingler, T. E. *et al.* The expression and function of microRNAs in chondrogenesis and osteoarthritis. *Arthritis Rheum.* **64**, 1909–1919. <https://doi.org/10.1002/art.34314> (2012).
- Culley, K. L. *et al.* Class I histone deacetylase inhibition modulates metalloproteinase expression and blocks cytokine-induced cartilage degradation. *Arthritis Rheum.* **65**, 1822–1830. <https://doi.org/10.1002/art.37965> (2013).
- Greco, K. V. *et al.* High density micromass cultures of a human chondrocyte cell line: a reliable assay system to reveal the modulatory functions of pharmacological agents. *Biochem. Pharmacol.* **82**, 1919–1929. <https://doi.org/10.1016/j.bcp.2011.09.009> (2011).
- Le, L. T. *et al.* The microRNA-29 family in cartilage homeostasis and osteoarthritis. *J. Mol. Med. (Berlin)* **94**, 583–596. <https://doi.org/10.1007/s00109-015-1374-z> (2016).
- Pais, H. *et al.* Analyzing mRNA expression identifies Smad3 as a microRNA-140 target regulated only at protein level. *RNA* **16**, 489–494. <https://doi.org/10.1261/rna.1701210> (2010).

22. Davidson, R. K. *et al.* Sulforaphane represses matrix-degrading proteases and protects cartilage from destruction in vitro and in vivo. *Arthritis Rheum.* **65**, 3130–3140. <https://doi.org/10.1002/art.38133> (2013).
23. Korinek, V. *et al.* Constitutive transcriptional activation by a beta-catenin-Tcf complex in APC-/- colon carcinoma. *Science* **275**, 1784–1787 (1997).
24. Goldring, M. B. Update on the biology of the chondrocyte and new approaches to treating cartilage diseases. *Best Pract. Res. Clin. Rheumatol.* **20**, 1003–1025. <https://doi.org/10.1016/j.berh.2006.06.003> (2006).
25. Gabay, C., Lamacchia, C. & Palmer, G. IL-1 pathways in inflammation and human diseases. *Nat. Rev. Rheumatol.* **6**, 232–241. <https://doi.org/10.1038/nrrheum.2010.4> (2010).
26. Grad, Y. *et al.* Computational and experimental identification of *C. elegans* microRNAs. *Mol. Cell* **11**, 1253–1263. [https://doi.org/10.1016/s1097-2765\(03\)00153-9](https://doi.org/10.1016/s1097-2765(03)00153-9) (2003).
27. Fan, J. *et al.* A simplified system for the effective expression and delivery of functional mature microRNAs in mammalian cells. *Cancer Gene Ther.* <https://doi.org/10.1038/s41417-019-0113-y> (2019).
28. Qu, B., Han, X., Tang, Y. & Shen, N. A novel vector-based method for exclusive overexpression of star-form microRNAs. *PLoS ONE* **7**, e41504. <https://doi.org/10.1371/journal.pone.0041504> (2012).
29. Nicolas, F. E., Hall, A. E., Csorba, T., Turnbull, C. & Dalmay, T. Biogenesis of Y RNA-derived small RNAs is independent of the microRNA pathway. *FEBS Lett.* **586**, 1226–1230. <https://doi.org/10.1016/j.febslet.2012.03.026> (2012).
30. Beitzinger, M. & Meister, G. Experimental identification of microRNA targets by immunoprecipitation of Argonaute protein complexes. *Methods Mol. Biol.* **732**, 153–167. [https://doi.org/10.1007/978-1-61779-083-6\\_12](https://doi.org/10.1007/978-1-61779-083-6_12) (2011).
31. Steck, E. *et al.* Chondrocyte secreted CRTAC1: a glycosylated extracellular matrix molecule of human articular cartilage. *Matrix Biol.* **26**, 30–41. <https://doi.org/10.1016/j.matbio.2006.09.006> (2007).
32. Tsang, J., Zhu, J. & van Oudenaarden, A. MicroRNA-mediated feedback and feedforward loops are recurrent network motifs in mammals. *Mol. Cell* **26**, 753–767. <https://doi.org/10.1016/j.molcel.2007.05.018> (2007).

## Acknowledgements

LL was funded by the Dunhill Medical Trust Project Grant (Number R371/0714); LN was funded by Action Arthritis; TES and MJB were funded by a Dunhill Medical Trust Programme Grant (Number R476/0516).

## Author contributions

L.L., L.N. and T.E.S. performed the research and analysed data; T.E.S. and I.M.C. supervised the research; T.E.S., D.A.Y., M.J.B., T.D. and I.M.C. provided research direction; all authors wrote and edited the manuscript.

## Additional information

**Supplementary Information** The online version contains supplementary material available at <https://doi.org/10.1038/s41598-020-78606-6>.

**Correspondence** and requests for materials should be addressed to I.M.C.

**Reprints and permissions information** is available at [www.nature.com/reprints](http://www.nature.com/reprints).

**Publisher's note** Springer Nature remains neutral with regard to jurisdictional claims in published maps and institutional affiliations.



**Open Access** This article is licensed under a Creative Commons Attribution 4.0 International License, which permits use, sharing, adaptation, distribution and reproduction in any medium or format, as long as you give appropriate credit to the original author(s) and the source, provide a link to the Creative Commons licence, and indicate if changes were made. The images or other third party material in this article are included in the article's Creative Commons licence, unless indicated otherwise in a credit line to the material. If material is not included in the article's Creative Commons licence and your intended use is not permitted by statutory regulation or exceeds the permitted use, you will need to obtain permission directly from the copyright holder. To view a copy of this licence, visit <http://creativecommons.org/licenses/by/4.0/>.

© The Author(s) 2020